Catalysis & Kinetics of Non-Phosgene Route to Synthesis of Dimethyl Carbonate (DMC)

By

Ziwei Song

Submitted to the graduate degree program in Chemical & Petroleum Engineering and the Graduate Faculty of the University of Kansas in partial fulfillment of the requirements for the degree of Doctor of Philosophy.

Chair: Raghunath V. Chaudhari

Bala Subramaniam

Laurence Weatherley

Kevin Leonard

James D. Blakemore

Date Defended: 22 August 2018

The dissertation committee for Ziwei Song certifies

that this is the approved version of the following dissertation:

Catalysis & Kinetics of Non-Phosgene Route to Synthesis of Dimethyl Carbonate (DMC)

Chair: Raghunath V. Chaudhari

Date Approved: 28 August 2018

Abstract

Converting CO_2 into value-added chemicals or fuels is one of the major sustainability challenges facing human society. Catalytic manufacture of dimethyl carbonate, a green chemical, using CO_2 as a starting material attracts increasing attention, because it provides an alternative environmentally friendly route. However, several fundamental issues need to be investigated to improve this technology: (a) development of heterogeneous catalyst with high activity, selectivity and stability; (b) kinetics and mechanism of transesterification required to provide a basis for catalyst improvement and design of suitable reactors.

In this thesis, a study on transesterification of alkyl carbonates has been presented using two types of catalysts: Metal Oxides (e.g. CaO) and Double metal cyanides. In one part, transesterification using CaO catalyst is presented to address the significant effect of catalyst pre-treatment using reactants on catalytic activity. Upon CaO pretreatment with methanol, the transesterification activity (TOF) increased significantly. In sharp contrast, pretreatment with cyclic carbonates resulted in a prolonged induction time and rate inhibition. Additionally, various characterization (SEM, CO_2-TPD, XRD, FT-IR, XANES and ^{13}C-NMR) was done on fresh CaO and treated CaO to explore the factors affecting catalytic activity. It is detected that strong basic sites have close correlation with catalytic activity. Furthermore, the formation of $Ca(OCH_3)_2$ is a key step during the pre-treatment process. Detailed investigations on catalyst recycle, effects of substrate types and reaction parameters (reactant concentrations, temperature and catalyst loading) on conversion, selectivity and initial rates are reported. The experiments revealed that with CaO as catalyst, significant contribution of the reaction is due to homogeneous catalysis from sparingly soluble CaO under reaction conditions. Therefore, an approach to analyze simultaneous homogeneous-heterogeneous catalytic transesterification has been discussed. Based on experimental

concentration-time data in batch slurry reactor, detailed kinetic modeling of transesterification of propylene carbonate to DMC in both homogeneous phase as well as heterogeneous phase is reported using both empirical power law and microkinetic (based on molecular level description of catalytic cycle) models, during which corresponding rate parameters for each model were fitted and determined.

In another part of the thesis, a truly heterogeneous double metal cyanide catalyst system is reported which eliminates the problems of leaching observed in metal oxide (CaO) catalysts. It is observed that transesterification of various cyclic carbonates, such as ethylene carbonate, propylene carbonate, and 1, 2-butalene carbonate to dimethyl carbonate can occur over double metal cyanide complex with high activity, selectivity and stability. Detailed investigation of the morphology and structure of the catalysts are done through different characterization techniques (BET, SEM, TEM, XRD, XPS, TGA, FT-IR and UV-Vis). Studies on different reaction parameters (catalyst loading, initial methanol/PC molar ratio, temperature and different cyclic carbonates) and surface characterization enabled the establishment of activity-performance correlation for cyclic carbonate conversion. Further, kinetic modeling using Fe-Mn double metal cyanide complex is reported in which different kinetic models based on different reaction mechanisms are discriminated to fit with the experimental data. The kinetic studies in this work provide guidance for postulating reaction mechanisms and better insight into activation mode of reactants.

In the last, a brief study of transesterification of DMC with phenol for synthesis of diphenyl carbonate (a key intermediate for polycarbonates) is presented. This is an example of a highly equilibrium limited reaction which gives very low reactant conversions (< 3-5%) in batch reactors. The preliminary results presented demonstrate that with simultaneous removal of a co-product methanol, significantly higher reactant conversions can be achieved. The preliminary study

suggest that reactive distillation approach can be effectively used to achieve high conversion in DPC synthesis.

The methodologies developed in this work will provide insights on rational design of catalysts for ring-opening reactions as well as understanding of the reaction mechanism and catalytic cycles.

Acknowledgments

I would like to offer my sincere gratitude to my academic advisor Dr. Raghunath V. Chaudhari, Deane E. Ackers distinguished professor of the Chemical and Petroleum Engineering department at the University of Kansas, and Deputy Director of the Center for Environmentally Beneficial Catalysis (CEBC), for all the support, encouragement and advice he provided during my PhD life. All the valuable suggestions and feedbacks he gave along the road would definitely benefit my whole life afterwards. I would like to thank my committee members, Dr. Bala Subramaniam, Dr. Laurence Weatherley, Dr. Kevin Leonard and Dr. James D. Blakemore, for their willingness to serve on my committee and the precious time they committed to my work, also for their critical review and valuable suggestions they provide on my graduate work.

I would like to thank my former and present friends and colleagues at CEBC: Dr. Kirk Snavely, Dr. Fenghui Niu and Ed Atchison for the invaluable assistance in building up reaction setups and maintaining the instruments. Dr. Anand Ramanathan, Dr. Andrzej Rokicki and Dr. Andrew M. Danby for the insightful discussion on my research work. Dr. Christopher Lyon, Dr. Claudia Bode, Ms. Nancy Crispy, Ms. Rhonda Patridge and Ms. Jane Jones for their kind assistance and instructions during all the official processes. Dr. Xin Jin, Dr. Arely Torres, Dr. Wenjuan Yan, Dr. Dupeng Liu, Dr. Hongda Zhu, Dr. Jianfeng Wu, Dr. Simin Yu, Ms. Pallavi Bobba and Ms. Honghong Shi for their friendship, great company and lively discussion along the PhD road. It would not be such wonderful adventure without them.

I would like to thank my family, for their consistent support and love in my highs and lows, for their encouragement during hard times, and for their being such a strong backing for every decision I made, even though sometimes they think I made the wrong ones.

I would like to acknowledge support for this work from the following sources: National Science Foundation and Environmental Protection Agency program Networks for Sustainable Material Synthesis and Design (NSF-EPA 1339661). I would like to thank Dr. Prem Thapa and Dr. Heather Shinogle of the Microscopy and Analytical Imaging Laboratory, University of Kansas for the fantastic XPS, SEM and TEM characterization. Dr. Victor W. Day of X-ray Crystallography Laboratory, University of Kansas for the XRD analysis, Dr. Justin T. Douglas of Nuclear Magnetic Resonance core laboratory, Molecular Structures Group, University of Kansas for the NMR analysis, which was acquired through an NSF Chemical Instrumentation Grant # 0840515. And Dr. Yongfeng Hu of Canadian Light Source Inc., University of Saskatchewan for the insightful EXANES analysis.

Table of Contents

List of Figures

List of Tables

List of Schemes

Chapter 1 Introduction

1.1 Background

Aromatic polycarbonates (PYC) are an important in day to day consumer products. Due to their outstanding impact resistance, good transparency, high heat resistance, high flame retardancy, they can be used in variety of industries, including construction, packaging, auto-motives, electrical and electronics etc.[1-3] The global polycarbonate market demand exceeded 4.30 million tons, with a total market value of about 15.24 billion dollars in 2015. The market demand of polycarbonate is expected to reach 7.72 million tons by 2024, growing at a CAGR (compound annual growth rate) of 6.9% from 2016 to 2024.[4] Therefore, the manufacture of PC is still a subject of intensive research. Conventionally, PC is manufactured via phosgenation of bisphenol A (BPA), which suffers from toxicity and corrosion problems associated with phosgene as well as the generation of large quantities inorganic salts as waste products, and treatment of large amount of wastewater (as shown in Figure 1-1).[1, 5-6] Therefore, alternative non-phosgene routes to manufacture PC need to be developed considering environmental and safety aspects.

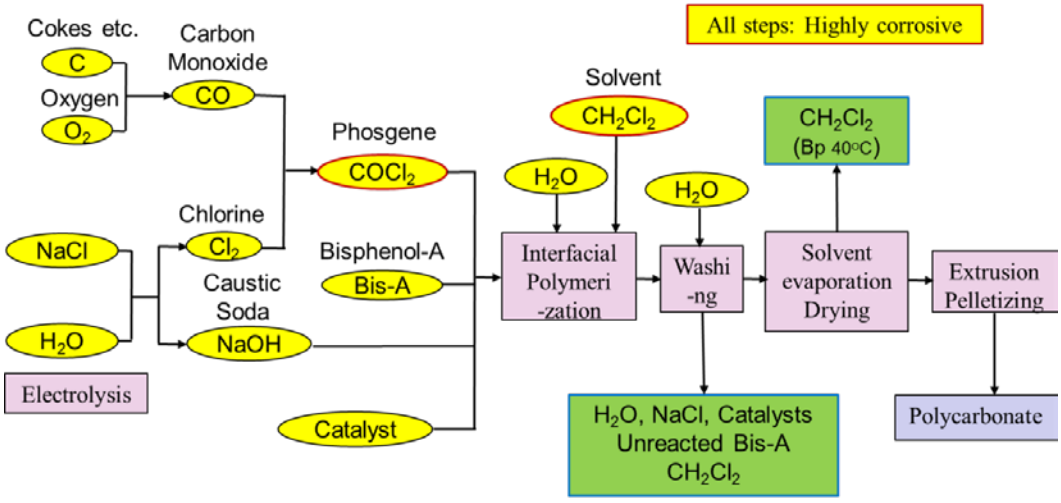

Figure 1-1 Phosgene route to manufacture polycarbonate

In 1993, the first non-phosgene process for the manufacturing PYC was developed and industrialized by GE Plastics, the reaction scheme for which is shown in Figure 1-2.[1, 7] In this non-phosgene process, CO, methanol and oxygen react by oxidative carbonylation to produce dimethyl carbonate (DMC) in the presence of CuCl-$CuCl_2$-HCl catalysts.[8-10] In subsequent steps, DMC is transesterified with phenol to produce diphenyl carbonate (DPC),[11] and finally DPC reacts with BPA to produce PYC.[1] Though toxic phosgene and issues associated with phosgene can be avoided during this non-phosgene process, there are still several disadvantages of this route, such as the catalyst deactivation due to loss of chlorine,[12] the catalytic system is highly corrosive,[13] and the chloride impurities affecting the stability of PYC as well as the final quality of PYC.[1]

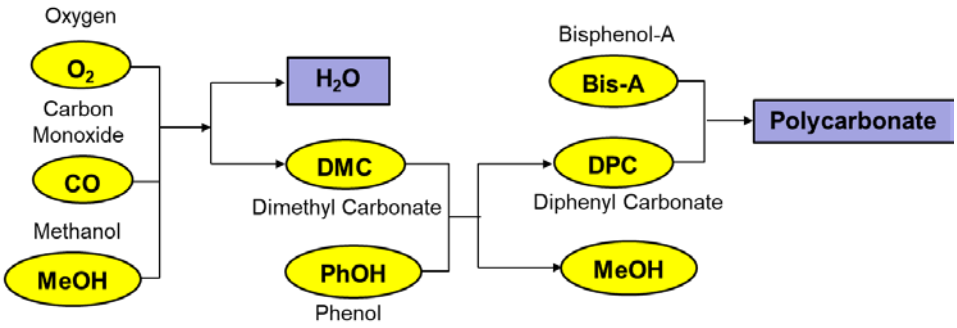

Figure 1-2 Non-phosgene route to manufacture polycarbonate using CO as starting material

Another non-phosgene route for the manufacture of PYC using CO_2 as a starting material was developed by Chimei Asahi in 2002, as shown in Figure 1-3.[1] This process is composed of four reaction steps. First, ethylene carbonate (EC) is produced through the reaction of ethylene oxide with CO_2,[14-15] then EC reacts with methanol to produce highly pure DMC and monoethylene glycol (MEG),[16-17] next highly pure DPC is produced through the transesterification of DMC with phenol,[11, 18] and in the last step, clear and high quality PYC is produced from the melting transesterification of DPC with bisphenol-A.[19-21] Compared to the phosgene and the oxidative carbonylation routes, the Asahi Kasei's process has several advantages, such as elimination of

toxic and corrosive phosgene as a raw material, use of CO_2, minimize waste generation, and co-production of highly pure MEG (important chemical to produce polyethylene terephthalate).[1]

For the two non-phosgene processes, DMC is a key intermediate. Various reports have been published on the manufacture of DMC, such as on different processes, catalysts development, etc. A detailed review of literature on the various catalysts and processes for the manufacture of DMC is presented in the following part.

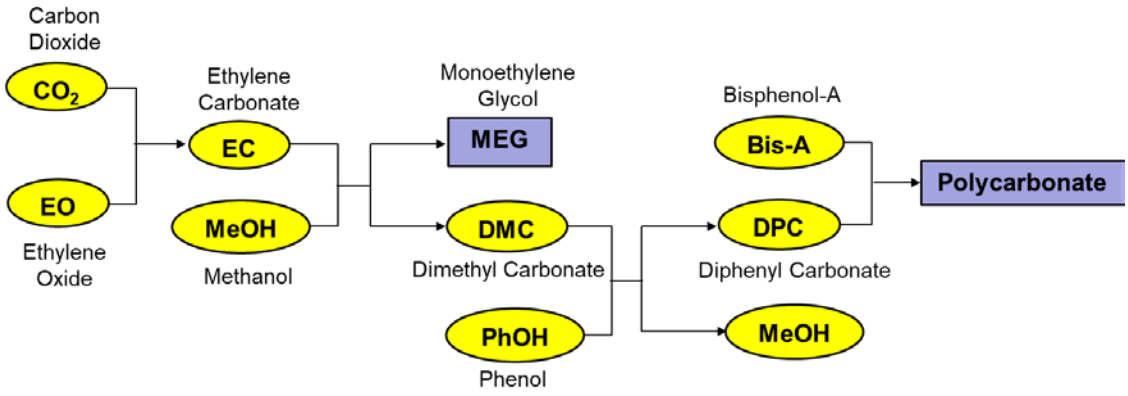

Figure 1-3 Non-phosgene route to manufacture polycarbonate using CO_2 as a starting material

1.2 Literature Review

1.2.1 Processes for Dimethyl Carbonate

Dimethyl carbonate (DMC) is an important chemical intermediate for a variety of industrial applications. Its increasing importance is mainly due to two reasons: green properties it possesses for human and environmental health, and its versatility as a reagent and solvent in various processes.[22] It can be used as an environmentally benign substitute for phosgene, dimethyl sulfate and methyl halide as well as carbonylation and methylation agent.[23] DMC is also widely used as an octane enhancer in gasoline and a key raw material for the production of commodity polymers such as polycarbonates avoiding the use of toxic and hazardous phosgene.[24-25]

Conventionally, DMC is manufactured *via* phosgenation of methanol, a process that suffers from toxicity and corrosion problems as well as the generation of large quantities of HCl

and inorganic salts as waste products.[9, 26-27] The process flow diagram is shown in Figure 1-4. In this process, the molar ratio of $COCl_2$:CH_3OH is typically 1:(1.5~2.5) following two consecutive reactions for 12~20 h at 50 °C, after which, crude DMC (90%) is obtained. Then, the crude DMC is introduced to the neutralizer, in which, the HCl residue is removed. The crude DMC is then pumped into the distillation column, to separate DMC with 95% purity. The overall yield of DMC based on methanol is about ~90%.[28] Though, high yield is achieved, this process suffers from serious safety and environmental problems related to using toxic and corrosive phosgene.[29] Currently, building of new phosgene based plants has been banned.

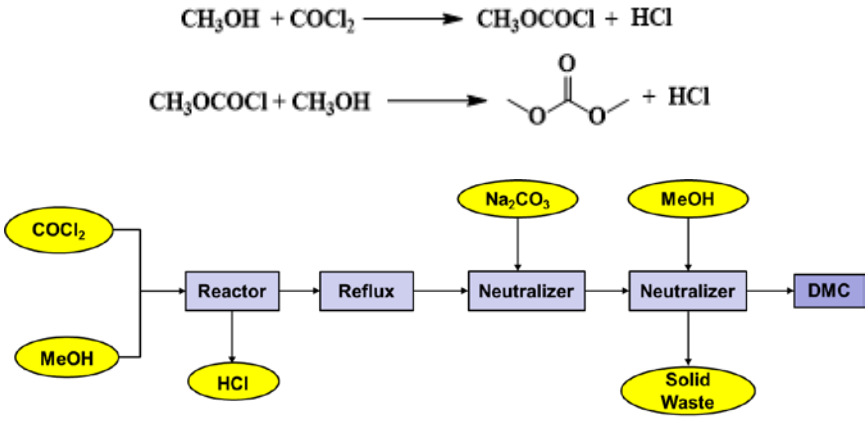

Figure 1-4 Reaction scheme and process flow diagram of phosgenation of methanol to DMC

The alternative Enichem process involving oxidative carbonylation of methanol with CO and O_2 using CuCl as a catalyst in the liquid phase has been commercialized since 1980s.[8] The process flow diagram is shown in Figure 1-5. In this process, the reaction is carried out in three continuous stirred tank reactors in series at 90~120 °C under 2~3 MPa. CO is bubbled through methanol and catalyst solution into the first reactor, while O_2 is introduced in the three reactors separately. The recovered catalyst and methanol are recycled in the first reactor. The final DMC selectivity achieved is ~90%.[28] This liquid phase oxidative carbonylation process eliminates the use of highly toxic phosgene. This process is considered as a great improvement in the history of

DMC industrialization. However, this reaction is carried out under high pressure, and large amounts of CO_2 as a by-product is generated during the process. Besides, using corrosive Cu halide as a homogeneous catalyst poses difficulties in separation of DMC from products as well as corrosion of the equipment.[12-13]

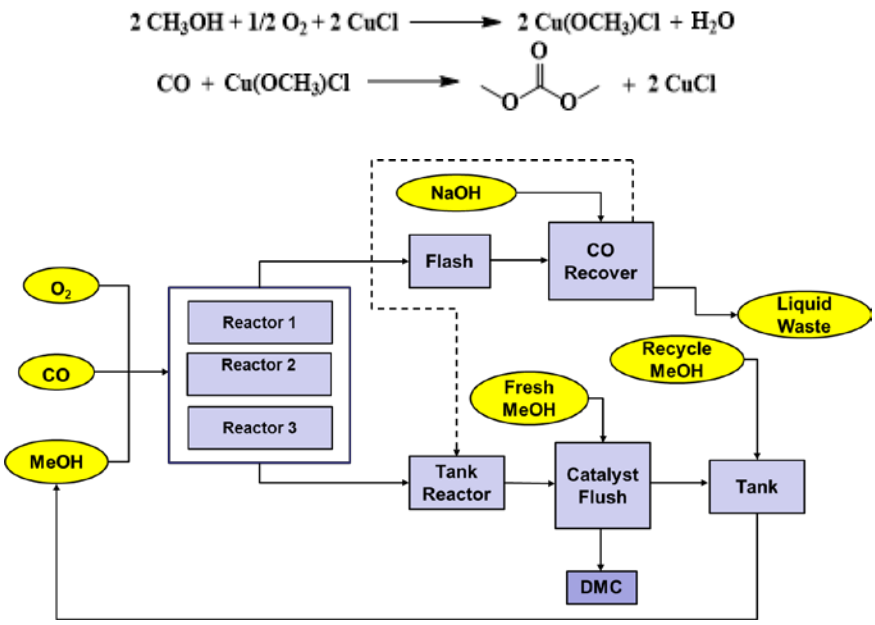

Figure 1-5 Reaction scheme and process flow diagram of liquid oxidative carbonylation

In 1992, an indirect gas phase oxidative carbonylation process (synthesis of DMC from intermediate methylnitrite (MN)) was developed by a Japanese company Ube, and commercialized with a capacity about 6 kt/y, the process flow diagram of which is shown in Figure 1-6.[30] For this process, the reaction takes place in the gas phase in two steps: in the first step, methanol, O_2 and NO react at ~50 °C under 0.28 MPa to form MN and H_2O without catalyst. Then, the formed MN is introduced into reactor 2 to conduct carbonylation with CO at around 100~120 °C under 0.5~1 MPa to form the final product DMC using supported Pd halide complex as a catalyst. In this process, co-catalyst is also needed just to prevent Pd from reduction to metal.[28] Compared to the liquid phase reaction, the Ube process prevents the formation of azeotropic component (MeOH-

H_2O-DMC). Additionally, it gives high productivity and selectivity of DMC. However, this process introduces issues of NO toxicity and CH_3ONO reactivity.[28, 30]

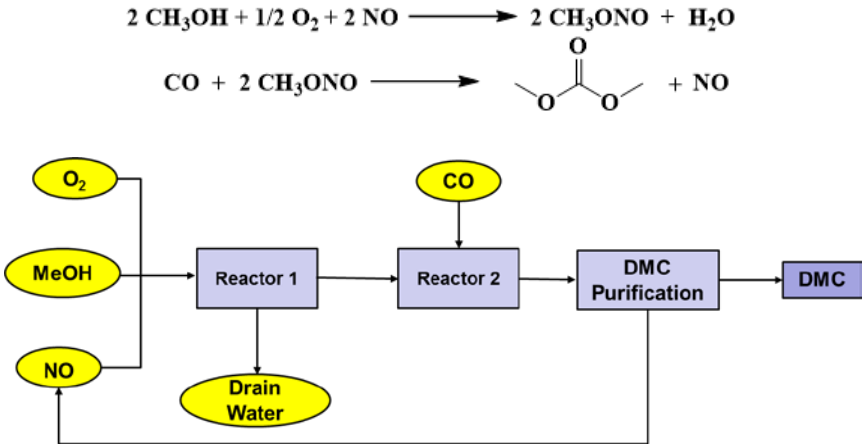

Figure 1-6 Reaction scheme and process diagram of indirect gas phase oxidative carbonylation

As early as 1986, a direct gas phase oxidative carbonylation (Scheme 1-1) was also reported by Dow Chemical, however, till now, this process is not commercialized. This direct gas phase oxidative carbonylation method eliminates the separation problem involved in the liquid phase process. Additionally, toxic gas NO is not used. For this process, the reaction is usually carried out at 100~120 °C under 1.96 ~3.92 MPa using $CuCl_2$ as catalyst, and the final DMC yield can reach 40~80 g/ (L· catalyst · hr).[28]

Scheme 1-1 Reaction scheme for direct gas oxidative carbonylation

In 1986, manufacture of DMC through cyclic carbonates and methanol was developed by American Company Texaco Inc.[31] The process flow chart is depicted in Figure 1-7. Mainly six process units are involved in this process, which are: reactive distillation, extractive distillation, light component removing unit, solvent recovery unit, PG recovery unit and methanol recovery unit. The reaction takes place at around 100~150 °C under moderate pressure. During the reaction, azeotropic component is formed at 63.5 °C between DMC and methanol in mass ratio m_{DMC}:$m_{methanol}$

= 30:70. Then, the azeotropic component is separated using extractive distillation, from which DMC is obtained.[28]

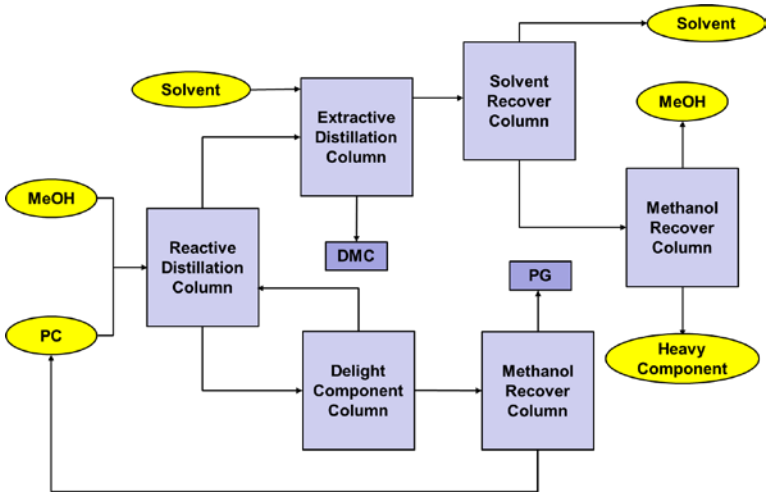

Figure 1-7 Reaction scheme and process diagram of transesterification

Direct synthesis of DMC from methanol and CO_2 (Scheme 1-2) is the most attractive as well as the most challenging route. The raw materials of direct synthesis are cheap and easy to obtain. The atom economy of the reaction can approach nearly 100%. However, due to thermodynamic limitations of the reaction, especially the low reactivity of CO_2, very low yield (0.18%~14%without using of dehydrating agent) of DMC is obtained.[32-35] At present, this process is still in exploratory stage of development. Different catalyst systems are reported with the goal of improving the conversion of methanol and DMC yield.

Scheme 1-2 Reaction scheme for direct synthesis of DMC

Among all the three commercialized processes, transesterification process is viewed as a cleaner alternative that can operate at mild reaction conditions with high selectivity and is hence

receiving increasing attention in recent years. All the raw materials involved in this process (methanol, EC or PC, DMC, and glycols) are non-corrosive and safe to handle by standard industrial practices.[36] Furthermore, naturally abundant CO_2 can be used as a starting material for the process to manufacture cyclic carbonates.[36-38] Additionally, the distilled DMC-methanol azeotropic composition can be used as a gasoline or diesel fuel additive without further treatment.[36] The co-products, glycols are also important chemical intermediates in polyesters, antifreeze products, and cosmetics.[39-40] Therefore, a more detailed account of transesterification is presented in following sections.

1.2.2 Transesterification of Propylene Carbonate with Methanol to DMC

1.2.2.1 Catalyst Development

Transesterification of cyclic carbonates (e.g. ethylene carbonate (EC) and propylene carbonate (PC)) with methanol has been studied previously using a variety of homogeneous and heterogeneous catalysts. Some important experimental studies are summarized in Table 1-1.

Typical homogeneous catalysts used are alkali metal methoxides[53], carbonates[36], tertiary phosphines, arsines or selenium compounds[31]. Homogeneous catalysts are usually used at mild reaction conditions with high catalytic activity.

a. *Alkali metal hydroxide, carbonates, alkoxides:* Inorganic bases have been reported as early as 1970s as catalysts for synthesis of carbonates.[61] For instance, with KOH, low DMC selectivity around 45% was obtained at 120 °C in a continuous process.[62] Sodium methoxide, as a homogeneous catalyst is used in commercial processes, with high activity for transesterification reactions. For example, transesterification with sodium methoxide was reported to give 53.9% PC conversion at 60 ^{o}C in just 10 min, with a TOF of 344 h^{-1}, which is much higher than other reported catalysts[53].

Table 1-1 Catalyst for transesterification of cyclic carbonate with methanol

#	Catalyst	T(°C)	Methanol/PC Ratio	PC conversion (%)	DMC selectivity (%)	TOF[a]	Ref
1	$NaOCH_3$	60	4	53.9	--	--	[53]
2	$Zr(C_5H_7O_2)_4$	130	4	25.8	98.0	--	[31]
3	$P(Bu)_3$	80	5.2	57.2	90.0	--	[54]
4	$Na_2Sn(OH)_6$	80	10	--	Yield (72.3)	--	[55]
5	Cu/Zn/Al mixed oxides	160	10	70.3	92.8	6.0	[56]
6	CaO	50	10	83.0	93.0	--	[25]
7	La modified Mg-Al hydrotalcite	150	10	33.1	87.7	57[b]	[23]
8	Au/CeO_2	140	10	63.0	55.0	30[c]	[57]
9	Ion exchange resin	40	8	55-65	97	--	[58]
10	TiO_2-SiO_2	150	10	86.0	51.2	--	[59]
11	Fe-Zn double metal	170	10	--	Yield (86.6)	26	[60]

[a]TOF = moles of PC converted /(mole of catalyst·time).
[b]TOF = moles of PC converted /(g of catalyst·time).
[c]TOF = moles of PC converted /(mole of Au·time).
[d]TON = moles of PC converted per mole of catalyst.

b. *Zirconium, titanium and tin homogeneous catalysts*: Organic metal salts and complexes based on zirconium, titanium and tin are known to be very active for transesterification reactions.[31] Though high DMC selectivity (>98%) is achieved with these catalysts, the reactions were carried out at much higher temperatures (~130 °C) compared to other catalysts.

c. *Tertiary phosphines, arsines and stibines.* Co-generation of DMC and diols through transesterification can also be realized in the presence of a homogeneous V-B group or VI-B group metal catalysts selected from tertiary phosphines, tertiary arsines, tertiary stibines, bivalent sulfur compounds and bivalent selenium compounds. In a typical example, a conversion of EC can reach

as high as 57.2%, with 90% DMC selectivity using PBu_3 as catalyst in a tubular reactor setup at 100 ^oC, when the methanol/EC ratio is 5.[54]

Although the homogeneous catalysts give high DMC yields under mild conditions, they are difficult to separate and recover from products. Several types of heterogeneous catalysts have also been investigated for the transesterification of cyclic carbonates with methanol, including metal oxides with[25] and without supports, ion exchange resins,[58] molecular sieves[59] and double metal cyanides[60].

a. *Metal oxides.* Metal oxides play an important role in catalytic reactions, such as hydrogenation reaction[63], oxidation reaction[64], esterification reaction[65], etc. Metal oxides are also the most studied catalysts for transesterification of cyclic carbonates with methanol, especially mixed metal oxides. Ce-M (M=Co, Fe, Cu, Zn), a bimetallic metal oxide catalyst (Ce-Cu) showed a TOF of 3.5 h^{-1}, when tested between 120 °C~180 °C, the highest DMC yield of 70% was derived at 160 °C after 4 h reaction[66]. Cu-Zn-Al hydrotalcite with layered structure was reported with TOF of 6.0 h^{-1}, 70% PC conversion and 94% DMC selectivity at 160 °C.[56] Mg-Al-CO_3 type hydrotalcite was reported to have much higher activity (TON 280.4 mmol DMC/g catalyst) than other metal oxides, such as ZnO (TON 12.5 mmol DMC/g), CeO_2 (TON 16.2 mmol DMC/g)[67]. The PC conversion can reach 72.2% with 97.1% DMC selectivity at 130 °C. Later, in Unnikrishnan and Srinivas's work, it is reported that, the activity of Mg-Al hydrotalcite can be significantly enhanced after modification with rare earth metals (La^{3+}, Ce^{3+}, Pr^{3+} et al).[23] CaO-ZrO_2, a mixed oxide, was reported to give 55% PC conversion at 117 °C and 95% PC conversion in a reactive distillation reactor but specific data on selectivity of DMC and activity is not reported.[37]

b. *Supported catalysts.* Several supported catalysts have also been reported for the transesterification reaction. One type of supported catalysts is the supported metal salts, such as

NaF/Al_2O_3, KF/Al_2O_3.[68] The second type of supported catalysts is the supported metal oxides, such as, CaO/ZrO_2[43], CaO/C[25]. The third type is the supported metals, for example Au/CeO_2[57]. KF supported on neutral alumina was reported to have higher activity than the one supported on acidic or basic alumina, which may be due to the concentration of basic sites between $7.2< H^- <9.8$. Supported Au nanoparticles (Au/CeO_2) have also been investigated,[69] for the transesterification reaction. They found that adding Au can significantly enhance the catalytic activity of CeO_2 for the transesterification of PC with various alcohols. The activity increased from 26.7 h^{-1} to 53.3 h^{-1} when Au content on CeO_2 was varied.

c. *Ion exchange resins.* A series of strong basic anion exchange resins having quaternary ammonium chloride with Cl^-, CO_3^{2-}, HCO_3^- and Cl^-/CO_3^{2-} counter ion, were tested in a lab-scale tubular reactor.[1] High DMC selectivity (above 99%) was obtained even at room temperature, with MeOH/EC molar ratio of 2 and liquid hourly space velocity (LHSV) of 0.33. A strong basic quaternary ammonium ion exchange resin with hydroxide counter ion was reported to give 55-65% PC conversion with 97% DMC selectivity at 40 °C. However, the activity of this catalyst decreased by 50% after 24 hrs.[58] Weak base ion exchange resin, Amberlyst A-21 was also reported to be active for the transesterification.[62]

d. *Molecular sieves.* As early as 1996, TS-1 was reported to have no activity for the transesterification, however, K_2CO_3 treated TS-1 molecular sieve was reported to be active for the reaction between EC and methanol.[70] In a later study, other two molecular sieves, Ti-MCM-41 and amorphous TiO_2-SiO_2 were reported. Amorphous TiO_2-SiO_2 was reported to have high activity, with a PC conversion of 86% and DMC selectivity of 51.2% at 150 °C.[59]

e. *Double metal cyanide.* Double metal cyanide is a group of heterogeneous catalysts that has been successfully used in epoxide polymerization reactions for several decades[71], and also in the

copolymerization of epoxide with CO_2 in polymer field[71-77]. Double metal cyanides are known to be insoluble in almost all solvents, including water, which can benefit the separation of catalyst from products.[60] Among the double metal cyanides, the ones based on Co-Zn and Fe-Zn are already shown to be excellent heterogeneous catalysts for transesterification.[71-77] Recently, double metal cyanide catalysts have also been successfully used in the manufacture of biodiesel.[78] Additionally, Srivastava and coworkers have found Fe-Zn as an excellent heterogeneous catalyst for transesterification of propylene carbonate with methanol.[60]

1.2.1.2 Reaction Mechanism

Understanding of the reaction mechanism is important for catalyst design and optimization of chemical processes. Several reports described possible reaction mechanisms for the transesterification of cyclic carbonates with methanol. It is generally believed that propylene carbonate would be first converted to two intermediates with one molecule of methanol. The two intermediates (2-HMC) (2-hydroxypropyl methyl carbonate) and 1-HP-2-MC (1-hydroxypropan-2-yl methyl carbonate) are obtained from different ring opening positions from propylene carbonate. However, both of the intermediates are transformed to final products DMC and PG through further transesterification with another methanol (as shown in Scheme 1-3). Though the main pathway of the reaction is known, the interaction of catalyst with the two reactants and intermediates is not clear.

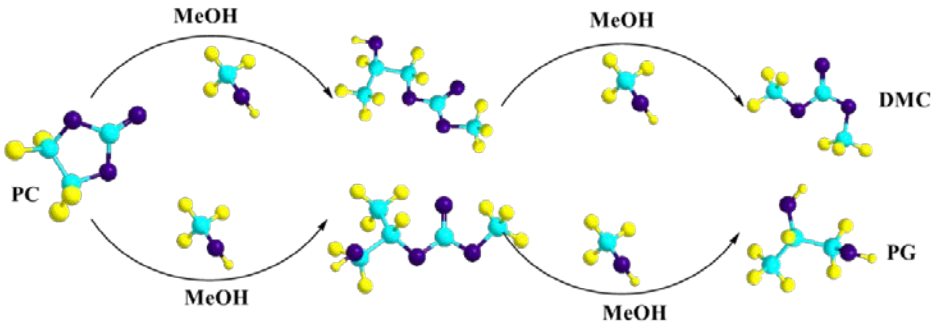

Scheme 1-3 Reaction pathway for transesterification of cyclic carbonate with methanol

For the transesterification of cyclic carbonates with methanol, the reaction mechanism relies on two important steps: the activation of methanol and activation of cyclic carbonate, to initialize the reaction.

(a) Activation of methanol

The basicity and acidity of catalysts has significant influence on the activation of methanol. The activation mode of methanol with basic catalysts is different from that with acidic catalysts. Previous studies, especially from transesterification in biodiesel field show that when solid basic catalysts are used, transesterification occurs with dissociated and non-dissociated methanol present in the system at the same time.[79-81] For the non-dissociated methanol, two weak interactions between methanol and catalysts are proposed. One involves physisorption while the other follows formation of a weak hydrogen bond between methanol and catalysts.[81] For the dissociated methanol, also two different kinds of interactions are possible. Two different intermediates can be formed (Like that shown in Figure 1-8). Intermediate I is a methoxy group bonded to the metal ion and an adjacent hydrogen atom bonded with an exposed oxygen ion of the surface, while intermediate II has been assigned to a surface methyl group linked to an oxygen ion and a hydroxyl group residing on a metal ion.[81-82] Theoretical studies showed that the dissociation ability of methanol on the surface of catalysts depends significantly on the coordination environment of the

metal and surface coverage of methanol.[79, 82-83] However, when homogenous basic catalysts, such as alkaline metal alkoxides, hydroxides or sodium or potassium carbonates are used, catalytically active species CH_3O^- would be formed through reaction of catalyst precursors and methanol.[84-88] After this, the nucleophilic attack from methanol on the carbon in carbonyl group from cyclic carbonates will continue the reaction.

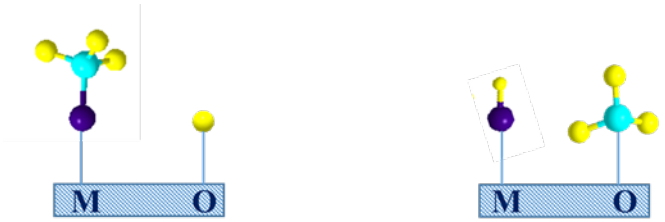

Figure 1-8 Interaction of methanol with basic metal oxides catalyst

For solid acid-catalyzed transesterification, the interaction between methanol and catalysts occurs through adsorption mechanism.[89-92] This follows a nucleophilic attack from methanol on the carbon in carbonyl group from cyclic carbonates. On other hand, when homogenous acid catalyst is used, instead of interaction with methanol, the proton from acid catalyst would form a stable bond with the oxygen in C=O bond due to its electron donor tendency.[93] The following steps would be the same as that in the solid-base case.

(b) Activation of cyclic carbonates

Unlike activation of methanol, there are very few studies on the activation of cyclic carbonates. However, several mechanisms have been proposed for different catalysts.[44, 60, 67, 94] Based on these, several possible interactions between cyclic carbonates and catalysts are possible.

The first activation mode of cyclic carbonate is due to the tendency to donor electrons of carbonyl oxygen in cyclic carbonate, during which the proton or acid site of catalysts can form stable bond with this oxygen.[67] The second type of interaction of cyclic carbonate with catalyst

is adsorption.[44, 95] The third activation mode of cyclic carbonate is direct nucleophilic attack by the methanol activated intermediate, which initializes the formation of mono-transesterified product 2-HMC and 1-HP-2-MC.[60, 94]

1.2.1.3 Reaction Kinetics

Understanding of the reaction kinetics is important for catalyst design, optimization of chemical processes and scale-up. Several studies on the kinetics of the transesterification of cyclic carbonates with methanol are reported. Empirical power law models are proposed in nearly all the reports.[53, 96-97] Reported kinetic models on transesterification of cyclic carbonates with methanol are summarized in Table 1-2. Little information is available on kinetic models of transesterification of cyclic carbonates with methanol, particularly, using heterogeneous catalysts. For the kinetics of transesterification in biodiesel synthesis, kinetic models based on Langmuir Hinshelwood type mechanism, Eley–Rideal type mechanism as well as kinetic models based on reaction mechanism have been proposed.[85, 98-101] In the kinetic studies of heterogeneous catalysts for transesterification in biodiesel synthesis, methanol adsorption is usually proposed as the rate-determining step.[85, 102] However, when strong basic catalysts are used, surface reaction step instead was assumed as the rate-determining step.[102] This information provides useful guidance for the kinetic studies of heterogeneous systems for the transesterification of cyclic carbonates with methanol.

Table 1-2 Kinetic models for transesterification of cyclic carbonates

Catalyst	Reactor Type	Reaction Rate Law	Note
KOH	Batch	$-r_{EC} = k_{for}C_{EC}^{0.87} - k_{rev}C_{DMC}^{1.25}C_{PG}^{0.9}$	97
$NaOCH_3$	Reactive Distillation Column	$-r_{EC} = k_{for}C_{EC}C_{MeOH}^{2} - k_{rev}C_{DMC}C_{PG}$	53
Verkade super bases (Proazaphosphatranes)	Batch	$-r_{EC} = k_{for}C_{PC}C_{MeOH}^{2} - k_{rev}C_{DMC}C_{PG}$	96

1.3 Challenges and Opportunities

1.3.1 Challenges

As discussed above, DMC manufacture from transesterification of cyclic carbonate with methanol attracts extensive interests compared to other synthesis route. Though this route has been commercialized successfully, several issues still exist, which need significant improvements:

(1) **Lack of stable, highly active and highly selective heterogeneous catalysts.** Although transesterification process has been commercialized, mainly alkali hydroxide or methoxide catalysts used, posing great difficulty in separation and recycle of catalysts due to deactivation as well as energy intensive and costly. Therefore, a stable, highly active and selective heterogeneous catalyst is still in demand.

(2) **Lack of fundamental understanding of the kinetics and mechanism.** Though, significant advances are made on the transesterification route for DMC as an environmentally benign route, the fundamental understanding of the reaction mechanism and catalytic cycle is far from complete. Particularly, the activation of substrates and nature of catalytic intermediates are not well understood. Reliable kinetic models representing wider range of conditions are also not available that can be used for reactor design and scale-up purpose.

1.3.2 Opportunities

The goal of this work is to investigate the performance of catalysts and understand the mechanism of transesterification reaction through kinetic studies to enable design of stable, active and selective heterogeneous catalysts for the synthesis of DMC. In order to achieve this goal, four major tasks have been carried out in this dissertation.

(1) Pretreatment effects and reaction mechanism of transesterification of cyclic carbonates on CaO catalyst. In this part of work, the activity and selectivity of metal oxides, especially

CaO for the transesterification reaction was investigated. Additionally, effect of experimental parameters such as substrate concentrations, substrates type, as well as pre-treatment time are studied Furthermore, based on the results, a possible reaction mechanism has been proposed. More importantly, various catalysts characterization techniques have been used to reveal the nature of active species.

(2) Kinetic modeling. Based on experimental concentration-time profiles and reaction mechanism, different kinetic models including power law model, molecular kinetic model have been proposed and simulated with experimental data to evaluate rate parameters. Simultaneous homogeneous/heterogeneous catalyzed transesterification of propylene carbonate has been investigated.

(3) Explore design of heterogeneous catalysts. The synthesis and testing of stable, active and selective double metal cyanide catalysts has been studied. The catalytic activity and reaction rates are correlated to metal composition. Further, various characterization techniques are used to understand the surface morphology and physical structure of the catalysts.

(4) Kinetic modeling of transesterification using double metal cyanide catalysts. Effect of different reaction parameters, including catalyst loading, PC/MeOH molar ratio, temperature, different cyclic carbonates has been studied. Furthermore, different kinetic models have been proposed and simulated based on the possible reaction mechanisms. Based on comparison of experimental and simulated results, several kinetic models are discriminated to propose the best fit model and evaluate rate parameters.

1.4 Outline of Dissertation

This dissertation composes of five chapters in addition to introduction (Chapter 1) and conclusions and future recommendations (Chapter 7) chapters. Chapter 2 describes the

pretreatment effect of methanol and cyclic carbonates on catalytic performance for transesterification of cyclic carbonates to dimethyl carbonate using metal oxide (CaO, BaO and SrO) catalysts. Stirred batch reactor experiments reveal that with untreated CaO as a catalyst, significant induction time was observed. The induction time was eliminated upon CaO pretreatment with methanol and the transesterification activity increased from 11 to 947 h^{-1}. In contrast, pretreatment with PC resulted in a prolonged induction time and rate inhibition. Pretreatment of CaO with other cyclic carbonates including ethylene carbonate (EC) and 1,2-butylene carbonate (BC) also showed similar trends on pretreatment. Based on these experimental results and complementary catalyst characterization results using SEM, CO_2-TPD, XRD, FT-IR, XANES and ^{13}C NMR, a possible reaction mechanism involving methoxy species as the key intermediate is proposed.

Chapter 3 presents a kinetic study of transesterification of propylene carbonate with methanol using CaO catalyst. In this chapter, experimental concentration-time profiles were obtained at different catalyst loadings, PC concentrations, and methanol concentrations in a temperature range of 20-50 ^oC in a stirred batch reactor for both the homogeneous-CaO catalyzed transesterification and the heterogeneous-CaO catalyzed transesterification reactions. Power law as well as models based on reaction mechanisms were evaluated. It is observed that the kinetic models based on molecularly described mechanisms fit better than the power law model, especially for the heterogeneous-CaO catalyzed reaction. The good fitting of kinetic models with experimental data indicates that the proposed mechanisms can be used to elucidate the kinetics of homogenous and heterogeneous CaO catalyzed reactions separately.

Chapter 4 presents transesterification of cyclic carbonates with methanol using double metal cyanide as a true heterogeneous catalyst with no leaching. The catalyst consisting of Fe-Mn

double metal cyanide complex with a Fe/Mn metal ratio of 8 was found to be highly active and non-leaching heterogeneous catalyst for the transesterification of cyclic carbonates with methanol with high selectivity and stability. Characterization of the catalyst using BET, SEM, TEM, XRD, XPS, TGA, FT-IR and UV-Vis analysis was carried out to understand the surface morphology and structure of this catalyst. Additionally, in this chapter, the effects of catalyst loading, methanol/PC ratio, temperature and different cyclic carbonate substrates (ethylene carbonate, propylene carbonate, and 1,2-butylene carbonate) on the initial reaction rate as well as concentration-time profiles have been investigated.

Based on the results in Chapter 4, detailed kinetic study of transesterification of PC with methanol over Fe-Mn double metal cyanide is presented in Chapter 5. Two-step power law model was found to well represent the experimental data. Furthermore, a kinetic model based on reaction mechanism involving an activation sequence of PC, methanol, and 2-HMC was found to demonstrate that the experimental data better than the power law.

Chapter 6 presents a brief introduction of the transesterification of DMC with phenol, the catalyst development, kinetic models and reaction mechanism. A continuous reaction setup of distilling off azeotropic component of methanol and DMC is used for some exploratory studies of the transesterification of DMC with phenol. It is found that the initial DMC/phenol ratio and temperature have significant effect on the conversion efficiency. Additionally, from screening of heterogeneous catalysts, it is found that Fe-Mn double metal cyanide is also an active catalyst for the transesterification of DMC with phenol.

Chapter 2 Catalyst (CaO) Pretreatment Effects in Propylene Carbonate Transesterification with Methanol

2.1 Introduction

Transesterification of cyclic carbonates with methanol, has been studied intensively using metal oxides such as CeO_2, ZrO_2, MgO et al.[37-38, 41-43] as heterogeneous catalysts as discussed in Chapter 1. Among the reported metal oxide catalysts, CaO is found to give high activity even at room temperature.[25, 44-45] It is also known as an effective heterogeneous catalyst for other transesterification reactions such as triglyceride conversion in bio-diesel production.[42, 46-49] CaO in various forms (nano-CaO, supported CaO, mixed CaO with other metals) has also been reported.[42, 50] In one of the recent studies, it was found that the catalytic activity of CaO can be further enhanced through pre-treatment with methanol during transesterification of rapeseed oil.[51-52] However, a detailed studies on the pretreatment effects and underlying mechanism are lacking. Furthermore, little information exists about the pretreatment effect of reactants during transesterification of cyclic carbonates such as ethylene carbonate (EC) and propylene carbonate (PC).

Therefore, in this work, the effect of pretreatment of CaO catalyst on catalytic performance in transesterification of PC with methanol was investigated. In particular, the influence of pretreating CaO with reactants PC and methanol was studied for DMC synthesis. Concentration-time profiles in the presence of fresh and pretreated CaO catalysts were obtained to better delineate the role of catalyst pretreatment. Characterization of fresh and pretreated catalysts using SEM, CO_2-TPD, XRD, FT-IR, XANES and ^{13}C-NMR analysis was carried out and structure-activity relations were studied. In addition, pretreatment effects of other cyclic carbonates, such as EC and 1, 2-butylene carbonate (BC) were also investigated. Additionally,

recycle experiments were conducted to verify the continuous usage of catalyst and test the stability. A plausible mechanism of transesterification has been proposed to explain the observed experimental results and provide new insights into the underlying reaction mechanism.

2.2 Experimental Section

2.2.1 Materials

All chemicals used in this part of work except BC were purchased from Sigma Aldrich. Methanol (99.8%), PC (99.7%), DMC (extra dry, 98+%), propylene glycol (PG, 99.5+%), EC (99%), ethylene glycol (EG, 99.8%), 1,2-butanediol (BG, 98+%), mesitylene (98%) and CaO (powder) were used without further treatment. BC (98+%) was obtained from Tokyo Chemical Industry Co., LTD.

2.2.2 Experimental Setup and Procedure

The transesterification experiments and pre-treatment studies were carried out in a stirred pressure reactor, with 300 ml capacity supplied by Parr Instrument Co. The setup is shown in Figure 2-1.

2.2.2.1 Evaluation of Catalyst Performance

For the evaluation of catalyst performance, in a typical experiment, 3.0 mol methanol, 0.15 mol PC and 0.025 mol mesitylene (internal standard for GC analysis) were charged into the reactor. The contents were heated to a desired temperature by using a temperature-controlled circulating bath. Following this step, 0.15 g of CaO was charged to the reaction mixture and the contents stirred at 1100 rpm, to start the reaction. The reaction progress was followed by withdrawing liquid samples at different time intervals and analyzed for the contents. To facilitate liquid sampling, the reactor was maintained at 0.69 MPa of N_2.

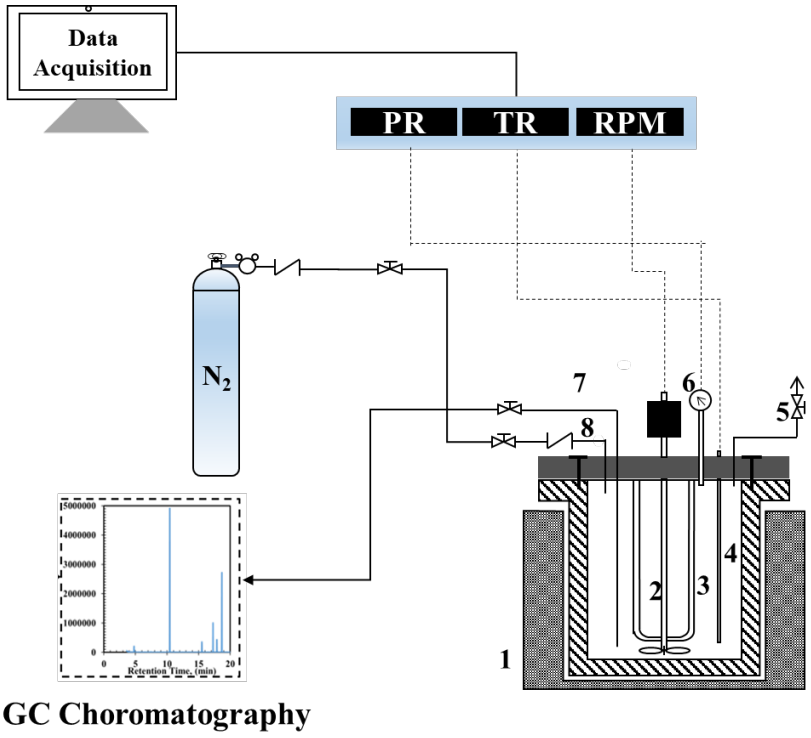

Figure 2-1 Schematic of experimental setup. 1. Heating jacket; 2. Stirring shaft; 3. Cooling coil; 4. Thermos well; 5. Gas vent; 6. Pressure gauge; 7. Liquid sampling tube; 8. Gas inlet; PR: reactor pressure indicator; TR: reactor temperature indicator.

2.2.2.2 Experiments for Pre-treatment Effect

For methanol pretreatment study, 0.15 g of fresh CaO catalyst was mixed with 3.0 mol methanol and stirred at a desired temperature for a fixed period of time. Then, 0.15 mol PC and 0.025 mol of mesitylene were added and the reaction carried out as described in section 2.2.2.1. For pretreatment of CaO with PC, 0.15 g of CaO and 0.15 mol PC were mixed first under stirring for a fixed period of time, after which methanol was charged and reaction was monitored as described in above section. In both cases, a constant temperature was maintained and the progress followed by analysis of liquid samples at different time intervals.

2.2.3 Analytical Methods

2.2.3.1 Description of Method

All the liquid samples were analyzed offline by gas chromatographic (GC) analysis (Agilent, GC-7890A). The GC was equipped with an autosampler (7683 B Series Injector) and a flame-ionization detector (FID). A ZB-WAX capillary column of 30 m length and an inner diameter of 0.32 mm was used as the stable phase. The inner surface of the column was a polyethylene glycol film. Helium at 30 std mL/min flow rate was used as the carrier gas.

A programmed temperature ramp was needed to separate and analyze the liquid samples. The oven temperature started from 80 °C, which was maintained for 4 min during the analysis. Then a temperature was increased at a rate of 40 °C/min until 250 °C, which was maintained for further 2 min. The liquid samples were separated completely using the above described temperature programming. Mesitylene was used as an internal standard for all samples. Typical retention times were 2.8 min for methanol, 3.1 min for DMC, 4.9 min for mesitylene, 7.1 min for PG and 8.3 min for PC, respectively. An example of GC result is shown in Figure 2-2. Two intermediates detected at 7.7 and 7.9 min, were identified as 1-hydroxypropan-2-yl methyl carbonate and 2-hydroxypropyl methyl carbonate (2-HMC) by GC-MS (Figure 2-2).

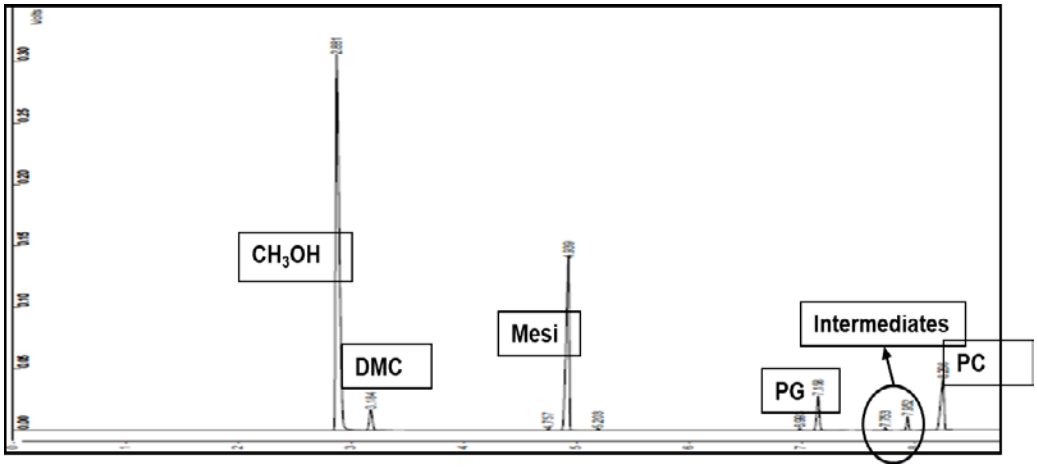

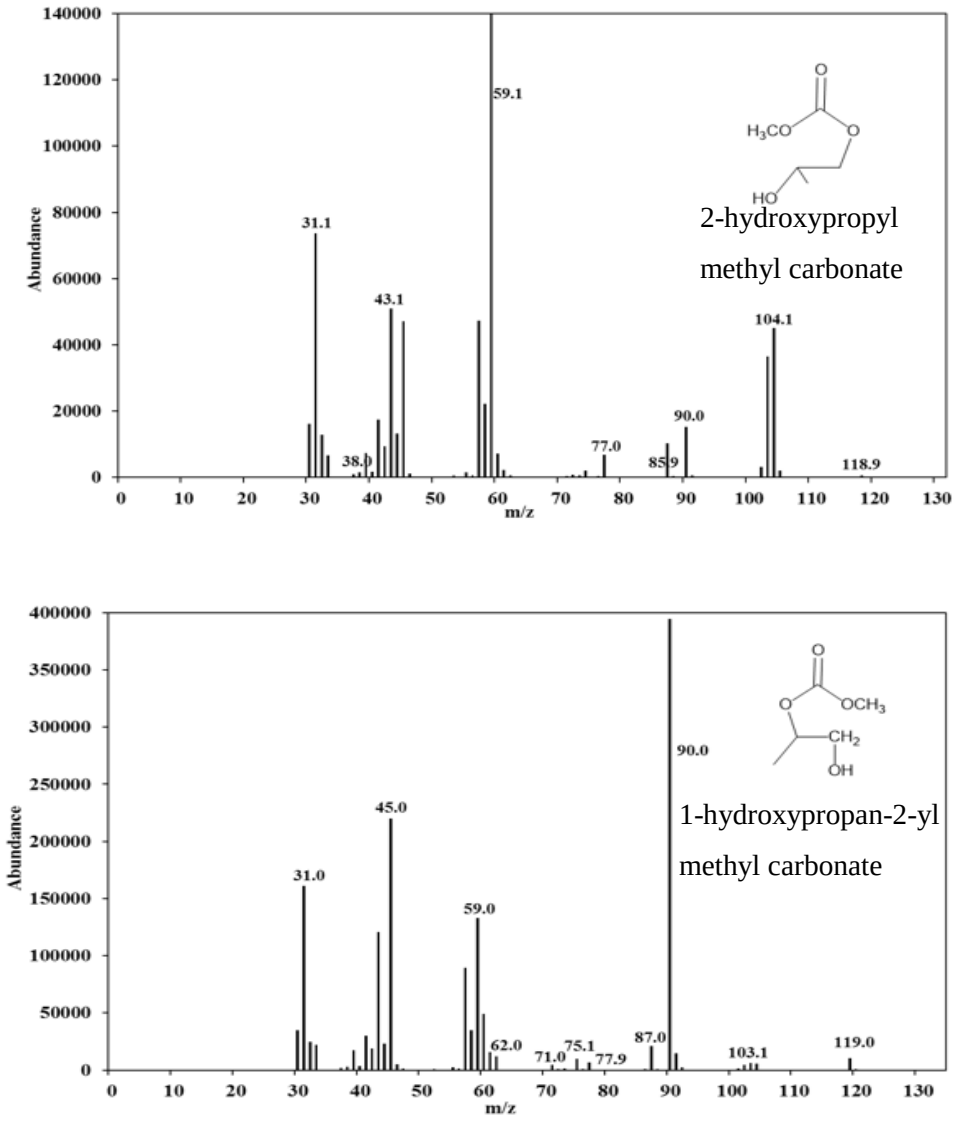

Figure 2-2 A typical GC result from transesterification of PC and mass spectra for the two intermediates

The calibration curve for each component was established to calculate the component concentration from the GC charts. For the calibration of one component, four samples were prepared, each sample was analyzed three times, and the mean value was used. To demonstrate the high accuracy of the GC analysis, synthetic standard samples were also prepared. The absolute value of the standard sample and the analyzed value from GC analysis were compared. The calibration curve and accuracy of calibration are presented in Appendix I.

2.2.3.2 Definitions

Conversion is defined as the ratio of moles of substrate converted to the moles of substrate charged initially. Selectivity is defined as the ratio of the moles of carbon in specific product to the moles of carbon equivalent to converted substrate. Turnover frequency (TOF) is defined as the amount of substrate converted (mol) in the presence of certain amounts of catalysts (mol) during reaction (h), expressed as mol/mol/h. The conversion of PC, selectivity of DMC and PG, and TOF were calculated using the following equations:

$$\%\text{Conversion} = \frac{(\text{Initial Moles of PC} - \text{Final Moles of PC})\ \text{x}\ 100}{\text{Initital Moles of PC}} \quad (1)$$

$$\%\text{Selectivity of Products} = \frac{(\text{Moles of Product Formed})\ \text{x}\ 100}{\text{Moles of PC Reacted}} \quad (2)$$

$$\text{TOF (for} < 15\ \%\ \text{PC conversion)} = \frac{(\text{Initial Moles of PC} - \text{Final Moles of PC})}{(\text{Molar Catalyst Loading})\ (\text{Reaction Time})} \quad (3)$$

2.2.3.3 Error Analysis

Error in an experiment includes the uncertainty from repeated experimental data under identical reaction conditions as well as the error in GC analysis. The (experimental) error (from repeated experiments) for a typical experiment was in the range of 2.24~17.3%. The relative error from GC analysis (repeated injection of one sample for three times) was as low as < 3.62% in all cases. The detailed procedures for error analysis are described in Appendix I.

2.2.4 Catalyst Characterization

A Versa 3D dual beam Scanning Electron Microscope (SEM)/ Focused Ion Beam (FEI, Hillsboro, OR, USA) was used to understand the surface morphology of various CaO catalysts. All the SEM images reported were obtained at an acceleration voltage of 10 kV, spot size 3.0 and the images were collected with an ET (Everhart Thornley) detector. CO_2-TPD was measured using AutoChem 2910 Instrument. In a typical measurement, solid catalyst sample was first vacuum dried at 120 °C for 2 h and then saturated with CO_2 at 50 °C, after which desorption tests were

conducted at a ramping rate of 10 °C till 1000 °C. CO_2 signal was recorded by a thermal conductivity detector. XRD patterns of the catalysts were obtained using a Bruker SMART APEX single-crystal diffractometer equipped with a graphite monochromator, with a scanning range of 5°-70°, and a step size of 0.02°. Diffuse Reflection Infrared Fourier Transform Spectroscopy (DRIFTS) spectra for the catalyst were collected in the range of 600-4000 cm^{-1}, using a Bruker Tensor 27 FT-IR equipped with a Pike diffuse reflectance cell. Ca K-edge XANES spectra were recorded using the SXRMB beamline of Canadian Light Source Inc., University of Saskatchewan. A Si (111) based monochromator was used to cover the energy range used in this work. A liquid cell setup was used to measure the Ca K-edge spectra. The fluorescence yield of aqueous samples was recorded using a 4-element Si drift detector. The total electron yield was used for reference samples, which are free from the self-absorption problem. All XANES data were analyzed using Athena package.[103] Solid state ^{13}C-NMR spectra were recorded on a Bruker DRX 400 MHz type spectrometer equipped with an HP amplifier. The spin rate of the sample was 10 kHz. The chemical shifts were determined in ppm using Alpha Glycine as a standard sample.

2.3 Results and Discussion

2.3.1 Evaluation of Various Catalysts

In order to benchmark the performance of various catalysts and establish the analytical protocols, several commonly available metal oxides were first tested for transesterification of PC with methanol. As summarized in Table 2-1, CaO gives the highest DMC yield (81%) compared with MgO, BaO and SrO and several other reported catalysts. The conversion and selectivity values observed for the CaO catalyst are similar to those reported by Cao et al,[104] who reported 83% PC conversion and 93% DMC selectivity at 50 °C.

Table 2-1 Summary of Results from Catalyst Screening Studies

Catalyst	T(°C)	Methanol/PC Ratio	PC conversion (%)	DMC selectivity (%)
CaO	50	20	88.1	92.0
MgO	50	20	12.0	19.3
SrO	50	20	86.4	92.9
BaO	50	20	46.5	98.2
CeO_2	50	20	0.54	Trace
γ-Al_2O_3	50	10	10.1	Trace
TiO_2-SiO_2	150	20	31.2	35
Mg-Al hydrotalcite	130	40	68.1	68.9
Dowex	50	10	4.7	0.3
La-10-TUD-1	100	20	8.9	32.8

Reaction conditions: PC: 1.07 kmol/ m^3; Methanol: 21.4 kmol/ m^3; CaO: 1.07 kg/ m^3; T = 20 °C; 0.69 MPa N_2

Though CaO is usually reported as a heterogeneous catalyst for transesterification reaction[46-47, 49], significant homogeneous reaction was observed in the range of reaction conditions studied. The initial homogeneous reaction rate during the reaction was compared with reaction rate obtained from solid CaO at different temperatures, shown in Table 2-2. From the comparison data, it is clear, that the contribution of dissolved CaO increases progressively with T, from approximately 6.5% at 20 °C to roughly 12% at 50 °C. Therefore, the heterogeneous catalytic reaction is still dominant.

In all the experiments, the amounts of PC and methanol reacted were found to be stoichiometrically consistent with the products formed (DMC and PG), as quantitatively shown in Figure 2-3 (a) for CaO catalyst. The maximum material balance deficit was < 8%, with trace amounts of intermediates, 2-hydroxypropyl methyl carbonate and 1-hydroxypropan-2-yl methyl carbonate formed under certain conditions (see GC-MS spectra in Figure 2-2). These trace compounds could not be reliably accounted for in the material balance calculations. Typical results

with fresh CaO catalyst [Figure 2-3 (a)] show an induction period of 20 min prior to the onset of transesterification. The concentration-time profiles for fresh CaO catalyst [Figure 2-3 (a)] show that PC concentration decreases from 1.07 to 0.2 kmol/m^3 within 120 min (86% conversion) with a constant DMC and PG selectivity throughout the run. The transesterification of EC under similar conditions [Figure 2-3 (b)] exhibits a slightly higher EC conversion (92%) after 120 min, with similar DMC selectivity (~98%). These preliminary observations motivated to investigate the effect of CaO pretreatment on the transesterification.

Table 2-2 Comparison of Homogenous and Heterogeneous Catalytic Reactions

	Catalyst	T(°C)	Initial reaction rate (kmol/(m^3·h))
1	Homogeneous CaO	20	0.65
2	Homogeneous CaO	40	2.3
3	Homogeneous CaO	50	5.3
4	CaO	20	10.1
5	CaO	40	31.9
6	CaO	50	45.6

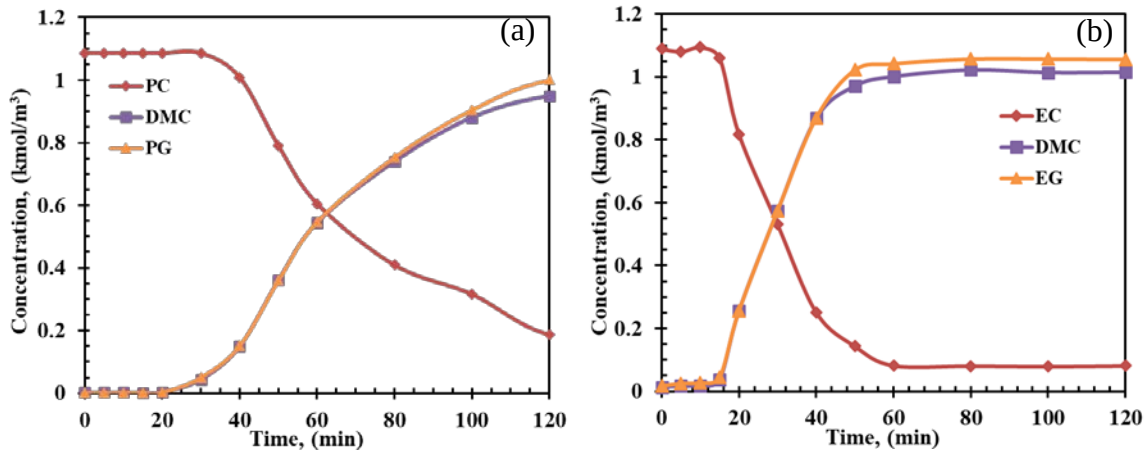

Figure 2-3 Concentration-time profiles for transesterification of PC (a) and EC (b) with methanol. Reaction conditions: PC or EC: 1.07 kmol/ m^3; Methanol: 21.4 kmol/ m^3; CaO: 1.07 kg/ m^3; T = 20 °C; 0.69 MPa N_2

2.3.2 Pretreatment Studies

2.3.2.1 Induction Period

In a few experiments, fresh CaO, PC pretreated CaO and methanol pretreated CaO were tested for transesterification of PC under identical conditions to those in Figure 2-3. The temporal PC and DMC concentration profiles are shown in Figure 2-4. Interestingly, it was found that DMC formation started after an induction period of approximately 20 min when fresh CaO catalyst (square symbols in Figure 2-4) was used with simultaneous addition of reactants initially. The reaction reached maximum PC conversion within approximately 150 min. When the reaction was carried out with PC pretreated CaO, the induction period was approximately 50 min (rhombus symbols in Figure 2-4) and the TOF value decreased from 11.8 to 6.7 h^{-1} (see Figure 2-5, TOF is calculated including the induction period). In sharp contrast, when methanol pretreated CaO was used, the catalyst activity increased significantly from 11.8 to 947.0 h^{-1} (see Figure 2-5). The DMC formation rate was substantially higher than the first two cases with no induction period (triangle symbols in Figure 2-4). For all the three cases, the maximum conversion for PC is around 86%, with approximately 85% DMC yield (with DMC selectivity ~98.2%). In previous studies, a significant increase in the activity of methanol pretreated CaO was also reported for transesterification of vegetable oil with methanol.[51-52, 105] However, for transesterification of PC to DMC, this is the first time that such pretreatment effects are reported. The sharp difference in DMC formation rate between fresh CaO and methanol pretreated CaO suggests that CaO and methanol might interact to form a substantially more active catalytic species compared to the other cases. Conversely, for the PC pretreated CaO case, PC is likely to be strongly adsorbed on CaO inhibiting the formation of the catalytically active species required to initiate the reaction.

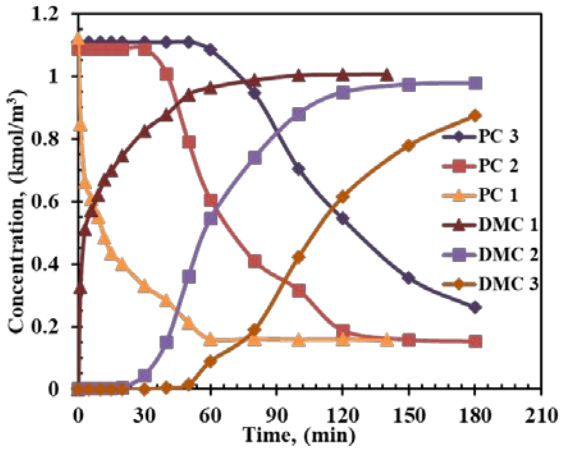

Figure 2-4 PC and DMC concentration-time profiles for transesterification of PC and methanol on CaO catalysts.

2.3.2.2 Influence of Pretreatment Time

The influence of pretreatment time on DMC formation rate is shown for methanol pretreated and PC pretreated CaO catalysts in Figure 2-5. Even when the methanol pretreatment time was only 10 min, a significant increase of activity was observed (increase from11.8 to 148 h^{-1}, Figure 2-5), suggesting rapid formation of catalytically active species on catalyst surface. When the methanol pretreatment time increased from 10 min to 30 min, further enhancement in activity (from 148 to 947 h^{-1}) was observed without change in DMC selectivity. Further activity increase (from 947 to 2210 h^{-1}) was observed when the methanol pretreatment time increased from 30 to 60 min. For PC pretreated CaO catalysts (Figure 2-5), progressively longer induction periods were observed, when the pretreatment time was extended from 10 min to 60 min, the catalyst activity decreased only marginally (from 7.2 to 6.6 h^{-1}).

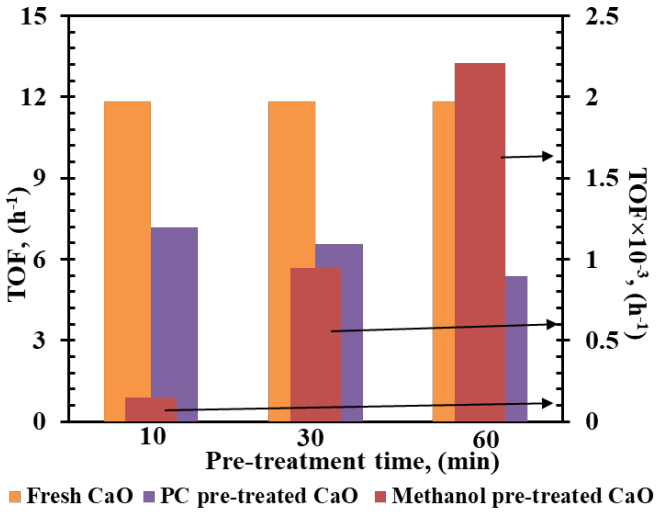

Figure 2-5 TOF values for non-pretreated catalysts and pretreated catalysts

2.3.2.3 Influence of PC Concentration

Three different initial PC concentrations 1.07 kmol/m^3, 2.14 kmol/m^3 and 3.24 kmol/m^3 were studied with methanol pretreated CaO catalyst. During these reactions, methanol was in excess. The PC concentration effect on the reaction is compared in Figure 2-6. It is clear that the initial reaction rate increased with increasing PC concentration. When PC concentration was increased from 1.07 kmol/m^3 to 3.24 kmol/m^3, the conversion of PC decreased from 86% to around 60%.

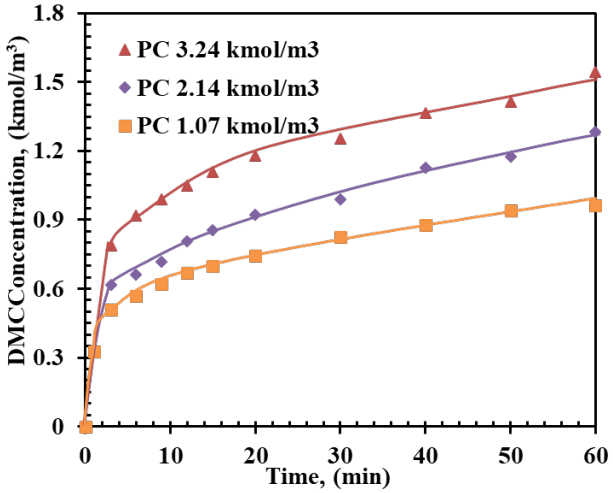

Figure 2-6 PC concentration effect. Reaction conditions: PC: 1.07-3.24 kmol/m^3, Methanol: 21.4-18.0 kmol/m^3, CaO: 1.07 kg/m^3; T = 20 °C; 0.69 MPa N_2

2.3.2.4 Pretreatment Effect for Other Cyclic Carbonates

The strong pretreatment effect on transesterification of PC and methanol observed on CaO motivated to investigate such effects for other cyclic carbonates. In particular, the transesterification of EC and BC were studied with fresh and pretreated CaO catalysts. It was found that the rate of transesterification of EC [see Figure 2-7 (a)] is much faster than PC. But similar to PC, when fresh CaO was used, an induction period was observed (15 min), after which the reaction ignition occurred and reached maximum conversion values within approximately 60 min. When the EC pretreated CaO was tested, a relatively longer induction time (50 min) was found for DMC formation, causing the TOF to drop from 26.3 to 6.4 h^{-1} [see Figure 2-7 (a)]. Methanol pretreated CaO displays extremely high catalytic activity (approximately 3,200 h^{-1}) reaching 92% EC conversion immediately after the EC was added. A similar pretreatment effect was also observed with BC [see Figure 2-7 (b)], although with lower activity [see Figure 2-7 (c)] and conversion (76%). Based on the reaction profiles and activity comparison in Figure 2-4, Figure 2-5 and Figure 2-7, it is clear that the reactivity of cyclic carbonates follows the order of EC > PC ≈ BC, and the maximum conversion also exhibits the order of EC > PC > BC. This difference in activity may be

due to steric hindrance associated with the bulky methyl and ethyl groups in PC and BC, as compared with the symmetrical EC.[36, 38]

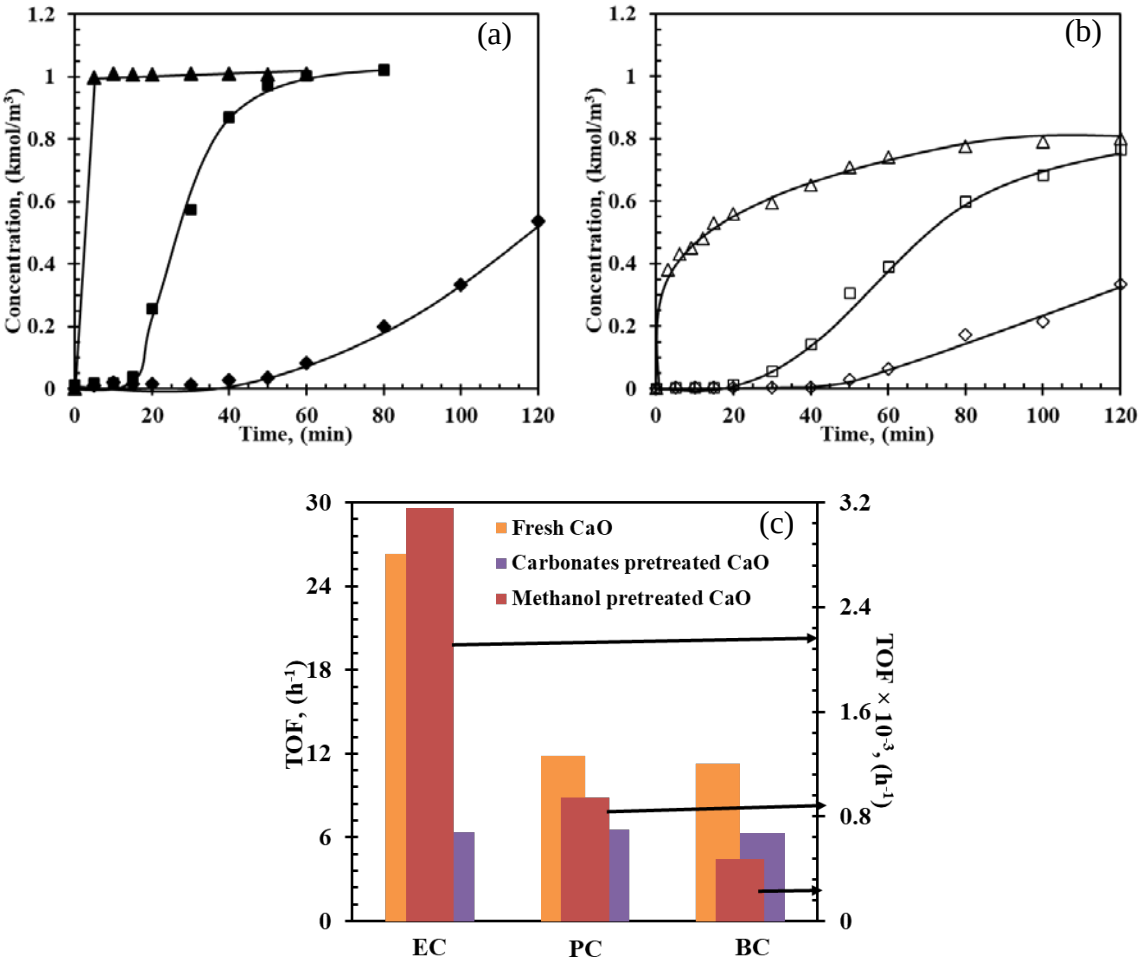

Figure 2-7 Pretreatment effects on temporal DMC concentration profiles during transesterification of EC and BC with methanol on CaO catalysts. Reaction conditions: EC/BC: 1.07 kmol/m^3, Methanol: 21.4 kmol/m^3, CaO: 1.07 kg/m^3; T = 20 °C; 0.69 MPa N_2

2.3.2.5 Reversibility of Pretreatment Effect

Experiments were also carried out to check the reversibility of pretreatment effects to further understand the methanol acceleration effect and PC inhibition effect, respectively. The catalyst pretreated with methanol for 30 min was centrifuged, separated from methanol and further treated with PC for another 30 min. After this, fresh methanol and internal standard mesitylene

were added and the reaction was carried out until maximum PC conversion was reached. The catalyst pretreated with PC for 30 min was centrifuged, separated from PC and further treated with methanol for another 30 min. Fresh PC and internal standard (mesitylene) were then added and the reaction was carried out until maximum PC conversion was attained.

As shown in Figure 2-8 (a), when the methanol pretreated CaO was treated with PC before experiments, no induction period was apparent, similar to the case of PC pretreated $Ca(OCH_3)_2$ (Figure 2-9). However, rate inhibition in rate was observed. This result suggests that the changes caused by methanol pretreatment are irreversible. In contrast, as shown in Figure 2-8 (b), when PC pretreated CaO was further treated with methanol, there was no induction period for the reaction, suggesting that PC pretreated CaO was reactivated by methanol to form catalytically active species. The activity after the first 30 min is similar to fresh CaO, suggesting that PC pretreatment is reversible. This reversibility of PC-pretreated CaO suggests that inhibition with PC is likely to be due to strong adsorption of PC on CaO.

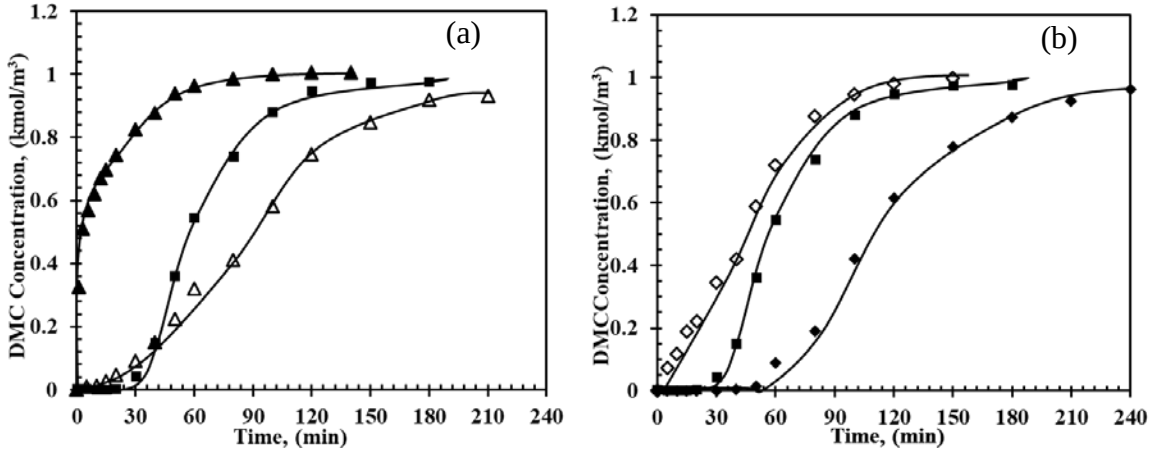

Figure 2-8 Catalyst pretreatment effects on DMC concentration profiles. (–▲–: Methanol pretreated CaO, –■–: Fresh CaO, –△–: PC treatment of methanol pretreated CaO, –◆–: PC pretreated $Ca(OCH_3)_2$, –□–: Fresh CaO, –◇–: Methanol treatment of PC pretreated CaO. Reaction conditions: PC: 1.07 kmol/m^3, Methanol: 21.4 kmol/ m^3, CaO: 1.07 kg/ m^3; T = 20 °C; 0.69 MPa N_2

2.3.3 Comparison of CaO with $Ca(OCH_3)_2$

To further understand the pretreatment effect, additional control experiments were conducted with two different precursors. The reaction of CaO with methanol to form $Ca(OCH_3)_2$ is known from previous work.[51-52, 105] In order to clarify whether $Ca(OCH_3)_2$ is the active species or not, fresh $Ca(OCH_3)_2$ and pretreated $Ca(OCH_3)_2$ were compared with the performance of CaO catalysts (see Figure 2-9 (a) and (b)). Unlike fresh CaO, $Ca(OCH_3)_2$ (hollow squares) exhibits even faster reaction rate with reduced induction time, with a much higher TOF (21.5 h^{-1}). Furthermore, the methanol pretreated $Ca(OCH_3)_2$ (hollow triangles in Figure 2-9) and methanol pretreated CaO (solid triangles) have nearly the same activity (947 h^{-1}) with no induction time, confirming that $Ca(OCH_3)_2$ and CaO both form similar types of species after methanol treatment. For the PC pretreated $Ca(OCH_3)_2$ (hollow rhombus symbols), even though a similar inhibition effect to that of PC pretreated CaO (solid rhombus symbols) was observed, a higher catalyst activity was observed (13.5 h^{-1}).

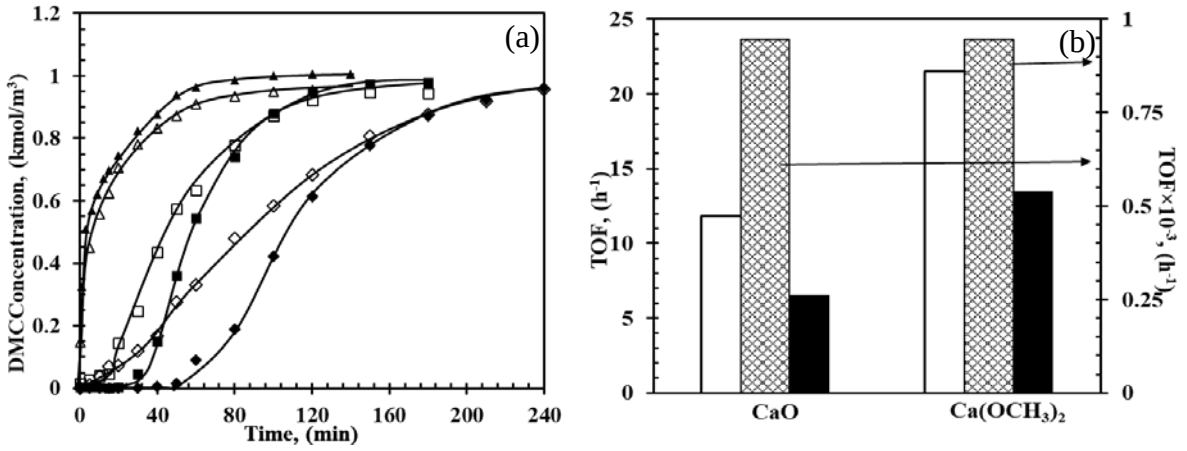

Figure 2-9 Comparison of fresh and pretreated CaO with $Ca(OCH_3)_2$

2.3.4 Catalyst Characterization

2.3.4.1 SEM Analysis

Micrographs of fresh and pre-treated CaO are shown in Figure 2-10. Specifically, Figure 2-10 (a) shows that the surface of fresh CaO is porous and flat. After PC pretreatment, the surface of catalyst becomes fluffy [see Figure 2-10 (b)], indicating interaction between PC and CaO. However, well developed layered and platelet structure was observed on the surface of catalyst after methanol pretreatment [see Figure 2-10 (c)]. The obvious change on the surface of catalysts clearly shows interaction between PC and methanol with CaO.

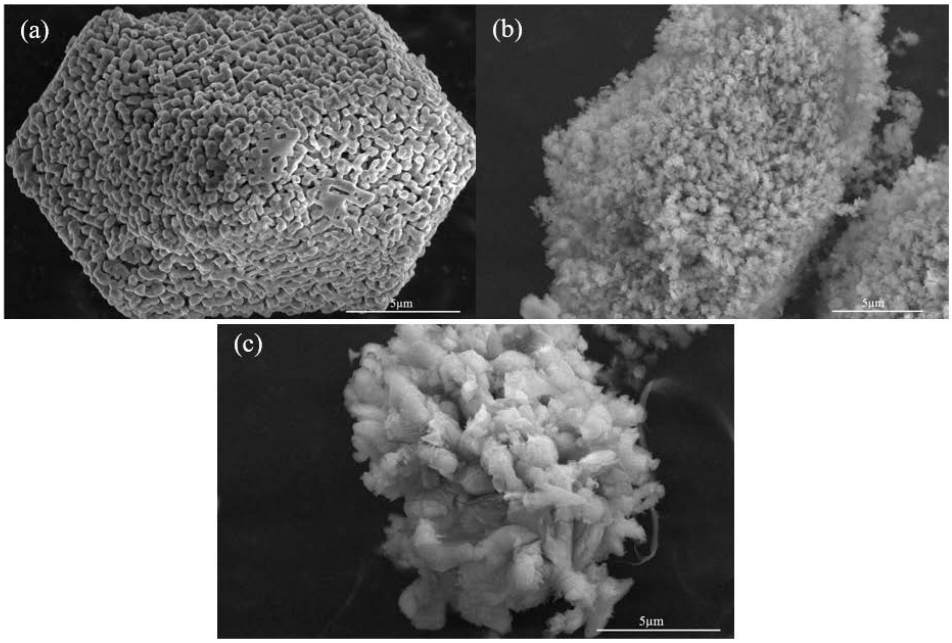

Figure 2-10 SEM images of fresh and pretreated CaO. (a). Fresh CaO, (b). PC pretreated CaO, (c). Methanol pretreated CaO

2.3.4.2 CO_2-TPD

The basicity analysis of fresh CaO and pretreated CaO using CO_2-TPD are shown in Figure 2-11. For the fresh CaO [Figure 2-11 (a)], four different basic sites were observed at 380 °C, 426 °C, 703 °C and 768 °C separately[45, 50]. Obviously, after PC pretreatment [Figure 2-11 (b)], the

weak basic sites of the catalyst at 380 °C and 426 °C shifted to a stronger basic site at 443 °C, while both the two strong basic sites at 703 °C and 768 °C decreased significantly. However, after methanol pretreatment [Figure 2-11 (c)], the weak basic sites at 380 °C disappeared, while the basic sites at 426 °C and 768 °C increased significantly. The experimental results in Figure 2-4 and Figure 2-5 clearly demonstrate that PC pretreated CaO has the lowest activity, while the methanol pretreated CaO has the highest activity. Therefore, it is reasonable to conclude that a strong correlation exists between strong basic sites and catalytic activity.

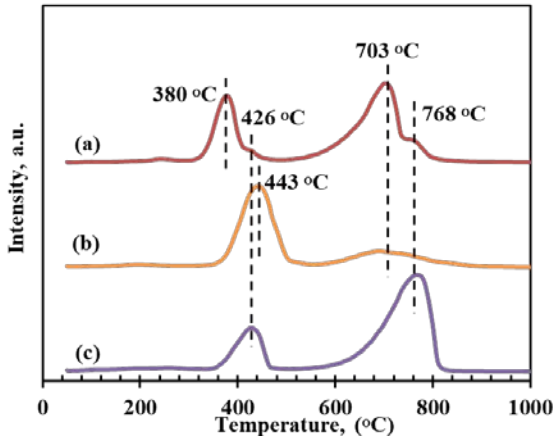

Figure 2-11 CO_2-TPD of fresh and pretreated CaO. (a). Fresh CaO, (b). PC pretreated CaO, (c). Methanol pretreated CaO

2.3.4.3 XRD Analysis

XRD patterns of the fresh CaO and the pretreated CaO are shown in Figure 2-12. It is observed that both fresh CaO and methanol pretreated CaO catalyst samples show intensive peaks at 18.1°, 28.7° and 34.1°, which correspond to the structure of $Ca(OH)_2$, indicating the presence of small amounts of $Ca(OH)_2$ in both of the samples.[106-107] Additionally, three clear peaks are detected at around 32.3°, 37.4° and 53.9°, which correspond to the [111], [200] and [220] planes respectively of the cubic structure of CaO (JCDPS No. 77-2376).[108-109] A characteristic peak of $Ca(OCH_3)_2$ (at around 10.8°) was detected for methanol pretreated CaO,[106] the relative

intensity of which increases with increasing pretreatment time. Especially when CaO was treated for 24 h, the characteristic peaks for CaO or $Ca(OH)_2$ diminished significantly. Furthermore, the shape of the XRD spectra of CaO is similar to that of fresh $Ca(OCH_3)_2$, suggesting most of CaO has been converted into $Ca(OCH_3)_2$ after pretreatment for 24 h. Therefore, when CaO is used as a catalyst for the transesterification reaction of PC with methanol, the actual active species is possibly $Ca(OCH_3)_2$.

2.3.4.4 FT-IR Spectrum

Figure 2-13 shows FTIR spectra of CaO catalysts and $Ca(OCH_3)_2$ catalysts. For all the catalyst samples, the characteristic absorption peaks at the wavenumbers around 3620 cm^{-1} are assigned to stretching and bending vibration peaks of O–H groups from H_2O absorbed on the surface of catalysts or the –OH stretching vibration of primary alcohol in catalysts.[109-110] The bands at 1800 cm^{-1} are related to asymmetric stretching of O–C–O bonds.[111] The absorption peaks at 1500 cm^{-1}, 1070 cm^{-1} and 880 cm^{-1} represent–C–H alkene bending, primary alcohol C–O stretching and the C–O bond related to carbonation of CaO, respectively. For methanol pretreated CaO, bands around 2800-3000 cm^{-1} appeared, which correspond to stretching of CH_3– in $Ca(OCH_3)_2$[112], (see Figure 2-13 (c)). The presence of the bands at 2800-3000 cm^{-1} indicates the formation of $Ca(OCH_3)_2$ during the methanol pretreatment which are not observed for CaO.

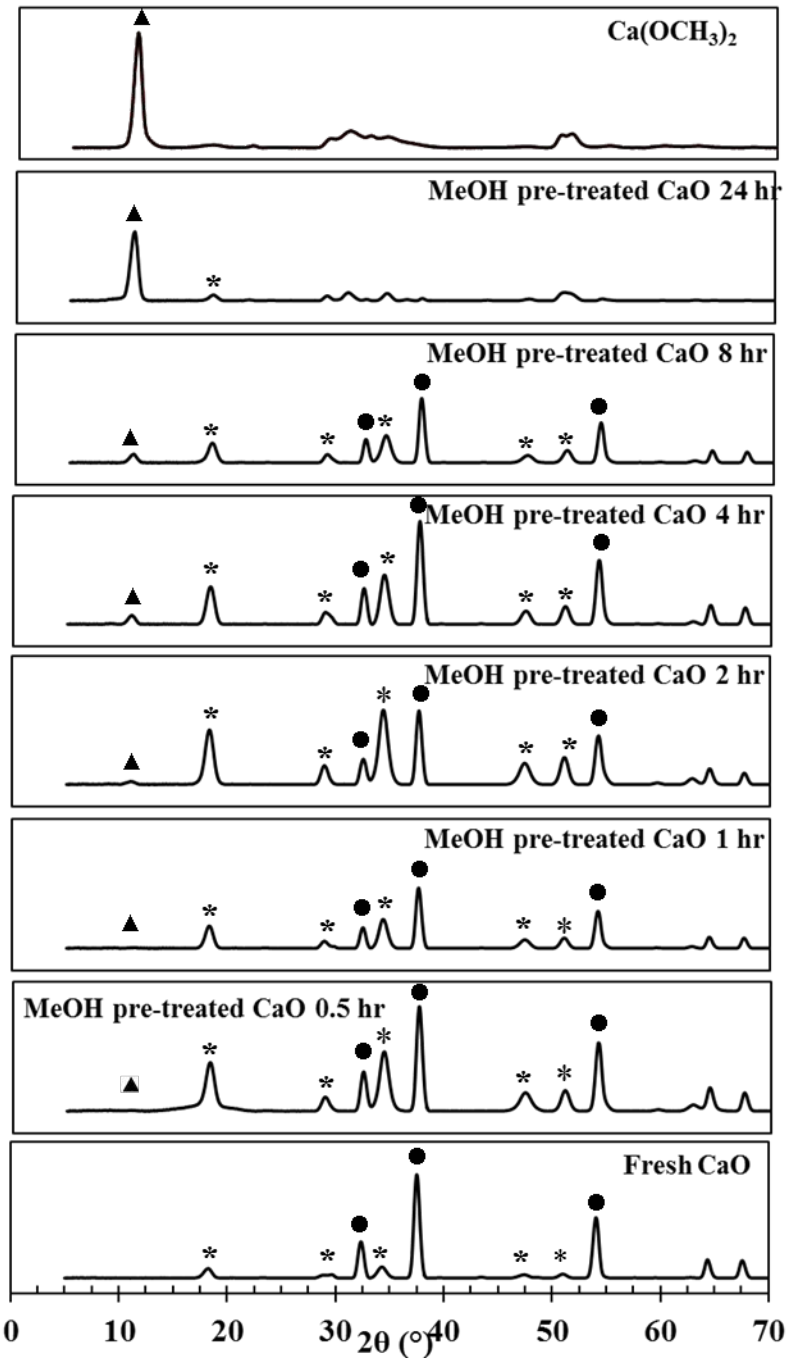

Figure 2-12 XRD Patterns of fresh CaO, methanol pretreated CaO and fresh $Ca(OCH_3)_2$ (* $Ca(OH)_2$, ▲ $Ca(OCH_3)_2$, ● CaO)

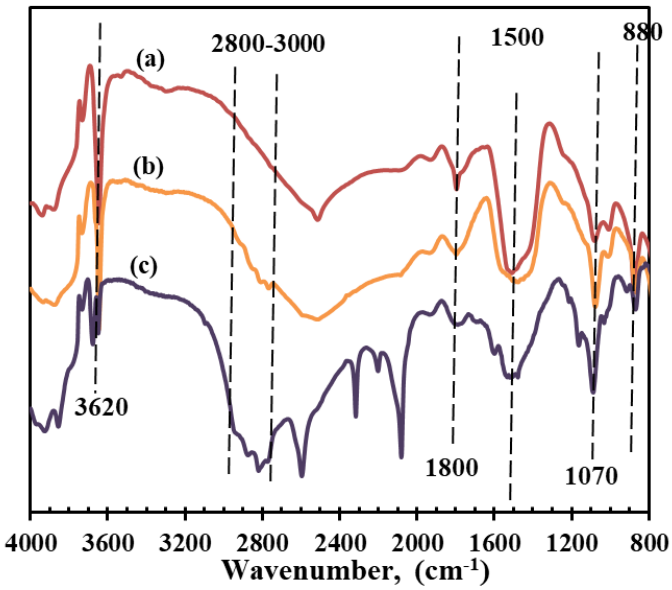

Figure 2-13 FT-IR Spectra of (a) Fresh CaO, (b) Methanol pretreated CaO, and (c) Fresh $Ca(OCH_3)_2$

2.3.4.5 XANES Spectra

It is well known that variation in the XANES region at Ca K edge is sensitive to the local structural environment.[113-114] XANES spectra for fresh CaO, $Ca(OCH_3)_2$, methanol pretreated CaO and PC pretreated CaO were therefore collected to provide insights into the chemical state of Ca species in the catalyst samples. As shown in Figure 2-14, XANES spectra show that the fresh CaO sample (solid line in Figure 2-14) exhibits a pre-edge peak at E=4043 eV (1s to 3d transition) for Ca element, which is reported to be related to the Ca coordination number and local symmetry of Ca environment, while the intensity of this peak is related to p-d mixing.[115-118] The main resonance peak appears at E = 4050 eV (1 s to 3 p transition). In addition, there exist two additional distinctive peaks at around E = 4058 eV (possibly due to transition to unoccupied states from 5s states) and E=4062 eV after the white line, which are strongly related to coordination conditions.[115] Different from the CaO sample, $Ca(OCH_3)_2$ (dash line in Figure 2-14) exhibits a weak and slightly shifted pre-edge peak at around E=4044 eV and one post-edge peak at E=4060 eV. For methanol pretreated CaO catalyst, the catalyst exhibits a weak pre-edge peak at E=4044 eV as observed from

$Ca(OCH_3)_2$ sample. This observation further suggests that the methanol pretreated catalyst is not CaO like and that Ca^{2+} species interact strongly with CH_3OH during catalyst pretreatment, the key step for the activation of CaO catalyst for transesterification reactions.

Compared with the observation in Figure 2-14, we find that the XANES spectra of PC pretreated CaO catalyst (dot dash line in Figure 2-14) showed almost identical pattern as that from Figure 2-14, which suggests that the surface of the CaO catalyst is still dominant by CaO species. The somewhat suppressed Ca K-edge spectrum of the PC pretreated CaO is likely a result of the strong adsorption of CaO with PC and the self-absorption associated with the fluorescence measurement. Overall, in conjunction with the experimental results from reversibility experiments, it can be concluded that the interaction between CaO and PC involves strong physical adsorption.

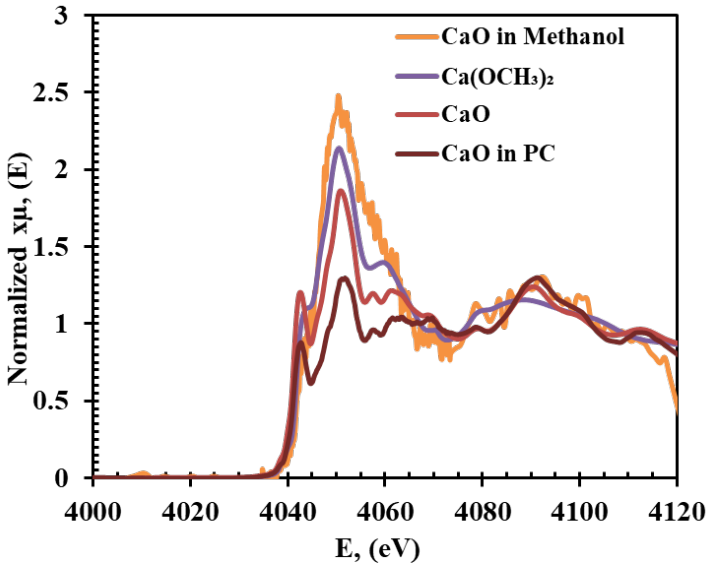

Figure 2-14 XANES spectra of fresh CaO and pretreated CaO

2.3.4.6 ^{13}C-NMR Analysis

Solid state ^{13}C-NMR spectra were obtained for fresh, pretreated $Ca(OCH_3)_2$ and pretreated CaO (Figure 2-15). For fresh $Ca(OCH_3)_2$, methanol pretreated $Ca(OCH_3)_2$ and methanol pretreated CaO, two different carbons were detected at ~52 ppm and ~50 ppm, which can be assigned to

carbon from $Ca(OCH_3)_2$ and methanol separately.[119-120] This suggests that after methanol pretreatment, $Ca(OCH_3)_2$ was formed, which is consistent with XRD, FTIR and XANES results. In contrast, for the PC pretreated CaO, the carbonyl group is shifted from ~155 ppm (pure PC)[121-122] to~166 ppm, while the other three carbons from $–CH_2O–$, –CH–O– and $CH_3–$ three groups were detected at similar range (Δ shift<5 ppm). This shifting of carbonyl group is possibly due to the coordinative interaction of Ca ion with the C=O group. This spectrum also suggests that $Ca(OCH_3)_2$ was formed after methanol pretreatment, while the interaction between PC and CaO is possibly due to strong adsorption, which is consistent with the conclusion derived from XRD, FTIR and XANES results.

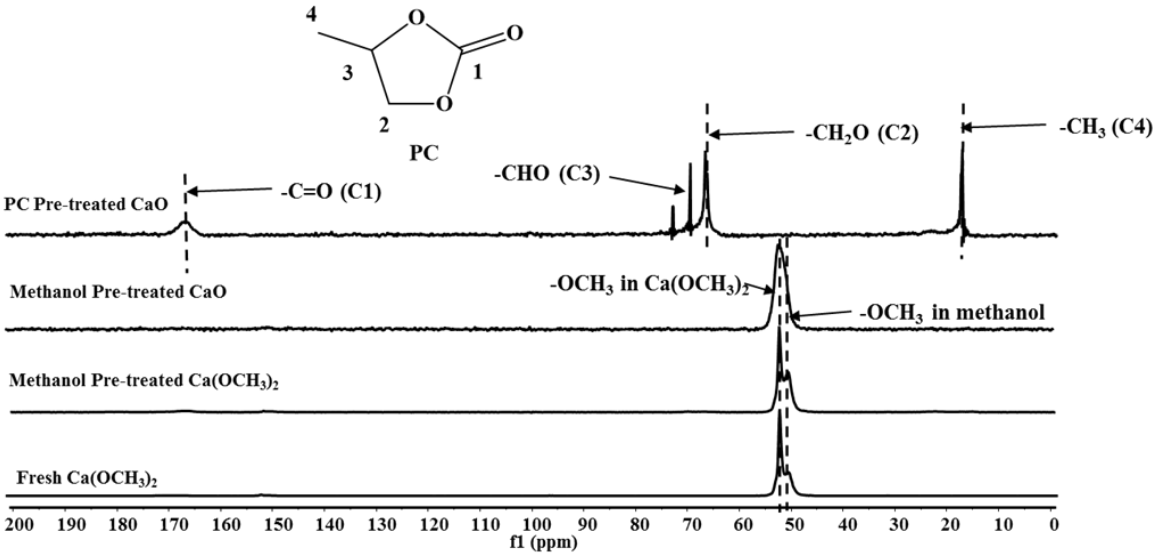

Figure 2-15 ^{13}C-NMR spectra of fresh CaO and pretreated CaO

2.3.5 Proposed Mechanism

Based on the foregoing results from reactions and complementary catalyst characterization studies, a plausible mechanism is proposed (Figure 2-16). We hypothesize that both CH_3O^- and H^+ (from methanol dissociation) are critical for catalytic transesterification reaction. This is because CH_3O^- alone cannot explain the complete catalytic cycle of transesterification, which

clearly requires the involvement of a proton (H^+). Based on our experimental and characterization results, as well as existing literature on transesterification of other substrates, a possible reaction mechanism involving the following steps is proposed:

(1) Methanol and CaO would react and form $Ca(OCH_3)_2$. This agrees well with the observation for other transesterification reactions.[52, 121, 123] As $Ca(OCH_3)_2$ has negligible solubility in methanol[54], it thus acts still mainly as a heterogeneous catalyst.

(2) Once $Ca(OCH_3)_2$ is formed, it would interact with methanol to form a more active species (Figure 2-4)[106], this is why after methanol pretreatment, both CaO and $Ca(OCH_3)_2$ have enhanced activity than untreated ones (Figure 2-9). At the same time, PC adsorbs strongly on the surface of $Ca(OCH_3)_2$, which agrees well with the experimental results with PC pretreated CaO and PC pretreated $Ca(OCH_3)_2$ as catalysts (Figure 2-9).

(3) Then, $Ca(OCH_3)_2$ activated methanol and adsorbed PC from step 2 would react to form two mono-transesterified intermediates[56-62], 1-hydroxypropan-2-yl methyl carbonate and 2-hydroxypropyl methyl carbonate. These two mono transesterified intermediates have been detected by GC and verified by GC-MS (Figure 2-2).

(4) The $Ca(OCH_3)_2$ activated methanol reacts further with the mono products from step 3 to form DMC and propylene glycol.

The proposed mechanism is consistent with our experimental findings and characterization results with fresh CaO, $Ca(OCH_3)_2$ and pretreated CaO, $Ca(OCH_3)_2$. Additionally, this mechanism is consistent with that proposed for the transesterification of vegetable oils over CaO catalyst to produce biodiesel.[52-60]

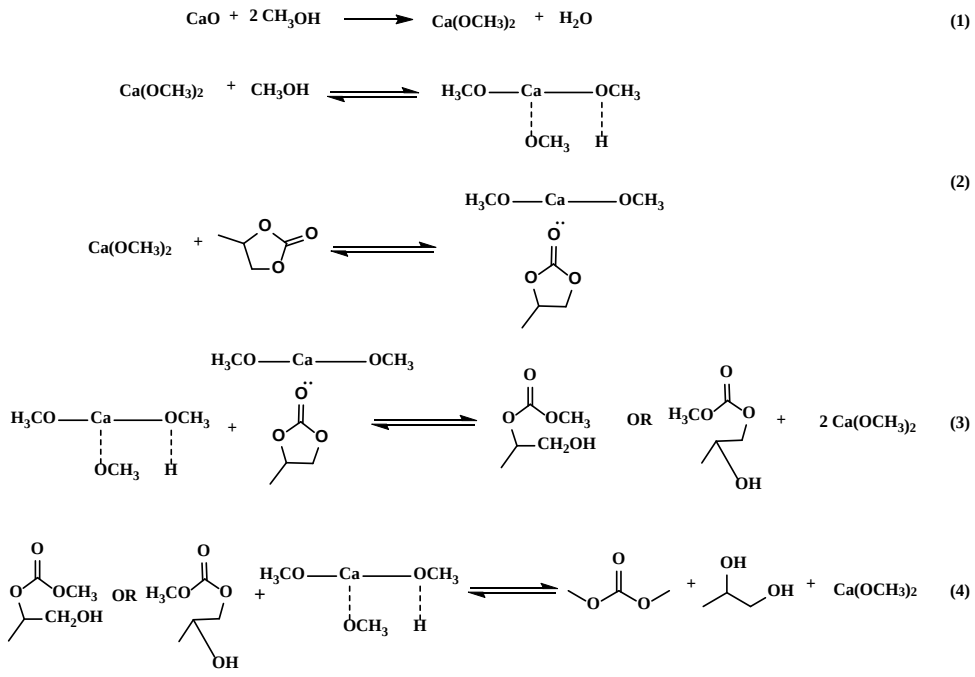

Figure 2-16 Proposed reaction mechanism steps

2.3.6 Recycle Experiments

The reusability is important to assess stability of catalysts, hence, experiments were carried out using methanol pretreated CaO. Methanol pretreated CaO is difficult to handle and easy to lose, hence, the following procedure was applied in recycle studies: 0.15 g of fresh CaO catalyst was mixed with 3.0 mol methanol and stirred at a desired temperature for a fixed period of time. After which, 0.15 mol PC and about 0.025 mol of mesitylene were added and the reaction was initiated by changing the stirring speed to 1100 rmp. After the reaction reached equilibrium, additional PC was added and the first cycle run was started. Once this run reached equilibrium, more PC was added. The results are shown in Figure 2-17. From this graph, it is clear that the first recycle had nearly the same reaction rate as the fresh start. While the second cycle had a much slower reaction rate than the fresh run and first cycle, which is mostly due to the formation of large amount of products.

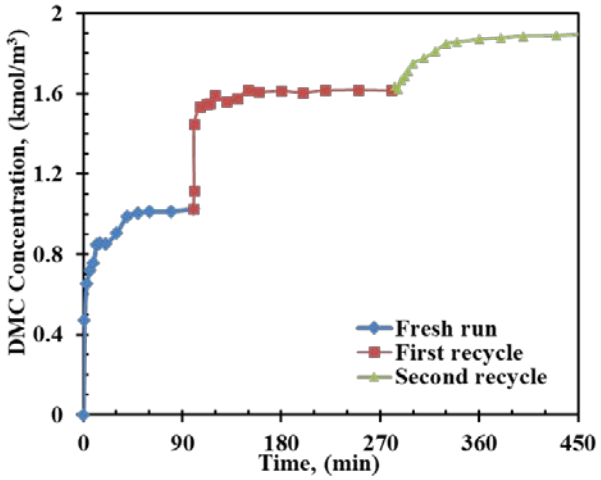

Figure 2-17 Reusability of methanol pre-treated CaO. Reaction conditions: PC: 1.07 kmol/m^3, methanol: 21.4 kmol/m^3, Methanol pre-treated CaO: 1.07 kg/m^3, T=20 °C under 0.69 MPa

Assume the reaction is elementary reaction, therefore, the reaction rate can be expressed as:

$$r = k_f \omega C_1 C_2^2 - k_r \omega C_3 C_4 \quad (5)$$

In which, k_f and k_r are the forward reaction constant and reversible reaction constant, respectively. C_1, C_2, C_3 and C_4 are the concentration for PC, methanol, DMC and PG, respectively. The two constants were fitted using experimental data for different recycles, the results are listed in Table 2-3. From the data in Table 2-3, it is clear that the variety between reaction rate constants of three runs is in 9%, which proves that the catalyst is stable during successive cycles of substrate addition.

Table 2-3 Fitted forward and reversible reaction constants for recycle experiments

	k_f ($m^9 \cdot h^{-1} \cdot kmol^{-3}$)	k_r ($m^6 \cdot h^{-1} \cdot mol^{-2}$)
Fresh Run	2.76	175.5
First Cycle	2.51	155.0
Second Cycle	2.58	163.4

2.4 Testing of Immobilized CaO

Though high activity and selectivity was observed for CaO, significant activity was due to the soluble CaO in methanol. Therefore, immobilization of CaO with other oxides or on various

supports have also been tested. The results of immobilization of CaO with other oxides are summarized in Table 2-4, while the results of CaO on various supports are in Table 2-5.

Table 2-4 Results of immobilization of CaO with other oxides

	Mg-Ca	Zn-Ca	Ba-Ca	Fe-Ca	Co-Ca	Ce-Ca	Ce-Ca Core shell
T(°C)	70	70	70	70	70	70	70
Methanol/PC Ratio	20	20	20	20	20	20	20
PC conversion (%)	7.2	63.9	79.8	4.7	73.7	66.8	71.0
DMC selectivity (%)	100	85.4	78.2	100	77.9	80.5	81.9
Ca leaching (%)	16.1	6.8	11.5	8.6	77.2	17.0	36.4
Metal leaching (%)	0.8	1.2	3.5	1.5	4.7	5.4	4.9

From the reaction results of the mixed oxides, it is clear that most of the CaO mixed oxides have high activity for PC transesterification reaction at mild reaction conditions with different DMC selectivity. However, from ICP analysis, it is found that severe Ca leaching as well as other metal leaching occurs during the reaction. The metal leaching from the mixed oxides is most probably the origin of the high catalyst activity. Similarly, as shown in Table 2-5, significant Ca leaching was also detected in supported CaO catalysts (concentration-time profiles are summarized in Appendix IV, which shows similar reaction trend as that of pure CaO). Based on these results, it is concluded that the total immobilization of CaO is difficult, therefore, other true heterogeneous catalysts systems need to be developed.

Table 2-5 Results of immobilization of CaO on other supports

	CaO/Al_2O_3	CaO/NaY	CaO/13X	CaO/C	CaO/TiO_2	CaO/SiO_2
T(°C)	50	50	50	50	50	50
Methanol/PC Ratio	20	20	20	20	20	20
PC conversion (%)	68.6	74.1	18.7	25.2	11.5	81.7
DMC selectivity (%)	100	85.5	100	100	100	91.9
Ca leaching (%)	16.1	6.8	11.5	8.6	77.2	17.0
Metal leaching (%)	0.8	1.2	3.5	1.5	4.7	5.4

2.5 Conclusion

Intriguing effects of pretreatment of CaO catalyst for transesterification of cyclic carbonates with methanol are reported herein for the first time. Methanol pretreated CaO catalyst significantly enhances catalytic activity and reduces induction time. In contrast, pretreatment with PC inhibits the transesterification rate. Further, while the inhibition effects of PC pretreatment are reversible with methanol treatment, the acceleration effects observed with methanol pretreatment are not reversible with PC treatment. Based on experimental results and detailed catalyst characterization, a reaction mechanism that involves the formation of $Ca(OCH_3)_2$ on the catalyst surface is a key step in the heterogeneous transesterification of cyclic carbonates has been proposed for transesterification of cyclic carbonates to DMC.

Additionally, immobilized CaO, with other mixed oxides or on different supports were evaluated. However, significant Ca leaching was detected, which leads to high activity.

Chapter 3 Kinetic Study of Homogenous and Heterogeneous CaO-Catalyzed Transesterification of Cyclic Carbonates with Methanol

3.1 Introduction

As discussed in Chapter 2, among metal oxides, CaO has been identified as a very promising basic heterogeneous catalyst for transesterification reactions in both biodiesel field[105-49] and DMC synthesis under mild reaction conditions[25]. However, studies have shown that, significant leaching of CaO in the reaction medium occurs posing difficulties in catalyst-product separation.[44, 105] The determination of the contribution of homogenous and heterogeneous CaO catalysts, as well as understanding the mechanism for both two steps is important, to provide guidance for rational design of catalysts in future. It is clearly noted from the review in Chapter 1 that there is lack of complete understanding on the plausible reaction mechanism involved in the conversion of cyclic carbonates and intrinsic kinetic data.

Therefore, in this part of the work, a kinetic study of homogeneous and heterogeneous catalytic reactions is presented. While, homogeneous catalytic reaction kinetics has been studied in the range of CaO concentration within solubility limits, kinetics of heterogeneous catalyzed reaction is determined from overall reaction by accounting for the homogeneous reaction. Additionally, plausible reaction mechanism is proposed though microkinetic modeling.

3.2 Experimental Section

3.2.1 Chemicals

All chemicals used in this work except butylene carbonate (BC) were purchased from Sigma Aldrich. Methanol (99.8%), PC (99.7%), DMC (extra dry, 98+%), propylene glycol (PG, 99.5+%), EC (99%), ethylene glycol (EG, 99.8%), 1,2-butanediol (BG, 98+%), mesitylene (98%) and CaO (powder). BC (98+%) was obtained from Tokyo Chemical Industry Co., LTD.

3.2.2 Experimental Setup and Procedure

The experiments for kinetic study were carried out in a stirred slurry reactor of 300 mL capacity (Parr reactor), with provisions for temperature control, sampling of liquids and variable agitation speed (The same setup as that in Figure 2-1). Typically, predetermined amount of fresh CaO catalyst was mixed with specific amount of methanol and stirred at room temperature for a fixed period of time as a step of catalyst pre-treatment.[44] Then, a known amount of PC and mesitylene (internal standard) were added and the reactor was heated to the target temperature at low stirring speed (< 50 rpm). When the desired temperature was reached, the reaction was initiated by switching the stirrer to 1000 rpm. The progress of reaction was followed by analysis of liquid samples withdrawn at different time intervals through a sampling filter. For convenience of liquid sampling, the reactor was maintained at 100 psi of N_2, while the samples were analyzed by Agilent GC.

3.2.3 Product Analysis

All samples were analyzed for concentrations of reactants (PC and methanol) and products (DMC and PG) using an Agilent Gas Chromatograph (GC-7890A). The GC is equipped with ZB-WAX capillary column and a flame-ionization detector (FID). The conditions used for the GC are the same as that described in section 2.2.3.1. Mesitylene was used as internal standard in the GC analysis.

3.3 Results and Discussion

3.3.1 Kinetic Study

Though CaO is usually reported as a heterogeneous catalyst for transesterification reaction[36, 44, 49, 51], significant homogeneous reaction was observed in the range of reaction conditions studied[44, 105]. In most of the previous works, the contribution of the homogeneous

reaction was neglected in analysis of the reaction rate data and no detailed kinetic studies are reported with CaO as a catalyst. However, quantifying for the homogenous and heterogeneous reactions separately is important to understand the intrinsic kinetics of the reaction.

Granados and coworkers investigated the solubility of CaO in methanol by measuring the conductivity of liquid.[105] In our work, the solubility data from Granados' report was used to determine the range of CaO concentration for homogeneous catalytic reactions. From Granados and coworkers' work, the solubility of CaO in methanol is 0.04 mg/ml at 60 °C and 0.17 mg/ml °C at 25 °C[105]. Assuming that the standard enthalpy of solution, ΔH_{sol}^{0} is approximately independent of temperature, the following Van't Hoff equation was used to extrapolate the data for different temperatures:

$$\log S_2 = \log S_1 - \frac{\Delta H_{sol}^{0}}{2.303R} \cdot \left(\frac{1}{T_2} - \frac{1}{T_1}\right) \quad (1)$$

Where, S_1, S_2 are solubility (mg/ml) at different temperatures T_1 and T_2, respectively.

The extrapolated solubility data and values of heat of solution are presented in Figure 3-1. From the slope of the plot, the heat solution can be derived, $\Delta H_{sol}^{0} = -34.1$ kJ/mol.

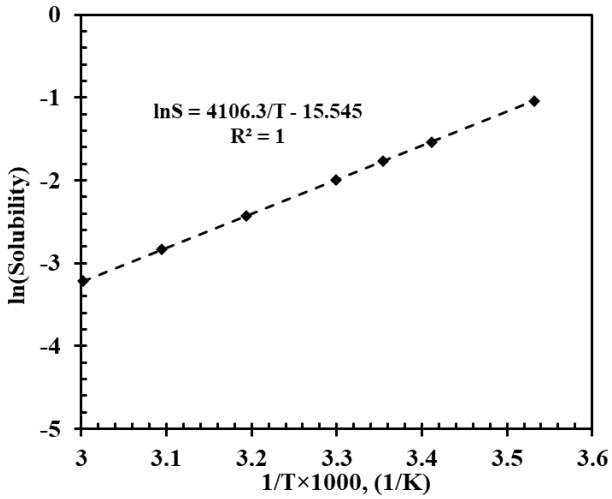

Figure 3-1 Solubility data of CaO in methanol

As a first step in kinetic study, the concentration-time profiles for the homogeneous reaction (at the solubility point of CaO in methanol) are determined and compared with the overall heterogeneous reaction as shown in Figure 3-2. It is clear that, though heterogeneous reaction is predominant, the homogenous reaction cannot be neglected. For both the homogeneous and the overall heterogeneous reactions, the selectivity of DMC is around 92%-98% under the reaction conditions.

Based on these observations, it was thought important to consider both homogeneous and heterogeneous reactions in analysis of the kinetics. Experiments were carried out to investigate the homogeneous and heterogeneous catalytic reactions separately as described below.

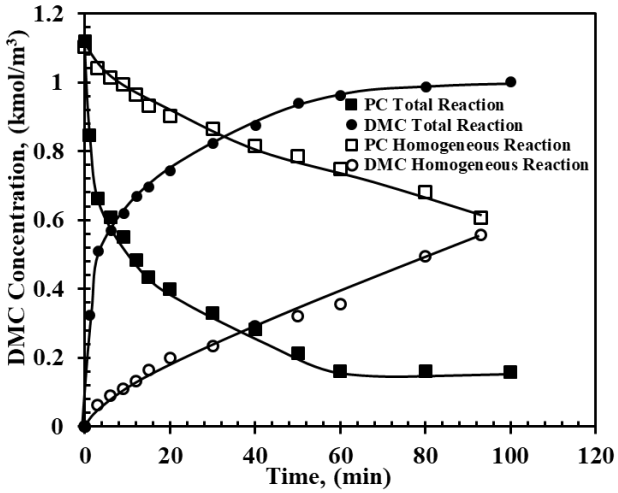

Figure 3-2 Comparison of homogeneous and over heterogeneous reaction. Reaction condition: PC: 1.1 kmol/m^3, MeOH: 21.4 kmol/m^3, CaO: 1.07 kg/m^3/0.235 kg/m^3, T= 20 ^oC, 0.69 MPa N_2

3.3.1.1 Experiments

For kinetic study, experiments were carried out in a batch reactor with CaO as the catalyst in both homogenous and heterogeneous regions. A total of 18 experiments were carried out at different substrate concentrations and temperatures. The operating ranges of parameters are: catalyst concentration: 1.4-6.63×10^{-3} kmol/m^3, PC concentration: 1.1-4.2 kmol/m^3, methanol concentration: 15.4-21.4 kmol/m^3 and temperature: 20-60 °C.

3.3.1.2 Mass Transfer Limitation

Before determination of intrinsic kinetic parameters using the experimental data, it is important to ensure the mass-transfer steps are not rate limiting for the observed experimental data. For homogenous reaction, such analysis is not necessary. To confirm that external and intraparticle mass transfer step are not rate limiting steps for the heterogeneous reaction, all the observed initial reaction rates of consumption of PC were compared with the maximum rates of liquid-solid mass transfer and intraparticle diffusion under the same conditions (sample calculations are given in Appendix II) using the criteria described by Ramachandran and Chaudhari[124]. Such ratios for liquid-solid mass transfer and intraparticle diffusion analysis were calculated to be 3.0×10^{-4}-6.2×10^{-3} and 2.7×10^{-6}-1.2×10^{-5} respectively, clearly indicating negligible mass transfer limitations.

3.3.1.3 Batch Reaction and Model Discrimination Criteria

In order to evaluate the kinetic parameters, a batch reactor model was used assuming that slurry reactor was perfectly mixed with no mass transfer limitations. Since negligible intermediate products [2-hydroxypropyl methyl carbonate (2-HMC) and 1-hydroxypropan-2-yl methyl carbonate (1-HP-2-MC)] were detected during the reaction, continuity equations for PC, methanol, DMC and PG only were considered based on power law rate equations as:

$$\frac{dC_{PC}}{dt} = -r; \tag{2}$$

$$\frac{dC_{Methanol}}{dt} = -2r; \tag{3}$$

$$\frac{dC_{DMC}}{dt} = r; \tag{4}$$

$$\frac{dC_{PG}}{dt} = r; \tag{5}$$

Where, $r = \omega_0(k_1[PC]^a[MeOH]^b - k_2[DMC]^c[PG]^d)$ (6)

Where, r is the specific reaction rate kmol/(m^3·h), ω_0 is the catalyst concentration, in kmol/m^3, [PC], [MeOH], [DMC], and [PG] are the concentrations of PC, methanol, DMC and PG respectively in kmol/m^3, and k_1 and k_2 are forward and reversible reaction constants, a, b, c, and d are the reaction orders for PC, methanol, DMC and PC respectively.

The initial conditions are:

at t=0, [PC]= $[PC]_0$, [MeOH]= $[MeOH]_0$, $[DMC]_0$= [PG] $_0$=0, where$[PC]_0$, $[MeOH]_0$, $[DMC]_0$ and $[PG]_0$ represent the initial concentrations of PC, methanol, DMC and PG respectively. For solving these ODEs, it is necessary to provide guess values of rate constants. From the concentration-time profiles, reasonable guess values (Example of calculation for guess values of rate constants are shown in Appendix I) for rate constants can be calculated using selected initial rate data. Using the guess values of rate constants, these equations were solved using Athena Visual Studio software for the reaction conditions of the experiments. For model discrimination and optimization of kinetic parameters, the following criteria were used:

(1) All reaction/adsorption constants must be positive.

(2) Uncertainty (95% confidence level) of rates should not increase or decrease significantly with changing reaction conditions.

(3) Reaction rate constants must follow thermodynamic consistency (Arrhenius relationship).

(4) The error in experimental and predicted functions should not indicate trends. (such as in Log Plot and Normal Probability Plot)

(5) Has minimum S_j.

$$S_j = \sum_1^N (C_{j,E} - C_{j,P})^2 \quad (7)$$

Where S_j is the sum of squares of (concentration) residuals of component j and $C_{j,E}$ and $C_{j,P}$ are the experimental (E) and predicted (P) concentrations, respectively.

3.3.1.4 Homogenous Reaction Kinetics

The experiments for homogeneous catalytic reactions were carried out under conditions such that CaO was completely soluble. To ensure homogeneous conditions, after each experiment, the final solution was checked to confirm the absence of solid particles.

3.3.1.4.1 Concentration-Time Profiles

The main products of transesterification were found to be DMC and PG, with negligible formation intermediates (2-HMC and 1-HP-2-MC). The markers in Figure 3-3 represent the temporal concentration-time profiles for transesterification of PC with methanol at different temperatures using homogeneous CaO as a catalyst. At 20 °C [Figure 3-3 (a)], the PC concentration decreases from 4.2 kmol/m^3 to 3.2 kmol/m^3 in 5 h. At the same time, the concentration of products, DMC and PG increased from 0 to around 0.8 kmol/m^3 gradually with time with stoichiometric consistency. At 30 °C [Figure 3-3 (b)], 40 °C [Figure 3-3 (c)] and 50 °C [Figure 3-3 (d)], the reaction rate increased with increase in temperature as expected. The concentration of DMC and PG are also consistent with stoichiometry.

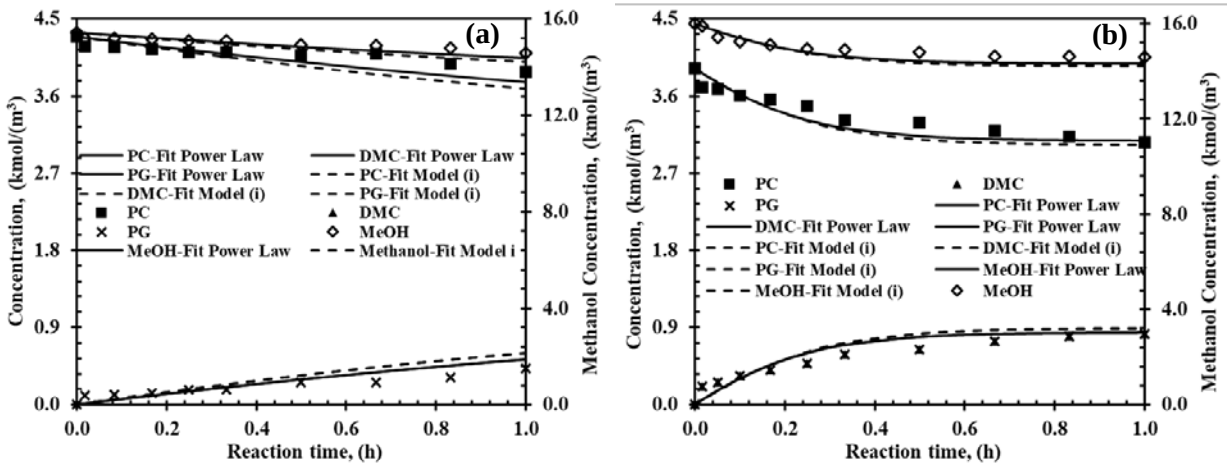

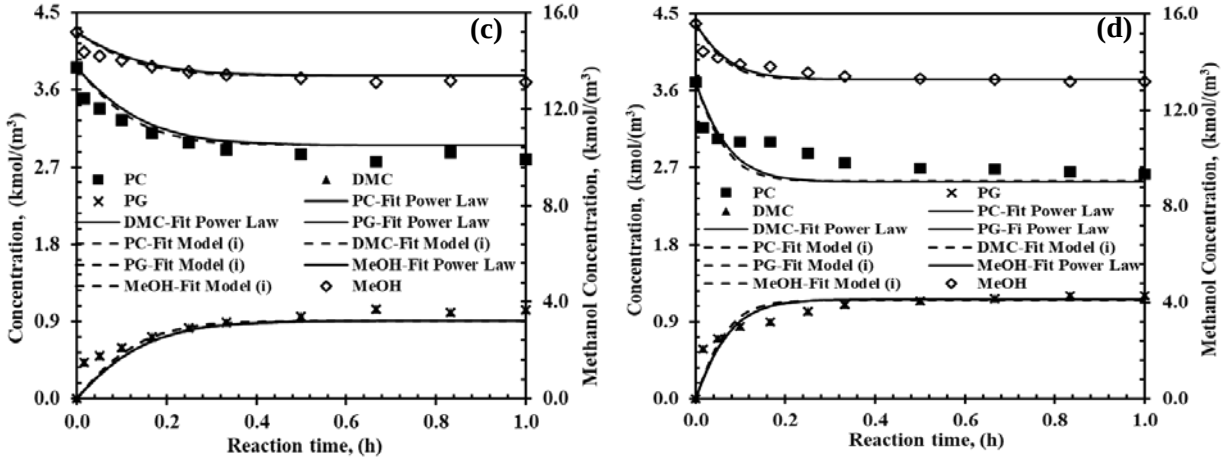

Figure 3-3 Temporal concentration-time profiles for homogenous transesterification of PC with methanol on methanol pretreated CaO at: (a) 20 °C, (b) 30 °C, (c) 40 °C, (d) 50 °C. Experimental conditions: PC: 3.7-4.3 kmol/m^3, MeOH: 15.2-16.0 kmol/ m^3, catalyst: 0.0014 kmol/m^3. Points: experimental values, lines: estimated values by power law model, dash lines: estimated values by Model (i) for homogeneous reaction

3.3.1.4.2 Initial Rate Data

Catalyst loading effect: The effect of catalyst loading on the initial reaction rate was studied, the results of which are shown in Figure 3-4. The markers represent the experimental results, and the solid line represents the linear regression from the experimental results. These results show that the initial reaction rate is linearly dependent on the catalyst concentration.

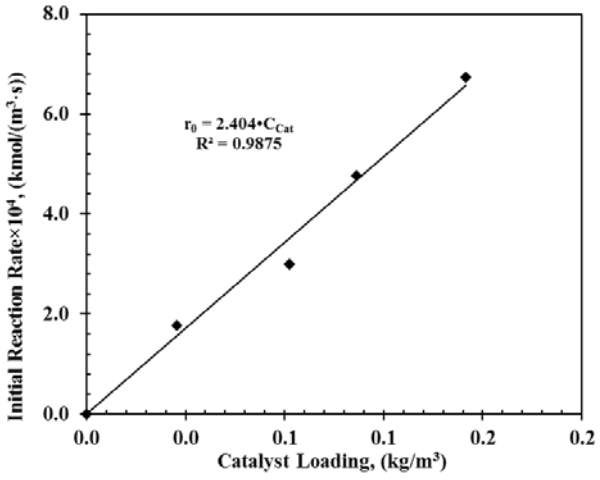

Figure 3-4 Dependence of initial reaction rate on homogeneous catalyst loading. Reaction conditions: methanol, 22.1 kmol/m^3; PC: 1.1 kmol/m^3; catalyst, 0.0014 -0.0032 kmol/m^3; T=20 °C; 0.69 MPa N_2

Effect of Initial Substrate Concentration: The effect of initial PC concentration on initial homogeneous reaction rate was studied, the results are summarized in Figure 3-5. As PC concentration increased from 1.1 to 4.3 kmol/m^3, the initial reaction rate increased from 0.28 to 20.66 kmol/(m^3·h) at 20 °C showing a linear dependence, suggesting first-order dependence of initial reaction rate on PC initial concentration. Similar trends were also observed at 30 °C, 40 °C and 50 °C with higher reaction rates.

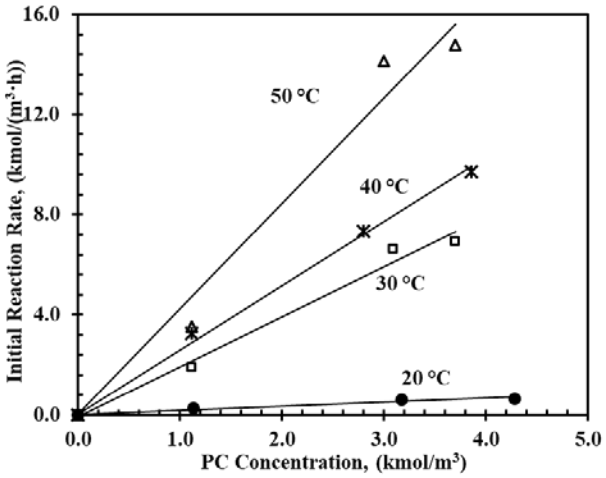

Figure 3-5 Effects of PC initial concentration and on initial reaction rates. Reaction conditions: methanol, 15.2-22.1 kmol/m^3; PC: 1.1-4.3 kmol/m^3; catalyst, 0.0014 kmol/m^3; T=20-50 °C; 0.69 MPa N_2

3.3.1.4.3 Power Law Rate Equation

To fit the experimental data, the mass balance equations of each component in a batch reactor as shown in Equations (2)-(6) are used. The homogeneous reaction rate r_{Homo} can be expressed with the concentration of different components and catalyst as follows:

$$r_{Homo}(T) = \omega^{\alpha}\left(k_{1,homo}(T)[PC]^{m}[MeOH]^{n} - k_{2,homo}(T)[DMC]^{p}[PG]^{q}\right) \quad (8)$$

where, $k_{1,homo}$ and $k_{2,homo}$ are temperature dependent forward and reversible reaction rate constants, ω is the homogeneous catalyst concentration, and α is used to quantify the effect of catalyst concentration on the reaction rate. The parameter α can be determined by varying catalyst loading.

The results from Figure 3-4 show that the initial reaction rate is linearly dependent on the catalyst concentration, indicating α in Equation (8) is unity.

Several different reaction orders have been tested, and compared with the experimental data. By meeting the optimization criteria in section 3.3.1.3, it is found that m=1, n=2, p=1, q=1 was found to be the best fit reaction orders. Under the reaction conditions used, a strong temperature dependence of forward and reversible reaction rate constants was observed. The Arrhenius equation was used to describe the temperature dependency of the two constants, as shown in Figure 3-6. Additionally, the equation of linear regression of Arrhenius equation is also shown in Figure 3-6.

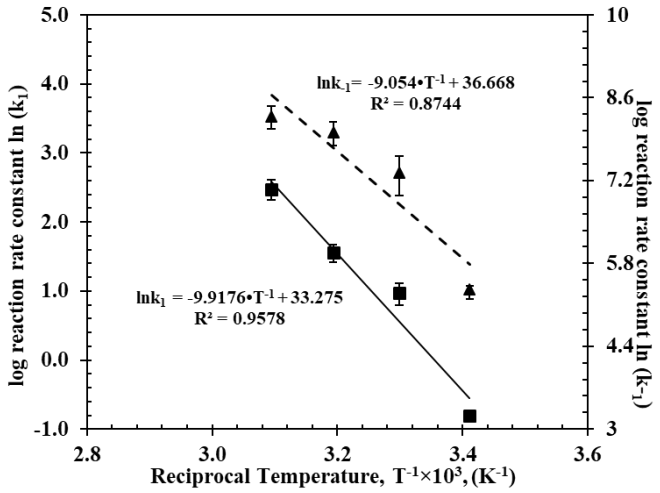

Figure 3-6 Arrhenius plot for the forward and reverse reaction rate constants for homogeneous reaction

The equation can be used to extrapolate reaction rate constants for other temperatures. The estimated reaction rate constants and activation energy can be obtained from the intercept and the slope of the dash line respectively. The estimated results are summarized in Table 3-1. An activation energy of 82.4±8.4 kJ/mol was observed for the transesterification of PC with MeOH using CaO in the homogeneous region as a catalyst. The comparison of simulated data (line in Figure 3-3) with experimental data (markers in Figure 3-3) is shown in Figure 3-3. The match

between the simulated results and experimental data indicates that the power rate equation fits the data well and can be used to describe to homogeneous CaO-catalyzed transesterification between PC and methanol.

Table 3-1 Estimated values for pre-exponential factor and activation energy for homogenous and heterogeneous reaction

	20 °C	30 °C	40 °C	50 °C	Activation energy (kJ/mol)
$k_{1,homo}$, ($m^9 \cdot h^{-1} \cdot kmol^{-3}$)	0.45±0.028	2.63±0.42	4.73±0.68	11.9±0.72	82.45±8.40
$k_{2,homo} \times 10^{-3}$, ($m^6 \cdot h^{-1} \cdot kmol^{-2}$)	0.21±0.014	1.53±0.49	3.02±0.58	3.96±0.76	75.27±16.94
$k_{1,heter} \times 10^{-2}$, ($m^{6.75} \cdot h^{-1} \cdot kmol^{-2.25}$)	0.18±0.07	—	1.22±0.42	1.34±0.57	56.80±22.32
$k_{2,heter} \times 10^{-4}$, ($h^{-1}$)	0.39±0.22	—	3.18±1.10	2.67±1.16	55.50±30.12

[a] Rate constants with 95% confidence level
[b] Unit of E_a: kJ/mol, error calculation is Appendix I.

3.3.1.5 Heterogeneous Reaction Kinetics

3.3.1.5.1 Concentration-Time Profiles

Similar to the procedure followed for homogenous reactions, the overall heterogeneous reactions were also carried out under different reaction conditions. Compared with the homogenous reaction, the contribution of heterogeneous catalytic reaction was observed to be significantly higher. The concentration-time profiles of each component for the overall reaction are presented in Figure 3-7. At 20 °C [Figure 3-7 (a)], the PC concentration decreased from 3.1 kmol/m^3 to 2.0 kmol/m^3 in just 15 min. At the same time, the concentration of products, DMC and PG increased from 0 to around 0.85 kmol/m^3 gradually with time with stoichiometric consistency. At 40 °C [Figure 3-7 (b)], and 50 °C [Figure 3-7 (c)], the reaction rate increased as expected. The concentration of DMC and PG are also consistent with stoichiometry.

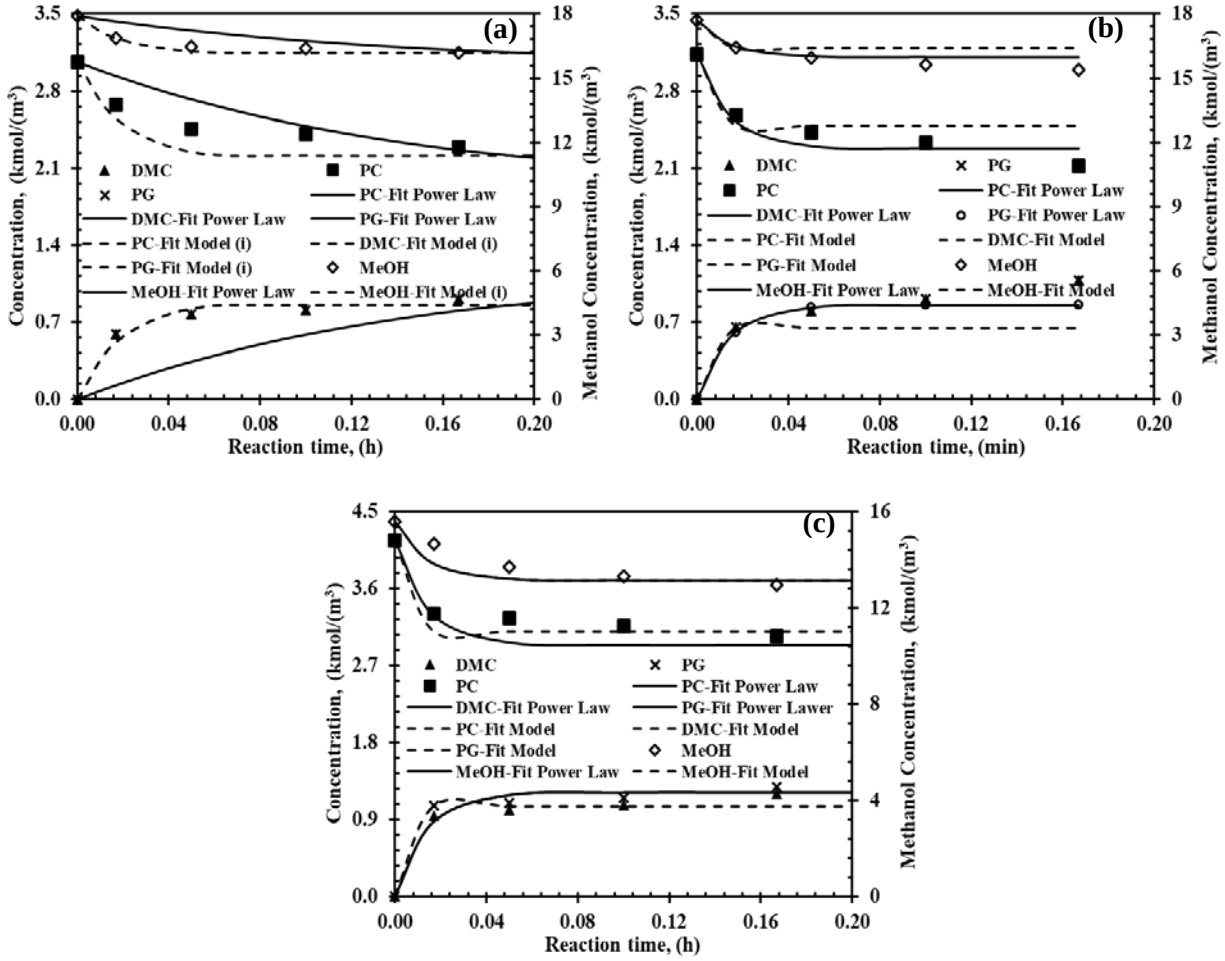

Figure 3-7 Temporal concentration-time profiles for overall transesterification of PC with methanol on methanol pretreated CaO at: (a) 20 °C, (b) 40 °C, (c) 50 °C. Experimental conditions: PC: 3.1/4.2 kmol/m^3, MeOH: 18.0/16.0 kmol/ m^3, catalyst: 0.0066 kg/m^3. Points: experimental values, lines: estimated value by power law model, dash lines: estimated value by model (i) for heterogeneous reaction

3.3.1.5.2 Initial Rate Data

Catalyst loading effect: The effect of CaO loading under conditions of significant heterogeneous reaction on the initial reaction rate was also studied, the results of which are shown in Figure 3-8. As homogeneous CaO is existing in the system when heterogeneous CaO system studied, the heterogeneous catalyst loading amount would be derived through the total amount minus the solubility of CaO. Additionally, the initial reaction rate of heterogeneous catalyst is obtained by the overall reaction rate minus the initial reaction rate of homogeneous reaction, determined from

already determined kinetics. Similar to that for homogeneous reaction, the initial reaction rate is also found to be linearly dependence on the catalyst amount.

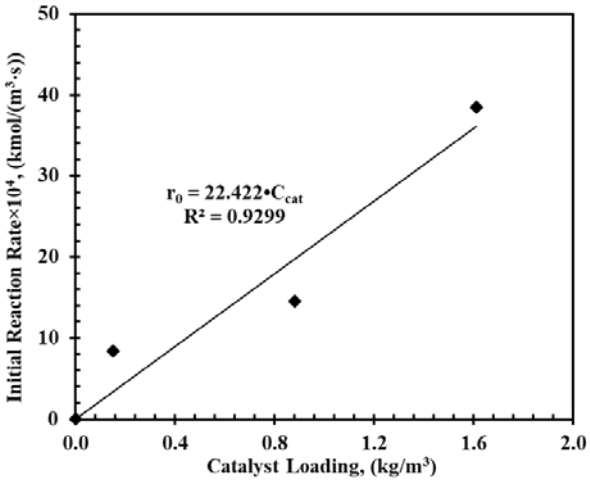

Figure 3-8 Dependence of initial reaction rate on catalyst loading for heterogeneous reaction

3.3.1.5.3 Power Law Fitting

As the reaction rate with a heterogeneous catalyst cannot be determined directly, the reaction rate of heterogeneous reaction was calculated using the observed overall reaction rate for homogeneous and heterogeneous reactions using the following equation.

$$r_T(T) = r_{Heter}(T) + r_{Homo}(T) \quad (9)$$

The overall reaction rate for a combined homogeneous/heterogeneous reaction can be expressed as follows:

$$r_T(T) = \omega\left(k_{1,homo}(T)[PC]MeOH^2 - k_{2,homo}(T)[DMC][PG]\right) + \omega_2^{\beta}\left(k_{1,heter}(T)[PC]^e[MeOH]^f - k_{2,heter}(T)[DMC]^s[PG]^t\right) \quad (10)$$

In which, $k_{1,heter}$ and $k_{2,heter}$ are temperature dependent forward and reversible reaction constants for heterogeneous reaction, ω is the concentration of CaO in methanol in homogeneous phase, ω_2 is the heterogeneous catalyst concentration, while *e*, f, s, t are the heterogeneous reaction orders, and β is used to quantify the effect of heterogeneous catalyst on the reaction rate. As shown in the plot

of Figure 3-8, the initial reaction rate of heterogeneous reaction is also linearly dependent on the heterogeneous catalyst loading. Therefore, unit 1 was determined for the parameter β.

For the parameter estimation of the heterogeneous reaction, the same optimization as described in section 3.3.1.3 was used. It is found that reaction orders of e=0.35, f=1.9, s=t=0 can best fit with the experimental data. Similarly, forward reaction rate and reversible reaction rate constant for heterogeneous reaction also show a strong dependence on temperature. The regression results are summarized in Figure 3-9 and Table 3-1. The activation energy of the heterogeneous CaO-catalyzed transesterification of PC with methanol is found to be 56.8±30.1 kJ/mol. The activation energy of the heterogeneous reaction is much less than that of the homogeneous reaction, indicating heterogeneous reaction may follow a different pathway compared to that of the homogeneous reaction.

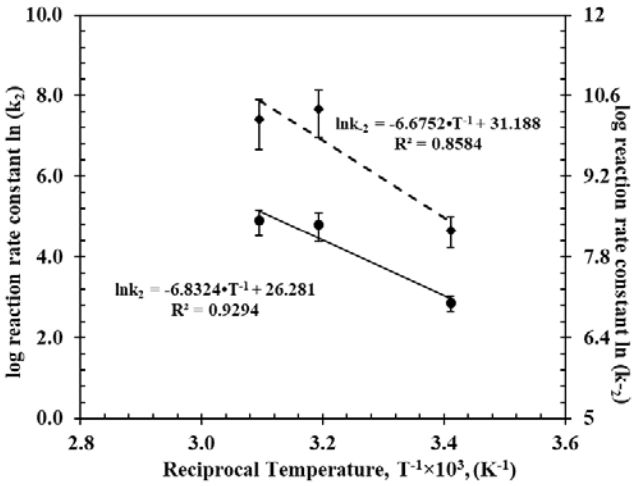

Figure 3-9 Arrhenius plot for the forward and reverse reaction rate constants for heterogeneous reaction

A comparison between the experimental and the simulated results is shown in Figure 3-10. In total, 836 data points from 18 experiments are included in this plot, demonstrating the high accuracy of the power law kinetic model. Therefore, the power law model is able to predict the

temporal concentration-time profiles of an experiment in the range of experimental parameters studied.

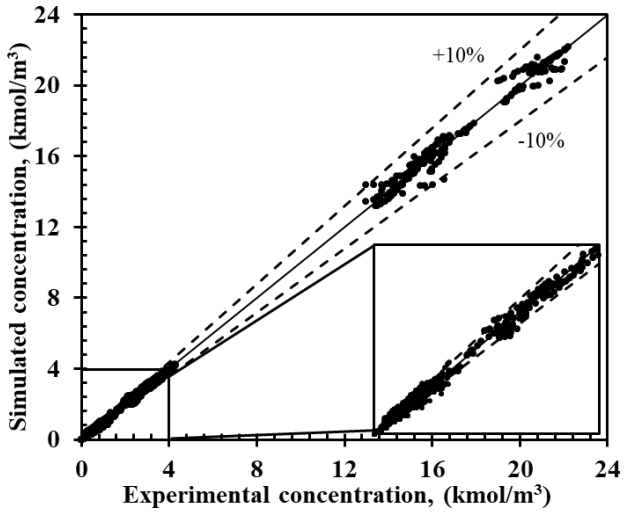

Figure 3-10 Parity plot of the simulated and experimental concentrations for the four chemicals.

3.3.1.6 Chemical equilibrium

Transesterification of PC is an equilibrium limited reaction, the equilibrium constant for which has been reported in previous work. William et al.[125] determined the molar-based chemical equilibrium to be 0.25 at standard conditions, while Holtbruegge et al.[53] found the equilibrium constant to be 0.302 at standard condition (20 °C and 1 atm). In this work also, the equilibrium constants were determined assuming ideal liquid phase behavior. The equilibrium constants were calculated according to the following equation:

$$K_x = \frac{x_{DMC}^{eq} x_{PG}^{eq}}{x_{PC}^{eq} x_{Methanol}^{eq\ 2}} \tag{11}$$

K_x depends on temperature, thus, the integral form of Van't Hoff equation can be used to correlate the temperature dependence of the equilibrium constant, as shown in equation (12).

$$\ln K_x(T) = \frac{\Delta h_R^0 - \Delta g_R^0}{RT^0} - \frac{\Delta h_R^0}{R}\left(\frac{1}{T}\right) \tag{12}$$

A linear regression of the experimentally determined equilibrium constants according to the Van't Hoff equation can be used to describe the temperature dependency of the chemical equilibrium constant. Furthermore, the standard enthalpy Δh_R^0 and standard Gibbs energy Δg_R^0 of reaction can be obtained from the slope and intercept of the linear regression.

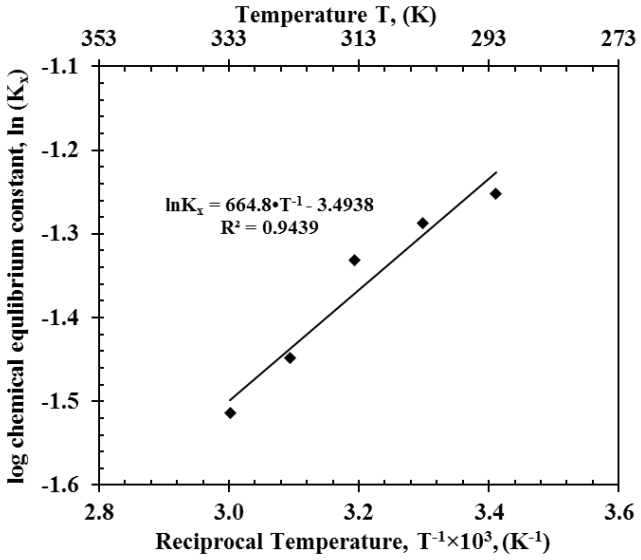

Figure 3-11 Van't Hoff plot for the molar-based chemical equilibrium constant K_x derived from experimental results.

Figure 3-11 displays a plot of chemical equilibrium constant for the transesterification of PC with methanol in the temperature range of 293 K-333 K. The solid line represents the linear regression of the experimental data. Additionally, the derived standard enthalpy and Gibbs energy values are summarized in Table 3-2. The diagram shows a decreasing chemical equilibrium constant with increasing temperature, indicating the formation of DMC and PG is unfavored at high temperatures. Furthermore, the chemical equilibrium constants calculated from the experimental data is in the same range as reported by William et al and Holtbruegge et al (Table 3-2).

Table 3-2 Estimated values for standard enthalpy and Gibbs energy

	Δh_R^0, (kJ/mol)	Δg_R^0, (kJ/mol)	$K_x{}^0$	Theoretical $K_x{}^0$	
This work (EC)	-1.74	1.37	0.576	0.171	This work
This work (PC)	-5.53	3.13	0.282	0.0587	This work
This work (BC)	-7.16	3.67	0.24	0.0862	This work
William et al. (PC)	-8.895	3.426	0.251	—	—
Holtbruegge et al. (PC)	-9.522	2.918	0.308	—	—

Similarly, the same procedure was applied for both EC and BC systems (Van't Hoff plot are presented in Appendix III) to determine equilibrium constants, the results of which are summarized in Table 3-2. From these data, it is clear, that the standard enthalpy of different cyclic carbonates follows the order of EC > PC > BC, indicating least energy is produced for EC system and most energy generated for BC system. The standard Gibbs energy exhibits a reverse order of EC < PC < BC, showing that the transesterification of PC and BC are less favorable than transesterification of EC. Furthermore, the gap between PC and BC systems is much less than the gap between PC and EC systems. This difference in these two properties is most likely due to steric hindrance associated with the bulky methyl and ethyl groups in PC and BC, as compared with the symmetrical EC[38,36,44]. Additionally, the theoretical reaction constants (Table 3-2) were also calculated using Equation (12) from standard enthalpy and standard entropy (Appendix III) of each component involved in the reaction. Since no reliable experimental data were available for most of the components, data from NIST database and some literature[126-127] were used for calculation of the properties. The unreliable thermodynamic properties are found to contribute to the difference between experimental and theoretical results.

3.3.2 Micro Kinetic Modelling

From the power law modeling results, it is clear that, the reaction order and activation energy for the heterogeneous reaction are different from that of the homogeneous reaction. It is

most probably because of different reaction mechanisms for homogenous CaO-catalyzed and heterogeneous CaO-catalyzed reactions. Further investigations of microkinetic models were carried out to provide a better insight on a possible reaction mechanism.

3.3.2.1 Microkinetic Modeling for Homogeneous Reaction

3.3.2.1.1 Homogeneous Reaction Mechanism

For the homogenous reaction, the dissociation of CaO in methanol involves a series of complex reaction networks.[105] Various ionic species are known to exist in the reaction medium, most predominant being Ca^{2+} and CH_3O^-.[105]. The generally accepted mechanism is described as follows: after CH_3O^- ion is formed as an initial step,[86, 90] nucleophilic attack of methoxy oxygen on carbonyl carbon in PC occurs to form intermediate I;[84-86, 90] then, the reaction between intermediate I and one mole of methanol would form intermediate II;[84-85, 90] next, intermediate II would decompose into DMC and intermediate III;[84-85, 90] Finally, PG and active species CH_3O^- would be formed from intermediate III and another mole of methanol.[85] The reaction mechanism is described in Scheme 3-1, in which intermediate II can also be intermediate formed by CH_3OH attach on carbonyl carbon from the other side.

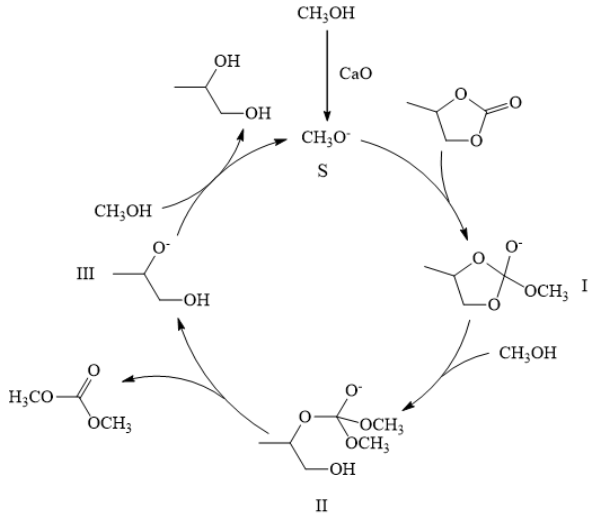

Scheme 3-1 Proposed reaction mechanism for homogeneous CaO-catalyzed transesterification reaction

3.3.2.1.2 Kinetic Modeling

As DMC and PG were formed with stoichiometric consistency from the start of reaction, the formation of DMC and the formation of PG would be considered as a combining step. Based on this assumption, the reaction pathway for formation of DMC and PG can be simplified to three steps [Scheme 3-2 (a)]. Based on the simplified pathway, reaction rate for each step is summarized in Scheme 3-2 (b). Additionally, the material balance for each component is summarized in Table 3-3.

$$S + PC \leftrightarrow I$$
$$I + MeOH \leftrightarrow II$$
$$II + MeOH \leftrightarrow DMC + PG + S$$

(a). Simplified reaction pathway for homogeneous CaO-catalyzed transesterification reaction

$$r_1 = k_1[S][PC] - k_{-1}[I]$$
$$r_2 = k_2[I][MeOH] - k_{-2}[II]$$
$$r_3 = k_3[II][MeOH] - k_{-3}[DMC][PG][S]$$

(b). Rate equation for each step based on simplified reaction pathway for homogeneous reaction

Scheme 3-2 Simplified pathway and reaction rate for homogeneous reaction

Table 3-3 Batch reactor equations for homogeneous reaction

Batch reactor equations for each component		
$\frac{d[PC]}{dt} = -r_1$	$\frac{d[MeOH]}{dt} = -r_2 - r_3$	$\frac{d[DMC]}{dt} = \frac{d[PG]}{dt} = r_3$
$\frac{d[S]}{dt} = -r_1 + r_3$	$\frac{d[I]}{dt} = r_1 - r_2$	$\frac{d[II]}{dt} = r_2 - r_3$

Where, [PC], [MeOH], [DMC] and [PG] represent the same thing as described in section 3.3.1.3, and [S], [I] and [II] represent the concentrations of the three catalyst species in liquid phase, kmol/m^3. During the kinetic modeling, no specific step has been assumed as rate-determining step, allowing the evaluation of rate parameters for the elementary steps involving catalytic intermediates.

The initial conditions are:

At t=0, $[PC]=[PC]_0$, $[MeOH]=[MeOH]_0$, $[S]=[S]_0$, $[DMC]=[PG]=[I]=[II]=0$, where $[PC]_0$, $[MeOH]_0$ and $[S]_0$ represent the initial concentrations of PC, methanol and catalyst precursor, respectively. For solving these ODEs, the same method and optimization procedure was applied as that in power law part.

Following the procedures described above, the optimum values of the rate constants at different temperatures were determined, as shown in Table 3-4. Each rate constant increases with temperature as well as showing consistency with the Arrhenius law (Appendix III). The activation energies for each single step calculated from the rate constants at different temperatures are also summarized in Table 3-4.

Additionally, the predicated and experimental data at different temperatures are compared in Figure 3-3. It is clear that the estimated values (dashed line) from micro-kinetic model fits better with the experimental data (markers), compared to the power law model. Therefore, the following mechanism involving only two intermediate species can be used to represent the homogeneous reaction. After the formation of active species CH_3O^-, PC is activated to form intermediate I, into which methanol is inserted to form intermediate II, which reacts with another methanol molecule to form final products DMC and PG.

Table 3-4 Rate constants and activation energy for homogeneous reaction

Rate Constants	20 °C [a]	30 °C [a]	40 °C [a]	50 °C [a]	E_a [b], (kJ/mol)
$k_1\times10^{-7}$, ($m^3\cdot h^{-1}\cdot kmol^{-1}$)	2.69±0.36	4.41±1.11	6.88±1.66	26.3±5.49	56.9±13.3
$k_{-1}\times10^{-5}$, (h^{-1})	0.86±0.12	3.71±0.97	11.9±3.02	24.3±5.87	88.3±13.8
$k_2\times10^{-4}$, ($m^3\cdot h^{-1}\cdot kmol^{-1}$)	0.69±0.04	2.90±0.44	6.10±1.13	20.7±4.16	86.3±10.6
$k_{-2}\times10^{-6}$, (h^{-1})	3.11±0.19	4.90±0.74	9.42±1.74	15.1±3.03	42.4±10.5
$k_3\times10^{-3}$, ($m^3\cdot h^{-1}\cdot kmol^{-1}$)	0.6±0.04	1.12±0.15	2.51±0.42	3.46±0.58	47.8±8.9
$k_{-3}\times10^{-5}$, ($m^6\cdot h^{-1}\cdot kmol^{-2}$)	2.03±0.27	5.80±1.51	7.01±1.78	19.2±4.62	54.5±13.8

[a] Rate constants with 95% confidence level
[b] Unit of E_a: kJ/mol, error calculation is Appendix III.

3.3.2.2 Microkinetic Modeling for Heterogeneous Reaction

3.3.2.2.1 Heterogeneous Reaction Mechanism

For the heterogeneous CaO catalyzed reaction, surface catalytic reactions need to be considered. The interaction between reactants and solid catalyst is assumed to involve dissociative adsorption and reaction.[128] A detailed mechanism is described in Scheme 3-4. Accordingly, methanol is dissociatively adsorbed on the surface of active catalyst to form intermediate I.[44, 79-82, 84-85] At the same time, PC would form intermediate II with active species through electric interaction;[44, 85] Then intermediate I and intermediate II would form intermediate III (intermediate III can also be the methoxy oxygen attack from the other side of PC) through the nucleophilic attack of methoxy oxygen on carbonyl carbon of PC from dissociatively adsorbed methanol;[44, 84-85] Then, intermediate III would react with another intermediate I to form the final product DMC and PG. [44]

3.3.2.2.2 Kinetic Modeling

For simplification of the modeling process, the reaction pathway above for heterogeneous CaO-catalyzed transesterification was simplified into three steps [Scheme 3-3 (a)]. Based on the simplified pathway, reaction rate for each step is summarized in Scheme 3-3 (b). Additionally, the material balance of each component is also summarized in Table 3-5.

$$S + MeOH \leftrightarrow I$$
$$S + PC \leftrightarrow II$$
$$II + 2I \leftrightarrow DMC + PG + 3S$$

(a). Simplified reaction pathway for heterogeneous CaO-catalyzed transesterification reaction

$$r_1 = k_1[S][MeOH] - k_{-1}[I]$$
$$r_2 = k_2[S][PC] - k_{-2}[II]$$
$$r_3 = k_3[II][I]^2 - k_{-3}[DMC][PG][S]^3$$

(b). Rate equation for each step based on simplified reaction pathway for heterogeneous reaction

Scheme 3-3 Simplified pathway and reaction rate for heterogeneous reaction

Table 3-5 Batch reactor equations for homogeneous reaction

Batch reactor equations for each component		
$\frac{d[PC]}{dt} = -r_2$	$\frac{d[MeOH]}{dt} = -r_1$	$\frac{d[DMC]}{dt} = \frac{d[PG]}{dt} = r_3$
$\frac{d[S]}{dt} = -r_1 - r_2 + 3 * r_3$	$\frac{d[I]}{dt} = r_1 - 2 * r_3$	$\frac{d[II]}{dt} = r_2 - r_3$

For the estimation of rate parameters for heterogeneous reaction, Equation (11) was used. The rate expressions of homogeneous reaction are used to account for homogeneous reaction. The same optimization procedure as that of homogeneous reaction was used. The estimated parameters are shown in Table 3-6. Similarly, the rate constants and activation energy at various temperatures for each step are calculated from Arrhenius Equations. (Appendix III). It is found that the activation energy of step 2 (PC activation step) is much higher than the activation energy of step 1 (methanol activation step) and step 3 (final formation of DMC and PG). Furthermore, the reaction constant is much higher than that of homogenous ones, which is consistent with the experimental results.

Additionally, comparison of predicated data with experimental data at different temperatures is also shown in Figure 3-7. It is clear that the estimated values from molecular kinetic models (dash line) based on reaction mechanisms fit much better with the experimental data (markers) than the power law model (lines). The excellent match between the experimental and predicted results at various reaction conditions indicate that the proposed reaction mechanism for heterogeneous reaction and corresponding kinetic models represents the transesterification reaction between PC and methanol satisfactorily.

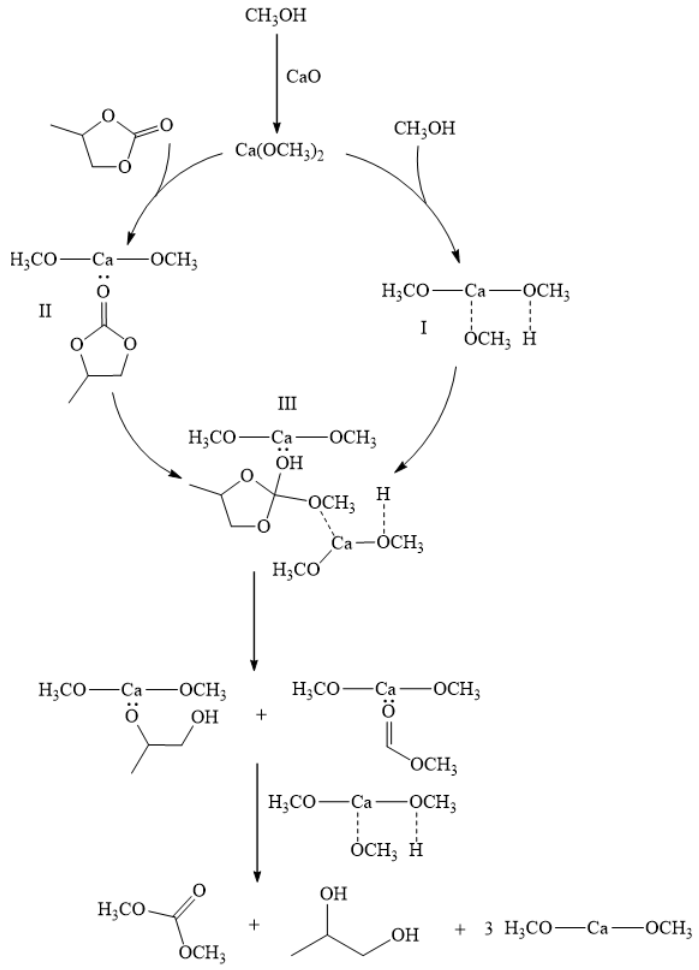

Scheme 3-4 Proposed reaction mechanism for homogeneous CaO-catalyzed transesterification reaction

Table 3-6 Rate constants and activation energy for heterogeneous reaction

Rate Constants	20 °C [a]	40 °C [a]	50 °C [a]	E_a [b]
$k_1\times10^{-6}$, ($m^3\cdot h\cdot kmol^{-1}$)	1.10±0.09	2.86±0.39	5.74±0.41	42.3±7.3
$k_{-1}\times10^{-6}$, (h^{-1})	0.35±0.07	2.45±0.34	2.54±0.18	55.6±11.1
$k_2\times10^{-6}$, ($m^3\cdot h\cdot kmol^{-1}$)	0.21±0.03	2.25±0.62	3.12±0.45	73.7±14.7
$k_{-2}\times10^{-6}$, (h^{-1})	0.89±0.13	2.50±0.69	4.50±0.64	42.0±14.5
$k_3\times10^{-14}$, ($m^6\cdot h^2\cdot kmol^{-2}$)	2.77±1.20	7.40±2.05	9.39±1.35	32.9±22.8
$k_{-3}\times10^{-18}$, ($m^{12}\cdot h^4\cdot kmol^{-4}$)	0.26±0.08	1.48±0.41	1.68±0.24	52.4±16.6

[a] Rate constants with 95% confidence level
[b] Unit of E_a: kJ/mol.

3.4 Conclusion

Transesterification of cyclic carbonates with CaO catalyst involves a reversible catalytic reaction which occurs in both homogeneous and heterogeneous phase due to significant activity of the sparingly soluble CaO in the reaction medium. In this work, kinetic modeling of the homogeneous/heterogeneous catalytic transesterification is reported for the first time. Homogeneous reaction kinetics was studied using the range of limiting CaO solubility in methanol. The intrinsic activation energy for the homogeneous reaction is 82.4 kJ/mol, which is greater than that for the heterogeneous reaction (56.8 kJ/mol). Micro-kinetic models based on reported reaction mechanisms were proposed for both the homogeneous and heterogeneous CaO-catalyzed transesterification. The excellent match between the simulated reaction data and the experimental ones indicate that the proposed mechanisms represent the transesterification reaction reasonably well. Although more rigorous analysis and characterization are needed to provide a strong support for the proposed mechanisms, the present work nevertheless provides valuable insights into the reaction mechanism and intrinsic kinetics on a molecular level.

Chapter 4 Transesterification of Propylene Carbonate with Methanol Using Fe-Mn Double Metal Cyanide Catalyst

4.1 Introduction

The results presented in Chapter 2 and the literature review indicate that, stable immobilization of CaO catalyst is difficult due to leaching of CaO under reaction conditions, hence efforts have been made in developing other heterogeneous catalysts for transesterification of cyclic carbonates. Double metal cyanide is a group of heterogeneous catalysts that has been successfully used in various ring-opening reactions. In this part of work, several double metal cyanide complexes were synthesized and evaluated for their performance as catalysts in transesterification of propylene carbonate with methanol. We report here for the first time that Fe-Mn double metal cyanide catalyst has significantly higher activity for transesterification reaction compared to previously reported metal oxides catalysts and other combinations of double metal cyanides (Fe-Zn[60, 129] or Co-Zn[130]). In this paper, a detailed study on the composition of Fe and Mn and effect of catalyst loading, methanol/PC ratio and temperature is presented on transesterification of different cyclic carbonates. In these experiments, concentration-time profiles were obtained to determine catalyst activity/selectivity behavior. In order to test the catalyst stability, recycle experiments were also performed. Comprehensive catalyst characterization using BET, SEM, TEM, XRD, XPS, TGA, FT-IR and UV-Vis analyses was carried out to understand morphological and surface characteristics and enable correlation of catalytic performance with surface structure.

4.2 Experimental Section

4.2.1 Materials

Methanol (99.9%), PC (99.7%), DMC (extra dry, 98+%), propylene glycol (PG, 99.5+%), EC (99%), ethylene glycol (EG, 99.8%), 1,2-butanediol (BG, 98+%), mesitylene (98%) and

$NiCl_2 \cdot 6H_2O$ were purchased from Sigma-Aldrich. $K_4Fe(CN)_6 \cdot 3H_2O$ (98%) was obtained from Alfa Aesar. $K_3Co(CN)_3$, $MnCl_2 \cdot 4H_2O$ (98.5%), and $ZnCl_2$ were obtained from Acros Organics. BC (98+%) was obtained from Tokyo Chemical Industry Co., LTD. All chemicals were used without further treatment.

4.2.2 Catalyst Preparation

The catalysts used in this work were prepared using the method described in previous work.[78] A typical preparation procedure of double metal cyanide complexes is outlined in Figure 4-1. Accordingly, 0.01 mol of $K_4[Fe(CN)_6] \cdot 3H_2O/K_4Co(CN)_6$ was dissolved in 40 mL distilled water in beaker A. Targeted amounts of $ZnCl_2/MnCl_2/NiCl_2$ were dissolved in 100 mL distilled water and 20 mL of *tert*-butanol mixture in beaker B. 15 g poly (ethylene glycol)-block-poly (propylene glycol)-block-poly (ethylene glycol) ($EO_{20}PO_{70}EO_{20}$; average molecular weight, 5800) was dissolved in a beaker C with 2 mL of distilled water and 40 mL of *tert*-butanol. Solution in beaker B was added to beaker A slowly over around 1 h at 323 K under vigorous stirring. Then the solution in beaker C was added to the above mixture over 5–10 min duration. After this, the mixture was vigorously stirred for 1 h at 323 K. The solid formed was then washed and filtered to remove the uncomplexed ions. Then the solid was vacuum dried at 333 K for two hours. The final catalyst was obtained after activation of the material at 453 K for 4 h.

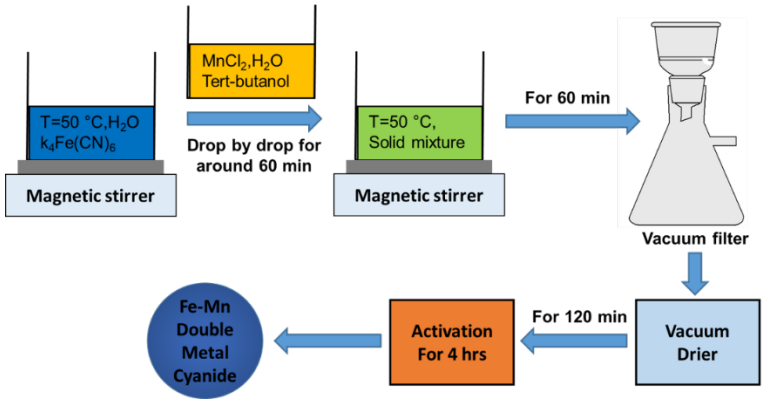

Figure 4-1 Outline of preparation of double metal cyanide catalyst

4.2.3 Catalyst Testing

Transesterification reactions were carried out in a 300 ml stirred slurry reactor (Parr reactor) with provisions for temperature control, stirring speed control and sampling of liquids at different time intervals. A schematic of the experimental setup is shown in Figure 4-2. In a typical experimental procedure, known amount of catalyst, methanol and mesitylene (internal standard for GC analysis) were charged into the reactor. The mixture was heated to the desired temperature by using a temperature-controlled circulating bath. Following this step, a predetermined amount of PC was pumped into the reactor using a HPLC pump [Scientific Systems, Inc. (SSI) Series I pump] to achieve the desired initial concentration. When the reaction mixture reached the desired temperature (~10-15 min), the reaction was started by switching the stirrer on to 1000 rpm. To facilitate sampling during reaction, the reactions were carried out in 0.69 MPa N_2. Liquid samples were withdrawn at different times to observe concentration-time profiles for the reactants and products.

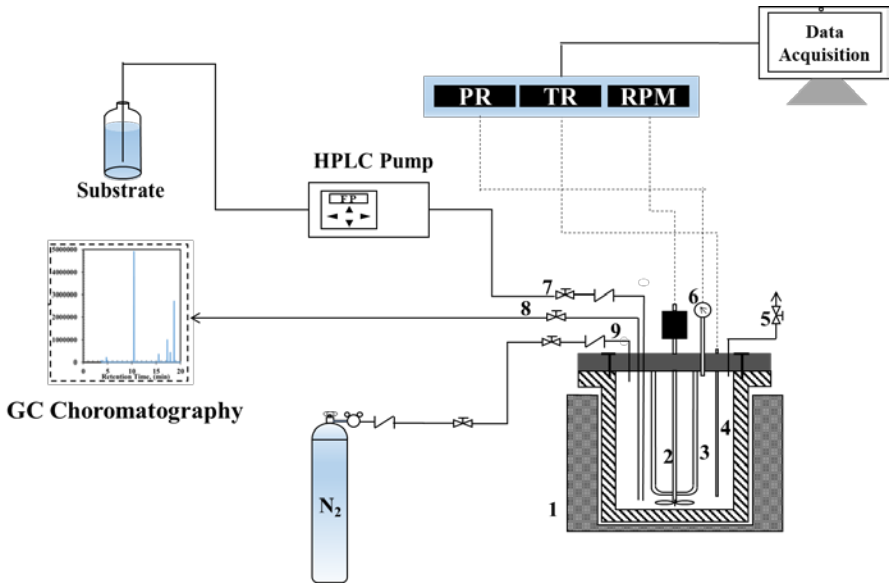

Figure 4-2 Schematic of experimental unit. 1. Heating jacket; 2. Stirring shaft; 3. Cooling coil; 4. Thermos well; 5. Gas vent; 6. Pressure gauge; 7. Liquid inlet; 8. Liquid sampling tube; 9. Gas inlet. PR: reactor pressure indicator; TR: reactor temperature indicator.

4.2.4 Analytical Methods

The liquid samples taken were analyzed using gas chromatographic (GC) analysis (Agilent, GC-7890A). The GC is equipped with a ZB-FFAP capillary column of 30 m length and a flame-ionization detector (FID). The inner surface of the column was nitroterephthalic acid modified polyethylene glycol film. Helium at 30 std mL/min flow rate was used as the carrier gas.

The same programmed temperature ramp as that in section 2.2.3 was used in this part of work. However, due to using different columns, different retention times were observed. Typical retention times were 3.3 min for methanol, 4.2 min for DMC, 6.4 min for mesitylene, 8.2 min for PG and 9.3 min for PC, respectively. An example of GC result is shown in Figure 4-3. Two intermediates were detected at 8.7 and 8.9 min, which were analyzed to be 1-hydroxypropan-2-yl methyl carbonate and 2-hydroxypropyl methyl carbonate (2-HMC) by GC-MS (Figure 2-2). Quantitative estimation of the concentrations of reactants and products was done using a calibration method with standards, which was found to give analytical accuracy within ±2.19%. The same calibration procedure was used for the calibration of chemical components as that in section 2.2.3. The calibration curves are shown in Appendix I.

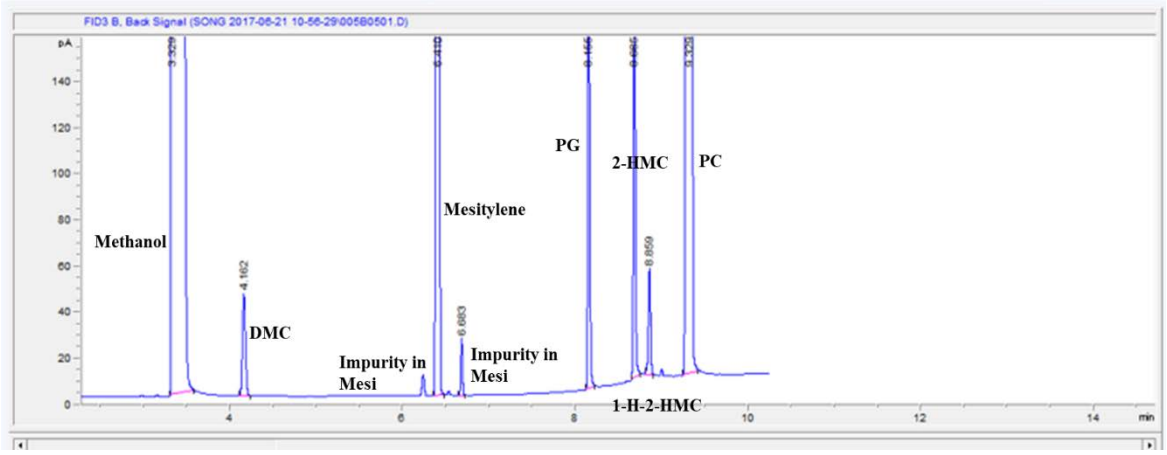

Figure 4-3 Typical GC graph

From the observed concentration-time profiles, the conversion of PC, selectivity of DMC

and PG, and the TOF (turn over frequency) were calculated using the following equations:

$$\%\text{Conversion} = \frac{(\text{Initial Moles of PC} - \text{Final Moles of PC}) \times 100}{\text{Initital Moles of PC}} \quad (1)$$

$$\%\text{Selectivity of Products} = \frac{\text{Moles of Product Formed} \times 100}{\text{Moles of PC Reacted}} \quad (2)$$

$$\text{TOF} = \frac{\text{Moles of PC Consumed}}{\text{Surface Mole of Mn} \cdot \text{Time}} \quad (3)$$

TOF values were estimated using conversion of carbonates between 10-15%. Mn content (from EDX analysis) was used to estimate TOFs as runs with either only FeO or only Fe_2O_3 showed that Fe alone is not active for the reaction.

4.2.5 Catalyst Characterization

Specific surface area, pore volume and the pore size of the catalyst were determined by the Brunauer–Emmett–Teller (BET) method from the N_2-adsorption–desorption isotherms using Autosorb iQ-Chemisorption & Physisorption Gas Sorption Analyzer. Average pore diameter was determined by the Barrett– Joyner–Halenda (BJH) method. Scanning electron microscope (SEM) images were obtained on a Leo 1550 field emission scanning electron microscope instrument. Transmission Electron Microscopy (TEM) and Scanning Transmission Electron Microscopy (STEM) images of catalyst samples were obtained using an FEI Tecnai F20 XT instrument at an electron acceleration voltage of 200 kV. Energy Dispersive X-Ray Spectroscopy (EDX) of elemental composition and distribution of metals were derived using a silicon drift EDX detector. Small angle X-ray scattering and wide-angle XRD patterns of catalyst samples were obtained in a PANalytical Empyrean instrument, operated at 45 kV and 40 mA. The scanning range is 10^o – 80^o, with a step size of 0.013^o. XPS spectra were recorded with X-ray photoelectron spectrometer PHI 5000 VersaProbe II ultrahigh vacuum (1×10^{-9} bar) apparatus with an Al-K_α X-ray source ($h\nu$=1486.6 eV) and a monochromator. Casa XPS software was used to analyze the XPS data. Shirley background subtraction and peak fitting with Levenberg–Marquardt method were used to

analyze the data. Thermogravimetric analysis (TGA) was done using a Q600 STD instrument with air flow (50 std cm^3/min) at a heating rate of 10 °C/min in the 50–600 °C range. Diffuse Reflection Infrared Fourier Transform Spectroscopy (DRIFTS) spectra for the catalyst samples were collected in the range of 1000-4000 cm^{-1}, using a Bruker Tensor 27 FT-IR equipped with a Pike diffuse reflectance cell. Diffuse-reflectance UV-vis absorption spectra in the range of 150~850 nm were acquired using a PerkinElmer Lambda 850 UV-VIS spectrophotometer at room temperature (23-25 °C). The scan speed used was 266.75 nm/min, while the data interval is 1 nm.

4.3 Results and Discussion

4.3.1 Evaluation of Double Metal Cyanide Catalysts

To benchmark the performance of double metal cyanide catalysts and establish the analytical protocols, several catalysts were tested. The results are summarized in Table 4-1. Among six different double metal cyanide catalysts tested (see Table 4-1), Fe-Mn double metal cyanide catalyst showed the highest TOF and DMC selectivity under identical reaction conditions. For the three Co-based catalysts, the TOF order observed is as follows: Co-Zn > Co-Ni > Co-Mn, which is attributed to the differences in the covalent radii [Zn (122±4 pm) < Ni (124±4 pm) < Mn (139±5 pm at low spin or 161±8 pm at high spin)]. Generally, shorter covalent radius leads to higher bond energies. However, for the three Fe-based catalysts, the activity follows a different order: Fe-Mn > Fe-Zn > Fe-Ni. This different order may be due to the unique cubic structure of the Fe-Mn double metal cyanide formed which was reported to have significant effect on the activity of catalysts.[130] Additionally, Fe-Mn double metal cyanide showed significantly higher activity than reported mixed oxides (Table 4-1), known as active catalyst in previous work for the transesterification reaction[44]. The Fe-Mn double metal cyanide complex was therefore chosen for further study.

In all the experiments, the products (DMC and PG) were found to be stoichiometrically consistent [see Figure 4-4 (a), the DMC formed is nearly the same as that of PG formed]]. Due to the low boiling points of DMC and methanol, they can be detected in the vapor phase at reaction conditions. The vapor phase concentrations were therefore taken into account in all calculations. The selectivity towards DMC and PG was found to increase with time (Appendix II) due to formation of intermediates [2-hydroxypropyl methyl carbonate (2-HMC) and 1-hydroxypropan-2-yl methyl carbonate (1-HP-2-MC)] at lower PC conversion, which were detected and confirmed by GC MS (in Appendix II). 2-HMC was observed in larger amounts compared to 1-HP-2-MC, especially at the beginning of the reaction[131]. These two intermediates cannot be reliably quantified due to unavailability of standard samples. However, the DMC selectivity was found to reach as high as 97% at the end of a typical reaction. Additionally, only the DMC and PG product peaks were dominant. The 2-HMC and 1-HP-2-MC concentrations were accounted for using the method described in Appendix I. The 2-HMC calculated from this method can quantify for more than 90% of the remaining material balance except for DMC formed. Therefore, the mass balance deficit was assumed to be 2-HMC, which was in the range of 1.60%-69.3% depending on the conversion of PC. The amount of 2-HMC reached a maximum at around 30 min, after which it gradually decreased to nearly zero [see Figure 4-4 (a)]. Specifically, when the molar ratio of methanol/PC decreased to 3.7, the amount of intermediate formed accounted for more than 50% of the products formed [Figure 4-4 (b)]. Similarly, the amount of 2-HMC reached a maximum at around 30 min, after which it decreased slowly accompanied by increasing DMC selectivity.

Table 4-1 Screening of different double metal cyanide catalysts

catalysts	PC X (%)	DMC S (%)	Intermediates S(%)[a]	TOF, (mol·mol^{-1}·h^{-1})[b]	Ref
Fe-Mn	49.4	96.1	7.0	57.1	This work
Fe-Ni	30.0	70.1	18.1	7.8	This work
Fe-Zn	29.1	75.4	21.2	20.0	This work
Co-Mn	16.1	89.7	30.9	4.0	This work
Co-Ni	8.8	53.8	51.8	21.6	This work
Co-Zn	19.1	92.2	30.2	36.2	This work
Fe-Zn[c]	-	Y_{DMC} 70.0	-	(TON) 26[d]	60
Au/CeO_2	63.0	55.0	-	30[f]	57
CaO-ZnO	-	Y_{DMC} 82.0[e]	-	17.8[g]	132
Cu/Zn/Al mixed oxides	70.3	92.8	-	6.0	56

Reaction conditions: PC, 1.1 kmol/m^3; methanol, 22.2 kmol/m^3; catalyst, 5 kg/m^3; T=140 °C; 0.69 MPa initial N_2; reaction time = 3 h

[a]See Supporting Information (Part 3) for details of calculation.

[b]Calculated using Equation (3).

[c]Reaction conditions: Fe–Zn (preactivated at 180 °C for 4 h), 0.25 g; PC, 10 mmol; MeOH, 100 mmol; reaction temperature, 170 °C; reaction time, 4 h.

[d]TON = moles of PC converted per mole of catalyst.

[e]DMC yield value=$S_{DMC}\times X_{PC}$.

[f]TOF = moles of PC converted /(mole of Au·time).

[g]TOF = moles of PC converted /(mole of catalyst·time).

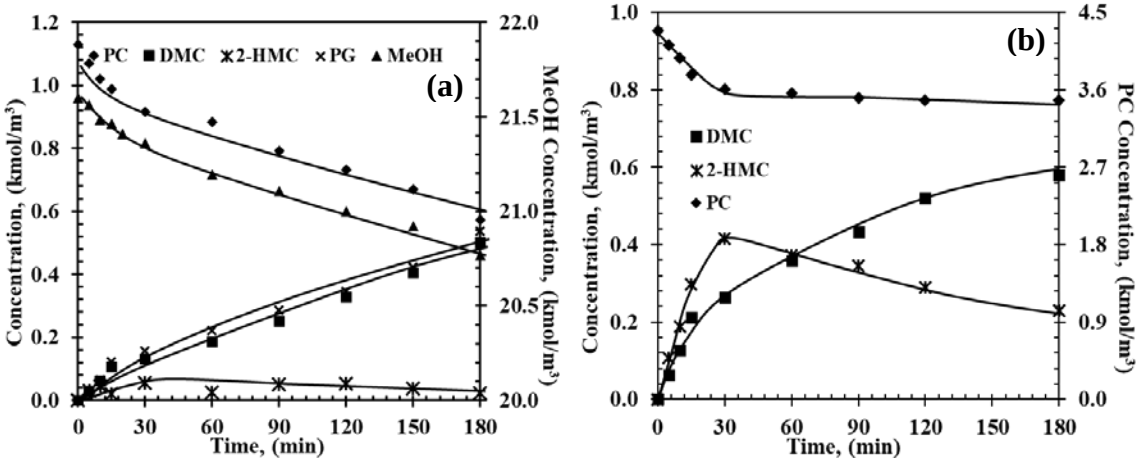

Figure 4-4 Temporal concentration-time profiles for PC with methanol. a. Reaction conditions: PC, 1.1 kmol/m^3; methanol, 22.2 kmol/m^3; catalyst, 5 kg/m^3; T=140 °C; 0.69 MPa initial N_2. b. Reaction conditions: PC, 4.3 kmol/m^3; methanol, 16.1 kmol/m^3; catalyst, 5 kg/m^3; T=140 °C; 0.69 MPa initial N_2.

4.3.2 Effect of Metal Ratio in Catalyst

Catalysts were prepared with different Fe/Mn metal ratios (1:2, 1:4, 1:8 and 1:12) and their performance are compared in Table 4-2. It is observed that the catalytic activity reaches a high value around a molar ratio of $K_4Fe(CN)_6$ to $MnCl_2$=1:8. Clearly, excess $MnCl_2$ was needed for superior activity. However, when the molar ratio of Fe/Mn reaches 1:12, a slight decrease in catalytic activity was observed. These preliminary observations suggest a significant effect of Mn on the catalytic activity.

Table 4-2 Catalyst preparation parameter screening

Experiment No.	Fe/Mn Ratio	PC,(%)	DMC S (%)	TOF[b], ($mol \cdot mol^{-1} \cdot h^{-1}$)
1	1:2	39.1	90.2	50.1
2	1:4	43.2	91.1	42.4
3	1:8	49.4	96.1	57.1
4	1:8[a]	22.1	89.9	29.5
5	1:12	32.9	90.3	34.9

Reaction conditions: PC: 1.1 kmol/m^3, methanol: 22.0 kmol/ m^3, catalyst: 5 kg/m^3, T = 140 °C; 0.69 MPa initial N_2; reaction time = 3 h
a: activated in N_2 flow.
b: Calculated using Equation (3).

4.3.3 Effect of Catalyst Activation Conditions

Two different activation procedures were examined. In one, the catalyst was calcined in air, while in another, the catalyst was calcined under N_2 at 50 cm^3/min flow rate of the gas. For the catalyst calcined in N_2 flow (Table 4-2, Entry#4), the activity decreased from 57.1 $mol \cdot mol^{-1} \cdot h^{-1}$ to 29.5 $mol \cdot mol^{-1} \cdot h^{-1}$. For the following studies, catalysts activated in air were therefore used.

4.3.4 Catalyst Characterization

4.3.4.1 Nitrogen adsorption–desorption isotherms

Textural properties of Fe-Mn catalyst (activated in air) and Fe-Mn-N_2 (activated in N_2 flow) were determined by nitrogen physisorption method. The adsorption isotherm of both these

two catalysts exhibited type III+IV behavior with H3 type hysteresis loop (Figure 4-5). Type III behavior suggests a nonporous or macroporous solid[133]. Type IV isotherms corresponded to mesoporous materials.[133-134] H3 type of loop indicates non-rigid aggregation of particles.[133] In combination with the results from SEM images [Figure 4-6 (a)], it is concluded that Fe-Mn catalyst is probably nonporous solid. The corresponding textural properties (BET surface area, pore volume, and pore size) are listed in Table 4-3. Fe-Mn complex showed higher surface area (83.8 m^2/g) than Fe-Zn catalyst. The total pore volume and average pore diameter were also higher for Fe-Mn complex than Fe-Zn (0.32 vs. 0.03-0.04 cm^3/g and 17.1 vs. 3-5 nm). Additionally, higher activity was observed for transesterification of PC with methanol with Fe-Mn complex (Table 4-1), which was most probably due to the cubic structure Fe-Mn complex (Fe-Zn has a spherical morphology[60]). Even though Fe-Mn-N_2 shows higher surface area than Fe-Mn, it has lower activity, suggesting the Mn content has more effect on the catalytic activity than the surface area.

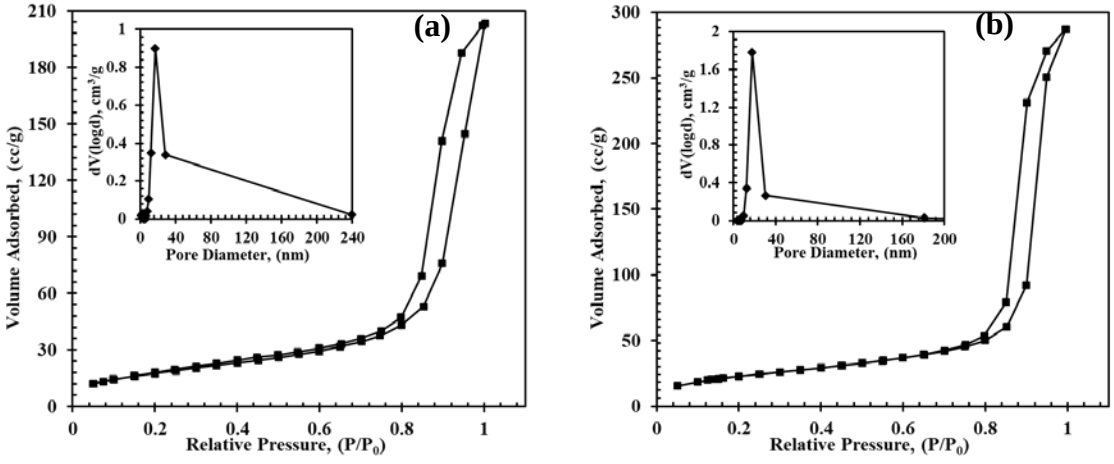

Figure 4-5 Nitrogen isotherm for (a) Fe-Mn catalyst and (b) Fe-Mn-N_2

Table 4-3 Textural properties of Fe-Mn catalyst

	Total surface area (m^2/g)	External surface (m^2/g)	pore volume (cm^3/g)	pore size (nm)	
Fe-Zn	35-40	22-25	0.03-0.04	3-5	[78]
Fe-Mn	83.8	63.9	0.32	17.1	This work
Fe-Mn-N_2	97.1	82.1	0.46	17.6	This work

4.3.4.2 SEM, TEM, STEM and EDX Mapping

The surface morphology of Fe-Mn and Fe-Mn-N_2 was examined from the SEM image (Figure 4-6 (a) and (b)). It is clear that Fe-Mn complex has fine fluffy surface without pores, which is consistent with the conclusion derived from N_2 adsorption-desorption isotherms. However, for the Fe-Mn-N_2 complex, small well developed petal by petal surface was observed.

TEM and STEM images provide clearer information on the morphological and structural aspects of the catalysts. TEM analysis was done for fresh Fe-Mn complex. Structured lattice with lattice spacing of 0.547 nm was observed for the Fe-Mn complex [(Figure 4-6 (c)], indicating a crystalline structure. STEM and EDX mapping was done for the precursor $K_4Fe(CN)_6$ and Fe-Mn complex. Interestingly, precursor $K_4Fe(CN)_6$ was observed to consist of smooth large particles (> 100 nm) while the Fe-Mn complex displayed much smaller particles [Figure 4-6 (d) and (e)]. In other words, the unit particles of the catalyst changed during the catalyst preparation process. Furthermore, in order to confirm the distribution of Mn, Fe and K species in the catalyst, EDX mapping was carried out. As seen from Figure 4-6 (e), Fe, K, Mn, N and O elements are homogeneously distributed throughout the catalyst. Furthermore, Cl was not detected in the Fe-Mn complex, indicating that free $MnCl_2$ was not present in the final catalyst.

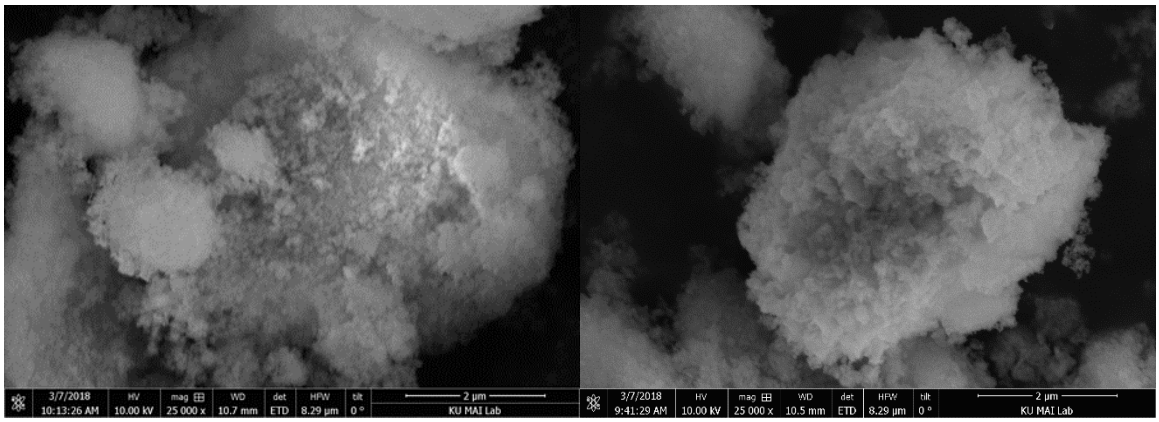

(a) SEM images of Fe-Mn Complex and (b) SEM images of Fe-Mn-N_2 complex

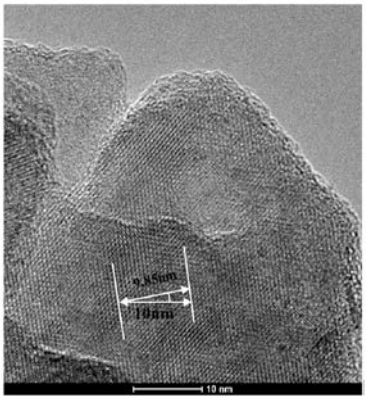

(c) TEM images for Fe-Mn Complex

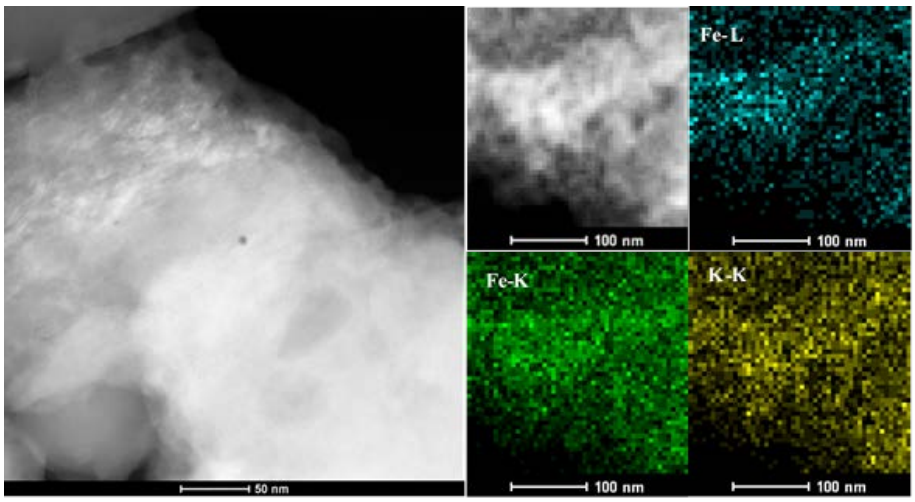

(d) STEM image and EDX mapping for $K_4Fe(CN)_6$

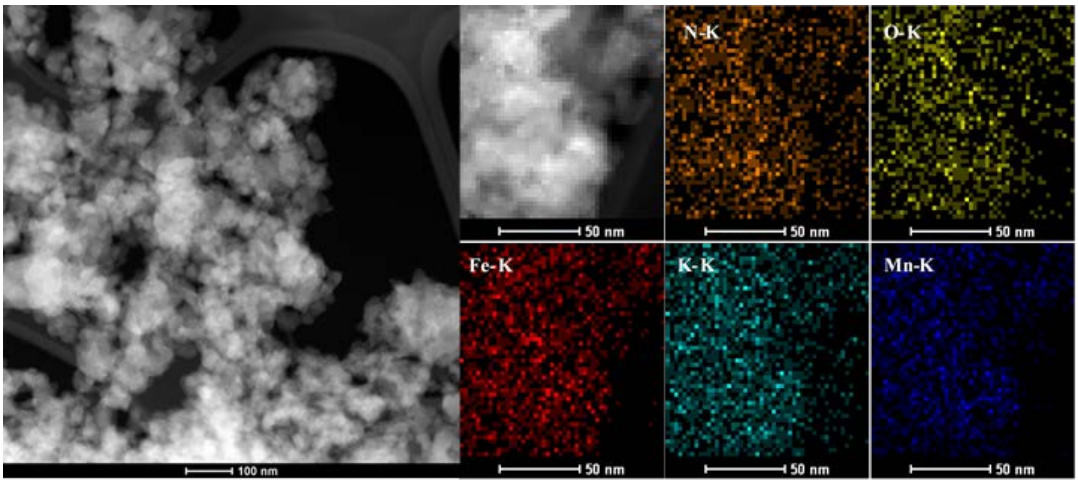

(e) STEM image and EDX mapping for Fe-Mn Complex

Figure 4-6 SEM, TEM, STEM images and EDX mapping for Fe-Mn catalysts

4.3.4.3 XRD Analysis

XRD patterns of the Fe-Mn double metal cyanide and its precursor compounds, $K_4Fe(CN)_6$ and $MnCl_2$ are shown in Figure 4-7. Unlike the $MnCl_2$ and $K_4Fe(CN)_6$ patterns [Figure 4-7 (b) and (c)], only a few distinct peaks [(100), (110), (200) and (211) planes of a cubic crystalline phase] were identified for the Fe-Mn complex [Figure 4-7 (a)]. In conjunction with the TEM results, it is hypothesized that the Fe-Mn complex possesses a cubic crystalline structure with a lattice spacing of 0.495 nm (calculated from indexing of x-ray diffraction), which is similar to that observed from TEM images [Figure 4-6 (c)]. Co-Zn double metal cyanide catalysts have been reported to possess cubic crystalline structure, which was reported to enhance catalytic activity for hydroamination reactions.[60, 74, 135-136] Therefore, we surmise that cubic structure of Fe-Mn double metal complex may play an important role in enhancing activity for the transesterification reaction compared with other double metal cyanides (Fe-Zn a spherical morphology).

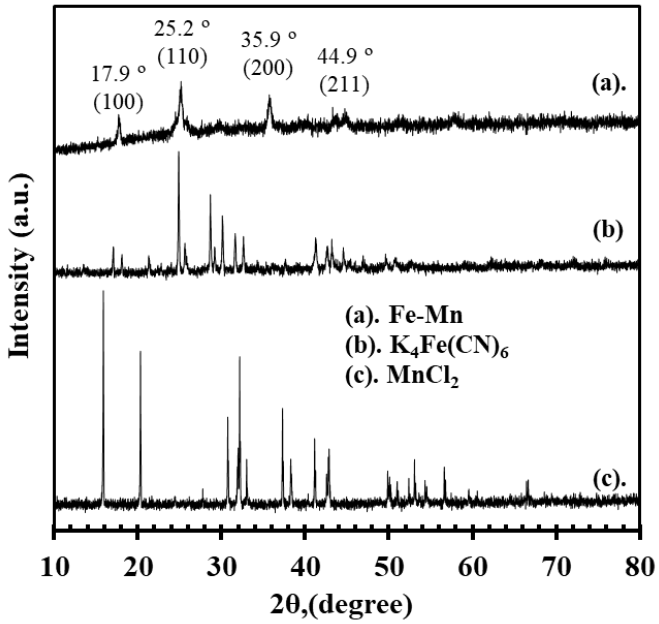

Figure 4-7 XRD patterns for Fe-Mn catalysts

4.3.4.4 XPS analysis

XPS analysis of fresh Fe-Mn catalyst was performed to elucidate the chemical state of elements in Fe-Mn. XPS data based on analysis of spectra of Fe 2p, Mn 2p, K 2p, O 1s, N 1s and C 1s electronic levels are presented. The spectra of Fe $2p_{3/2}$, and Mn $2p_{3/2}$ are displayed in Figure 4-8 (a)-(b). Two chemical states of Fe were deconvoluted in the Fe $2p_{3/2}$ spectrum at binding energies of 707.4 and 708.4 eV, which are attributed to $[Fe(CN)_5H_2O]^{3-}$ and $[Fe(CN)_6]^{4-}$ bonds, respectively.[137-138] The deconvoluted Mn $2p_{3/2}$ spectrum showed that mainly three chemical bonds contribute to the Mn spectrum: $[Mn(CN)_6]^{4-}$ (640.1 eV), MnO (642.1 eV) and MnO_2 (646.2 eV)[139]. The N 1s XPS spectra of investigated materials are characterized by the peaks at BE of 396.5, which can be attributed to –CN group[140]. Three characteristic binding energy peaks in O 1s XPS spectra are detected, 530.4, 530.7 and 532.3 eV, which can be ascribed to MnO_2[141], C=O[142] and C-OH atomic bonds[140], respectively.

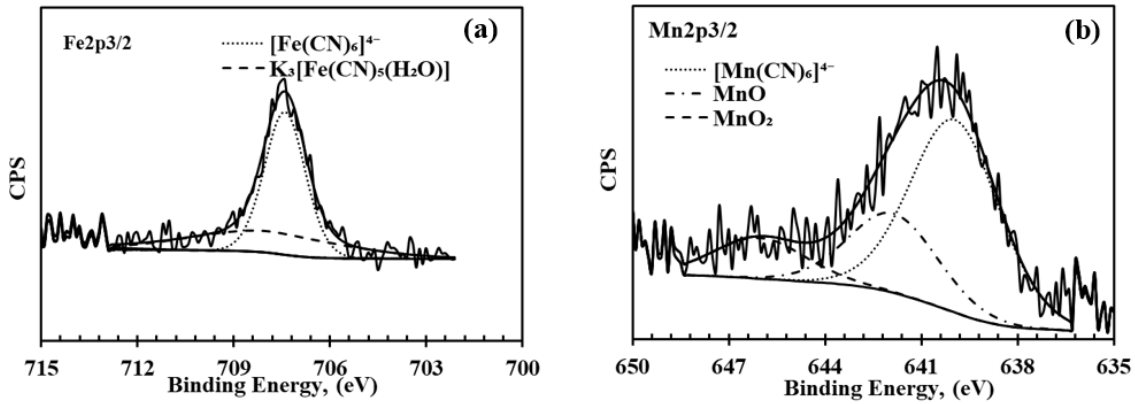

Figure 4-8 XPS spectra for (a) Fe 2p3/2 and (b) Mn 2p3/2 (Survey Spectra of Fe-Mn complex in Appendix II)

4.3.4.5 TG

Thermogravimetric analysis (see Figure 4-9) showed four stages of weight loss. The first stage is the noticeable mass loss step (~5.6 wt%) in the 25–130 °C range, which is attributed to the liberation of water and tert-butanol molecules.[130, 143-144] The second stage exhibits a sharp mass

decrease (7.5%) in the 280–316 °C range probably due to decomposition of the cyanide group.[60, 130, 144] The following stage (316-378 °C) is most probably due to the transformation of the double-metal cyanide complexes into metal nitrates and carbonates.[60, 130, 144] During the fourth stage (316-586 °C), only a 1.8% mass loss was detected. In our work, the catalysts were exposed to Stage 2 temperatures wherein the CN group as coordination bridge between Fe and Mn is stable.

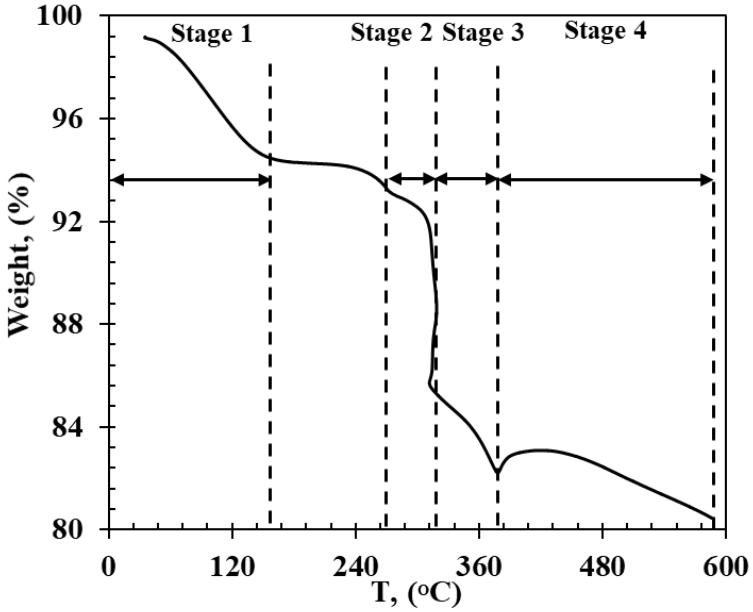

Figure 4-9 TGA analysis for Fe-Mn catalysts

4.3.4.6 FT-IR Spectra (DRIFT mode)

The -CN band in the IR spectrum is known to be sensitive to the mode of cyanide coordination and the metal to which it is coordinated[145], which can bridge the metal atoms Fe/Mn in Fe-Mn catalyst. The $K_4Fe(CN)_6$ precursor showed an intensive characteristic stretching band at 2069.5 cm^{-1} due to -CN, which shifted to a higher wave number in Fe-Mn complex at 2090.7 cm^{-1} in the Fe-Mn complex. Previous studies[60, 71, 73-75] reported a similar shift of CN band to higher frequencies in other double metal cyanide catalysts. For example, Co–Zn double-metal cyanides show a shift of this band from 2133 cm^{-1} to 2187 cm^{-1}, compared to the precursor $K_3Co(CN)_6$.[136] The *ν*(CN) shift to higher frequencies demonstrates that the CN ion acts as not only a σ-donor by

donating electrons to Fe but also as a π-electron donor by chelating to Mn metal.[136, 146] Additionally, the existence of complexing agent tert-BuOH in the Fe-Mn catalyst was confirmed from the characteristic bands at 1440.7 cm^{-1}–1261.4 cm^{-1} (symmetric and anti-symmetric C–H deformation and out-of-plane C_3C–O anti-symmetric stretching vibrations) and 1103.2 cm^{-1} (CH_3 rocking vibrations).[60, 147-148] Furthermore, a broad band attribute to OH was detected due to H_2O and tert-butanol around 3650 cm^{-1}.[60, 148]

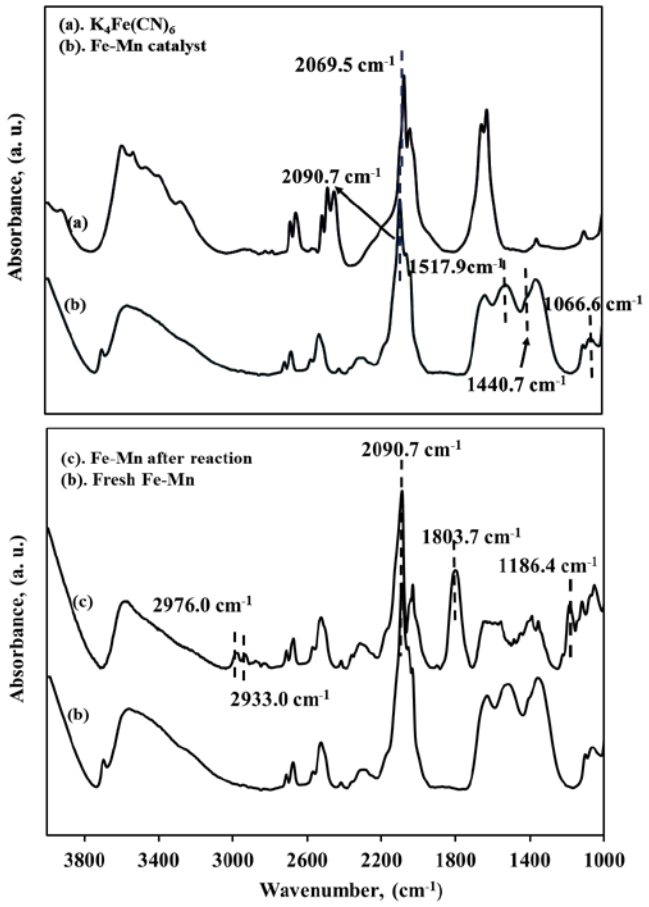

Figure 4-10 FTIR spectra for Fe-Mn catalyst and used Fe-Mn catalyst

4.3.4.7 Diffuse-reflectance UV–visible spectra

The UV-Visible spectra of the solid $K_4Fe(CN)_6$ powder and Fe-Mn double metal cyanide complex are illustrated in Figure 4-11. From the figure, it is clear that all the bands are in the ultraviolet region. A strong absorption band around 210 nm was observed for both $K_4Fe(CN)_6$ and

Fe-Mn complex, which is reported to be the fingerprint of $[Fe(CN)_6]^{4-}$ (the deviation from literature value may be due to differences between liquid and solid sample).[149] Three additional adsorption bands at 248 nm, 280 nm and 332 nm were also observed for $K_4Fe(CN)_6$. The latter two bands (280 nm, 332 nm) are attributed to ligand-to-metal (Fe) charge transfer (LMCT) transitions, the former (at 248 nm) is probably attributed to π–π∗ charge transfers in the CN ligand, which is different from previous literature[60, 150]. In the case of Fe–Mn catalysts, the π–π∗ charge transfer band shifted to higher energy side (from 248 nm to 239 nm). However, for the LMCT bands (280 nm and 332 nm), one moves a little bit to the higher energy side (280 nm to 279 nm), while the other shifted significantly to higher energy side (from 332 nm to 318 nm). The shift from 332 nm to 318 nm is most probably due to CN ligand donation of antibonding electrons to Mn ions. This shift of bands (248 nm to 239 nm and 332 nm to 318 nm) suggested that Fe–Mn catalysts contain bridging cyano groups between Fe and Mn, which is consistent with the conclusion derived from FTIR results. Furthermore, no adsorption bands were detected in the visible region, indicating that Fe is in a low spin +2 oxidation state,[60] which is consistent with the conclusion from XPS results.

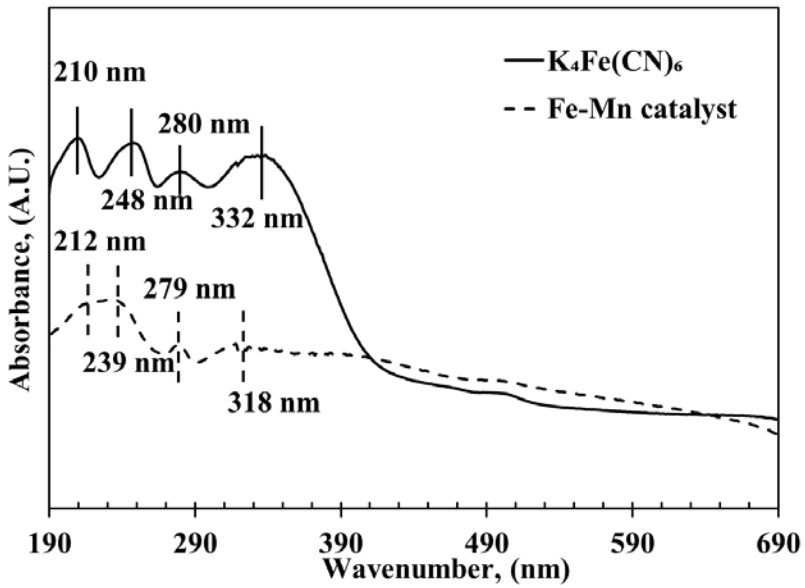

Figure 4-11 UV-Vis spectra for Fe-Mn complex

4.3.5 Effect of Reaction Conditions

Fe-Mn double metal cyanide complex as a heterogeneous catalyst shows better catalytic activity than other double metal cyanides (Table 4-1) for the transesterification of PC with methanol. Therefore, it was used to study the effect of reaction parameters (catalyst loading, PC/Methanol ratio, temperature and different cyclic carbonates) and stability.

4.3.5.1 Catalyst loading effect

First, the effect of catalyst loading on PC conversion, DMC selectivity and initial reaction rates was investigated by keeping other parameters constant. Figure 4-12 shows that with increase in catalyst loading from 0.5 kg/m^3 to 4 kg/m^3, the PC conversion increased from 11.8% to 46.1%, DMC selectivity also increased from 62.3% to 89.7%. At the same time, there is a continuous increase in the initial reaction rate when catalyst loading was increased from 0.5 kg/m^3 to 4 kg/m^3. However, further increase in the catalyst loading from 4 kg/m^3 to 5 kg/m^3 did not significantly affect either the PC conversion (from 46.1 to 49.4%) or the initial reaction rate (from 3.4×10^{-3} to 3.5×10^{-3} kmol/m^3/min), with a minor change in DMC selectivity (from 89.7% to 96.2%) as well.

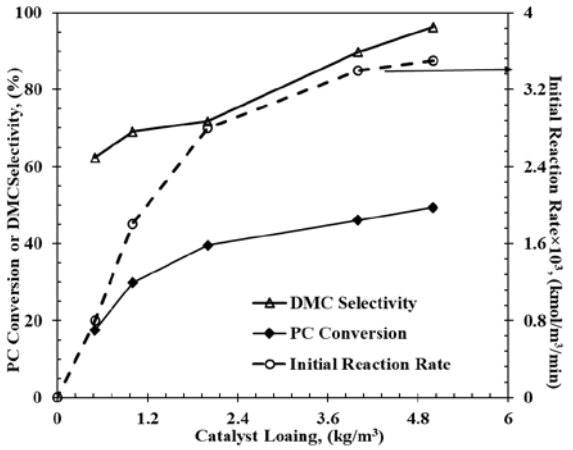

Figure 4-12 Catalyst loading effect: Reaction conditions: PC, 1.1 kmol/m^3; methanol, 22.2 kmol/m^3; T=140 °C; 0.69 MPa N_2, t=3 h.

4.3.5.2 Methanol/PC Ratio Effect

Figure 4-13 (a) shows the effect of methanol/PC ratio on concentration-time profiles, PC conversion and DMC selectivity. In these experiments, the reaction mixture volume was kept constant while changing the methanol/PC ratio. It was observed that the PC conversion increased from 22.1% to 49.4% with increasing methanol/PC molar ratio from 3.7 to 20, while the DMC selectivity increased from 65.6% to 96.1%. At low conversion, the DMC selectivity was lower mainly due to significant formation of intermediate product 2-HMC (see Figure 2-2). As expected, increasing the reactant ratio shifts the reaction equilibrium towards the formation of final products. Additionally, the initial reaction rate decreased with increasing methanol/PC ratio, as a result of reduced PC concentration. Concentration-time profiles for different methanol/PC ratios are shown in Figure 4-13 (b)-(e). It is clear that when the ratio decreases, the intermediate 2-HMC formation is higher. At low methanol/PC ratio, the reaction between 2-HMC and methanol is slower compared to that at higher methanol/PC ratio.

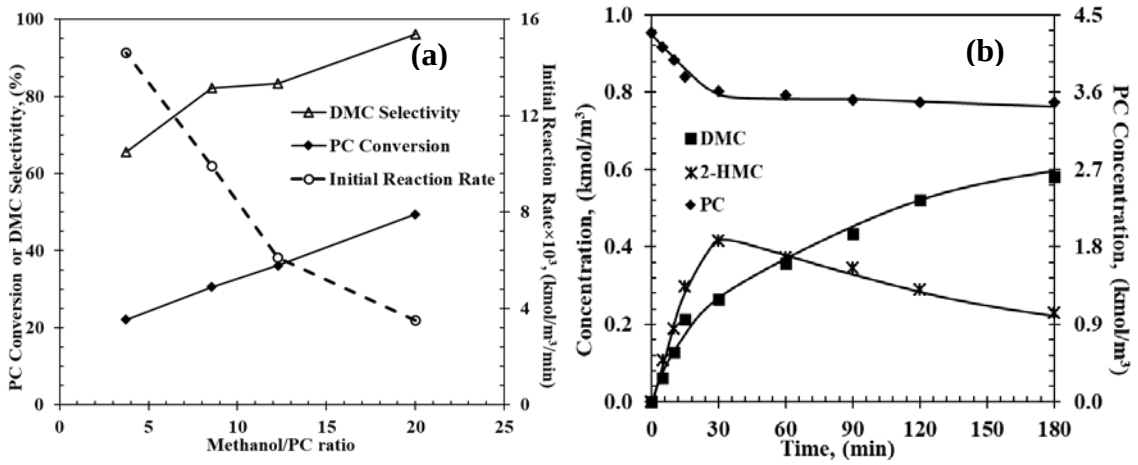

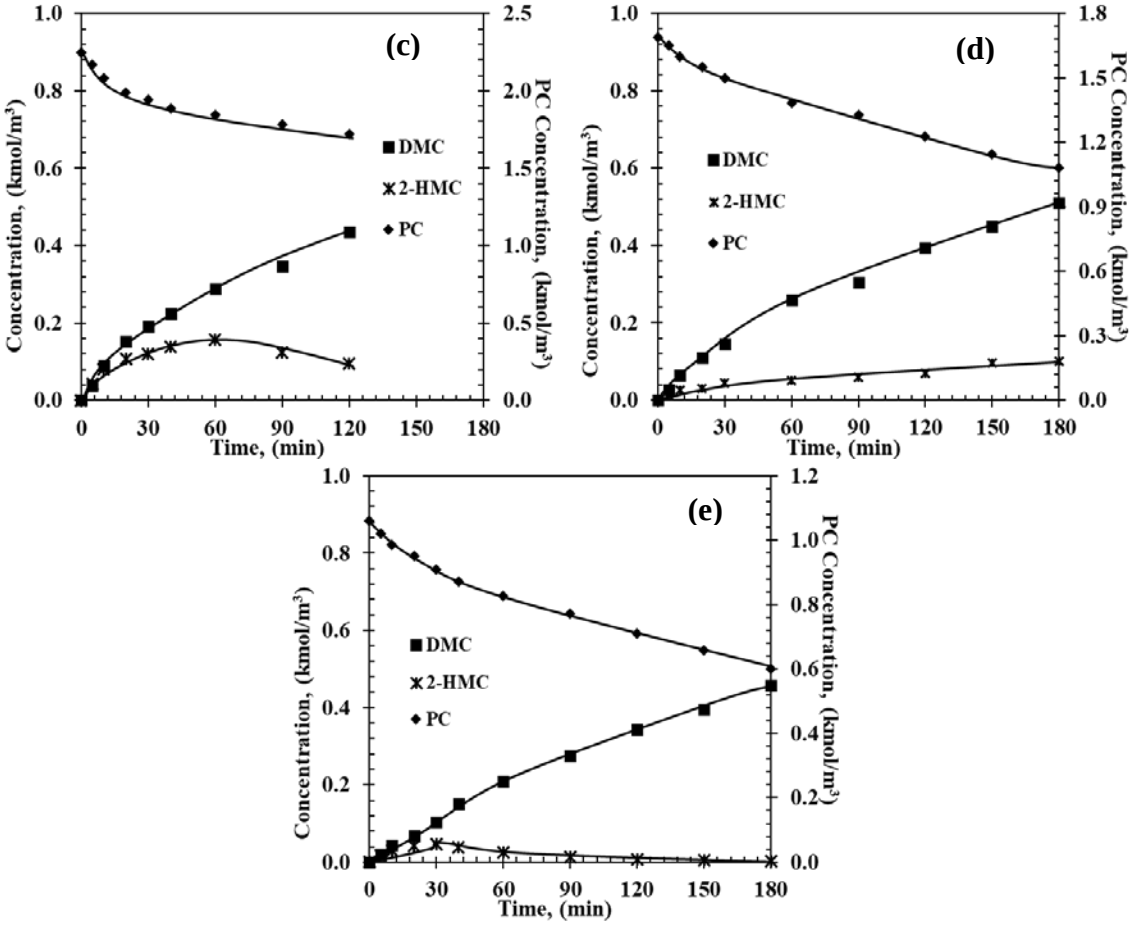

Figure 4-13 Methanol/PC ratio effect. (a) PC conversion and DMC selectivity with different methanol/PC ratio, (b) Concentration-time profile for Methanol/PC=3.7, (c) Concentration-time profile for Methanol/PC=8, (d) Concentration-time profile for Methanol/PC=12, (e) Concentration-time profile for Methanol/PC=20. Reaction conditions: PC, 1.1-4.3 kmol/m^3; methanol, 16.1-22.2 kmol/m^3; catalyst, 5 kg/m^3; T=140 °C; 0.69 MPa initial N_2.

4.3.5.3 Temperature Effect

At a low temperature of 140 °C, the conversion of PC was 49.4% (Figure 4-14). At 200 °C, the PC conversion increased to 79.1% with nearly the same DMC selectivity at lower temperatures. Previously, lower DMC selectivity was reported at higher temperatures, which may ascribe to PC decomposition at higher temperatures.[23, 56-57, 132] However, with Fe-Mn catalyst, the DMC selectivity at 200°C remained high (96.7%) during a 3 h reaction. Even though PO (a decomposition product of PC) was observed, it was negligible. From the concentration-time profiles at different temperatures, it is clear that the formation of 2-HMC is favored when the

temperature is increased from 140 °C to 180 °C. However, with further increase in temperature to 200 °C, the formation of 2-HMC decreased.

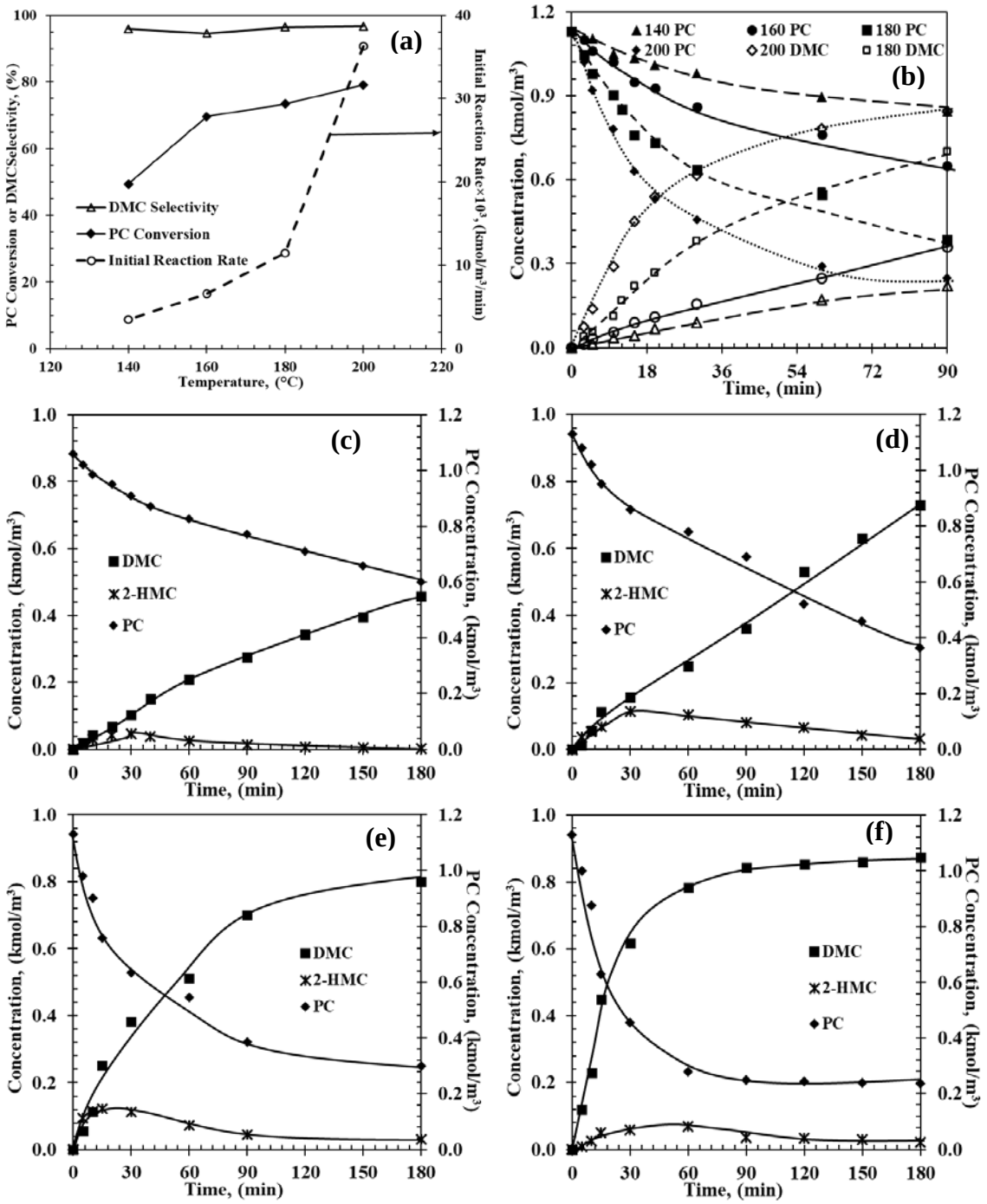

Figure 4-14 Temperature effect. (a) PC conversion and DMC selectivity with different temperature (b) PC and DMC concentration-time profiles with different temperature, (c) Concentration-time profile for 140 °C, (d) Concentration-time profile for 160 °C, (e) Concentration-time profile for 180 °C, (f) Concentration-time profile for 200 °C.

Reaction conditions: PC, 1.1-4.3 kmol/m^3; methanol, 16.1-22.2 kmol/m^3; catalyst, 5 kg/m^3; T=140 °C; 0.69 MPa initial N_2.

4.3.5.4 Effect of Cyclic Carbonate Substrates

Transesterification of two other cyclic carbonates (ethylene carbonate, EC and butylene carbonate, BC) was also studied using Fe-Mn catalyst at different temperatures, typical concentration-time profiles are shown in Figure 4-15. It was found that the reaction rate with EC is much faster than those observed with PC and BC as substrates. After a 3 h reaction, the EC reaction reached 90.5% conversion, with a small amount of intermediate, identified as 2-hydroxyethyl methyl ester by GC MS (Appendix II). In contrast, a much lower BC conversion (~34.7%) was observed under the same conditions. Similar to the case of PC, two intermediates 1-hydroxybutan-2-yl methyl carbonate (1-HB-2-MC) and 2-hydroxybutyl methyl carbonate (2-HBMC) were detected in significant amounts by GC MS analysis (Appendix II). The transesterification activity of the three substrates was found to vary in the following order: EC > PC≈BC [Figure 4-15 (a)], which is attributed to the steric hindrance associated with the bulky methyl and ethyl group in PC and BC, as compared with the symmetrical EC[44].

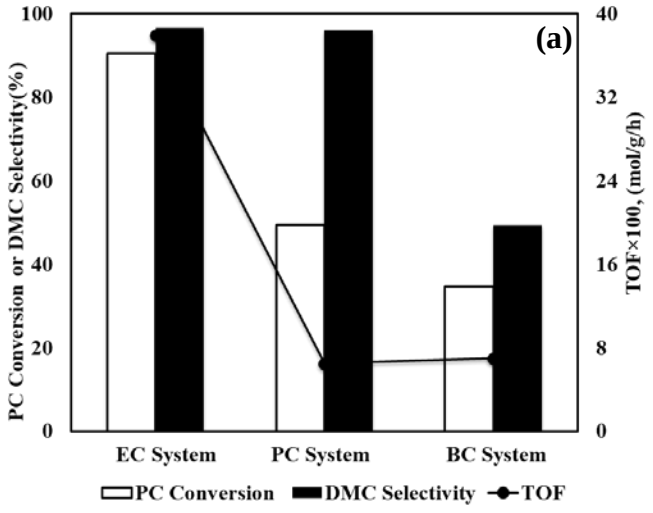

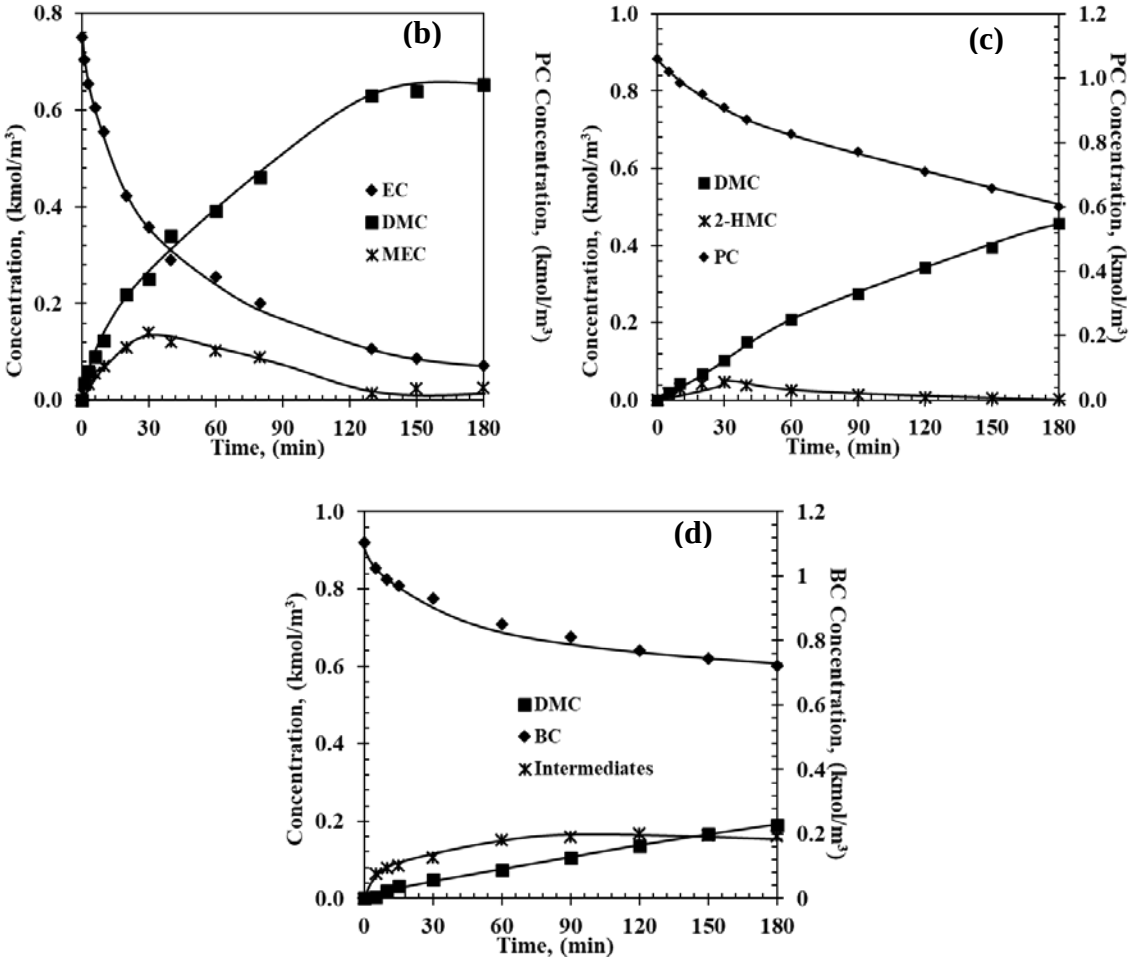

Figure 4-15 Effect of different cyclic carbonates. (a) comparison of EC, PC and BC systems (b) concentration-time profile for EC, (c) concentration-time profile for PC, (d) concentration-time profile for BC. Reaction conditions: PC, 1.1 kmol/m^3; methanol, 22.2 kmol/m^3; catalyst, 5 kg/m^3; T=140 °C; 0.69 MPa initial N_2

4.3.6 Catalyst Leaching and Recycle Experiments

For the leaching experiments, after a 2 h transesterification reaction, the reaction mixture was centrifuged. Then the clear solution was taken for a further experiment under the same reaction conditions. The results [Figure 4-16 (a)] show that after the solid catalyst was removed, no further reaction was detected [compare to the results in Figure 4-4 (a)], confirming that no active species leach out during the reaction.

For the catalyst recycle experiments, after a 3 h transesterification reaction, the catalysts were recovered by centrifugation, then reused in another fresh reaction without further treatment. The catalyst loss during the recycling process was found to be 11.2% after 4 runs. The results for consecutive reaction runs are summarized in Figure 4-16 (b), with the catalyst loss considered in the TOF calculation.. It is clear from Figure 4-16 (b) that the catalytic activity decreased slightly from the fresh run to the first cycle, after which, the activity was found to be constant. Specifically, from the fresh run to the first cycle, the PC conversion decreased from 49.4% to 42.1%. After the fresh run, the following 3 cycles had nearly the same PC conversion. The activity decreasing from the fresh run to the first cycle is most likely due to active sites being occupied by reactants or products (most probably PC), which can be seen from FTIR spectra of used catalyst [Figure 4-10 (c)]. The sharp absorption band at 1803 cm^{-1} is characteristic of the C=O functional group. Besides, the peaks observed at 2976 cm^{-1} and 2933 cm^{-1} are attributed to CH_2 and CH vibrations of PC, respectively.[151-152] Moreover, the C-O ring stretching at 1186.4 cm^{-1} was detected.

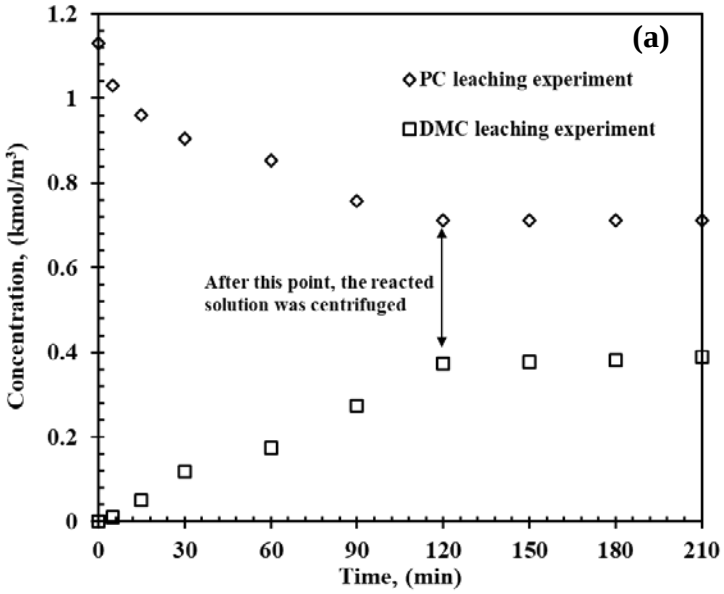

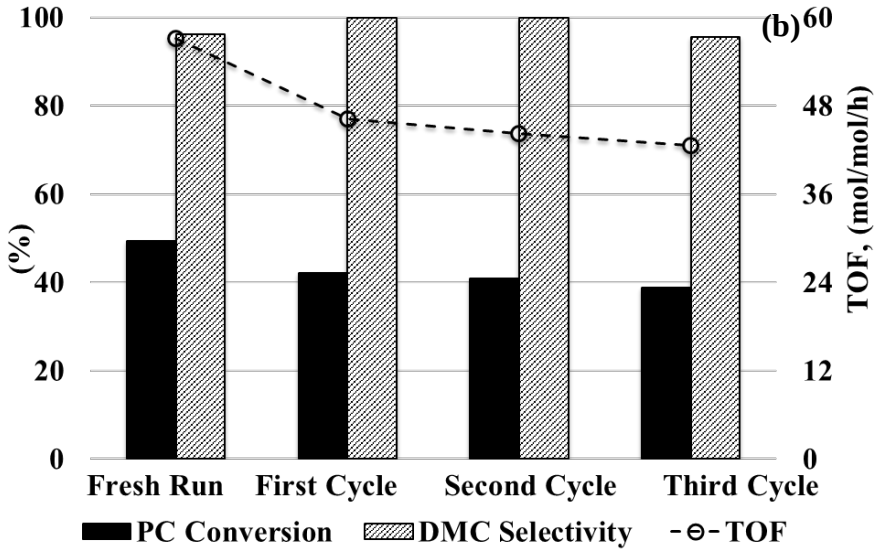

Figure 4-16 (a) Leaching testing and (b) Recycle experiments. Reaction conditions: PC, 1.1 kmol/m^3; methanol, 22.2 kmol/m^3; catalyst, 5 kg/m^3; T=140 °C; 0.69 MPa N_2.

4.3.7 Proposed Mechanism

As Fe is not active for the reaction, we propose that Mn in the Fe–Mn complex forms the active sites. Fe in the catalyst structure acts as a metal-dispersing agent and a stabilizer of the cyano-bridged complex.[60] Additionally, double metal cyanide-catalyzed ring-opening polymerization of propene oxide has been reported previously.[74, 129, 153] Based on the foregoing results from reaction and complementary catalyst characterization studies, a plausible mechanism is proposed (Scheme 4-1). First, methanol would get activated by catalysts to form intermediate I.[60, 74, 129] Then, intermediate I assists in the ring-opening of the cyclic carbonate to form intermediate II.[60, 74, 129, 136, 153] This is followed by intermediate II decomposing into monotransesterified product 2-HMC, which was detected by GC MS. At the same time, intermediate II goes through transesterification with another molecular of intermediate I present in the reaction medium to form intermediate III. In the last step, intermediate III would decompose into DMC, PG and catalyst precursor consecutively.[85]

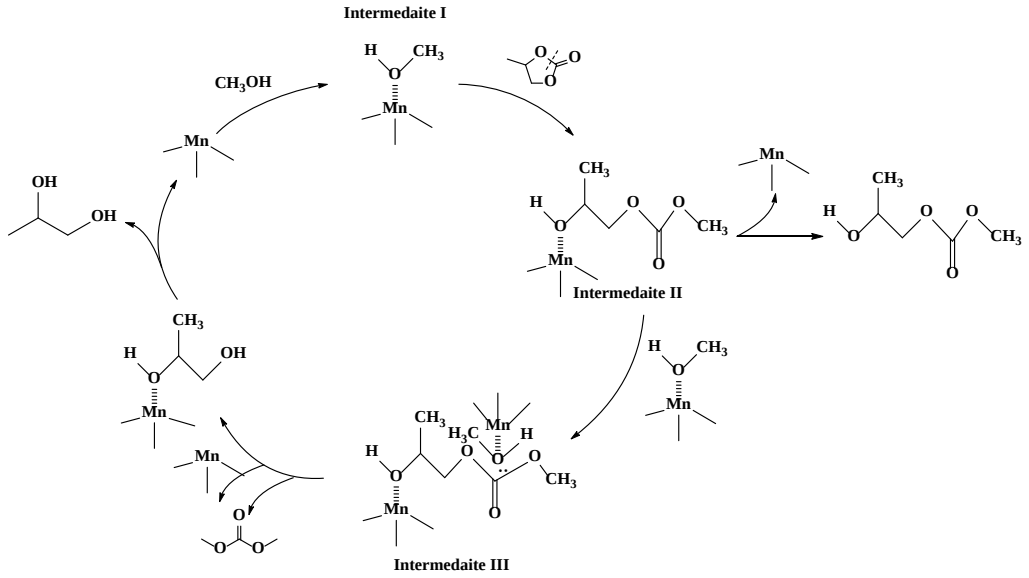

Scheme 4-1 Proposed reaction mechanism for transesterification of PC with methanol over Fe-Mn complex

4.4 Conclusion

In this chapter, several different double metal cyanide catalysts (Fe-Mn, Fe-Ni, Fe-Zn, Co-Mn, Co-Ni, Co-Zn) were prepared and their catalytic activity for transesterification of cyclic carbonates with methanol were measured. It is found that Fe-Mn catalyst has the highest TOF with stable activity in several consecutive experiments. Additionally, no leaching of active species was found, unlike the previously reported heterogeneous catalysts. The experimental results showed that Mn content has a significant influence on the catalytic activity. Various characterization techniques were tested to explore the structure and morphology of the double metal cyanide complex. TEM and XRD analyses confirmed that Fe-Mn complex represents a cubic crystalline structure. XPS analysis showed that all Fe exists in Fe^{2+} state. However, for the Mn element, 86.8% of Mn exists in Mn^{2+} state with only 13.2% in Mn^{4+} state. Furthermore, FTIR and DRIFT UV-Vis results verified the formation of a new mixed-metal complex of ferrocyanide moiety and Mn ions via bridging cyanide ligands. These results provide valuable insights into the reaction pathways underlying transesterification.

Chapter 5 Kinetic Modeling and Mechanistic Investigations of Transesterification of Propylene Carbonate with Methanol over Fe-Mn Double Metal Cyanide Catalyst

5.1 Introduction

Double metal cyanide catalysts were reported previously, but most of the reports were focused on exploring the morphological and structural aspects of different double metal cyanides. There is little information in published literature on the underlying reaction mechanism and kinetics over this kind of catalysts. Although, several reports discussed some insights on the possible activation modes of cyclic carbonates and methanol on metal catalysts,[44, 60, 67] there is lack of understanding on the intrinsic kinetics of transesterification of cyclic carbonates over double metal cyanide catalysts.

In this part of work, we report detailed kinetic modeling of transesterification of propylene carbonate (PC) with methanol over Fe-Mn double metal cyanide catalyst, which was found to be a non-leaching and stable catalyst for this reaction. The effects of several experimental parameters, including temperature (140-200 °C), initial PC concentration (1.1-4.3 kmol/m^3), initial methanol concentration (1.2-4.8 kmol/m^3) were studied. Power law rate model was examined by fitting the experimental concentration-time data and intrinsic kinetic parameters were estimated ensuring that the rate data were obtained under conditions of negligible mass transfer limitations. Additionally, different mechanistic models were also proposed and evaluated by fitting the model with the experimental data. Based on model discrimination procedure, a mechanistic models involving sequential activation of reactants and intermediates with catalyst was found to best fit the experimental data. The kinetic study in this chapter also provide a method for validating the reaction mechanism and better insight into the reaction mechanism.

5.2 Experimental

5.2.1 Materials

The chemicals used in this chapter is as that described in Chapter 4 section 4.2.1.

5.2.2 Reactor Setup and Procedures

The kinetic experiments on transesterification of PC with methanol were conducted in the same setup as described in Chapter 4 Section 4.2.3. The same experiment procedure was used.

5.3 Results and Discussion

5.3.1 Reaction Kinetics

Detailed kinetic models for PC transesterification were investigated using experimentally measured concentration-time profiles at different temperatures and different reaction conditions (Appendix IV Chapter 5). These profiles were used to capture the temporal evolution of various products including intermediates.

5.3.1.1 Concentration-Time Profiles

It is clear from the concentration-time profiles that the major products formed are DMC and PG, with a smaller but significant amount of mono transesterified product 2-hydroxypropyl methyl carbonate (2-HMC) under certain conditions. At 140 °C [Figure 5-1 (a)], the concentration of reactant PC decreased from 1.1 kmol/m^3 to 0.56 kmol/m^3 in 3 h. Concentrations of DMC and PG increased gradually with reaction time, while the formation of 2-HMC first increased and then decreased to nearly zero. When the temperature increased from 140 °C to 200 °C, the formation rates of products show a significant leap. More reaction profiles are available in Appendix IV Chapter 5. It is important to mention that data from 16 profiles at four different temperatures were used for the parameter estimation and model discrimination.

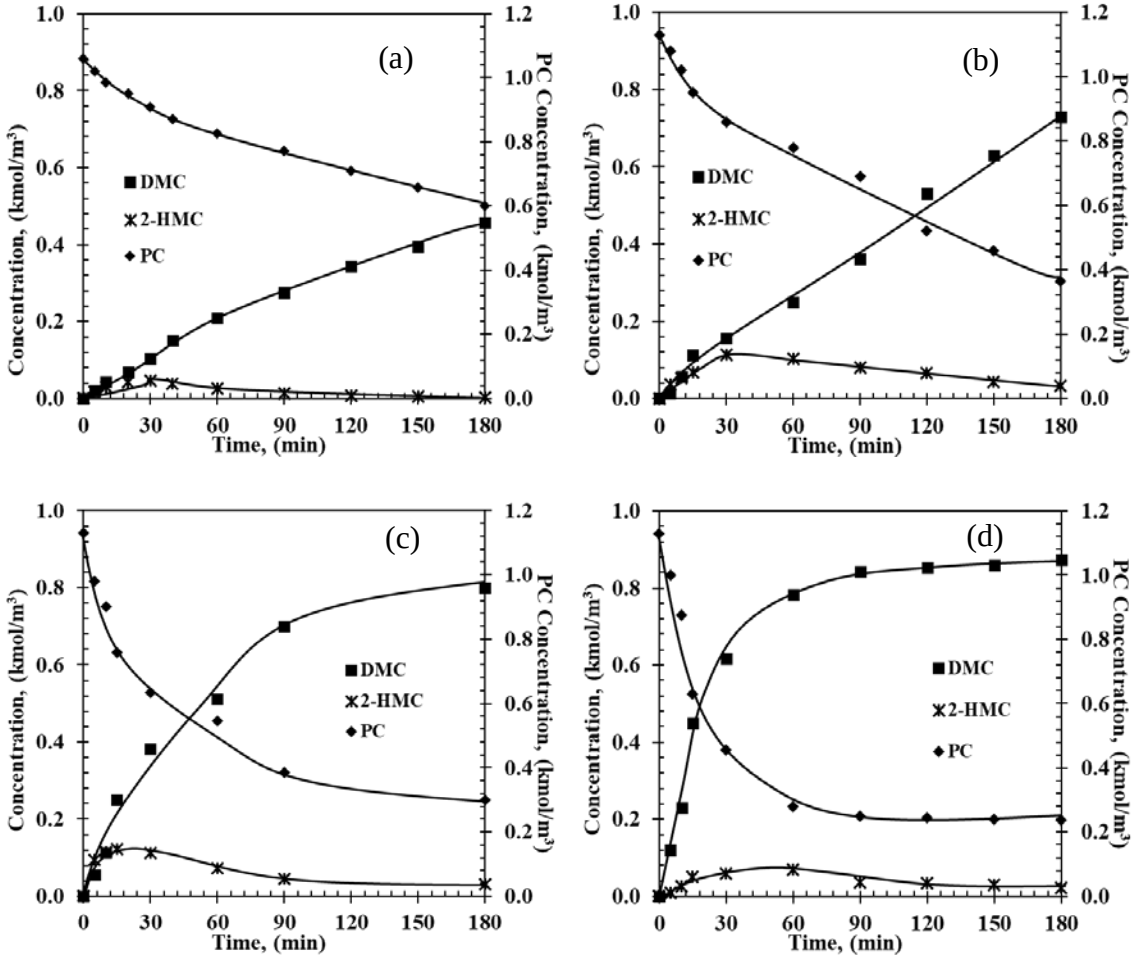

Figure 5-1 Temporal concentration-time profiles of PC conversion over Fe-Mn catalyst at (a) 140 °C; (b) 160 °C; (c) 180 °C; (d) 200 °C. Reaction conditions: PC: 1.1 kmol/m^3; methanol: 22.2 kmol/m^3; catalyst: 5 kg/m^3; 0.69 MPa initial N_2.

5.3.1.2 Analysis of mass transfer effect

Since transesterification reaction involves a liquid-solid catalytic reaction, mainly, liquid-solid and intraparticle mass transfer limitations for the limiting reactant, PC were considered, with methanol being in large excess. To assess the liquid-solid mass-transfer limitation between the reactant and catalyst, and intraparticle diffusion in the catalyst, the criteria described by Ramachandran and Chaudhari were used.[124] In these criteria, experimentally observed rates were compared with maximum rates of the mass transfer steps (liquid-solid and intraparticle). The

details of the calculations for a few cases are shown in Appendix II. This analysis showed that both liquid-solid and intraparticle diffusion limitations for the limiting reactant PC were negligible for this case and the experimental data were obtained in kinetic regime.

5.3.1.3 Effect of Substrates Concentration

The effect of initial substrate concentration on initial reaction rate was studied. Specifically, the effect of PC concentration on the reaction rate is shown in Figure 5-2 (a). As PC concentration increased from 1.1 to 4.3 kmol/m^3, the initial reaction rate increased from 0.65×10^{-2} to 2.32×10^{-2} kmol/(m^3·min) at 140 °C, suggesting first-order dependence if the initial reaction rate with PC concentration. Similar trends were also observed at 160 °C, 180 °C and 200 °C with higher reaction rates. The effect of methanol concentration on initial reaction rate shows a similar trend at 200 °C [Figure 5-2 (b)].

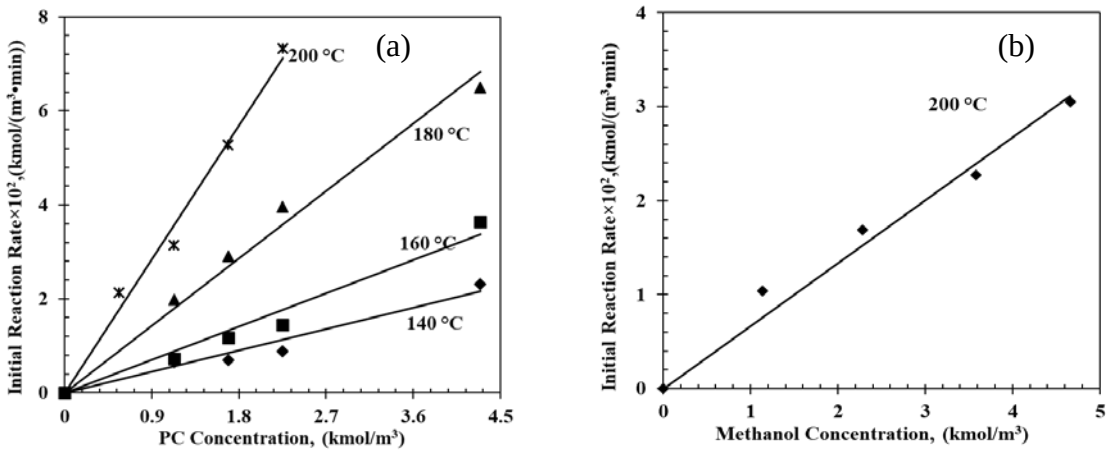

Figure 5-2 Effects of (a) PC initial concentration and (b) methanol concentration on initial reaction rates. Reaction conditions: (a). methanol, 17.9-22.8 kmol/m^3; catalyst, 5 kg/m^3; T=140 °C; 0.69 MPa N_2; (b). PC, 9.3-10.8 kmol/m^3; catalyst, 5 kg/m^3; T=140 °C; 0.69 MPa N_2

5.3.1.4 Apparent activation energy

First-order forward reaction rate constants were obtained from the slope of the regression line in Figure 5-2 (a). The estimated forward reaction rate constants at 140 °C, 160 °C, 180 °C and

200 °C for PC transesterification reaction were 0.50 min^{-1}, 0.79 min^{-1}, 1.60 min^{-1} and 3.17 min^{-1}, respectively. The apparent activation energy for the PC systems was estimated as 50.4 kJ/mol, the pre-exponential factor was found to be 1.07×10^4 min^{-1} [Figure 5-3 (a)].

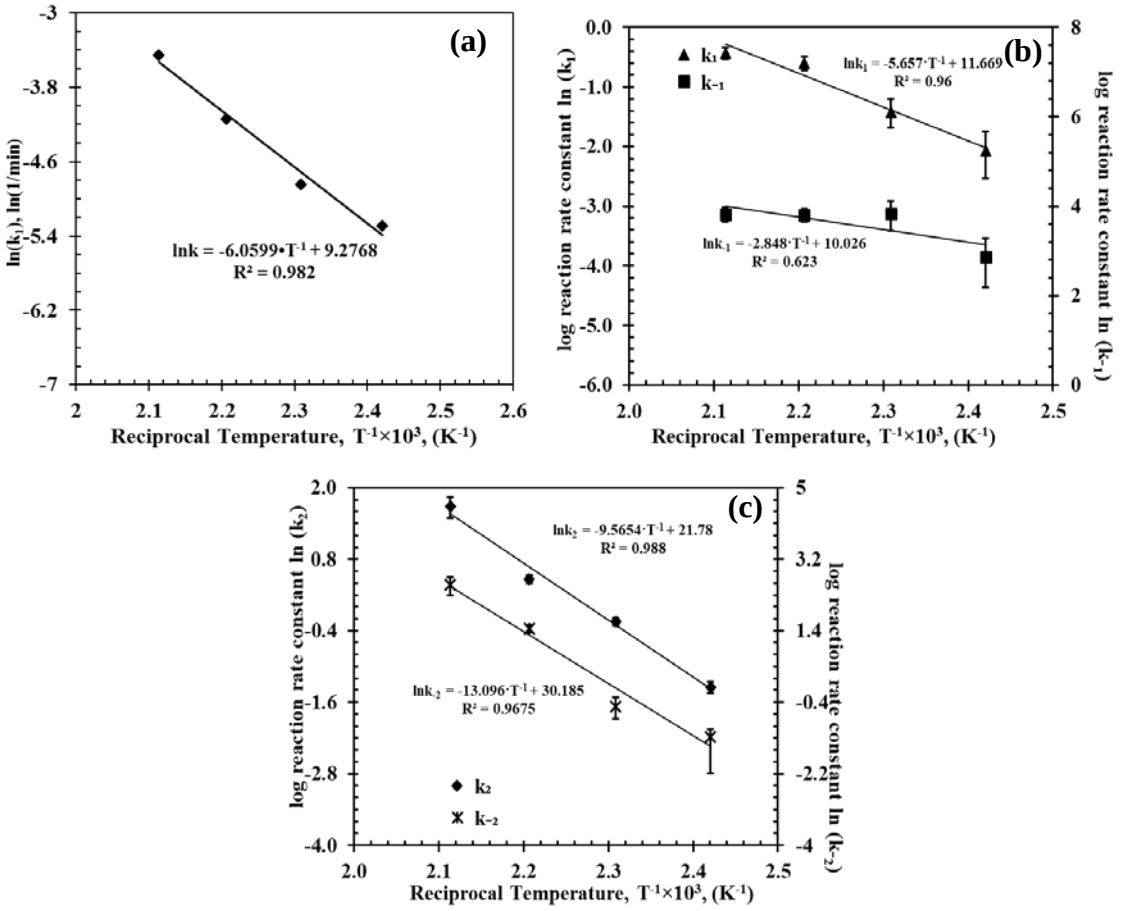

Figure 5-3 Arrhenius plot. (a) Initial reaction rate, Parameters estimation from modelling with two-step power law for (b) first step, (c) second step

5.3.1.5 Two-step Power Law Model

The following reaction scheme (Scheme 5-1) was considered for kinetic analysis. The mass balance equations of each component in a batch reactor are given in Equation (1)-(6).

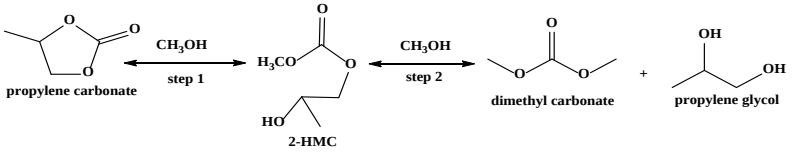

Scheme 5-1 Two-step reaction scheme

$$r_1 = k_1[PC][MeOH] - k_{-1}[2-HMC] \quad (1)$$

$$r_2 = k_2[2-HMC][MeOH] - k_{-2}[DMC][PG] \quad (2)$$

$$\frac{d[PC]}{dt} = -\omega r_1 \quad (3)$$

$$\frac{d[MeOH]}{dt} = -\omega(r_1 - r_2) \quad (4)$$

$$\frac{d[DMC]}{dt} = \frac{d[PG]}{dt} = \omega r_2 \quad (5)$$

$$\frac{d[2HMC]}{dt} = \omega(r_1 - r_2) \quad (6)$$

Where, r_1 and r_2 are specific reaction rates for step 1 and step 2, k_1, k_{-1} and k_2, k_{-2} are temperature dependent forward and reversible reaction rate constants for step 1 and step 2, respectively, while ω is the catalyst concentration.

To simulate the experimental concentration-time data, Equations (1)-(6) were solved with an optimization routine using Athena Visual Studio software. For the parameter estimation and model discrimination, several convergence criteria were used, as summarized in section 3.2.4. Typical results of experimental and predicated concentration-time profiles for various chemical components are shown in Figure 5-4. It can be seen that the two-step power law model fits the experimental data reasonably well.

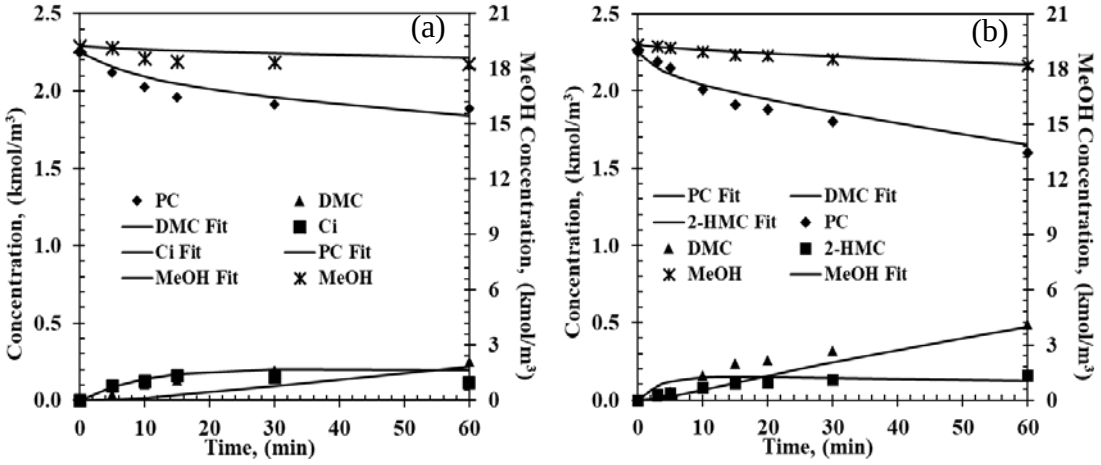

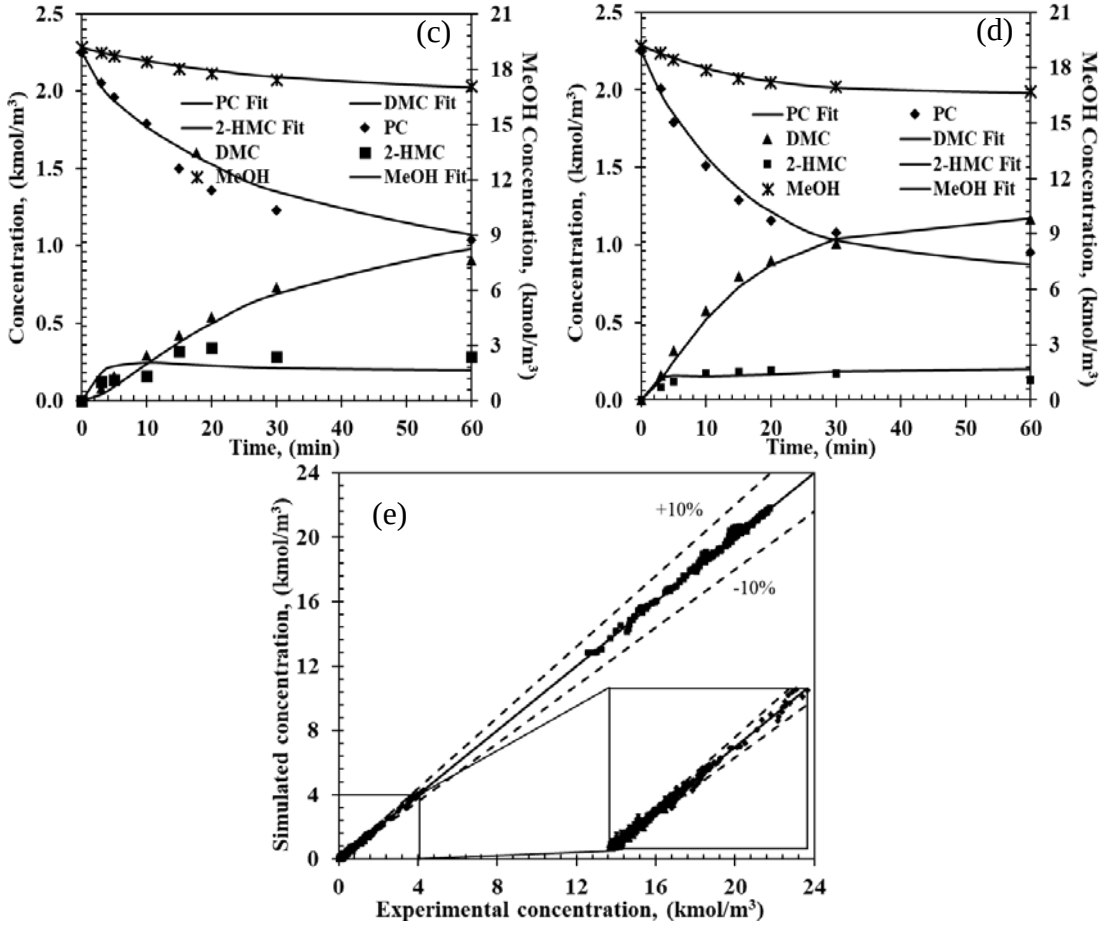

Figure 5-4 Experimental and predicated concentration-time profiles from two-step power law. Reaction conditions: PC, 2.25 kmol/m^3; methanol, 20.5 kmol/m^3; catalyst, 5 kg/m^3; 0.69 MPa N_2. (a) 140 °C, (b) 160 °C, (c) 180 °C, (d) 200 °C, (e) Parity plot of the simulated and experimental concentrations for the four chemicals

A similar procedure was followed for all the 16 experiments at four different temperatures. The predicated data are compared with the experimental data in Figure 5-4 (e), which shows a high accuracy of the power law model. Therefore, the two-step power law can be applied to predict the temporal concentration-time profiles in the range of the experimental conditions studied. The first order dependence on methanol concentration is not consistent with the overall stoichiometry but is consistent with the two step reaction pathway shown in Scheme 5-1.

Optimized values of the rate parameters are shown in Arrhenius plot in Appendix III while the reaction rate constants and activation energies are presented in Table 5-1. An activation energy

of 47.0±20.2 kJ/mol was observed for the mono-transesterification of PC with methanol using Fe-Mn as the catalyst. In contrast, a much higher activation energy (79.6±9.8 kJ/mol) was observed for the second step transesterification of 2-HMC with methanol.

Table 5-1 Values of activation energy and rate constants derived from power law

Rate Constants	140 °C[a]	160 °C[a]	180 °C[a]	200 °C[a]	E_a[b]
$k_1\times10^1$, ($m^6\cdot min^{-1}\cdot kmol^{-2}$)	1.26±0.47	2.42±0.57	5.50±0.61	6.52±0.59	47.0±20.2
$k_{-1}\times10^{-1}$, ($m^3\cdot min^{-1}\cdot kmol^{-1}$)	1.76±0.88	4.64±1.47	4.49±0.63	4.57±0.72	23.7±27.2
k_2, ($m^6\cdot min^{-1}\cdot kmol^{-2}$)	0.26±0.024	0.78±0.049	1.60±0.12	5.38±0.97	79.6±9.8
k_{-2}, ($m^6\cdot min^{-1}\cdot kmol^{-2}$)	0.28±0.06	0.60±0.16	4.29±0.43	12.9±2.89	108.9±14.6

[a] Rate constants with 95% confidence level
[b] Unite of E_a: kJ/mol, detailed error analysis is in Appendix I.

5.3.2 Mico Kinetic Modeling

5.3.2.1 Reaction Mechanism and Proposed Models

Transesterification reaction between cyclic carbonates and methanol generally follows the following main steps: 1) the formation of -M-O-CH_3 intermediate through the interaction between CH_3O^- from methanol and active metal center[52, 121, 123], 2) the formation of mono-transesterified product (2-HMC and 1-HP-2-MC) from activated methanol with PC or with activated PC[67, 84, 154-157]; 3) further transesterification of mono-transesterified product/activated mono-transesterified product with activated methanol to form the final product DMC and PG. However, a specific activation sequence of methanol, PC and 2-HMC is not obvious from the general trends observed. To assess this problem and better understand the catalytic reaction mechanism, four kinetic models (which can clarify this problem) were proposed (Scheme 5-2) based on possible sequential reaction steps. Each model was fitted with experimental data and discriminated based on the predictive ability of the models with reaction parameters.

$S + MeOH \leftrightarrow I$	$S + MeOH \leftrightarrow I$
$I + PC \leftrightarrow II$	$I + PC \leftrightarrow II$
$II \leftrightarrow 2 - HMC + S$	$II \leftrightarrow 2 - HMC + S$
$II + I \leftrightarrow III + S$	$2 - HMC + I \leftrightarrow III$
$III \leftrightarrow DMC + PG + S$	$III \leftrightarrow DMC + PG + S$
Model (i)	**Model (ii)**
$S + MeOH \leftrightarrow I$	$S + MeOH \leftrightarrow I$
$S + PC \leftrightarrow II$	$S + PC \leftrightarrow II$
$I + II \leftrightarrow III + S$	$I + II \leftrightarrow III + S$
$III \leftrightarrow 2 - HMC + S$	$III \leftrightarrow 2 - HMC + S$
$III + I \leftrightarrow IV + S$	$2 - HMC + I \leftrightarrow IV$
$IV \leftrightarrow DMC + PG + S$	$IV \leftrightarrow DMC + PG + S$
Model (iii)	**Model (iv)**

Scheme 5-2 Proposed kinetic models of transesterification of PC with methanol using Fe-Mn as catalyst

For model (i), methanol is first activated by Fe-Mn complex to form the intermediate I[60, 74] Then, PC would react with intermediate I to form intermediate II,[60, 74] followed by decomposition of intermediate II into mono-transesterified product, 2-HMC while releasing the catalytic site. Further, intermediate II reacts with another activated methanol (intermediate I) to form intermediate III followed by decomposition into product DMC and PG. The only difference between model (ii) and model (i) is in step (4), where 2-HMC is assumed to react with activated methanol (intermediate I).

For model (iii), methanol is first activated by Fe-Mn complex to form the intermediate I[60, 74]; simultaneously, PC is activated to form intermediate II[131]. Then, intermediates I and II react to form intermediate III followed by decomposition into mono-transesterified product 2-HMC and catalyst. Intermediate III further reacts with another activated methanol (intermediate I) species to form intermediate IV which decomposes into product DMC and PG. The only difference between model (iv) and model (iii) is in step (5), where 2-HMC is assumed to react with activated methanol (intermediate I) instead.

5.4.2 Rate Equations and Batch Reactor Equations

Rate equations for each step of the models are summarized in Scheme 5-3 while the corresponding batch reactor equations are summarized in Table 5-2.

$$r_1 = k_1[S][MeOH] - k_{-1}[I] \qquad r_1 = k_1[S][MeOH] - k_{-1}[I]$$
$$r_2 = k_2[I][PC] - k_{-2}[II] \qquad r_2 = k_2[I][PC] - k_{-2}[II]$$
$$r_3 = k_3[II] - k_{-3}[HMC][S] \qquad r_3 = k_3[II] - k_{-3}[HMC][S]$$
$$r_4 = k_4[II][I] - k_{-4}[III][S] \qquad r_4 = k_4[HMC][I] - k_{-4}[III]$$
$$r_5 = k_5[III] - k_{-5}[DMC][PG][S] \qquad r_5 = k_5[III] - k_{-5}[DMC][PG][S]$$

Model (i) **Model (ii)**

$$r_1 = k_1[S][MeOH] - k_{-1}[I] \qquad r_1 = k_1[S][MeOH] - k_{-1}[I]$$
$$r_2 = k_2[S][PC] - k_{-2}[II] \qquad r_2 = k_2[S][PC] - k_{-2}[II]$$
$$r_3 = k_3[I][II] - k_{-3}[III][S] \qquad r_3 = k_3[I][II] - k_{-3}[III][S]$$
$$r_4 = k_4[III] - k_{-4}[HMC][S] \qquad r_4 = k_4[III] - k_{-4}[HMC][S]$$
$$r_5 = k_5[III][I] - k_{-5}[IV][S] \qquad r_5 = k_5[HMC][I] - k_{-5}[IV]$$
$$r_6 = k_6[IV] - k_{-6}[DMC][PG][S] \qquad r_6 = k_6[IV] - k_{-6}[DMC][PG][S]$$

Model (iii) **Model (iv)**

Scheme 5-3 Rate equations for each step in each model

Table 5-2 Batch reactor equations

Models	Batch reactor equations			
Model i	$\frac{d[PC]}{dt} = -r_2$	$\frac{d[MeOH]}{dt} = -r_1$	$\frac{d[C_{2-HMC}]}{dt} = r_3$	$\frac{d[DMC]}{dt} = \frac{d[PG]}{dt} = r_5$
	$\frac{d[S]}{dt} = -r_1 + r_3 + r_4 + r_5$	$\frac{d[I]}{dt} = r_1 - r_2 - r_4$	$\frac{d[II]}{dt} = r_2 - r_3 - r_4$	$\frac{d[III]}{dt} = r_4 - r_5$
Model ii	$\frac{d[PC]}{dt} = -r_2$	$\frac{d[MeOH]}{dt} = -r_1$	$\frac{d[C_{2-HMC}]}{dt} = r_3 - r_4$	$\frac{d[DMC]}{dt} = \frac{d[PG]}{dt} = r_5$
	$\frac{d[S]}{dt} = -r_1 + r_3 + r_5$	$\frac{d[I]}{dt} = r_1 - r_2 - r_4$	$\frac{d[II]}{dt} = r_2 - r_3$	$\frac{d[III]}{dt} = r_4 - r_5$
Model iii	$\frac{d[PC]}{dt} = -r_2$	$\frac{d[MeOH]}{dt} = -r_1$	$\frac{d[C_{2-HMC}]}{dt} = r_4$	$\frac{d[DMC]}{dt} = \frac{d[PG]}{dt} = r_6$
	$\frac{d[S]}{dt} = -r_1 - r_2 + r_3 + r_4 + r_5 + r_6$	$\frac{d[I]}{dt} = r_1 - r_3 - r_5$	$\frac{d[II]}{dt} = r_2 - r_3$	$\frac{d[III]}{dt} = r_3 - r_4 - r_5$
	$\frac{d[IV]}{dt} = r_5 - r_6$			

	$\frac{d[PC]}{dt} = -r_2$	$\frac{d[MeOH]}{dt} = -r_1$	$\frac{d[C_{2-HMC}]}{dt} = r_4 - r_5$	$\frac{d[DMC]}{dt} = \frac{d[PG]}{dt} = r_6$
Model iv	$\frac{d[S]}{dt} == -r_1 - r_2 + r_3 + r_4 + r_6$	$\frac{d[I]}{dt} = r_1 - r_3 + r_5$	$\frac{d[II]}{dt} = r_2 - r_3$	$\frac{d[III]}{dt} = r_3 - r_4$
	$\frac{d[IV]}{dt} = r_5 - r_6$			

For all the four kinetic models, no specific step was assumed as rate-determining, which allows the evaluation of rate parameters for each reaction step including those involving catalytic intermediate species.

The initial conditions are:

at t=0, [PC]=$[PC]_0$, [MeOH]=$[MeOH]_0$, [DMC]=[PG]=[2-HMC]=0, [S]=C_0, [I]=[II]=[III]=[IV]=0,

where, $[PC]_0$, $[MeOH]_0$, C_0 represent the initial concentrations of PC, methanol and catalyst precursor, respectively. For solving these ODEs, reasonable initial guesses were provided for all the rate constants. The ODEs were solved using Athena Visual Studio. Identical convergence criteria and constraints were used as those used in the power law models.

5.4.3 Proposed Mechanism Based on Model Discrimination

The quality of the fit of models (i)–(iv), is compared in Table 5-3. The estimated parameters for model (ii)–(iv) are shown in Appendix III. Model (i) fits the best compared to the other three models and also realistic parameter values. The bases for discrimination of the various models is summarized in Table 5-3.

Table 5-3 Basis for Discrimination of Models (i)-(iv)

Models	Model Discrimination
Model i	Best fitted with experimental data
Model ii	Rate constants (k_{-3} and k_{-4}) decrease with increasing temperature, and 95% confidence level > 120% for k_2 and k_{-2}
Model iii	Negative k_{-1} at 160 °C, the constants do not agree with Arrhenius Equation
Model iv	95% confidence level > 120% for k_4 at 160 °C, activation energy of step 4 > 400 kJ/mol

Therefore, the mechanism represented by model (i) was deemed to best represent the experimental kinetic data. A schematic description of the mechanism represented in Model (i) is presented in Scheme 5-4. The kinetic parameters obtained from fitting Model (i) with experimental data are listed in Table 5-4. The activation energy values for each step are estimated from the Arrhenius Equations (Appendix III). Additionally, a comparison of predicated and experimental data at different temperatures is shown in Figure 5-5. The excellent match between the experimental and predicated results at various reaction conditions indicates that the proposed reaction mechanism in Scheme 5-4 represents the transesterification of PC and methanol satisfactorily.

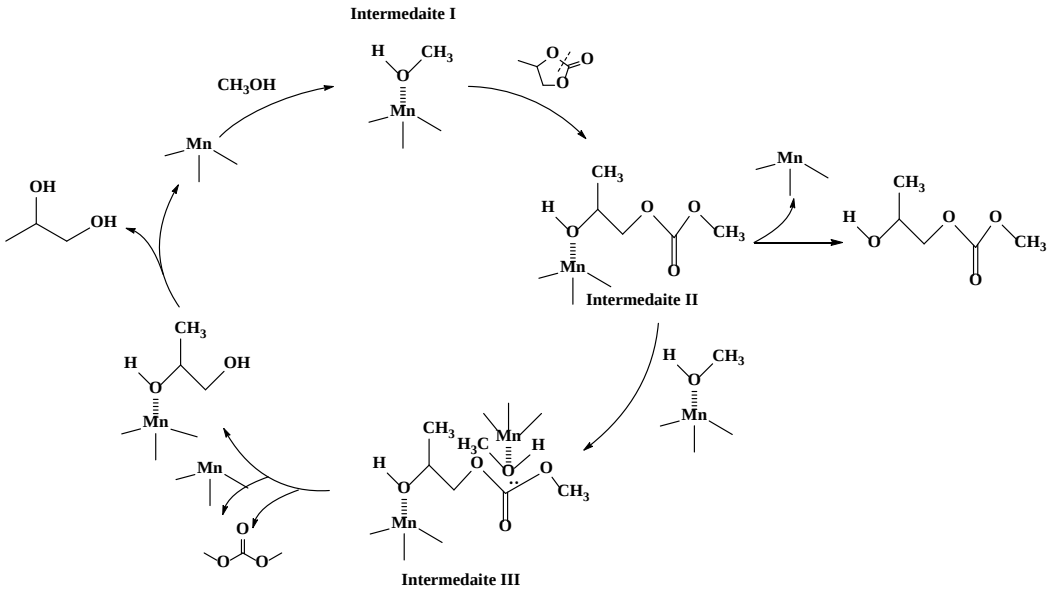

Scheme 5-4 Proposed reaction mechanism based on model discrimination

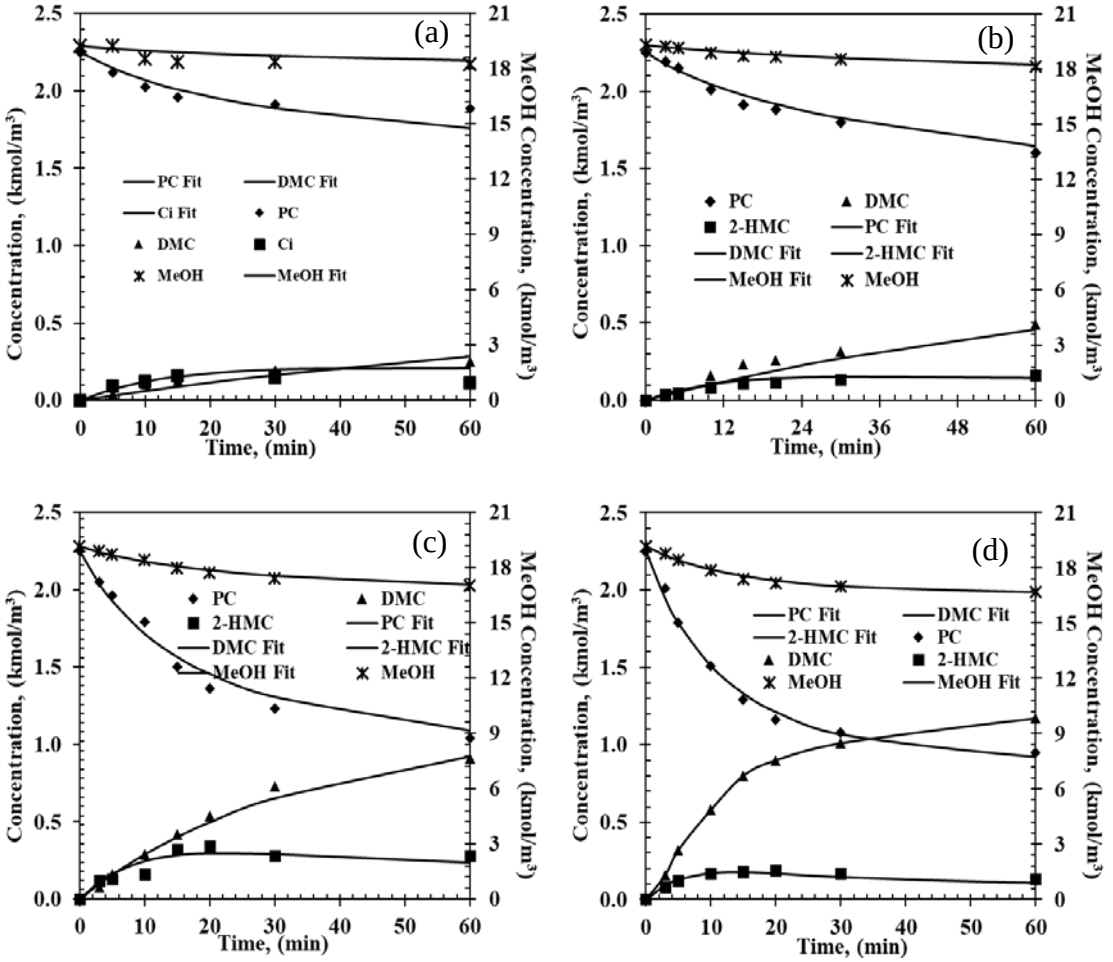

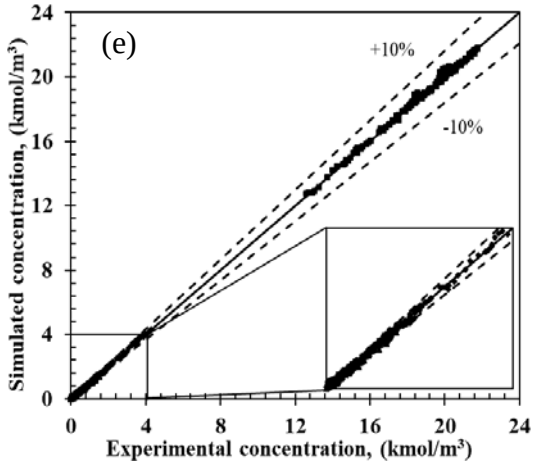

Figure 5-5 Experimental and predicated concentration-time profiles from the micro kinetic model. Reaction conditions: PC, 2.25 kmol/m^3; methanol, 20.5 kmol/m^3; catalyst, 5 kg/m^3; 0.69 MPa N_2. (a) 140 °C, (b) 160 °C, (c) 180 °C, (d) 200 °C, (e) parity plot

Table 5-4 Rate constants and activation energy for each reaction step

Rate Constants	140 °C[a]	160 °C[a]	180 °C[a]	200 °C[a]	E_a[b]
$k_1\times10^{-2}$, ($m^3\cdot min^{-1}\cdot kmol^{-1}$)	0.51±0.01	1.22±0.06	2.79±0.06	4.81±0.11	61.7±2.7
$k_{-1}\times10^{-4}$, (min^{-1})	2.15±0.31	5.11±0.20	8.15±0.52	14.0±1.04	49.6±7.8
$k_2\times10^{-4}$, ($m^3\cdot min^{-1}\cdot kmol^{-1}$)	2.80±0.26	7.18±0.27	1.24±0.82	17.20±0.85	49.1±5.1
$k_{-2}\times10^{-6}$, (min^{-1})	0.48±0.10	2.11±0.0.06	4.28±0.50	6.26±0.17	68.8±11.3
$k_3\times10^{-2}$, (min^{-1})	1.21±0.10	2.56±0.04	8.13±1.25	9.50±0.70	60.0±8.4
k_{-3}, ($m^3\cdot min^{-1}\cdot kmol^{-1}$)	2.32±0.19	3.98±0.69	6.85±1.36	8.34±0.67	35.8±10.8
$k_4\times10^{-5}$, ($m^3\cdot min^{-1}\cdot kmol^{-1}$)	1.84±0.25	5.06±1.30	8.17±0.46	16.80±2.39	58.0±13.9
$k_{-4}\times10^{-4}$, ($m^3\cdot min^{-1}\cdot kmol^{-1}$)	0.68±0.20	1.66±1.36	1.99±0.33	2.48±0.39	33.4±44.2
$k_5\times10^{-3}$, (min^{-1})	0.23±0.06	0.90±0.21	2.96±0.48	5.16±0.68	86.2±14.8
k_{-5}, ($m^6\cdot kmol^{-2}\cdot min^{-1}$)	3.17±0.62	8.23±5.67	9.20±1.59	18.68±2.78	44.29±37.3

[a] Rate constants with 95% confidence level
[b] Unit of E_a: kJ/mol, the detail error calculation is in Appendix I.

5.5 Conclusion

A detailed kinetic study for transesterification of PC with methanol using Fe-Mn double metal cyanide revealed that both a two-step power law model and a microkinetic model based on

transesterification mechanism were found to fit the experimental data well. Four microkinetic models based on different activation sequence of methanol, PC and 2-HMC were considered. Through model discrimination based on the quality of fit between experimental and model-predicted data, it was concluded that methanol was first activated to form intermediate I, then PC was activated by activated methanol (intermediate I) instead of the catalyst precursor to form intermediate II. Next, the intermediate II instead of 2-HMC itself reacted with activated methanol (intermediate I) to form intermediate III, which decomposed into to DMC and PG, the major products. These results provide valuable insights into the reaction pathways underlying transesterification.

Chapter 6 Transesterification of Dimethyl Carbonate (DMC) with Phenol for the Synthesis of Diphenyl Carbonate (DPC)

6.1 Introduction

Diphenyl carbonate (DPC) is used as an important intermediate in the non-phosgene route for polycarbonate and also as phenylating and methoxycarbonylating agent.[30, 158-159] It is also an excellent solvent in pharmaceuticals, cosmetics, and synthetic resins manufacture.[160] Conventionally, DPC is manufactured through phosgenation of phenol in the presence of bases (Scheme 6-1), which accounts for around 70% of the DPC manufactured. However, this method uses highly toxic and corrosive phosgene as a raw material. Additionally, stoichiometric amounts of HCl and NaCl are formed as co-products posing serious environmental threats in waste disposal.[30, 161]

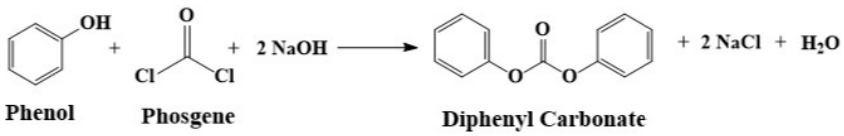

Scheme 6-1 DPC synthesis by reaction of phosgene and phenol

Compared to the phosgene route, manufacture of DPC through the transesterification of DMC and phenol is an more environmentally friendly and greener route.[162-163] This involves a two-step process consisting of the transesterification of phenol and DMC to methyl phenyl carbonate (MPC), followed by further transesterification of phenol and MPC or the disproportionation of MPC to DPC, as shown in Scheme 6-2. Due to critical thermodynamic limitations, this reaction suffers from low DPC yields and selectivity.[162-165] Step (2) is reported to be more restricted than step (1) (Kp =10^{-3}~10^{-4} for step 1 and 10^{-7} for step 2).[1, 30, 164] In a batch reactor with an equimolar feed of DMC and phenol, an equilibrium DMC conversion of 3% can be expected.[163] Therefore, instead of transesterification of MPC with phenol to DPC,

disproportionation of MPC to DPC and DMC (step 3 in Scheme 6-2) is considered more preferable. The DMC produced from step 3 can be recycled to step 1, and the methanol produced in step 1 can be recycled to the DMC production step. Additionally, anisol and CO_2 can be produced as easily occurring side reactions, such as etherification and decarboxylation. Furthermore, the reaction suffers from lower reaction rates. To overcome the technical barriers described above, many alternative methods have been proposed, involving development of active catalyst systems, optimization of reaction conditions and reactive distillation.[30]

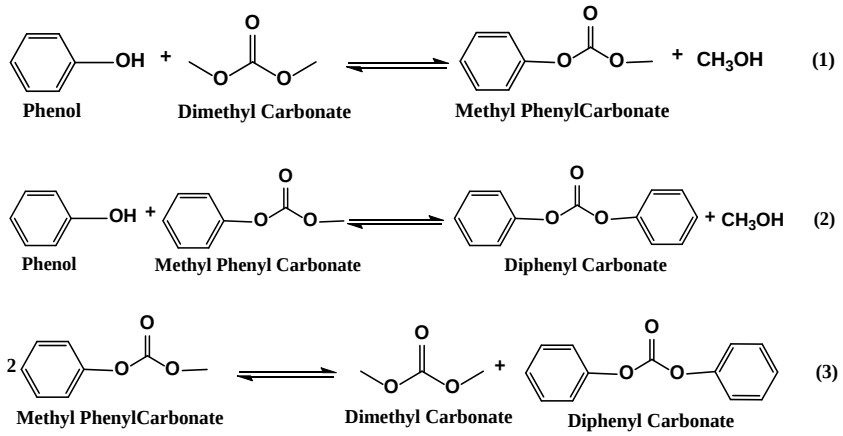

Scheme 6-2 DPC synthesis from the transesterification reaction of phenol with DMC

6.2 Previous Work

6.2.1 Reaction Methods

Several attempts on alternative methods have been investigated to push the chemical equilibrium in forward direction, such as using azeotrope-forming agent[166], using adsorbers[167], batch-column setup,[11, 168] and reactive distillation technology. When azeotrope-forming agent such as heptane was used, low MPC and DPC yield was obtained and also a large amount of azeotropic agent was needed.[166] If methanol adsorber is used, not only large amount of adsorber is needed, the desorption of methanol from the adsorber is not quantitative. Furthermore, if batch-column setup was used, the reaction rate is slow, leading to low productivity of MPC and DPC. Compared

to these methods, reactive distillation technology is more attractive. As the reaction proceeds at higher reaction rates, and higher MPC and DPC yields can be obtained in RD column.[169]

In recent years, there has been increasing interest in process intensification involving integrated or hybrid operations or units, which can improve the energy efficiency to increase the sustainability.[170] Reactive distillation (RD), integrating chemical reaction with simultaneous distillation separation is one of the best-known example of a process intensification process.[171-172] RD process results in cost reduction through reducing the number of equipment required to achieve the same goal compared to the conventional processes. RD is a well-established operation unit and has been successfully applied industrially for several chemical equilibrium-limited reactions, such as esterification, transesterification and etherifications.[173-176]

The transesterification reaction between DMC and phenol is a thermodynamic equilibrium reaction, for which the equilibrium constant was reported to be very low.[177] Sun et al. reported equilibrium constant for step 1 (Scheme 6-2) as 9×10^{-4}, while 1.86×10^{-4} and 0.27 were reported for step 2 and 3 respectively.[178] Additionally, the complex thermodynamic behavior (DMC and methanol forms azeotropic components) results in difficulties in separation and purification steps. Hence, a conventional chemical process requires large amount of recycle streams, leading to difficult separation as well as high operational cost.[179] The reaction is an excellent candidate for conducting in a reactive distillation column to achieve high conversions of reactants.[180-181] By using reactive distillation technology, the intermediate product methanol and DMC can be easily separated from the other components. Therefore, the conversion of DMC and phenol in the transesterification step can be increased. RD technology has been successfully used for the transesterification of DMC with phenol, with high DPC selectivity (99.999%).[1]

6.2.2 Catalyst Development

Transesterification of DMC with phenol has been studied previously using a variety of homogeneous and heterogeneous catalysts. Some of the typical results are summarized in Table 6-1.

Table 6-1 Catalyst for transesterification of DMC with phenol

#	Catalyst	T(°C)	X (Phenol) (%)	Y(DPC) (%)	Y(MPC) (%)	Ref
1	Bu_2SnO	180	DMC 21	4.0	16.7	[182]
2	$AlCl_3$	98	15.5	—	14.7	[11]
3	$Ti(OBu)_4$	150-180	DMC 20.2	1.5	18.7	[163]
4	$Pb(OPh)_2$	195				[183]
5	MoO_3/SiO_2	160-170	17.3	48	17.1	[184]
6	Pb_3O_4-ZnO	180	40.8	45.6	—	[185]
7	Core shell TiO_2/SiO_2	150-180	41.8	17.7	24.1	[186]
8	V-Cu compound	15.-180	37.2	15.6	20.2	[187]

Typical homogeneous catalysts used are lead compounds, Lewis acids and Lewis acid-forming transition metals,[11, 188] organotin compounds,[189] alkali metals and metal alkoxides,[166] complex compounds of zinc, copper, titanium.[166] These proposed catalysts are all reported to give high MPC or DPC yields with high catalytic activity.

Although, high DPC yield can be derived using homogeneous catalysts using RD technology, it is difficult to separate and recover catalysts from products. Therefore, intensive research has been focused on developing heterogeneous catalyst systems. Several types of heterogeneous catalysts have been investigated and reported for the transesterification of DMC with phenol, including supported molybdenum oxide[184, 190], different silica–titania [165, 186, 191-193] and a series of lead oxides.[185, 194] Heterogeneous catalysts have comparatively lower DPC yield, and hence development of heterogeneous catalysts is still a subject of extensive study.

6.1.3 Reaction Mechanism

Conversion of DMC to DPC involves several steps, including transesterification of DMC, transesterification of MPC, disproportionation of MPC and side reactions such as methylation. However, detailed mechanisms of these steps are still debated.

Shaikh and Sivaram proposed a mechanism of formation of diaryl carbonates over dibutyltin oxide [$(C_4H_9)_2SnO$] catalyst.[195] They proposed that carbonyl activation by tin coordination was a main step, initialized by nucleophilic attack of the aryloxy or alkoxy group on the carbonyl group.[196-197] Two step consecutive nucleophilic attack of the aryloxy or alkoxy group on the carbonyl group leads to the final product. Later, Wang and coworkers proposed another mechanism for transesterification of dimethyl carbonate with phenol in the presence of dibutyltin oxide [$(C_4H_9)_2SnO$] catalysts.[198] Three steps involving, generation of active species, transesterification and disproportion, and regeneration of active species were proposed in this mechanism. It was believed that instead of dibutyltin oxide, intermediate I [dimeric tetraorganodistannoxane $[Bu_2Sn(OPh)OSnBu_2O(Ph)]_2$ Scheme 6-3] formed from phenol and dibutyltin oxide was the true active species. Another two intermediates were also verified by GC MS to be existing during the reaction. Except for mechanisms proposed based on tin catalysts, there is little information available on the activation of reactants or reaction routes for transesterification of DMC based on other catalysts.

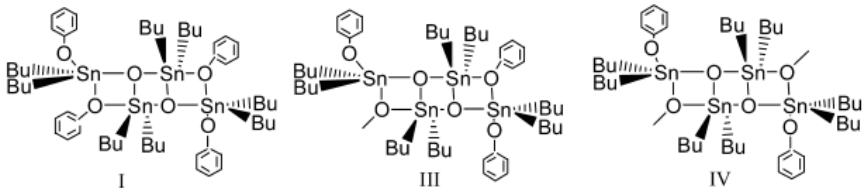

Scheme 6-3 Intermediates involved in the reaction

6.2.3 Reaction Kinetics

Kinetic models on DPC synthesis from DMC transesterification are summarized in Table 6-2. Haubrock's group proposed a reaction network for the formation of MPC and DPC based on experimental data from a batch reactor using tetrabutyl titanate [$Ti(OBu)_4$].[177] It was believed that over this catalyst, the formation of by-products can be negligible. Therefore, the three reversible reactions in Scheme 6-2 were considered during the kinetic modeling. Activation energies of 73.5 kJ/mol and 59.9 kJ/mol were calculated for the two different transesterification steps respectively.

A different reaction network was proposed by Sun's group[178], in which the formation of anisol as well as MPC and DPC are considered over mixed catalysts consisting of tetrabutyl titanate [$Ti(OBu)_4$] and dibutyltin oxide [$(C_4H_9)_2SnO$]. In this model, seven reactions were considered, including three pairs of forward and reversible reactions [Equation (1) to (3) in Scheme 6-2] and the formation of anisol from DMC and phenol through methylation. The overall reaction rates of phenol, DMC, MPC, DPC, MeOH and anisol were the combination of the four reactions. The activation energies for the steps 1 and 2 were 38.5 kJ/mol and 40.9 kJ/mol, respectively.

Yin's group[180] proposed an empirical kinetic model based on the mechanism proposed by Wang et al over dibutyltin oxide [$(C_4H_9)_2SnO$].[198] A detailed information on this mechanism is discussed in section 6.1.3. For this model, seven reversible pseudo-second-order reactions were considered. This empirical kinetic model was found to fit the experimental results well.

Table 6-2 Kinetic models for DPC synthesis from DMC transesterification

Catalyst	Reactor Type	Reaction Rate Law	Ref
$Ti(OBu)_4$	Batch	$R_1 = k_1 x_{cat}(\gamma_{PhOH} x_{PhOH} \gamma_{DMC} x_{DMC} - \frac{1}{K_{a,1}} \gamma_{MPC} x_{MPC} \gamma_{MeOH} x_{MeOH})$ $R_2 = k_2 x_{cat}(\gamma_{PhOH} x_{PhOH} \gamma_{MPC} x_{MPC} - \frac{1}{K_{a,2}} \gamma_{DPC} x_{DPC} \gamma_{MeOH} x_{MeOH})$	177

		$R_3 = k_3 x_{cat}(\gamma_{MPC}{}^2 x_{MPC}{}^2 - \frac{1}{K_{a,3}}\gamma_{DPC}x_{DPC}\gamma_{DMC}x_{DMC})$	
$Ti(OBu)_4$ + $(C_4H_9)_2SnO$	Batch	$R_1 = k_1 m_{cat}(C_{PhOH}C_{DMC} - \frac{1}{K_1}C_{MPC}C_{MeOH})$ $R_2 = k_2 m_{cat}(C_{PhOH}C_{MPC} - \frac{1}{K_2}C_{DPC}C_{MeOH})$ $R_3 = k_3 m_{cat}(C_{MPC}{}^2 - \frac{1}{K_3}C_{DPC}C_{DMC})$ $R_4 = k_4 m_{cat}C_{DMC}C_{PhOH}$	178
$(C_4H_9)_2SnO$	RD	$R_1 = k_1 C_{PhOH}C_{Cat} - k_{-1}C_I C_{H2O}$ $R_2 = k_2 C_I C_{DMC} - k_{-2}C_{III}C_{MPC}$ $R_3 = k_3 C_{III}C_{DMC} - k_{-3}C_{IV}C_{MPC}$ $R_4 = k_4 C_I C_{MPC} - k_{-4}C_{III}C_{DPC}$ $R_5 = k_5 C_{III}C_{MPC} - k_{-5}C_{IV}C_{DPC}$ $R_6 = k_6 C_{III}C_{PhOH} - k_{-6}C_I C_{MeOH}$ $R_7 = k_7 C_{IV}C_{PhOH} - k_{-7}C_{III}C_{MeOH}$	180

6.2.4 Challenges and Opportunities

As discussed above, DPC manufacture from transesterification of DMC with phenol is the most attractive route compared to other alternatives. Though, this transesterification process has been commercialized successfully, sever challenges need to be resolved for an improved process:

(1) Lack of stable, highly active and highly selective heterogeneous catalysts. As summarized previously, it is mainly the lead or titanium complexes that have been commercially used for the manufacture of DPC. Besides the environmental problems generated by lead catalysts, these homogenous catalysts are difficult to separate and recycle. Therefore, a stable, highly active and selective heterogeneous catalyst is still in demand.

(2) Lack of information on kinetics and mechanism. Transesterification reaction of DMC with phenol often involves several steps of reaction with equilibrium limitations, which is difficult to analyze accurately. The kinetics of the reaction and activation of reactants with catalysts are

not well understood. However, this information is important, to provide insightful information on optimizing and designing of improved catalysts and process.

6.3 Scope of Work

The scope of this work is to investigate the performance of different catalysts and understand the significant effect of reaction method through different reaction setup study as well as reaction parameter studies. Results from these fundamental studies provide guidance for the future design of active and stable heterogeneous catalyst, as well as understanding the mechanism of transesterification reaction between DMC with phenol.

6.4 Experimental Section

6.4.1 Materials

Phenol (99.0%, extra pure) was purchased from Acros Organics; diphenyl carbonate (DPC, 99.0%) and methyl phenyl carbonate (MPC, 97%) were purchased from Alfa Aesar; ethyl benzoate (EB, 99.0+%), DMC (extra dry, 98+%), and anisol (99.0+%) were purchased from Sigma-Aldrich. All chemicals were used without further treatment.

6.4.2 Experimental Setup and Procedure

As elaborated in introduction part, the transesterification reaction between DMC and phenol is critical thermodynamic limited reaction, low reactants conversion and products yield are usually derived. To improve the reactants conversion and products yield, three experimental setups (Figure 6-1) were tested and compared in this part of work.

For setup 1, reactions were carried out in a 100 ml stirred slurry reactor (Parr reactor) with provisions for temperature control, stirring speed control and pressure gauge for pressure monitor. A typical reaction was carried out as follows: certain amount of phenol, dimethyl carbonate, catalyst and EB (internal standard for GC analysis) were charged into the reactor. Then, the reactor

was flushed with N_2 for several times to get rid of air in the system. Next, the contents were heated to a desired temperature at stirring speed < 50 rpm. After the desired temperature was attained, the stirring rate was set to 1000 rpm, to initiate the reaction. After reaction, the liquid mixture was analyzed using GC after the reactor system cooling down.

For setup 2, the experiments were carried out in a three-necked round bottom flask made of glass, equipped with nitrogen inlet, magnetic stirring bar, thermometer and fractionating column connected to a liquid dividing head. Typical experimental procedure was as follows: certain amount of phenol, DMC, catalyst, and EB (internal standard for GC analysis) were charged into the three neck flask. The contents were heated to a desired temperature. When the temperature reached around 100 °C, liquid began to appear in the receiving flask. During the reaction procedure, an azeotrope of DMC and methanol was slowly collected in a receiver flask. When the distillation off rate of the DMC and methanol, reaction rate and heating rate reached equilibrium, the temperature in the reactor stayed constant. During the reaction, the vapor phase at the top of the fractionating column kept between 40~50 °C. At the end of the reaction, the liquid in both the reactor and the receiving flask was analyzed using GC.

Similar to the setup 2, typical experimental procedure for setup 3 is as follows: certain amount of phenol, catalyst, and EB (internal standard for GC analysis) were charged into the three neck flask. The contents were heated to a desired temperature. When the mixture was heated to around the desire temperature, DMC was pumped into the system and the reaction temperature was kept in a range of temperature under refluxing condition. When the distillation off rate of the DMC and methanol, reaction rate, heating rate and DMC pumping in rate reached equilibrium, the temperature in the reactor stayed constant. During the reaction, the vapor phase at the top of the fractionating column kept between 40~50 °C. Similar to the case in setup 2, DMC and methanol

azeotropic component was collected. At the end of the reaction, the liquid in both the reactor and the receiving flask was analyzed using GC.

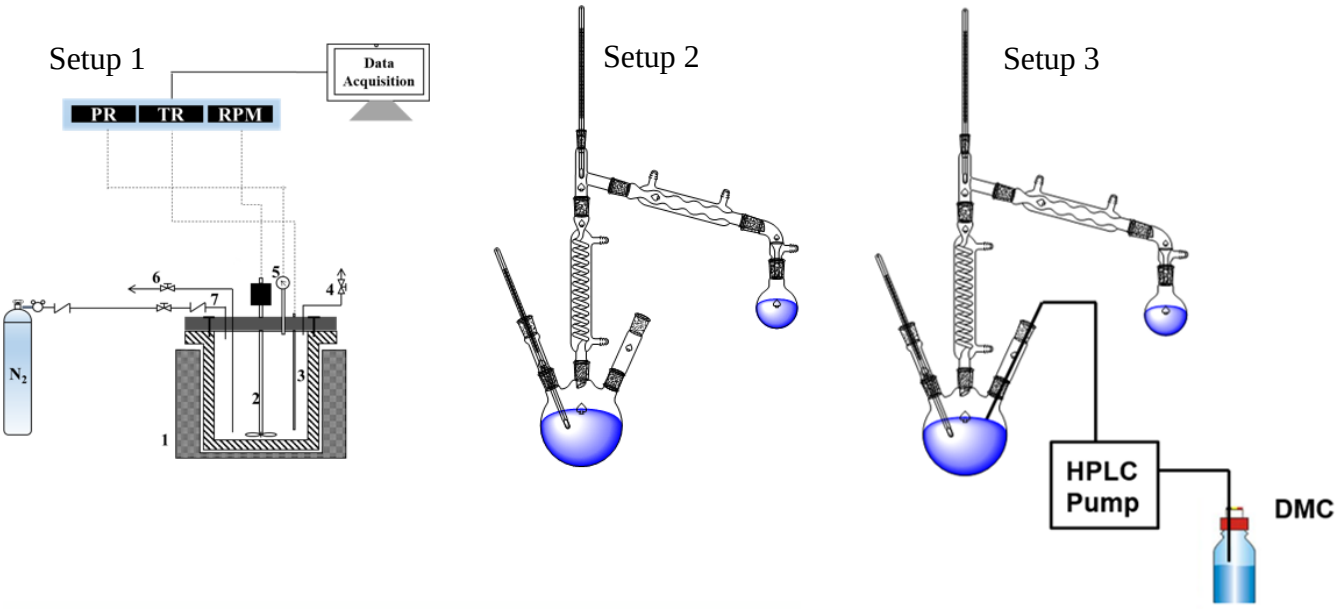

Figure 6-1 Schematic of experimental unit

6.4.3 Analytical Methods

All the final liquid product mixtures were analyzed offline by gas chromatography (GC) (Agilent, GC-7890A). The GC was equipped with an autosampler (7683 B Series Injector) and a flame-ionization detector (FID). A ZB-FFAP capillary column of 30 m length and an inner diameter of 0.32 mm was used as the stable phase. The inner surface of the column was a polyethylene glycol film. Helium at 30 std mL/min flow rate was used as the carrier gas.

A programmed temperature ramp was needed to separate and analyze the liquid samples for concentrations of reactants and products. The oven temperature starting from 85 °C, was maintained for 4 min during the analysis. Then a temperature was increased at a rate of 40 °C/min up to 160 °C, which was maintained for further 3 min. In the last stage, a temperature increase rate of 50 °C/min was applied to reach the final temperature 250 °C, kept for 10 min. The liquid samples can be separated completely using the above described temperature ramp. Ethyl Benzoate (EB)

was used as internal standard for this study. Typical retention times were 3.1 min for methanol, 3.7 min for DMC, 7.2 min for anisol (side product), 10.3 min for internal standard EB, 11.0 min for MPC, 12.4 min for phenol and 17.1 min for DPC, respectively. An example of GC result is shown in Figure 6-2. The same calibration procedure was used for the calibration of chemical components as that in section 2.2.3. The calibration curves are shown in Appendix I. The analytical error for the DPC system (Methanol, DMC, Phenol, Anisol, Ethyl Benzolate, MPC and DPC) are 4.1%, 4.6%, 11.8%, 7.3%, 10%, 10.6%, and 15.6%, respectively.

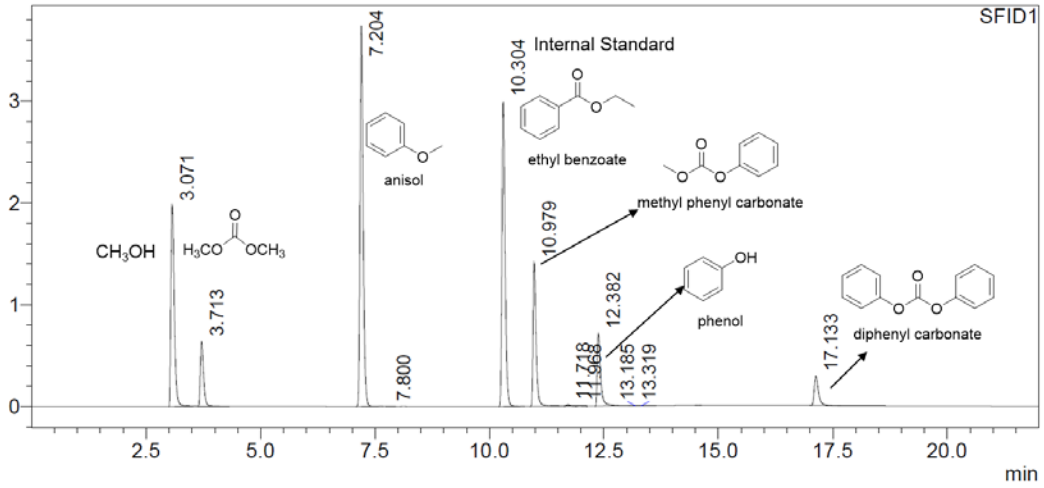

Figure 6-2 Typical GC graph for DPC system

6.5 Results and Discussion

6.5.1 Comparison of Different Setups

The transesterification of DMC with phenol were tested in three different setups, the results are summarized in Table 6-3. When tested in a batch reactor as described in setup 1, only 2.1% of phenol conversion was observed, which is similar to the results reported previously in literature.[163] Therefore, a suitable modification was required in the design of a reaction setup to successfully carry out the reaction of DMC to DPC at higher reactant conversion levels. When setup 2 was used, 32.9% phenol conversion was observed, and DPC selectivity can reach 35.7%. Additionally,

compared to setup 2, higher phenol conversion (43.4%) can be derived using setup 3. It is mainly because of the continuous distilling of the azeotropic components of DMC and methanol favoring the forward transesterification reaction, leading to higher phenol conversion in both setup 2 and 3. Except for the continuous distillation of DMC and methanol, the continuous pumping in of DMC also contributes to higher phenol conversion using setup 3. Therefore, setup 3 was chosen for further studies.

Table 6-3 Comparison of results from three different setups

Catalyst	T (°C)	X (phenol) (%)	S(DPC) (%)	S(MPC) (%)
n-Bu_2SnO	150-180	29.7 (DMC)	7.4	92.9
n-Bu_2SnO (batch)	160	2.1	0	100
n-Bu_2SnO (removal)	160	32.9	35.7	64.1
n-Bu_2SnO (removal+charge)	160	43.4	29.0	65.7

Reaction conditions: DMC: 1.07 kmol/ m^3; Phenol: 21.4 kmol/ m^3; n-Bu_2SnO: 1.07 kg/ m^3; T = 160 °C, t=6 h

6.5.2 Repeatability of Experiments

Typical experiment was repeated twice and the values of phenol conversion and product selectivity were evaluated (see Table 6-4), the average experimental error during these reactions was 5.7%, which was acceptable for this part of work.

Table 6-4 Repeatability results

Catalyst	T (°C)	X (phenol) (%)	S(DPC) (%)	S(MPC) (%)
n-Bu_2SnO (removal+charge)	170	46.8	34.2	61.3
n-Bu_2SnO (removal+charge)	170	48.8	37.7	59.1

Reaction conditions: DMC: 1.07 kmol/ m^3; Phenol: 21.4 kmol/ m^3; n-Bu_2SnO: 1.07 kg/ m^3; T = 170 °C, t= 6 h

6.5.3 Initial DMC/Phenol Ratio Effect

Table 6-5 shows the effect of DMC/phenol ratio on conversion of phenol and selectivity of DPC and MPC. It was observed that the phenol conversion increased from 41.4% to 46.8% with increasing DMC/phenol molar ratio from 0:1 to 4:1, while the DPC selectivity increased from

26.9% to 34.2%. At low conversion, the selectivity of DMC observed was lower mainly due to the formation of intermediate product MPC (see Scheme 6-2). As expected, during such equilibrium reactions, increasing the reactant ratio facilitates the reaction equilibrium to shift towards the formation of final products.

Table 6-5 Initial DMC/phenol molar ratio effect

Catalyst	T (°C)	t	Initial DMC/Phenol	X (phenol) (%)	S(DPC) (%)	S(MPC) (%)
n-Bu_2SnO	170	6	4:1	46.8	34.2	61.3
n-Bu_2SnO	170	6	1:1	40.7	29.2	68.7
n-Bu_2SnO	170	6	0:1	41.4	26.9	65.3

Reaction conditions: n-Bu_2SnO: 1.07 kg/ m^3; T = 170 °C, t= 6 h

6.5.4 Temperature Effect

The temperature effect was also investigated (Table 6-6). At 160 °C, the conversion of phenol was 43.4% and the selectivity of DPC was 29.0%. When the reaction temperatures increased to 170 °C, the phenol conversion increased to 46.8% and DPC selectivity increased to 34.2%.

Table 6-6 Temperature effect

Catalyst	T (°C)	X (phenol) (%)	S(DPC) (%)	S(MPC) (%)
n-Bu_2SnO (removal+charge)	160	43.4	29.0	65.7
n-Bu_2SnO (removal+charge)	170	46.8	34.2	61.3

Reaction conditions: DMC: 1.07 kmol/ m^3; Phenol: 21.4 kmol/ m^3; n-Bu_2SnO: 1.07 kg/ m^3; t= 6 h

6.5.5 Screening of Heterogeneous Catalysts

As the benchmark of reaction setup has been done for transesterification of DMC with phenol using n-Bu_2SnO catalyst, this setup was used for screening of heterogeneous catalysts (Table 6-7). Heterogeneous catalysts based on Ti or Mo were tested. However, low phenol conversion was observed (3.1% and 5.9% respectively) in these experiments. Fe-Mn double metal cyanide was successfully used for the transesterification of cyclic carbonate with methanol to synthesis DMC (Chapter 4). Therefore, Fe-Mn complex was also tested in the transesterification

of DMC with phenol. It is found that much higher conversion (31.8%) was achievable compared to Ti or Mo heterogeneous catalysts. However, significant side product, anisol was observed. Additionally, no DPC was found.

Table 6-7 Screening of heterogeneous catalysts

Catalyst	T(°C)	t(h)	X (phenol) (%)	S(DPC) (%)	S(MPC) (%)	S(Anisol) (%)
Ti-Fe-Mg	170	6	3.1	9.92	165.3	—
Fe-Mn	170	6	31.8	—	20.0	22.32
Nb/EISA	170	6	1.0	—	87.8	10.9
Mo/GIA	170	6	5.9	—	23.6	—

Reaction conditions: DMC: 1.07 kmol/ m^3; Phenol: 21.4 kmol/ m^3; catalyst: 1.07 kg/ m^3; t= 6 h

6.6 Conclusion

In this chapter, three different reaction setups were tested for DPC synthesis, the preliminary results presented demonstrate that with simultaneous removal of a co-product methanol, significantly higher reactant conversions can be achieved (phenol conversion increased from 2.1% to 43.4%). Initial DMC/phenol molar ratio as well as temperature has significant effect on reactants conversion and products selectivity. Several different heterogeneous catalysts were tested, it is found that Fe-Mn double metal cyanide complex, which was found to be highly active for the transesterification of cyclic carbonates with methanol, is also active for the transesterification of DMC with phenol.

6.7 Recommendations for Future Work

Based on previous literature reports and the preliminary experiments reported in this chapter, several future studies are recommended:

6.7.1 Development of Heterogeneous Catalysts

From the experimental results of screening of heterogeneous catalysts, it is observed that Fe-Mn double metal cyanide complex has significantly higher activity for the transesterification of DMC with phenol to MPC. However, it showed poor activity for transesterification of MPC to

DPC. Therefore, detail study of different catalyst parameters, such as different metals, Fe/Mn metal ratio, activation mode etc is necessary, which may give guidelines for rational design of active heterogeneous catalysts for the two steps in transesterification of DMC with phenol.

6.7.2 Investigating the Reaction Mechanism

The mechanism of transesterification with phenol as a substrate is not well understood and hence further studies on activation of phenol and DMC with homogeneous and heterogeneous catalysts is necessary to identify the parameters that can be tuned to achieve better catalyst performance with respect to activity, selectivity and stability. It is clear that the work on catalysis has to be coupled with separation techniques such as reactive distillation to intensify the equilibrium limited reactions.

Chapter 7 Conclusions and Future Recommendations

7.1 Conclusions

This thesis was focused on investigations on catalysis and reaction engineering aspects of conversion of cyclic carbonates, such as ethylene carbonate (EC), propylene carbonate (PC) and 1,2-butylene carbonate (BC) to high value chemicals, dimethyl carbonate (DMC) and glycols [*e.g.* propylene glycol (PG) and ethylene glycol (EG)]. The reactions involved liquid-solid multiphase reaction systems, and equilibrium limited reactions posing challenges to achieve high conversions. Through detailed investigations on catalysis and kinetic modeling, this work has contributed to advances in (a) fundamental understanding of the reaction behavior of transesterification reactions, (b) rational design of active catalysts for effective cyclic carbonate conversion to chemicals and (c) kinetic modeling on molecular level. A brief summary of important contributions is presented here.

7.1.1 Catalyst (CaO) Pretreatment Effects in Propylene Carbonate Transesterification with Methanol

Catalytic conversion of cyclic carbonates through transesterification using metal oxides, specifically CaO, was discussed. Significant pretreatment effect was observed during the reaction.

(a). With fresh CaO as catalyst for transesterification of cyclic carbonates, significant induction time (around 20 min) was observed. However, with methanol pretreated CaO as catalyst, the induction time was eliminated and the transesterification activity (TOF) increased from 11 to 947 h^{-1}. In contrast, with PC pretreated CaO, a prolonged induction time was observed.

(b). Various characterization technique (SEM, CO_2-TPD, XRD, FT-IR, XANES and ^{13}C NMR) were used to explore the fresh and treated CaO. It is found that strong basic sites correlative

closely to the activity of catalyst. Additionally, the formation of $Ca(OCH_3)_2$ during the methanol pretreatment process was believed to be a key step for the reaction.

7.1.2 Kinetic Study of Homogenous and Heterogeneous CaO-Catalyzed Transesterification of Cyclic Carbonates with Methanol

Homogeneous reaction was observed during the catalytic conversion of cyclic carbonate to DMC over CaO catalyst. Though heterogeneous reaction was detected to be predominant, the homogenous reaction cannot be neglected. Therefore, both homogeneous and heterogeneous reactions were considered in analysis of the kinetics.

(a) Empirical power law model was used for both homogeneous CaO-catalyzed transesterification and heterogeneous CaO-catalyzed transesterification. Different reaction orders were determined for homogeneous reaction (1, 2, 1, 1 for PC, methanol, DMC and PG) and heterogeneous reaction (0.35, 1.9, 0, 0 for PC, methanol, DMC and PG).

(b) For the homogeneous CaO-catalyzed transesterification, the formation of CH_3O^- ion initialized the reaction. In contrast, for heterogeneous CaO-catalyzed transesterification reaction, methanol dissociative adsorbing as well as PC's adsorption on the surface of active catalyst initialize the reaction.

7.1.3 Catalytic Transesterification of Cyclic Carbonates Over Fe-Mn Double Metal Cyanide

A highly active and selective heterogeneous catalyst consisting of Fe-Mn double metal cyanide is reported for the transesterification of cyclic carbonates with methanol.

(a). Precursor molar ratio [$K_4Fe(CN)_6/MnCl_2$] effect combined with the N_2-adsorption-desorption result demonstrated that the Mn ions are responsible for the high activity, selectivity and stability.

(b). TEM and XRD analyses confirmed that Fe-Mn complex presents a cubic crystalline structure with a lattice spacing of 0.5 nm. XPS and UV-Vis analysis results showed that all Fe exists in Fe^{2+} state. However, for the Mn element, 86.8% of Mn exists in Mn^{2+} state with only 13.2% in Mn^{4+} state. Furthermore, FTIR and DRIFT UV-Vis results verified the formation of a new mixed-metal complex of ferrocyanide moiety and Mn ions via bridging cyanide ligands.

(c). Catalyst leaching experiment results showed that after filtering out the solid, no further reaction was detected, confirming no active species leach out during the reaction. The catalyst recycle experiments presented that the catalytic activity decreased slightly from the fresh run to the first cycle, after which, the activity was found to be constant. However, the activity decrease from fresh run to the first cycle was due to active sites being occupied by PC, which was confirmed by the FTIR spectra.

7.1.2 Kinetic Modeling of Transesterification of Propylene Carbonate with Methanol over Fe-Mn Double Metal Cyanide Catalyst

Detailed kinetic modeling of transesterification of propylene carbonate (PC) with methanol over Fe-Mn double metal cyanide was done using a batch slurry reactor in a various range of reaction conditions.

(a) Empirical two-step power law model (first step is mono-transesterification of PC with methanol, and the second step is transesterification of 2-HMC with methanol) represents the experimental data well. An activation energy of 47.0±20.2 kJ/mol was observed for the mono-transesterification of PC with methanol. In contrast, a much higher activation energy (79.6 ± 9.8 kJ/mol) was observed for the second step transesterification of 2-HMC with methanol.

(b) Four different kinetic models based on different activation sequence of methanol, PC and 2-HMC (mono-transesterified product) were considered. It is found that a model based on the

following sequence of steps provides the best description of the experimental data with respect to reaction parameters over a wide range of conditions: methanol was first activated to form intermediate I, then PC was activated by activated methanol (intermediate I) instead of the catalyst precursor to form intermediate II. Next, the intermediate II instead of 2-HMC itself reacted with activated methanol (intermediate I) to form intermediate III, which decomposed into DMC and PG, the major products.

7.2 Future Recommendations

The results of this work pave the way for several follow-up studies:

7.2.1 Structure Study of the Fe-Mn Complex

Various characterization techniques have been applied in this work to characterize the double metal cyanide catalyst. However, this information is not enough for proposing of a proper structure of the catalyst. EXAFS (Extended X-ray Absorption Fine Structure) analysis, especially in-situ EXAFS can give information about the coordination condition of the main metals in the catalysts, which can provide direct evidence for the structure of the catalysts.

The accurate structure of the catalyst can give insight into the reaction mechanism as well as give evidence for the rational design of functional catalysts in the future.

7.2.2 Developing Supported Fe-Mn Double Metal Cyanide

As described in the above dissertation, currently the major research efforts have been focused on designing double metal catalysts in powder form, which is not practical for continuous studies in a fixed bed reactor. Therefore, developing new strategies on pelletizing active powder catalysts into particles or immobilize active power catalysts on larger particles will be a promising research direction, facilitating the test of such catalysts in continuous setup, which is a key step for the further usage of such catalysts in an industrial scale.

7.2.3 Computational Studies on Reaction Mechanism

Though through kinetic study, the most possible reaction mechanism was proposed. Interactions between reactant and catalyst are still unknown. Current bond characterization techniques like IR or NMR cannot be successfully used to address the interaction, due to the organic complexing agent used during the catalyst preparation stage and the magnetic properties of the catalyst. The unsolved problems can be potentially addressed by the aid of computational calculation:

a. The position where the cyclic ring opens and the preference opening conditions for each position

b. The interaction between intermediates and catalyst. Several possible interactions between mono-transesterified product and catalyst have been proposed in this study. However, with computational calculation, accurate interaction between mono-transesterified product and catalyst may be derived.

The information derived from computational studies will provide insight on the reaction mechanism and further design of ring-opening catalysts.

7.2.4 Development of Catalyst for One Pot Synthesis of DMC from Methanol, CO_2 and Epoxide and Direct Synthesis of DMC Using CO_2 and Methanol

Current project for synthesis of DMC is a three step process using olefin (ethylene or propylene) as staring material. During the first step, ethylene or propylene would be oxidized into epoxide. Then, through carboxylation, epoxide would be turned into cyclic carbonates. In the last step, cyclic carbonates would be transesterified into DMC with methanol.

However, for the last decade, researchers have made effort to optimize the DMC manufacture processes. Two of the most important routes are: (1) one pot synthesis of DMC from

methanol, CO_2 and epoxide, (2) direct synthesis of DMC from CO_2 and methanol. For the first route, the separation step of cyclic carbonates can be eliminated. Additionally, the complete conversion of epoxide can be easily achieved. However, low selectivity of DMC and cyclic carbonates are obtained due to the alcoholysis of epoxide with methanol. For the second route, low DMC yield is derived due to thermodynamic limitation.

Therefore, development of catalysts with high DMC selectivity and yield is a key factor for both the one pot synthesis of DMC and direct synthesis of DMC.

References

1. Fukuoka, S.; Fukuoka, S., Non-phosgene polycarbonate from co_2: industrialization of green chemical process. Nova Science Publishers: **2012**.
2. Haba, O.; Itakura, I.; Ueda, M.; Kuze, S., Synthesis of polycarbonate from dimethyl carbonate and bisphenol-a through a non-phosgene process. *Journal of Polymer Science Part A: Polymer Chemistry* **1999,** *37* (13), 2087-2093.
3. Ueda, M.; Mizoguchi, K., Synthesis of polycarbonate by melt self-polycondensation of 4,4′-isopropylidenedi(p-phenylene)bis(2,2,2-trichloroethyl) carbonate. *Polymer* **1997,** *38* (13), 3369-3372.
4. Research, G. V. *Polycarbonate market size to reach $25.37 billion by 2024*; 10, 2016.
5. Clagett, D. C.; Shafer, S. J., Polycarbonates. *Pergamon Press plc, Comprehensive Polymer Science.* **1989,** *5*, 345-356.
6. Freitag, D.; Fengler, G.; Morbitzer, L., Routes to new aromatic polycarbonates with special material properties. *Angewandte Chemie International Edition in English* **1991,** *30* (12), 1598-1610.
7. Shimoda, T., *Development of Environmentally Friendly Chemical Technology (Japanese)* **2000**, 198-208.
8. Ugo, R.; Renato, T.; Gioacchino, C.; Lidio, M., US4218391, **1980**.
9. Romano, U.; Tesel, R.; Mauri, M. M.; Rebora, P., Synthesis of dimethyl carbonate from methanol, carbon monoxide, and oxygen catalyzed by copper compounds. *Industrial & Engineering Chemistry Product Research and Development* **1980,** *19* (3), 396-403.
10. Romano, U.; Rivetti, F., US 5206409, **1993**.
11. Illuminati, G.; Romano, U.; Tesei, R.,US 4182726, **1980**.
12. Rivetti, F.; Romano, U., US 5686644, **1997**.
13. Rivetti, F.; Romano, U.; Garone, G.; Ghirardini, M., US 5527943, **1996**.
14. Mcclellan, P. P., US 2873282, **1959**.
15. Emmons, A. H., US 3535342, **1970**.
16. Buysch, H.-J.; Krimm, H.; Rudolph, H., US 4181676, **1980**.
17. Romano, U.; Melis, U., US 4062884, **1977**.
18. Tundo, P.; Trotta, F.; Moraglio, G.; Ligorati, F., Continuous-flow processes under gas-liquid phase-transfer catalysis (GL-PTC) conditions: the reaction of dialkyl carbonates with phenols, alcohols, and mercaptans. *Industrial & engineering chemistry research* **1988,** *27* (9), 1565-1571.
19. Hachiya, H.; Komiya, K., US 6277945, **2001**.
20. Kakihara, I.; Hachiya, H., US 7563858, **2005**.
21. Komiya, K.; Hasegawa, K., US 6037437, **2000**.
22. Pacheco, M. A.; Marshall, C. L., Review of Dimethyl Carbonate (DMC) Manufacture and Its Characteristics as a Fuel Additive. *Energy & Fuels* **1997,** *11* (1), 2-29.
23. Unnikrishnan, P.; Srinivas, D., Calcined, rare earth modified hydrotalcite as a solid, reusable catalyst for dimethyl carbonate synthesis. *Industrial & Engineering Chemistry Research* **2012,** *51* (18), 6356-6363.
24. Haba, O.; Itakura, I.; Ueda, M.; Kuze, S., Synthesis of polycarbonate from dimethyl carbonate and bisphenol-a through a non-phosgene process. *Journal of Polymer Science Part A: Polymer Chemistry* **1999,** *37* (13), 2087-2093.

25. Wei, T.; Wang, M.; Wei, W.; Sun, Y.; Zhong, B., Synthesis of dimethyl carbonate by transesterification over CaO/carbon solid base catalysts. In *Studies in Surface Science and Catalysis*, Sang-Eon Park, J.-S. C.; Kyu-Wan, L., Eds. Elsevier: **2004**; *153*, 41-46.
26. Tomishige, K.; Ikeda, Y.; Sakaihori, T.; Fujimoto, K., Catalytic properties and structure of zirconia catalysts for direct synthesis of dimethyl carbonate from methanol and carbon dioxide. *Journal of Catalysis* **2000,** *192* (2), 355-362.
27. Fang, S.; Fujimoto, K., Direct synthesis of dimethyl carbonate from carbon dioxide and methanol catalyzed by base. *Applied Catalysis A: General* **1996,** *142* (1), L1-L3.
28. Yi, Hua-yan.; Shang, Hua-yan.; Mei L.; Wang L.; Li L.; Lei Ben-yong.; Zhu Y.; Summarize on synthesis process of dimethyl carbonate. *Guang Dong Chem* **2010,** *9*, 63-65.
29. Delledonne, D.; Rivetti, F.; Romano, U., Developments in the production and application of dimethylcarbonate. *Applied Catalysis A: General* **2001,** *221* (1–2), 241-251.
30. Gong, J.; Ma, X.; Wang, S., Phosgene-free approaches to catalytic synthesis of diphenyl carbonate and its intermediates. *Applied Catalysis A: General* **2007,** *316* (1), 1-21.
31. Knifton, J. F., US4661609, **1987**.
32. Kabra, S. K.; Turpeinen, E.; Keiski, R. L.; Yadav, G. D., Direct synthesis of dimethyl carbonate from methanol and carbon dioxide: A thermodynamic and experimental study. *The Journal of Supercritical Fluids* **2016,** *117*, 98-107.
33. Tamboli, A. H.; Chaugule, A. A.; Kim, H., Catalytic developments in the direct dimethyl carbonate synthesis from carbon dioxide and methanol. *Chemical Engineering Journal* **2017,** *323*, 530-544.
34. Li, A.; Pu, Y.; Li, F.; Luo, J.; Zhao, N.; Xiao, F., Synthesis of dimethyl carbonate from methanol and CO_2 over Fe–Zr mixed oxides. *Journal of CO_2 Utilization* **2017,** *19*, 33-39.
35. Tamboli, A. H.; Chaugule, A. A.; Kim, H., Highly selective and multifunctional chitosan/ionic liquids catalyst for conversion of CO_2 and methanol to dimethyl carbonates at mild reaction conditions. *Fuel* **2016,** *166*, 495-501.
36. De Filippis, P.; Scarsella, M.; Borgianni, C.; Pochetti, F., Production of dimethyl carbonate via alkylene carbonate transesterification catalyzed by basic salts. *Energy & fuels* **2006,** *20* (1), 17-20.
37. Wang, H.; Wang, M.; Zhang, W.; Zhao, N.; Wei, W.; Sun, Y., Synthesis of dimethyl carbonate from propylene carbonate and methanol using CaO–ZrO_2 solid solutions as highly stable catalysts. *Catalysis Today* **2006,** *115* (1–4), 107-110.
38. Bhanage, B. M.; Fujita, S.-i.; Ikushima, Y.; Arai, M., Synthesis of dimethyl carbonate and glycols from carbon dioxide, epoxides, and methanol using heterogeneous basic metal oxide catalysts with high activity and selectivity. *Applied Catalysis A: General* **2001,** *219* (1–2), 259-266.
39. Sullivan, C. J., Propanediols. In *Ullmann's Encyclopedia of Industrial Chemistry*, Wiley-VCH Verlag GmbH & Co. KGaA: 2000.
40. Bausmith, D. S.; Neufeld, R. D., Soil biodegradation of propylene glycol based aircraft deicing fluids. *Water Environment Research* **1999,** *71* (4), 459-464.
41. Abimanyu, H.; Kim, C. S.; Ahn, B. S.; Yoo, K. S., Synthesis of dimethyl carbonate by transesterification with various MgO–CeO_2 mixed oxide catalysts. *Catalysis Letters* **2007,** *118* (1), 30-35.
42. Thitsartarn, W.; Kawi, S., An active and stable CaO-CeO_2 catalyst for transesterification of oil to biodiesel. *Green Chemistry* **2011,** *13* (12), 3423-3430.

43. Liu, S.; Huang, S.; Guan, L.; Li, J.; Zhao, N.; Wei, W.; Sun, Y., Preparation of a novel mesoporous solid base Na–ZrO_2 with ultra high thermal stability. *Microporous and Mesoporous Materials* **2007,** *102* (1), 304-309.
44. Song, Z.; Jin, X.; Hu, Y.; Subramaniam, B.; Chaudhari, R. V., Intriguing catalyst (CaO) pretreatment effects and mechanistic insights during propylene carbonate transesterification with methanol. *ACS Sustainable Chemistry & Engineering* **2017**, *5*, 4718-4729.
45. Wei, T.; Wei, W.; Wang, M.; Sun, Y.; Zhong, B., Effect of the amount of base site on catalytic behavior of CaO for synthesis of dimethyl carbonate from propylene carbonate and methanol. 2002; *47 (*1*)*, 88-89.
46. Liu, X.; He, H.; Wang, Y.; Zhu, S.; Piao, X., Transesterification of soybean oil to biodiesel using CaO as a solid base catalyst. *Fuel* **2008,** *87* (2), 216-221.
47. Gopal, S.; Sajitha, C.; Krishnakumar, U., Production of biodiesel from vegetable oil using CaO catalyst & analysis of its performance in four stroke diesel engine. *International Journal of Scientific and Research Publications* **2013,** *3* (11), 2250-3153.
48. Yan, S.; Lu, H.; Liang, B., Supported CaO catalysts used in the transesterification of tapeseed oil for the purpose of biodiesel production. *Energy & Fuels* **2008,** *22* (1), 646-651.
49. Lengyel, J.; Cvengrošová, Z.; Cvengroš, J., Transesterification of triacylglycerols over calcium oxide as heterogeneous catalyst. *Petroleum & coal* **2009,** *51* (3), 216-224.
50. Wei, T.; Wang, M.; Wei, W.; Sun, Y.; Zhong, B., Effect of base strength and basicity on catalytic behavior of solid bases for synthesis of dimethyl carbonate from propylene carbonate and methanol. *Fuel processing technology* **2003,** *83* (1), 175-182.
51. Kawashima, A.; Matsubara, K.; Honda, K., Acceleration of catalytic activity of calcium oxide for biodiesel production. *Bioresource Technology* **2009,** *100* (2), 696-700.
52. Kumar, A.; Some, D.; Kiriamiti, K. H. In Pretreatment of CaO Catalyst for transesterification of croton megalocarpus oil, Proceedings of Sustainable Research and Innovation Conference, **2014**; *5*, 150-153.
53. Holtbruegge, J.; Leimbrink, M.; Lutze, P.; Górak, A., Synthesis of dimethyl carbonate and propylene glycol by transesterification of propylene carbonate with methanol: Catalyst screening, chemical equilibrium and reaction kinetics. *Chemical Engineering Science* **2013,** *104*, 347-360.
54. Knifton, J. F., US 4734518, **1988**.
55. Zhang, S.-G.; Wei, Y.-D.; Yin, S.-F.; Luo, S.-L.; Au, C.-T., Superbasic sodium stannate as catalyst for dehydrogenation, Michael addition and transesterification reactions. *Applied Catalysis A: General* **2011,** *406* (1-2), 113-118.
56. Kumar, P.; Srivastava, V. C.; Mishra, I. M., Dimethyl carbonate synthesis from propylene carbonate with methanol using Cu–Zn–Al catalyst. *Energy & Fuels* **2015,** *29* (4), 2664-2675.
57. Juarez, R.; Corma, A.; Garcia, H., Gold nanoparticles promote the catalytic activity of ceria for the transalkylation of propylene carbonate to dimethyl carbonate. *Green Chemistry* **2009,** *11* (7), 949-952.
58. Pyrlik, A.; Hoelderich, W. F.; Müller, K.; Arlt, W.; Strautmann, J.; Kruse, D., Dimethyl carbonate via transesterification of propylene carbonate with methanol over ion exchange resins. *Applied Catalysis B: Environmental* **2012,** *125*, 486-491.
59. Srinivas, D.; Srivastava, R.; Ratnasamy, P., Transesterifications over titanosilicate molecular sieves. *Catalysis Today* **2004,** *96* (3), 127-133.
60. Srivastava, R.; Srinivas, D.; Ratnasamy, P., Fe–Zn double-metal cyanide complexes as novel, solid transesterification catalysts. *Journal of Catalysis* **2006,** *241* (1), 34-44.
61. Frevel, L. K.; Gilpin, J. A., US 3642858, **1972**.

62. Dhuri, S. M.; Mahajani, V. V., Studies in transesterification of ethylene carbonate to dimethyl carbonate over Amberlyst A-21 catalyst. *Journal of Chemical Technology & Biotechnology* **2006,** *81* (1), 62-69.
63. Kattel, S.; Liu, P.; Chen, J. G., Tuning selectivity of CO_2 hydrogenation reactions at the metal/oxide interface. *Journal of the American Chemical Society* **2017,** *139* (29), 9739-9754.
64. Haruta, M.; Tsubota, S.; Kobayashi, T.; Kageyama, H.; Genet, M. J.; Delmon, B., Low-temperature oxidation of CO over gold supported on TiO_2, α-Fe_2O_3, and Co_3O_4. *Journal of Catalysis* **1993,** *144* (1), 175-192.
65. Borges, M. E.; Díaz, L., Recent developments on heterogeneous catalysts for biodiesel production by oil esterification and transesterification reactions: A review. *Renewable and Sustainable Energy Reviews* **2012,** *16* (5), 2839-2849.
66. Kumar, P.; Srivastava, V. C.; Mishra, I. M., Dimethyl carbonate synthesis by transesterification of propylene carbonate with methanol: Comparative assessment of Ce-M (M= Co, Fe, Cu and Zn) catalysts. *Renewable Energy* **2016,** *88*, 457-464.
67. Murugan, C.; Bajaj, H., Transesterification of propylene carbonate with methanol using Mg-Al-CO_3 hydrotalcite as solid base catalyst. *Indian journal of chemistry. Section A, Inorganic, bio-inorganic, physical, theoretical & analytical chemistry* **2010,** *49* (9), 1182.
68. Murugan, C.; Bajaj, H. C.; Jasra, R. V., Transesterification of propylene carbonate by methanol using KF/Al_2O_3 as an efficient base catalyst. *Catalysis Letters* **2010,** *137* (3), 224-231.
69. Hashmi, A. S. K.; Hutchings, G. J., Gold Catalysis. *Angewandte Chemie International Edition* **2006,** *45* (47), 7896-7936.
70. Tatsumi, T.; Watanabe, Y.; Koyano, K. A., Synthesis of dimethyl carbonate from ethylene carbonate and methanol using TS-1 as solid base catalyst. *Chemical Communications* **1996,** (19), 2281-2282.
71. Jack, M., US 3278457, **1966**.
72. Dienes, Y.; Leitner, W.; Müller, M. G.; Offermans, W. K.; Reier, T.; Reinholdt, A.; Weirich, T. E.; Müller, T. E., Hybrid sol–gel double metal cyanide catalysts for the copolymerisation of styrene oxide and CO_2. *Green Chemistry* **2012,** *14* (4), 1168-1177.
73. O'connor, J. M.; Lickei, D. L.; Grieve, R. L., US 6359101, **2002**.
74. Kim, I.; Ahn, J.-T.; Ha, C. S.; Yang, C. S.; Park, I., Polymerization of propylene oxide by using double metal cyanide catalysts and the application to polyurethane elastomer. *Polymer* **2003,** *44* (11), 3417-3428.
75. Kim, I.; Ahn, J.-T.; Lee, S.-H.; Ha, C.-S.; Park, D.-W., Preparation of multi-metal cyanide catalysts and ring-opening polymerization of propylene oxide. *Catalysis today* **2004,** *93*, 511-516.
76. Kim, I.; Yi, M. J.; Lee, K. J.; Park, D.-W.; Kim, B. U.; Ha, C.-S., Aliphatic polycarbonate synthesis by copolymerization of carbon dioxide with epoxides over double metal cyanide catalysts prepared by using ZnX_2 (X= F, Cl, Br, I). *Catalysis today* **2006,** *111* (3), 292-296.
77. Eleveld, M. B. A., NL), Grotenbreg, Robert Adrianus Wilhelmus (Amsterdam, NL), Van Kempen, Ronald (Amsterdam, NL) Preparation of a double metal cyanide catalyst. **2005**.
78. Srinivas, D.; Srivastava, R.; Ratnasamy, P., US 7754643, **2010**.
79. Petitjean, H.; Tarasov, K.; Delbecq, F.; Sautet, P.; Krafft, J. M.; Bazin, P.; Paganini, M. C.; Giamello, E.; Che, M.; Lauron-Pernot, H.; Costentin, G., Quantitative investigation of MgO Brønsted basicity: DFT, IR, and Calorimetry study of methanol adsorption. *The Journal of Physical Chemistry C* **2010,** *114* (7), 3008-3016.
80. Branda, M. M.; Ferullo, R. M.; Belelli, P. G.; Castellani, N. J., Methanol adsorption on magnesium oxide surface with defects: a DFT study. *Surface Science* **2003,** *527* (1), 89-99.

81. Tench, A. J.; Giles, D.; Kibblewhite, J. F. J., Adsorption and desorption of methyl alcohol on magnesium oxide. *Transactions of the Faraday Society* **1971,** *67* (0), 854-863.
82. Liang, S. H.; Gay, I. D., Adsorption and thermal decomposition of methanol on magnesium oxide. Carbon-13 NMR studies. *Langmuir* **1985,** *1* (5), 593-599.
83. Peng, X. D.; Barteau, M. A., Acid-base properties of model magnesium oxide surfaces. *Langmuir* **1991,** *7* (7), 1426-1431.
84. Kouzu, M.; Kasuno, T.; Tajika, M.; Sugimoto, Y.; Yamanaka, S.; Hidaka, J., Calcium oxide as a solid base catalyst for transesterification of soybean oil and its application to biodiesel production. *Fuel* **2008,** *87* (12), 2798-2806.
85. Dossin, T. F.; Reyniers, M.-F.; Marin, G. B., Kinetics of heterogeneously MgO-catalyzed transesterification. *Applied Catalysis B: Environmental* **2006,** *62* (1), 35-45.
86. Ochoa-Gómez, J. R.; Gómez-Jiménez-Aberasturi, O.; Maestro-Madurga, B.; Pesquera-Rodríguez, A.; Ramírez-López, C.; Lorenzo-Ibarreta, L.; Torrecilla-Soria, J.; Villarán-Velasco, M. C., Synthesis of glycerol carbonate from glycerol and dimethyl carbonate by transesterification: Catalyst screening and reaction optimization. *Applied Catalysis A: General* **2009,** *366* (2), 315-324.
87. Matsuoka, S.-i.; Shimakawa, S.; Takagi, K.; Suzuki, M., Organocatalytic head-to-tail dimerization of methacrolein via conjugate addition of methanol: an alcohol activation mechanism proved by electrospray ionization mass spectrometry. *Tetrahedron Letters* **2011,** *52* (50), 6835-6838.
88. Helwani, Z.; Othman, M. R.; Aziz, N.; Kim, J.; Fernando, W. J. N., Solid heterogeneous catalysts for transesterification of triglycerides with methanol: A review. *Applied Catalysis A: General* **2009,** *363* (1), 1-10.
89. López, D. E.; Goodwin, J. G.; Bruce, D. A., Transesterification of triacetin with methanol on Nafion® acid resins. *Journal of Catalysis* **2007,** *245* (2), 381-391.
90. Meher, L. C.; Vidya Sagar, D.; Naik, S. N., Technical aspects of biodiesel production by transesterification—a review. *Renewable and Sustainable Energy Reviews* **2006,** *10* (3), 248-268.
91. Kulkarni, M. G.; Gopinath, R.; Meher, L. C.; Dalai, A. K., Solid acid catalyzed biodiesel production by simultaneous esterification and transesterification. *Green Chemistry* **2006,** *8* (12), 1056-1062.
92. Štich, I.; Gale, J. D.; Terakura, K.; Payne, M. C., Role of the zeolitic environment in catalytic activation of methanol. *Journal of the American Chemical Society* **1999,** *121* (14), 3292-3302.
93. Lotero, E.; Liu, Y.; Lopez, D. E.; Suwannakarn, K.; Bruce, D. A.; Goodwin, J. G., Synthesis of biodiesel via acid catalysis. *Industrial & Engineering Chemistry Research* **2005,** *44* (14), 5353-5363.
94. Wang, J.-Q.; Sun, J.; Cheng, W.-G.; Shi, C.-Y.; Dong, K.; Zhang, X.-P.; Zhang, S.-J., Synthesis of dimethyl carbonate catalyzed by carboxylic functionalized imidazolium salt via transesterification reaction. *Catalysis Science & Technology* **2012,** *2* (3), 600-605.
95. Tatsumi, H.; Sasahara, A.; Tomitori, M., Adsorption of propylene carbonate molecules on a TiO_2 (110) surface. *The Journal of Physical Chemistry C* **2013,** *117* (20), 10410-10416.
96. Han, M. S.; Lee, B. G.; Ahn, B. S.; Park, K. Y.; Hong, S. I., Kinetics of dimethyl carbonate synthesis from ethylene carbonate and methanol using alkali-metal compounds as catalysts. *Reaction Kinetics and Catalysis Letters* **2001,** *73* (1), 33-38.
97. Abimanyu, H., Studies on kinetics of dimethyl carbonate synthesis by homogeneous transesterification. *Jurnal Kimia Terapan Indonesia* **2009,** *11* (2), 15-18.

98. Alenezi, R.; Leeke, G. A.; Winterbottom, J. M.; Santos, R. C. D.; Khan, A. R., Esterification kinetics of free fatty acids with supercritical methanol for biodiesel production. *Energy Conversion and Management* **2010,** *51* (5), 1055-1059.
99. Zeng, D.; Yang, L.; Fang, T., Process optimization, kinetic and thermodynamic studies on biodiesel production by supercritical methanol transesterification with CH_3ONa catalyst. *Fuel* **2017,** *203*, 739-748.
100. Doná, G.; Filho, L.; Silva, C.; Castilhos, F., Biodiesel production using supercritical methyl acetate in a tubular packed bed reactor. *Fuel Processing Technology,* **2013**; *106*, 605–610.
101. Bernard, F.; O., B. R.; H., P. E., Transesterification kinetics of soybean oil 1. *Journal of the American Oil Chemists' Society* **1986,** *63* (10), 1375-1380.
102. Hattori, H.; Shima, M.; Kabashima, H., Alcoholysis of ester and epoxide catalyzed by solid bases. *Studies in surface science and catalysis* **2000,** *130*, 3507-3512.
103. Yao, Y.; Patzig, C.; Hu, Y.; Scott, R. W., In Situ X-ray Absorption Spectroscopic Study of $Fe@Fe_xO_y$/Pd and $Fe@Fe_xO_y$/Cu Nanoparticle Catalysts Prepared by Galvanic Exchange Reactions. *The Journal of Physical Chemistry C* **2015,** *119* (36), 21209-21218.
104. Gao, Y.; Xu, C., Synthesis of dimethyl carbonate over waste eggshell catalyst. *Catalysis today* **2012,** *190* (1), 107-111.
105. Granados, M. L.; Alonso, D. M.; Sadaba, I.; Mariscal, R.; Ocón, P., Leaching and homogeneous contribution in liquid phase reaction catalysed by solids: the case of triglycerides methanolysis using CaO. *Applied Catalysis B: Environmental* **2009,** *89* (1), 265-272.
106. Teo, S. H.; Taufiq-Yap, Y. H.; Rashid, U.; Islam, A., Hydrothermal effect on synthesis, characterization and catalytic properties of calcium methoxide for biodiesel production from crude Jatropha curcas. *RSC Advances* **2015,** *5* (6), 4266-4276.
107. Mirghiasi, Z.; Bakhtiari, F.; Darezereshki, E.; Esmaeilzadeh, E., Preparation and characterization of CaO nanoparticles from $Ca(OH)_2$ by direct thermal decomposition method. *Journal of Industrial and Engineering Chemistry* **2014,** *20* (1), 113-117.
108. Safaei-Ghomi, J.; Ghasemzadeh, M. A.; Mehrabi, M., Calcium oxide nanoparticles catalyzed one-step multicomponent synthesis of highly substituted pyridines in aqueous ethanol media. *Scientia Iranica* **2013,** *20* (3), 549-554.
109. Liu, T.; Zhu, Y.; Zhang, X.; Zhang, T.; Zhang, T.; Li, X., Synthesis and characterization of calcium hydroxide nanoparticles by hydrogen plasma-metal reaction method. *Materials Letters* **2010,** *64* (23), 2575-2577.
110. Salvadori, B.; Dei, L., Synthesis of $Ca(OH)_2$ Nanoparticles from Diols. *Langmuir* **2001,** *17* (8), 2371-2374.
111. Ghiasi, M.; Malekzadeh, A., Synthesis of $CaCO_3$ nanoparticles via citrate method and sequential preparation of CaO and Ca $(OH)_2$ nanoparticles. *Crystal Research and Technology* **2012,** *47* (4), 471-478.
112. Galván-Ruiz, M.; Hernández, J.; Baños, L.; Noriega-Montes, J.; Rodríguez-García, M. E., Characterization of calcium carbonate, calcium oxide, and calcium hydroxide as starting point to the improvement of lime for their use in construction. *Journal of Materials in Civil Engineering* **2009,** *21* (11), 694-698.
113. Zhao, L., Novel solid base catalysts for the production of biodiesel from lipids. **2010**.
114. Quartieri, S.; Chaboy, J.; Merli, M.; Oberti, R.; Ungaretti, L., Local structural environment of calcium in garnets: a combined structure-refinement and XANES investigation. *Physics and Chemistry of Minerals* **1995,** *22* (3), 159-169.

115. Takahashi, Y.; Miyoshi, T.; Yabuki, S.; Inada, Y.; Shimizu, H., Observation of transformation of calcite to gypsum in mineral aerosols by Ca K-edge X-ray absorption near-edge structure (XANES). *Atmospheric Environment* **2008,** *42* (26), 6535-6541.
116. Sowrey, F. E.; Skipper, L. J.; Pickup, D. M.; Drake, K. O.; Lin, Z.; Smith, M. E.; Newport, R. J., Systematic empirical analysis of calcium–oxygen coordination environment by calcium K-edge XANES. *Physical Chemistry Chemical Physics* **2004,** *6* (1), 188-192.
117. Barkyoumb, J.; Mansour, A., Electronic and atomic structure of Mn-doped CaF_2: An x-ray-absorption near-edge structure and extended x-ray-absorption fine-structure study. *Physical Review B* **1992,** *46* (14), 8768.
118. Martin-Diaconescu, V.; Gennari, M.; Gerey, B.; Tsui, E.; Kanady, J.; Tran, R.; Pécaut, J.; Maganas, D.; Krewald, V.; Gouré, E.; Duboc, C.; Yano, J.; Agapie, T.; Collomb, M.-N.; DeBeer, S., Ca K-Edge XAS as a probe of calcium centers in complex systems. *Inorganic Chemistry* **2015,** *54* (4), 1283-1292.
119. Chaboy, J.; Quartieri, S., X-ray absorption at the Ca K edge in natural-garnet solid solutions: A full-multiple-scattering investigation. *Physical Review B* **1995,** *52* (9), 6349.
120. Cornish, A.; Nicholls, K.; Scott, D.; Hunter, B.; Aston, W.; Higgins, I.; Sanders, J., In vivo ^{13}C NMR investigations of methanol oxidation by the obligate methanotroph methylosinus trichosporium OB_3b. *Microbiology* **1984,** *130* (10), 2565-2575.
121. Kouzu, M.; Kasuno, T.; Tajika, M.; Yamanaka, S.; Hidaka, J., Active phase of calcium oxide used as solid base catalyst for transesterification of soybean oil with refluxing methanol. *Applied Catalysis A: General* **2008,** *334* (1–2), 357-365.
122. Reddy, V. P.; Smart, M. C.; Chin, K. B.; Ratnakumar, B. V.; Surampudi, S.; Hu, J.; Yan, P.; Prakash, G. S., ^{13}C NMR spectroscopic, CV, and conductivity studies of propylene carbonate-based electrolytes containing various lithium salts. *Electrochemical and Solid-State Letters* **2005,** *8* (6), A294-A298.
123. Tanabe, K.; Misono, M.; Ono, Y.; Hattori, H.; Tanabe, K.; Misono, M.; Ono, Y.; Hattori, H., New solid acids and bases studies in the surface science and catalysis. Elsevier, Amsterdam: **1989**.
124. Ramachandran, P.; Chaudhari, R., *Three-phase catalytic reactors*. Gordon & Breach Science Pub: **1983**; *2*, 399-422.
125. Williams, D. B. G.; Sibiya, M. S.; van Heerden, P. S.; Kirk, M.; Harris, R., Verkade super base-catalysed transesterification of propylene carbonate with methanol to co-produce dimethyl carbonate and propylene glycol. *Journal of Molecular Catalysis A: Chemical* **2009,** *304* (1), 147-152.
126. Benson, S. W.; Cruickshank, F.; Golden, D.; Haugen, G. R.; O'neal, H.; Rodgers, A.; Shaw, R.; Walsh, R., Additivity rules for the estimation of thermochemical properties. *Chemical Reviews* **1969,** *69* (3), 279-324.
127. Guo X.; Shi You-min.; Zheng Hua-an.; Cheng J.; Zhao Xian-ze.; Yang Bo-lun., Thermodynamic study on diphenyl carbonate synthesis with different feedstocks. *Journal of Chemical Engineering of Chinese Universities* **2016**, *4*, 754-760.
128. Man, I.-C.; Soriga, S. G.; Parvulescu, V., Effect of Ca and Sr in MgO (100) on the activation of methanol and methyl acetate. *Catalysis Today* **2018,** *306*, 207-214.
129. Chen, S.; Zhang, P.; Chen, L., Fe/Zn double metal cyanide (DMC) catalyzed ring-opening polymerization of propylene oxide: Part 3. Synthesis of DMC catalysts. *Progress in Organic Coatings* **2004,** *50* (4), 269-272.

130. Peeters, A.; Valvekens, P.; Ameloot, R.; Sankar, G.; Kirschhock, C. E.; De Vos, D. E., Zn–Co double metal cyanides as heterogeneous catalysts for hydroamination: A structure–activity relationship. *ACS Catalysis* **2013,** *3* (4), 597-607.
131. Song, Z.; Jin, X.; Hu, Y.; Subramaniam, B.; Chaudhari, R. V., Intriguing catalyst (CaO) pretreatment effects and mechanistic insights during propylene carbonate transesterification with methanol. *ACS Sustainable Chemistry & Engineering* **2017,** *5* (6), 4718-4729.
132. Meenakshisundaram, S.; Srikanth, S.; Palanichamy, M., Transesterification of cyclic carbonates to dimethyl carbonate using solid oxide catalyst at ambient conditions: Environmentally Benign Synthesis. *ChemSusChem* **2010,** *3* (5), 575-578.
133. Thommes, M.; Kaneko, K.; Neimark Alexander, V.; Olivier James, P.; Rodriguez-Reinoso, F.; Rouquerol, J.; Sing Kenneth, S. W., Physisorption of gases, with special reference to the evaluation of surface area and pore size distribution (IUPAC Technical Report). In *Pure and Applied Chemistry*, **2015**; *87*, 1051.
134. Ravindran, A.; Srivastava, R., Catalytic activity of dual metal cyanide complex in multi-component coupling reactions. *Chinese Journal of Catalysis* **2011,** *32* (9), 1597-1603.
135. Kotwal, M.; Deshpande, S.; Srinivas, D., Esterification of fatty acids with glycerol over Fe–Zn double-metal cyanide catalyst. *Catalysis Communications* **2011,** *12* (14), 1302-1306.
136. Tharun, J.; Dharman, M. M.; Hwang, Y.; Roshan, R.; Park, M. S.; Park, D.-W., Tuning double metal cyanide catalysts with complexing agents for the selective production of cyclic carbonates over polycarbonates. *Applied Catalysis A: General* **2012,** *419*, 178-184.
137. Yatsimirskii, K. B.; Nemoshkalenko, V. V.; Nazarenko, Y. P.; Aleshin, V. G.; Zhilinskaya, V. V.; Tomashevsky, N. A., Use of X-ray photoelectron and Mössbauer spectroscopies in the study of iron pentacyanide complexes. *Journal of Electron Spectroscopy and Related Phenomena* **1977,** *10* (3), 239-245.
138. Yang, H.; Li, H.; Zhai, J.; Yu, H., In situ growth of prussian blue nanocrystal within Fe3+ crosslinking PAA resin for radiocesium highly efficient and rapid separation from water. *Chemical Engineering Journal* **2015,** *277*, 40-47.
139. Biesinger, M. C.; Payne, B. P.; Grosvenor, A. P.; Lau, L. W. M.; Gerson, A. R.; Smart, R. S. C., Resolving surface chemical states in XPS analysis of first row transition metals, oxides and hydroxides: Cr, Mn, Fe, Co and Ni. *Applied Surface Science* **2011,** *257* (7), 2717-2730.
140. Lawniczak-Jablonska, K.; Dynowska, E.; Lisowski, W.; Sobczak, J. W.; Chruściel, A.; Hreczuch, W.; Libera, J.; Reszka, A., Structural properties and chemical bonds in double metal cyanide catalysts. *X-Ray Spectrometry* **2015,** *44* (5), 330-338.
141. Nefedov, V.; Gati, D.; Dzhurinskii, B.; Sergushin, N.; Salyn, Y. V., X-ray electron study of oxides of elements. *Zhurnal Neorganicheskoi Khimii* **1975,** *20* (9), 2307-2314.
142. Gervais, M.; Douy, A.; Gallot, B.; Erre, R., Surface studies of polypeptidic block copolymers by electron spectroscopy for chemical analysis: Poly(N'-trifluoroacetyl-l-lysine)-polysarcosine diblock copolymers. *Polymer* **1986,** *27* (10), 1513-1520.
143. Chruściel, A.; Hreczuch, W.; Czaja, K.; Ławniczak-Jabłońska, K.; Janik, J., The complementary structural studies of the double metal cyanide type catalysts for the ring opening polymerization of the oxiranes. *Polimery* **2016,** *61*, 421-432.
144. Patil, M. V.; Yadav, M. K.; Jasra, R. V., Prins condensation for synthesis of nopol from β-pinene and paraformaldehyde on novel Fe–Zn double metal cyanide solid acid catalyst. *Journal of Molecular Catalysis A: Chemical* **2007,** *273* (1), 39-47.
145. Nakamoto, K.; Nakamoto, K., *Infrared and Raman spectra of inorganic and coordination compounds*. Wiley: 1977.

146. Dharman, M. M.; Ahn, J.-Y.; Lee, M.-K.; Shim, H.-L.; Kim, K.-H.; Kim, I.; Park, D.-W., Moderate route for the utilization of CO_2-microwave induced copolymerization with cyclohexene oxide using highly efficient double metal cyanide complex catalysts based on Zn3[Co(CN)6]. *Green Chemistry* **2008,** *10* (6), 678-684.
147. Raut, R. K.; Shaikh, M.; Darbha, S., Synthesis of fatty monoester lubricant base oil catalyzed by Fe-Zn double-metal cyanide complex. *Journal of Chemical Sciences* **2014,** *126* (4), 997-1003.
148. Sebastian, J.; Darbha, S., Solid, double-metal cyanide catalysts for synthesis of hyperbranched polyesters and aliphatic polycarbonates. *Journal of Chemical Sciences* **2014,** *126* (2), 499-509.
149. Mandal, B.; Basumallick, I.; Ghosh, S., Electrochemical studies on Li^+/K^+ ion exchange behaviour in $K_4Fe(CN)_6$ cathode material for Li, K-ion battery. *Journal of Chemical Sciences* **2015,** *127* (1), 141-148.
150. Carlin, R. L., Inorganic electronic spectroscopy (Lever, A. B. P.). *Journal of Chemical Education* **1969,** *46* (9), A628.
151. Rokicki, G.; Rakoczy, P.; Parzuchowski, P.; Sobiecki, M., Hyperbranched aliphatic polyethers obtained from environmentally benign monomer: glycerol carbonate. *Green Chemistry* **2005,** *7* (7), 529-539.
152. Indran, V. P.; Zuhaimi, N. A. S.; Deraman, M. A.; Maniam, G. P.; Yusoff, M. M.; Hin, T.-Y. Y.; Rahim, M. H. A., An accelerated route of glycerol carbonate formation from glycerol using waste boiler ash as catalyst. *RSC Advances* **2014,** *4* (48), 25257-25267.
153. Neyvis, A. B.; Sergey, P.; Luca, B.; Max, G. M.; Guillem, R. L.; Miquel, G. R.; Belén, V. G. A.; Pedro, H. A.; Núria, L., Structure, activity, and deactivation mechanisms in double metal cyanide catalysts for the production of polyols. *ChemCatChem* **2015,** *7* (6), 928-935.
154. Schuchardt, U.; Sercheli, R.; Vargas, R. M., Transesterification of vegetable oils: a review. *Journal of the Brazilian Chemical Society* **1998,** *9* (3), 199-210.
155. Gryglewicz, S., Rapeseed oil methyl esters preparation using héterogeneous catalysts. *Bioresource Technology* **1999,** *70* (3), 249-253.
156. Liu, X.; He, H.; Wang, Y.; Zhu, S., Transesterification of soybean oil to biodiesel using SrO as a solid base catalyst. *Catalysis Communications* **2007,** *8* (7), 1107-1111.
157. Masood, H.; Yunus, R.; Choong, T. S. Y.; Rashid, U.; Taufiq Yap, Y. H., Synthesis and characterization of calcium methoxide as heterogeneous catalyst for trimethylolpropane esters conversion reaction. *Applied Catalysis A: General* **2012,** *425–426*, 184-190.
158. Ono, Y., Dimethyl carbonate for environmentally benign reactions. *Catalysis Today* **1997,** *35* (1), 15-25.
159. Zhang, Y.; Wang, S.; Xiao, Z.; Chen, T.; Wang, G., Mesoporous silica-anchored organotin as heterogeneous catalyst for the transesterification of dimethyl carbonate with phenol. *Res. Chem. Intermed.* **2016**, *42* (9), 7213-7222.
160. Park, S.-J.; Hwang, I.-C.; Shin, S.-H., Liquid–liquid equilibria for ternary mixtures of methylphenyl carbonate, dimethyl carbonate, diphenyl carbonate, anisole, methanol, phenol, and water at several temperatures. *Journal of Chemical & Engineering Data* **2014,** *59* (2), 323-328.
161. Ono, Y., Catalysis in the production and reactions of dimethyl carbonate, an environmentally benign building block. *Applied Catalysis A: General* **1997,** *155* (2), 133-166.
162. Cheng, K.; Wang, S.-J.; Wong, D. S. H., Steady-state design of thermally coupled reactive distillation process for the synthesis of diphenyl carbonate. *Computers & Chemical Engineering* **2013,** *52*, 262-271.

163. Haubrock, J.; Raspe, M.; Versteeg, G. F.; Kooijman, H. A.; Taylor, R.; Hogendoorn, J. A., Reaction from dimethyl carbonate to diphenyl carbonate. 1. Experimental determination of the chemical equilibria. *Industrial & Engineering Chemistry Research* **2008,** *47* (24), 9854-9861.
164. Wang, S.; Tang, R.; Zhang, Y.; Chen, T.; Wang, G., 12-Molybdophosphoric acid supported on titania: A highly active and selective heterogeneous catalyst for the transesterification of dimethyl carbonate and phenol. *Chemical Engineering Science* **2015,** *138*, 93-98.
165. Zhou, X.; Ge, X.; Tang, R.; Chen, T.; Wang, G., Preparation and catalytic property of modified multi-walled carbon nanotube-supported TiO_2 for the transesterification of dimethyl carbonate with phenol. *Chinese Journal of Catalysis* **2014,** *35* (4), 481-489.
166. Krimm, H.; Buysch, H.-J.; Rudolph, H., US 4252737, **1981**.
167. Hallgren, J. E., US 4410464, **1983**.
168. Mark, V., US 4552704, **1985**.
169. Oyevaar, M. H.; To, B. W.; Doherty, M. F.; Malone, M. F., US 6093842, **2000**.
170. Holtbruegge, J.; Kuhlmann, H.; Lutze, P., Process analysis and economic optimization of intensified process alternatives for simultaneous industrial scale production of dimethyl carbonate and propylene glycol. *Chemical Engineering Research and Design* **2015,** *93*, 411-431.
171. Keller, T.; Holtbruegge, J.; Górak, A., Transesterification of dimethyl carbonate with ethanol in a pilot-scale reactive distillation column. *Chemical Engineering Journal* **2012,** *180*, 309-322.
172. Holtbruegge, J.; Wierschem, M.; Lutze, P., Synthesis of dimethyl carbonate and propylene glycol in a membrane-assisted reactive distillation process: pilot-scale experiments, modeling and process analysis. *Chemical Engineering and Processing: Process Intensification* **2014,** *84*, 54-70.
173. Harmsen, G. J., Reactive distillation: The front-runner of industrial process intensification: A full review of commercial applications, research, scale-up, design and operation. *Chemical Engineering and Processing: Process Intensification* **2007,** *46* (9), 774-780.
174. Harmsen, G.; Chewter, L., Industrial applications of multi-functional, multi-phase reactors. *Chemical engineering science* **1999,** *54* (10), 1541-1545.
175. Hiwale, R. S.; Bhate, N. V.; Mahajan, Y. S.; Mahajani, S. M., Industrial applications of reactive distillation: recent trends. *International Journal of Chemical Reactor Engineering* **2004,** *2* (1), 1542-6580.
176. Sharma, M.; Mahajani, S., Industrial applications of reactive distillation. *Reactive distillation: Status and future directions* **2003**, 1-29.
177. Haubrock, J.; Wermink, W.; Versteeg, G. F.; Kooijman, H. A.; Taylor, R.; van Sint Annaland, M.; Hogendoorn, J. A., Reaction from dimethyl carbonate (DMC) to diphenyl carbonate (DPC). 2. Kinetics of the reactions from DMC via methyl phenyl carbonate to DPC. *Industrial & Engineering Chemistry Research* **2008,** *47* (24), 9862-9870.
178. Weizhen, S.; Jianqiang, S.; Zhenhao, X.; Ling, Z., Thermodynamics and kinetics of transesterification reactions to produce diphenyl carbonate from dimethyl carbonate catalyzed by tetrabutyl titanate and dibutyltin oxide. *The Canadian Journal of Chemical Engineering* **2017,** *95* (2), 353-358.
179. Buchanan, J. S.; Jiang, Z.; Kowalski, J. A.; Santiesteban, J. G., US 6407279, **2002**.
180. Yin, X.; Zeng, Y.; Yao, J.; Zhang, H.; Deng, Z.; Wang, G., Kinetic modeling of the transesterification reaction of dimethyl carbonate and phenol in the reactive distillation reactor. *Industrial & Engineering Chemistry Research* **2014,** *53* (49), 19087-19093.

181. Wang, Q.; Li, C.; Guo, M.; Luo, S.; Hu, C., Transesterification of dimethyl carbonate with phenol to diphenyl carbonate over hexagonal $Mg(OH)_2$ nanoflakes. *Inorganic Chemistry Frontiers* **2015,** *2* (1), 47-54.
182. Lee, H.; Yong Bae, J.; Kwon, O. S.; Joon Kim, S.; Deuk Lee, S.; Sik Kim, H., Sulfonate-bonded tin complexes for the production of diphenyl carbonate. *Journal of Organometallic Chemistry* **2004,** *689* (10), 1816-1820.
184. Fu, Z.-h.; Ono, Y., Two-step synthesis of diphenyl carbonate from dimethyl carbonate and phenol using MoO_3-SiO_2 catalysts. *Journal of Molecular Catalysis A: Chemical* **1997,** *118* (3), 293-299.
185. Weiqing, Z.; Xinqiang, Z.; Yanji, W.; Jiyan, Z., Synthesis of diphenyl carbonate by transesterification over lead and zinc double oxide catalyst. *Applied Catalysis A: General* **2004,** *260* (1), 19-24.
186. Tang, R.; Chen, T.; Chen, Y.; Zhang, Y.; Wang, G., Core-shell TiO2@SiO2 catalyst for transesterification of dimethyl carbonate and phenol to diphenyl carbonate. *Chinese Journal of Catalysis* **2014,** *35* (4), 457-461.
187. Tong, D.; Chen, T.; Yao, J.; Wang, Y.; Wang, G.; Shi, D.; Li, Z.; Chen, Z., V–Cu composite oxide catalyst for transesterification of dimethyl carbonate with phenol to diphenyl carbonate. *Chinese Journal of Catalysis* **2007,** *28* (3), 190-192.
188. Romano, U.; Tesei, R., US 4045464, **1977**.
189. Mark, V., US 4554110, **1985**.
190. Kim, Y. T.; Park, E. D., Deactivation phenomena of MoO_3/SiO_2 and TiO_2/SiO_2 during transesterification between dimethyl carbonate and phenol. *Applied Catalysis A: General* **2009,** *356* (2), 211-215.
191. Kim, W. B.; Lee, J. S., Gas phase transesterification of dimethyl carbonate and phenol over supported titanium dioxide. *Journal of Catalysis* **1999,** *185* (2), 307-313.
192. Kim, W. B.; Kim, Y. G.; Lee, J. S., The role of carbon deposition in the gas phase transesterification of dimethylcarbonate and phenol over TiO_2/SiO_2 catalyst. *Applied Catalysis A: General* **2000,** *194–195*, 403-414.
193. Gao, Y.; Li, Z.; Su, K.; Cheng, B., Excellent performance of TiO_2(B) nanotubes in selective transesterification of DMC with phenol derivatives. *Chem. Eng. J. (Amsterdam, Neth.)* **2016,** *301*, 12-18.
194. Cao, M.; Meng, Y.; Lu, Y., Synthesis of diphenyl carbonate from dimethyl carbonate and phenol using O_2-promoted PbO/MgO catalysts. *Catalysis Communications* **2005,** *6* (12), 802-807.
195. Shaikh, A. A. G.; Sivaram, S., Dialkyl and diaryl carbonates by carbonate interchange reaction with dimethyl carbonate. *Industrial & Engineering Chemistry Research* **1992,** *31* (4), 1167-1170.
196. Davies, A. G.; Kleinschmidt, D. C.; Palan, P. R.; Vasishtha, S. C., Organotin chemistry. Part XI. The preparation of organotin alkoxides. *Journal of the Chemical Society C: Organic* **1971,** (0), 3972-3976.
197. Otera, J.; Danoh, N.; Nozaki, H., Novel template effects of distannoxane catalysts in highly efficient transesterification and esterification. *The Journal of Organic Chemistry* **1991,** *56* (18), 5307-5311.
198. Wang, Y.; Yao, J.; Zeng, Y.; Wang, G. Y., Mechanism study of dibutyltin oxide catalyzed transesterification of dimethyl carbonate with phenol. *Huaxue Xuebao* **2005**; *63*, 603-611.

Appendix I Calibration of GC

Calibration of GC (Example)

Calibration of PC, MeOH, DMC and PG are described as follows: (a) certain amount of PC, MeOH, DMC, PG and certain amount of mesitylene were measured accurately and charged into a 25 mL flask; (b) shake the flask vigorously to mix the mixture evenly; (c) 1 ml of the aqueous solution was added into the GC analysis vials and analyzed by GC; (d) three other samples and one verify sample with different concentrations of PC, MeOH, DMC and PG were made and analyzed by GC. The calibration curves for PC, MeOH, PG and DMC are shown in Figure A-1. Verify sample was used to verify the accuracy of the calibration curve. Actuate amount of verified sample and calculation from GC calibration were compare in Table A-1 , it is clear that the error is below 3.62%.

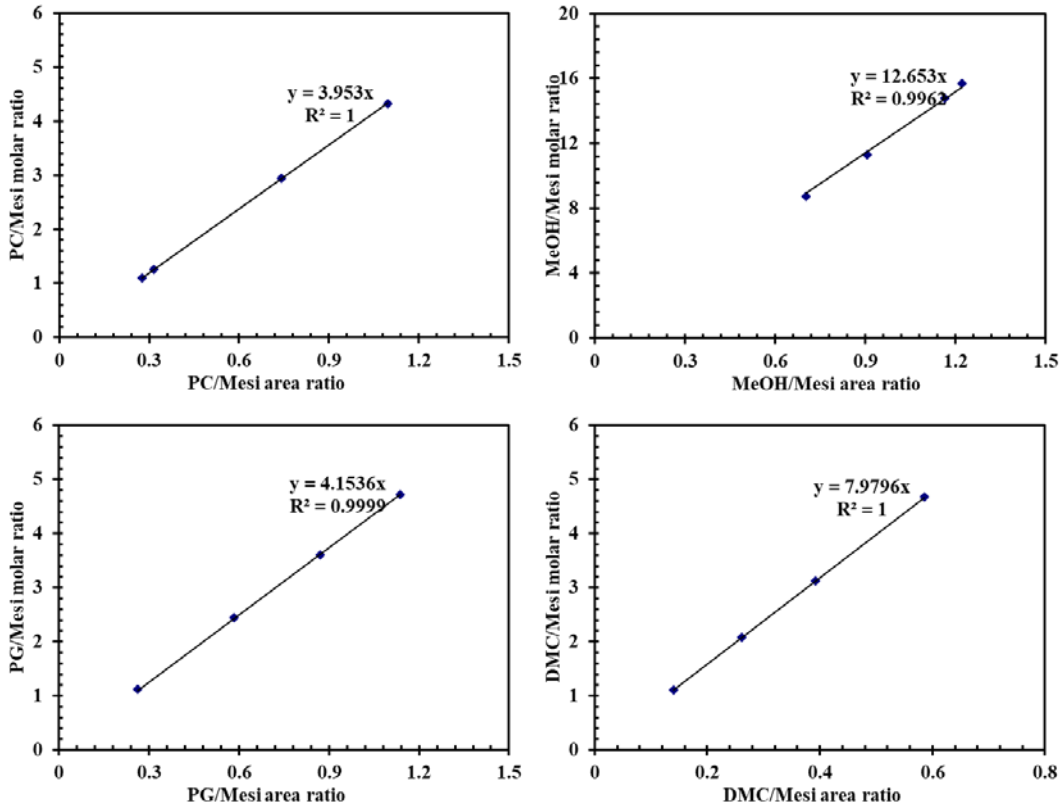

Figure A-1 Calibration of PC, MeOH, DMC, and PG using ZB-WAX column

Table A-1 Errors of accurate amount of verify sample and calculation from calibration curve

Verify sample	PC	DMC	PG
Real amount	1.878	1.5616	1.5236
Calculated amount	1.9460	1.5105	1.5536
Deviation	3.62%	-3.27%	1.97%

Similarly, the calibration of EC system and BC system was done using the same method. The calibration curves are shown in Figure A-2. Verify sample were also prepared for EC and BC system, respectively. The maximum error for the EC system is 2.96% and for BC system is 4.02%.

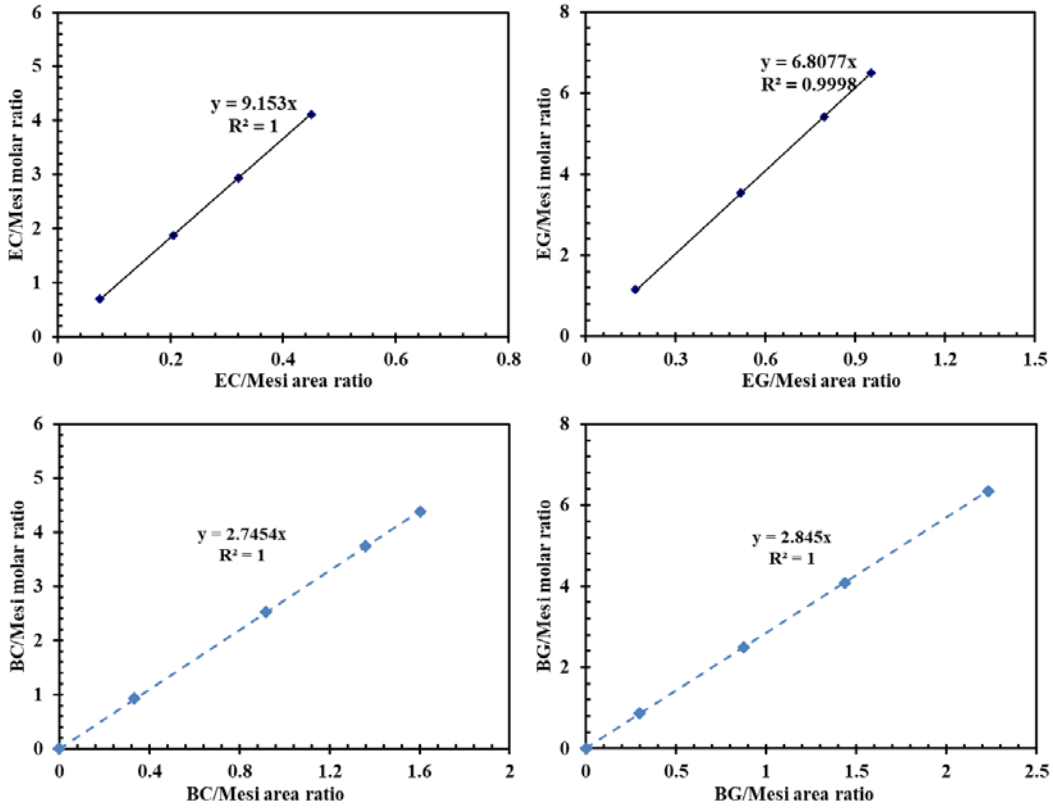

Figure A-2 Calibration curve for EC and BC systems

The calibration of DPC system was also done using the above method. The calibration curves are shown in Figure A-3. Verify sample were also prepared for every component in DPC

system. The analytical error for the DPC system (Methanol, DMC, Phenol, Anisol, Ethyl Benzolate, MPC and DPC) are 4.1%, 4.6%, 11.8%, 7.3%, 10%, 10.6%, and 15.6%, respectively.

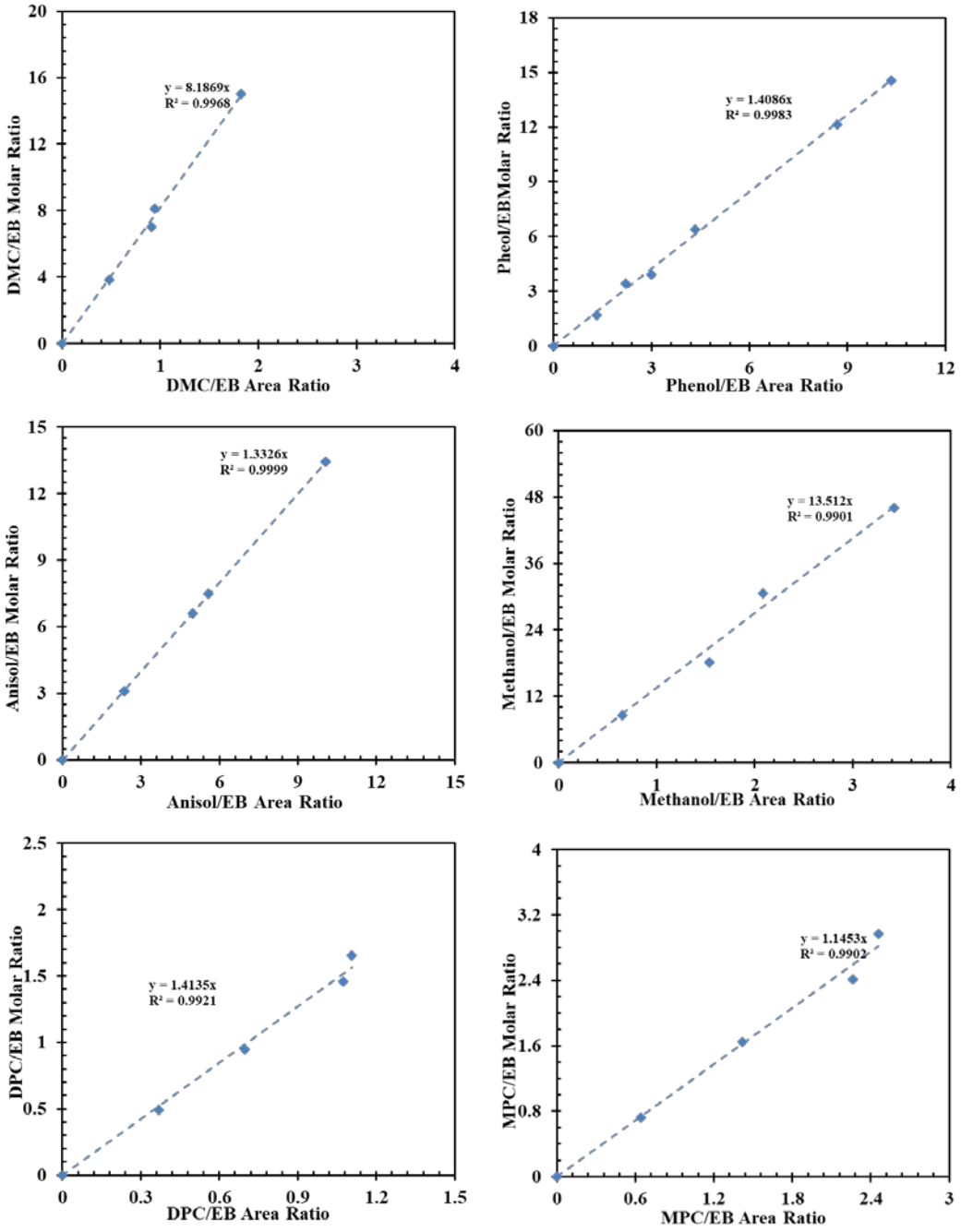

Figure A-3 Calibration curve for DPC system

Calibration of HPLC pump

Calibration of HPLC pump is described as follows: (a) set the HPLC pump at a certain flowrate; (b) then measure the volumetric of the liquid that at the outlet of the pump in 5 minutes using graduated cylinder; (c) the flowrate of the pump was compared with the one at the outlet; (d) five different flowrates were compared. The calibration curves HPLC pump is shown in Figure A-4.

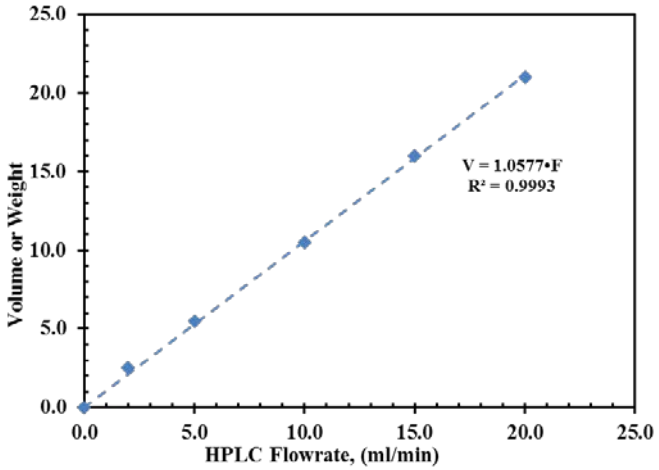

Figure A-4 Calibration of HPLC pump

Error analysis (Example)

Error analysis for transesterification using CaO as catalysts

(1) Experimental error

Typical experiment was repeated for two times and values of substrate/product concentration were derived (see Figure A-5), the error is in the range of 2.24%-17.3%, which was taken into account when parameter estimation was carried out.

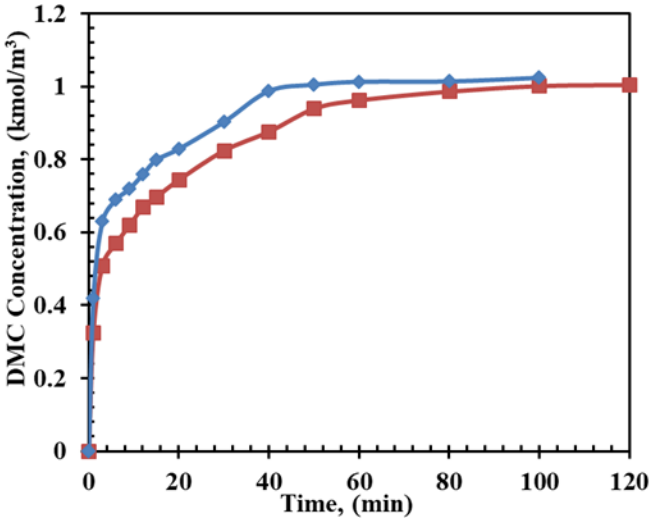

Figure A-5 Repeatability of experiment. Reaction conditions: PC, 1.1 kmol/m^3; methanol, 22.2 kmol/m^3; catalyst, 5 kg/m^3; T=20 °C; 0.69 MPa N_2.

(2) Analysis error from GC

The maximum error for GC analysis (repeated injection of one for three times) between each injection is only < 2.26%, while the maximum error between GC analysis and the actual amount is < 3.62%.

Error analysis for transesterification using Fe-Mn double metal cyanide catalysts

(1) Experimental error

Typical experiment was repeated for two times and values of substrate/product concentration were derived (see Figure A-6), the average experimental error during the reaction is 4.82%, which was taken into account when parameter estimation was carried out.

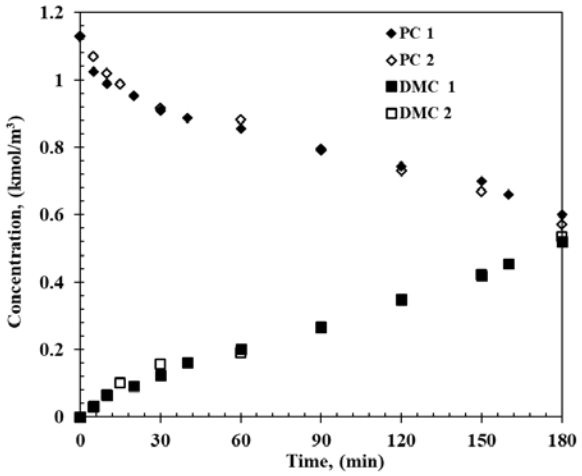

Figure A-6 Repeatability of experiment. Reaction conditions: PC, 1.1 kmol/m^3; methanol, 22.2 kmol/m^3; catalyst, 5 kg/m^3; T=140 °C; 0.69 MPa N_2

(2) Analysis error from GC

The maximum error for GC analysis (repeated injection of one for three times) between each injection is only < 0.6%, while the maximum error between GC analysis and the actual amount is < 2.2%. Both errors are lower compared with experimental error (< 4.82%).

(3) Uncertainty of activation energy from uncertainty of reaction rate constant

The activation energy was estimated based on estimated reaction rate constants from experimental data at each temperature, therefore, the uncertainty of activation energy relies on the uncertainty of reaction rate constants. The procedure for estimation of uncertainty of activation energy is summarized as follows.

The relationship between activation energy and reaction rate constant is $k=k_o \times e^{(-Ea/RT)}$

(a) Functions for error propagation are listed in Table A-2, which will be used to calculate uncertainty of activation energy.

Table A-2 Functions for propagation of error

Function	Propagated error
$z = a + b$	$\Delta z = [(\Delta a)^2 + (\Delta b)^2]^{1/2}$
$z = ca$	$\Delta z = \lvert c \rvert \Delta a$
$z = a \times b$	$\frac{\Delta z}{z} = \left[\left(\frac{\Delta a}{a}\right)^2 + \left(\frac{\Delta b}{b}\right)^2\right]^{1/2}$
$z = lna$	$\Delta z = \frac{\Delta a}{a}$

c is known exactly as constant, Δa is the uncertainty of a.

(b) The uncertainty for activation energy is determined by the following equation:

$$\ln(k_T) = \ln(k_0) - {}^{E_a}/_{RT}$$

After rearrangement,

$$E_a = RT[\ln(k_0) - \ln(k_T)]$$

Therefore, the uncertainty for activation energy can be expressed as,

$$\frac{\Delta E_a}{E_a} = \left[\left(\frac{\Delta T}{T}\right)^2 + \frac{\left[\frac{\Delta k_0}{k_0}\right]^2 + \left[\frac{\Delta k_T}{k_T}\right]^2}{[\ln(k_0) - \ln(k_T)]^2}\right]^{1/2}$$

(c) Take E_{a1} from power law for example,

The error from k_1 at 140 ^{o}C (413 K) is expressed in the following equation:

$$\Delta E_{a1T1} = E_{a1}\left[\left(\frac{\Delta T}{T_1}\right)^2 + \frac{\left[\frac{\Delta k_0}{k_0}\right]^2 + \left[\frac{\Delta k_{T_1}}{k_{T_1}}\right]^2}{\left[\ln(k_0) - \ln\left(k_{T_1}\right)\right]^2}\right]^{1/2}$$

$$= 47.03\,\frac{kJ}{mol} \times \left[\left(\frac{1\text{ K}}{413\text{ K}}\right)^2 + \frac{(1 - 0.96) + \left(\frac{0.047}{0.0.126}\right)^2}{[11.669 - \ln(0.126)]^2}\right]^{\frac{1}{2}} = 0.74\text{ kJ/mol}$$

(d) Similarly, error from 160 °C, 180 °C and 200 °C is 0.78 kJ/mol, 1.24 kJ/mol and 2.11 kJ/mol respectively.

(e) Therefore, the average activation energy uncertainty ΔE_{a1} is:

$$\Delta E_{a1} = \sqrt{\Delta E_{a_{T1}}{}^2 + \Delta E_{a_{T2}}{}^2 + \Delta E_{a_{T3}}{}^2 + \Delta E_{a_{T4}}{}^2} = 2.68\ \text{kJ/mol}$$

Calculation of intermediates

In this system, the components PC, MeOH, DMC and PG are the main components can be detected from GC. The responsive factor of PC, methanol, DMC and PG can be determined from the calibration curve using internal standard mesitylene, as shown below in Figure A-7. However, for the intermediates 2-HMC and 1-HP-2-MC, due to the absence of standard samples, the responsive factors were decided using a different method.

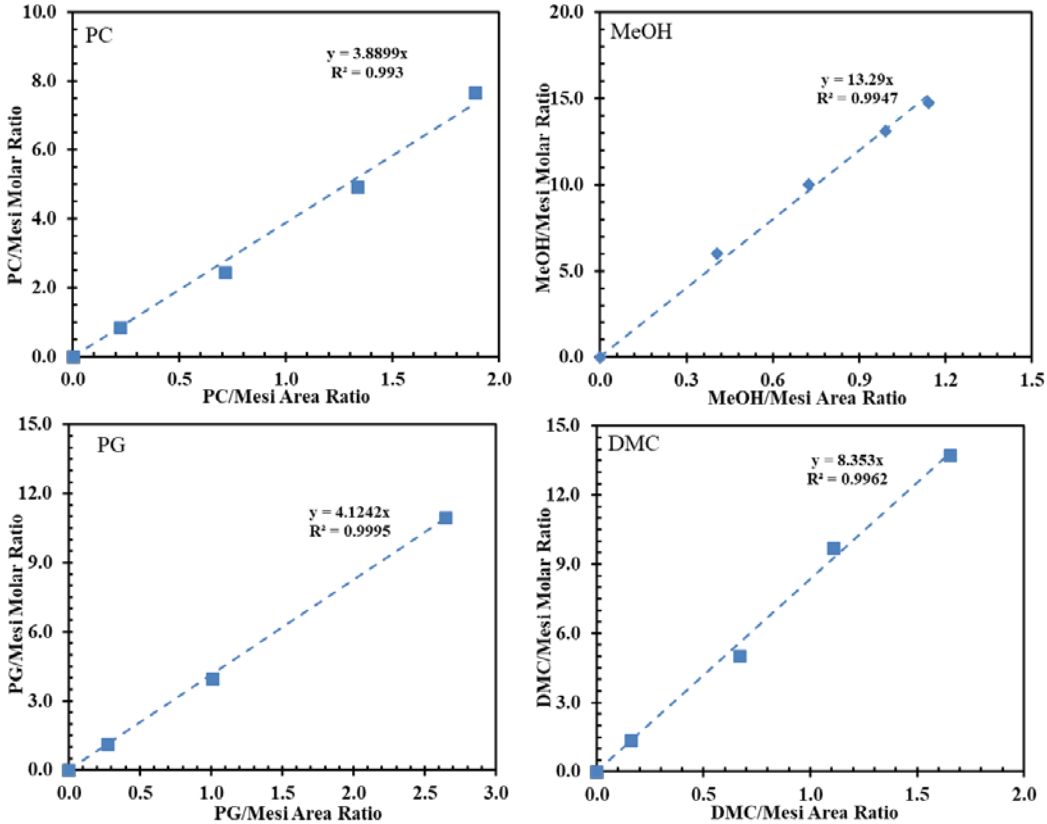

Figure A-7 Calibration of PC, MeOH, PG and DMC using ZB-FFAP column

Average responsive factors for the two intermediates were derived from three different GC graphs from three different reactions (under difference initial PC and methanol concentration) under 200 °C listed in Table A-3.

The detail of the process is described as follows: from selectivity data in Table 1-1, the mass balance loss can be derived, which believed to be caused by the formation of the two intermediates. Therefore, equations (1) and (2) were solved using Excel. The derived responsive factors are 37.29 and 0 for 2-HMC and 1-HP-2-MC, respectively. Through using these responsive factors, the average loss of mass balance is about 3.70%.

$$a \times \frac{A_1}{A} \times N + b \times \frac{A_2}{A} \times N = n_1 - n_2 \quad (1)$$

$$S_j = \sum_1^N (a \times \frac{A_1}{A} \times N + b \times \frac{A_2}{A} \times N + n_2 - n_1)^2 \quad (2)$$

in which, a, b are responsive factors for two intermediates separately, A, A_1, A_2 are peak areas for internal standard, 2-HMC and 1-HP-2-MC respectively, N is the molar for internal standard, n_1 is the molar PC consumed and n_2 is the molar DMC formed. S_j is the sum of squares of residues. Applying these responsive factors to reaction profiles under 140 °C, 160 °C and 180 °C, respectively. It is found that the average error from loss of mass balance is 5.06%, 11.28% and 6.58% at 140 °C, 160 °C and 180 °C, respectively, indicating the responsive factor actually can be used for the calculation of the intermediates in the range of the reaction conditions used in this work.

Table A-3 Mass balance profile for different reactions under 200 °C

PC Initial Concentration: 2.82 kmol/m^3		PC Initial Concentration: 1.69 kmol/m^3		PC Initial Concentration: 1.13 kmol/m^3	
time	selectivity of DMC (%)	time	selectivity of DMC (%)	time	selectivity of DMC (%)
15	76.8	15	74.51	15	90.96
30	79.3	30	75.97	30	96.3
60	85.2	60	82.42	60	92.22
95	88.62	90	86.97	90	96.91

125	88.68	120	87.92	120	96.54
150	92.01	150	91.16	150	96.44
180	90.25	180	95.41	180	98.39

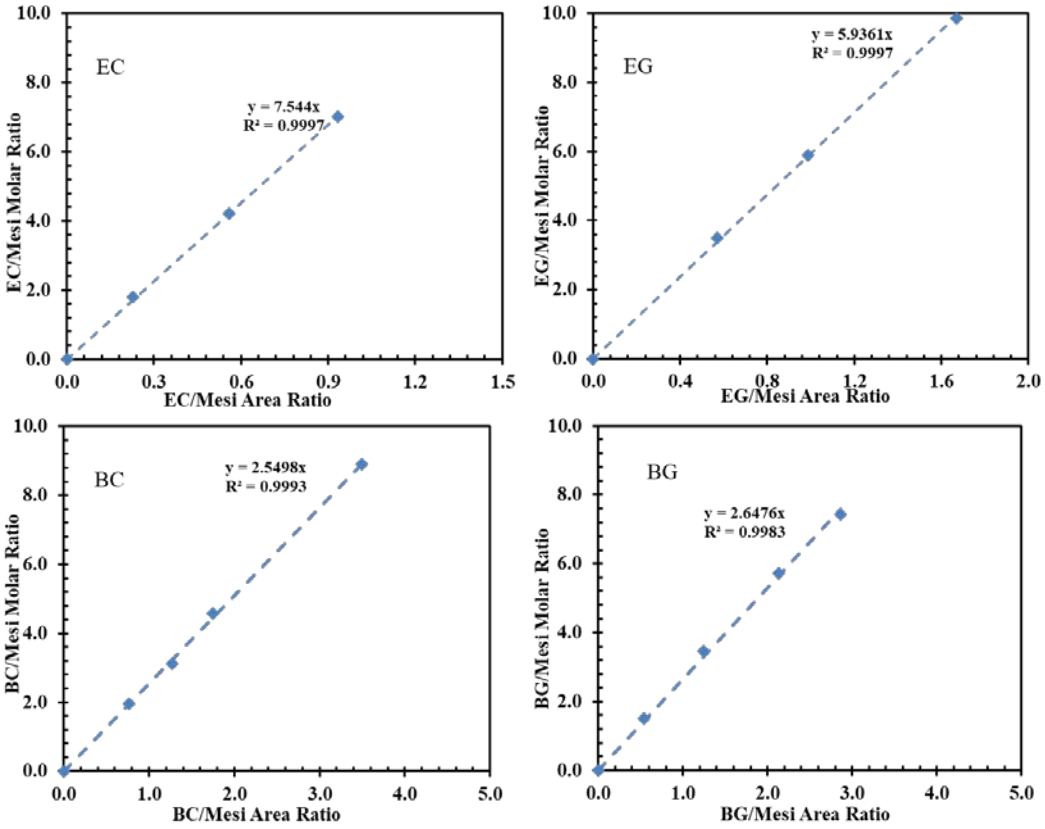

Figure A-8 Calibration of EC system and BC system using ZB-FFAP column

Calculation for guess value of rate constants

The guess values of rate constants are calculated from the initial reaction rate and equilibrium reaction rate. For the transesterification reaction of PC with methanol,

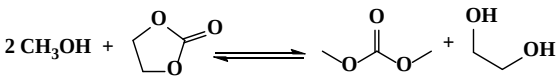

Assume the reaction is elementary reaction, therefore the reaction rate is as follows:

$$r = k_f \omega C_{PC} C_{MeOH}^2 - k_r \omega C_{DMC} C_{PG}$$

In which, k_f and k_r are the forward reaction constant and reversible reaction constant, respectively. C_{PC}, C_{MeOH}, C_{DMC} and C_{PG} are the concentration for PC, methanol, DMC and PG, respectively.

At the beginning of reaction, the concentration of DMC and PG are 0, therefore, the initial reaction rate is

$$r = k_f \omega C_{PC} C_{MeOH}^2$$

At the end of the reaction, when the reaction reaches equilibrium, the reaction rate is 0.

An example for estimated values is demonstrated as follows:

The concentration-time data of transesterification reaction of PC with methanol over CaO (concentration of 0.003839 kmol/m^3) at 20 °C is as follows:

Table A-4 Concentration-time profile of reaction of PC with methanol over CaO

Time, (h)	PC	Methanol	DMC	PG
0	1.105	22.03	0	0
0.017	0.978	20.79	0.169	0.213
0.05	0.801	20.67	0.329	0.377
0.1	0.684	20.63	0.44	0.488
0.15	0.624	20.57	0.493	0.543
0.2	0.6	20.49	0.52	0.576
0.25	0.468	20.42	0.63	0.695
0.33	0.428	20.35	0.681	0.76
0.5	0.363	20.26	0.733	0.815
0.67	0.32	20.19	0.76	0.858
0.83	0.295	20.17	0.805	0.904
1	0.27	20.13	0.825	0.924
1.33	0.215	20.03	0.872	0.987
1.67	0.181	19.97	0.901	1.012
2.0	0.17	19.94	0.914	1.051

At the beginning of the reaction, the initial reaction rate is 1.056 kmol/(m^3·h), thus,

$r=k_f*22.03*22.03*1.105*0.003839=1.056$

$k_f=0.5\ m^9/(kmol^3 \cdot h)$

when the reaction reaches equilibrium,

$r=0.5*19.94*19.94*0.17*0.003839-k_r*0.914*1.051*0.003839=0$

$k_r=35.2\ m^6/(kmol^2 \cdot h)$

Therefore, the guessed value of 0.5 and 35.2 will be used as the initial value for the estimation of reaction rate parameters of power law model.

Appendix II Calculation of Mass Transfer Limitation and GCMS Graph

Mass transfer limitation for transesterification using CaO as catalyst

Intraparticle transfer limitation of PC:

$$\varphi = \frac{d_p}{6}\left[\frac{(\mathrm{m}+1)\cdot\rho_p\cdot \mathrm{R_{Initial}}}{2\cdot \mathrm{D_e}\cdot\omega_{\mathrm{cat}}\cdot \mathrm{C_{PC}}}\right]^{0.5}$$

$d_p \leq 10^{-7}$ m (catalyst particle diameter)

$\rho_p \approx 3300$ kg/m^3 (density of catalyst))

$\mathrm{R_{Initial}} = 0.0035–1.387$ kmol/(m^3·min) (initial reaction rate)

$\mathrm{D_e} = \frac{\mathrm{D_M}\varepsilon}{\tau} \approx 0.004$ m^2/s (effective diffusivity)

$\mathrm{D_M} = \frac{7.8\times10^{-8}\cdot \mathrm{T}\cdot(\mathrm{XM_W})^{0.5}}{\mu_l \mathrm{V_m}^{0.6}} \approx 0.004$ m^2/s (molecular diffusivity)

$\omega_{\mathrm{cat}} = 0.073$-$0.365$ kg/m^3 (catalyst loading)

$\mathrm{C_{PC}} = 1.1–4.2$ kmol/m^3

$\varphi \approx 2.7\times10^{-6}$ -1.2×10^{-5}

The calculated parameter above is far smaller than the criteria 0.2.

Liquid-solid mass transfer limitation:

$$\alpha = \frac{\mathrm{R_{Initial}}}{\mathrm{k_{l-s}}\cdot \mathrm{a_p}\cdot \mathrm{C_{PC}}}$$

$\mathrm{R_{Initial}} = 0.0035–1.387$ kmol/(m^3·min) (initial reaction rate)

$\mathrm{k_{l-s}} = \mathrm{D_M F_C}\left(2 + 0.4\left[\frac{\mathrm{e}(\mathrm{d_p})^4 \rho_l^3}{\mu_l^3}\right]^{0.25}\left[\frac{\mu_l}{\rho_l \mathrm{D_M}}\right]^{0.333}\right)/\mathrm{d_p} \approx 0.008$ m/s (liquid-solid mass transfer coefficient)

$\mathrm{a_p} = \frac{6\omega_{cat}}{\rho_p\cdot \mathrm{d_p}} \approx 1330$-$6636$ (m^{-1}) (specific surface area)

$\rho_p \approx 3300$ kg/m^3 (density of catalyst)

$d_p \leq 10^{-7}$ m (catalyst particle diameter)

ω_{cat} = 0.073-0.365 kg/m^3 (catalyst loading)

C_{PC} = 1.1–4.2 kmol/m^3

$\alpha \approx 3.0\times10^{-4}$ -6.22×10^{-3}

Even if the error of parameter is 10000%, the external liquid-solid mass transfer limitation (3.0×10^{-2}– 6.22×10^{-1}) is still much lower than 0.1.

Mass transfer limitation for transesterification using Fe-Mn double metal cyanide as catalyst

Intraparticle transfer limitation of PC:

$$\varphi = \frac{d_p}{6}\left[\frac{(m+1)\cdot\rho_p\cdot R_{Initial}}{2\cdot D_e\cdot\omega_{cat}\cdot C_{PC}}\right]^{0.5}$$

$d_p \leq 0.000125$ m (catalyst particle diameter)

$\rho_p \approx 744$ kg/m^3 (density of catalyst))

$R_{Initial} = 0.0065$–0.0732 kmol/(m^3·min) (initial reaction rate)

$D_e = \frac{D_M\varepsilon}{\tau}$ m^2/s (effective diffusivity)

$D_M = \frac{7.8\times10^{-8}\cdot T\cdot(XM_W)^{0.5}}{\mu_l V_m^{0.6}} \approx 3.11\times10^{-5}$ m^2/s (molecular diffusivity)

ω_{cat} = 5 kg/m^3 (catalyst loading)

C_{PC} = 1.1–4.2 kmol/m^3

$\varphi \approx 4.52\times10^{-4}$– 7.77×10^{-4}

Even if the error of parameter is 10000%, the intraparticle mass transfer limitation (0.0452-0.0777) is still much lower than 0.2.

Liquid-solid mass transfer limitation:

$\alpha = \frac{R_{Initial}}{k_{l-s} \cdot a_p \cdot C_{PC}}$

$R_{Initial} = 0.0065–0.0732$ kmol/(m^3·min) (initial reaction rate)

$k_{l-s} = D_M F_C (2 + 0.4 \left[\frac{e(d_p)^4 \rho_l{}^3}{\mu_l{}^3}\right]^{0.25} \left[\frac{\mu_l}{\rho_l D_M}\right]^{0.333}) / d_p \approx 0.498$ m/s (liquid-solid mass transfer coefficient)

$a_p = \frac{6\omega_{cat}}{\rho_p \cdot d_p} \approx 322.6$ (m^{-1}) (specific surface area)

$\rho_p \approx 744$ kg/m^3 (density of catalyst)

$d_p \leq 0.000125$ m (catalyst particle diameter)

$\omega_{cat} = 5$ kg/m^3 (catalyst loading)

$C_{PC} = 1.1–4.2$ kmol/m^3

$\alpha \approx 6.13\times10^{-7} – 1.81\times10^{-6}$

Even if the error of parameter is 10000%, the external liquid-solid mass transfer limitation ($6.13\times10^{-5} – 1.81\times10^{-4}$) is still much lower than 0.1.

GCMS graph for intermediates

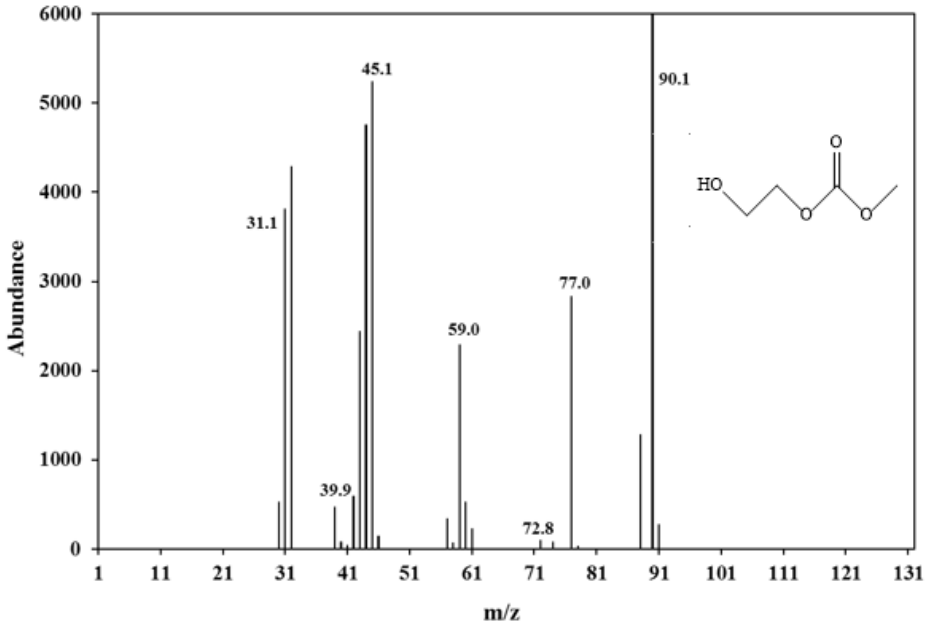

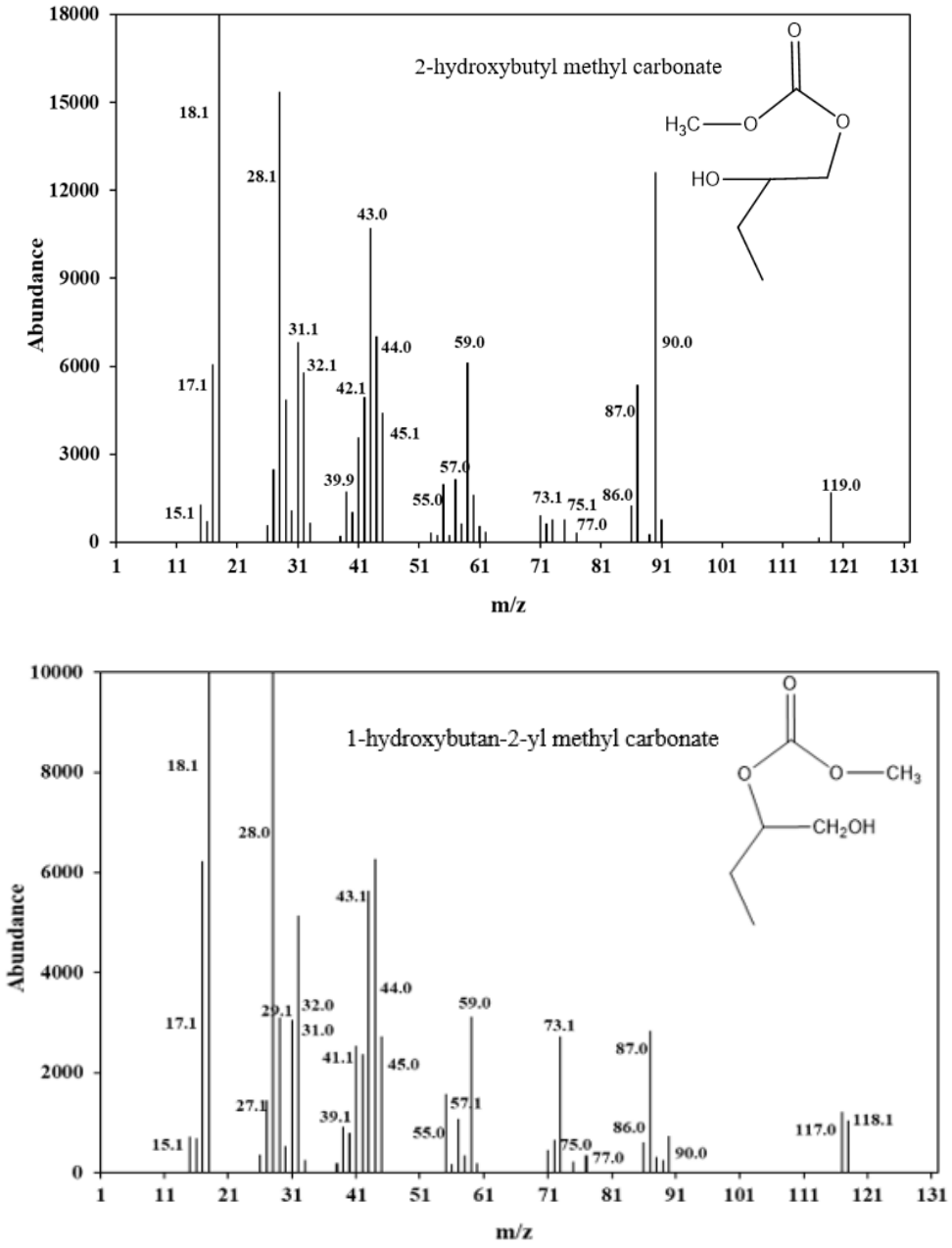

Figure A-9 GCMS for intermediates of EC system and BC system

Survey Spectra of Fe-Mn complex

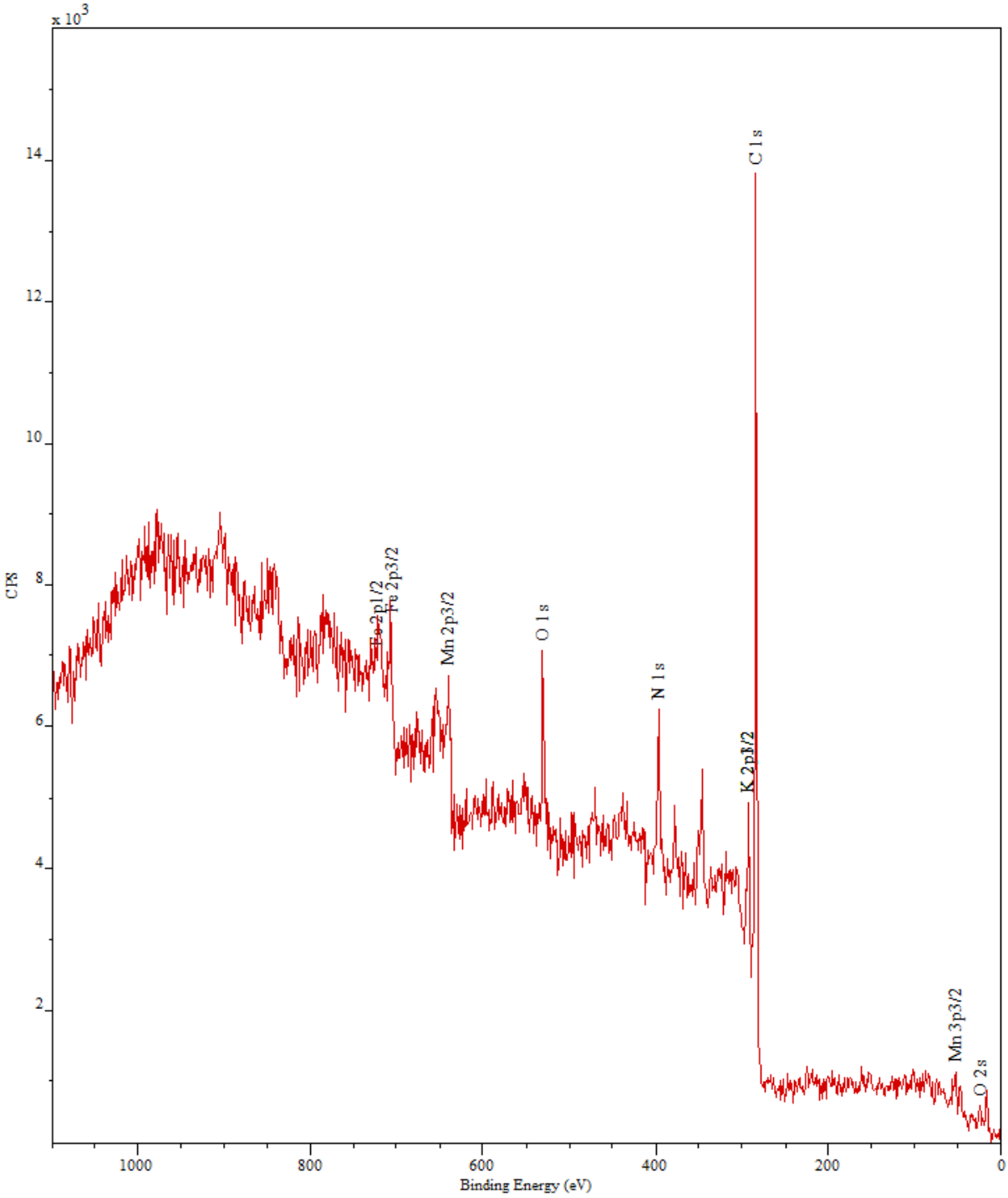

Figure A-10 Survey spectra of Fe-Mn complex

Appendix III Estimated Parameters from Kinetic Models

Parameter estimation for transesterification using CaO as catalyst

Table A-5 Parameter estimation for homogenous reaction from Model (ii)

Rate Constants	20 ℃	30 ℃	40 ℃	50 ℃
$k_1\times10^{-3}$, ($m^3\cdot h\cdot kmol^{-1}$)	1.87±0.61	7.21±2.93	31.5±14.1	32.9±16.7
$k_{-1}\times10^{-2}$, (h^{-1})	0.11±0.44	6.78±4.38	42.8±16.6	58.7±13.6
$k_2\times10^{-4}$, ($m^3\cdot h\cdot kmol^{-1}$)	0.41±0.18	0.62±0.27	1.32±0.37	5.98±4.28
$k_{-2}\times10^{-6}$, (h^{-1})	1.86±0.06	1.37±0.80	3.56±0.96	9.42±8.20
$k_3\times10^{-8}$, ($m^3\cdot h\cdot kmol^{-1}$)	2.36±0.20	3.78±0.45	5.79±0.41	24.4±1.66
$k_{-3}\times10^{-10}$, ($m^9\cdot h^3\cdot kmol^{-3}$)	3.39±1.92	4.76±3.10	6.44±2.07	13.7±12.3

Table A- 6 Parameter estimation for heterogeneous reaction from Model (ii)

Rate Constants	20 ℃	40 ℃	50 ℃
$k_1\times10^{-2}$, ($m^3\cdot h\cdot kmol^{-1}$)	1.84±0.04	4.14±1.88	5.04±2.34
$k_{-1}\times10^{-2}$, (h^{-1})	1.23±0.46	2.06±1.84	0.70±0.22
$k_2\times10^{-6}$, ($m^6\cdot h^2\cdot kmol^{-2}$)	1.17±0.003	9.70±20.6	3.17±2.92
$k_{-2}\times10^{-5}$, (h^{-1})	0.19±0.0004	0.76±1.61	7.91±1.28
$k_3\times10^{-9}$, ($m^6\cdot h^2\cdot kmol^{-2}$)	7.57±0.13	9.25±18.30	87.10±14.10
$k_{-3}\times10^{-15}$, ($m^{15}\cdot h^5\cdot kmol^{-5}$)	0.99±0.60	8.20±2.57	9.74±1.57

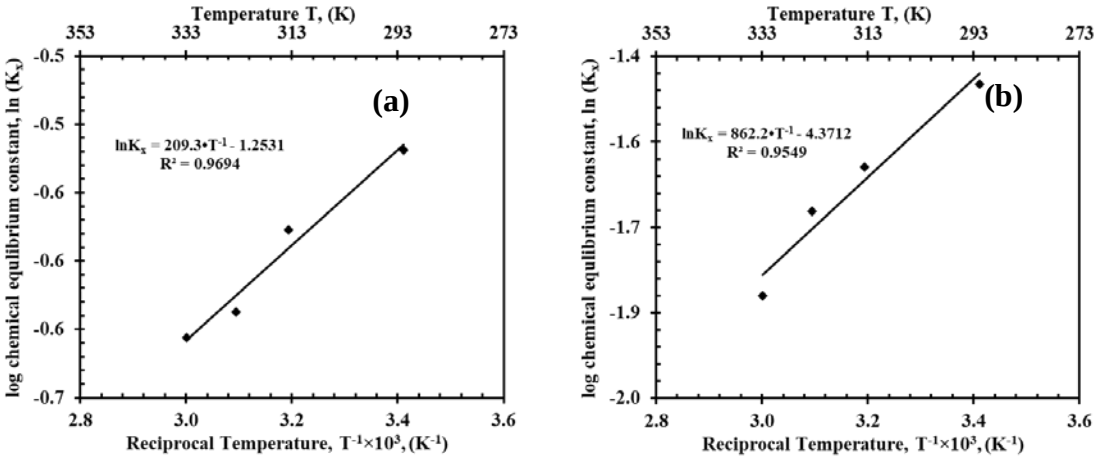

Figure A-11 Van't Hoff plot for the molar-based chemical equilibrium constant K_x derived from experimental results, (a) EC system, (b) BC system.

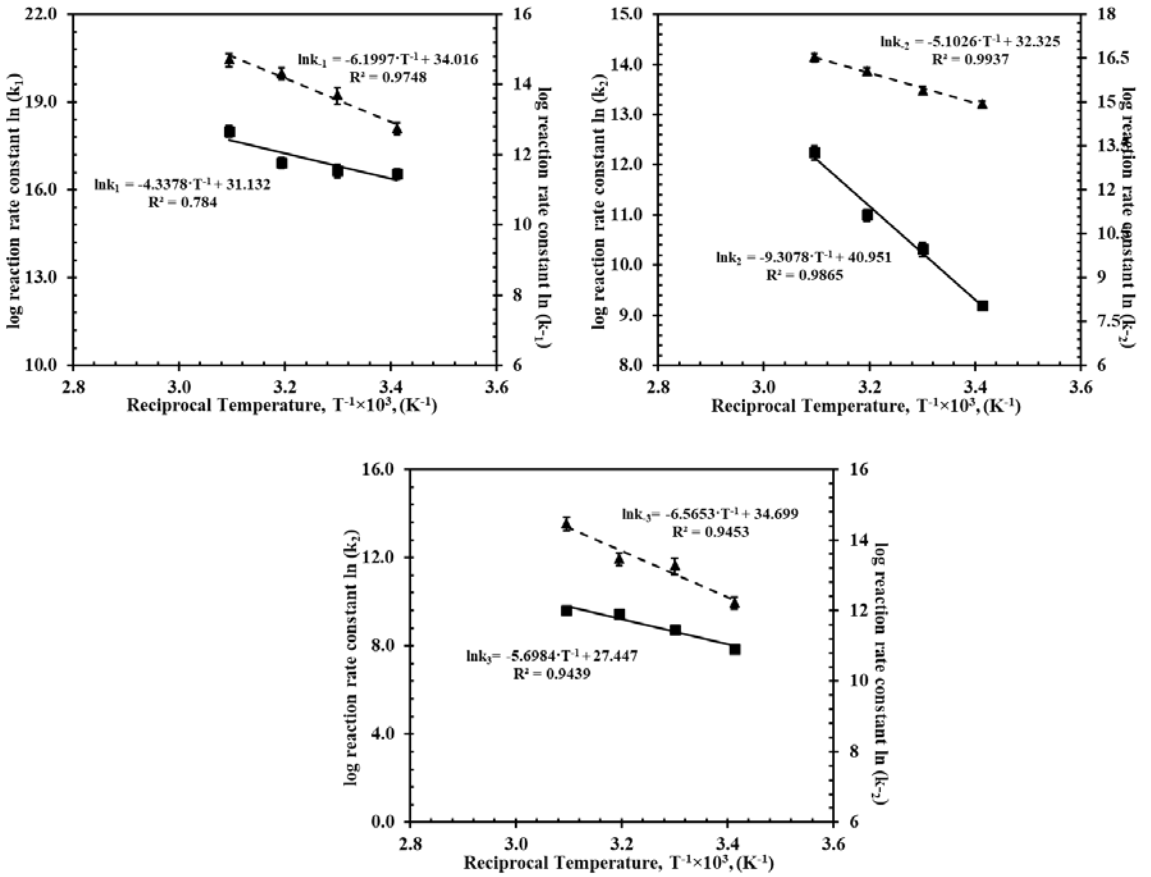

Figure A-12 Arrhenius plot. Parameters estimation from model (i) for homogeneous reaction for (a) first step, (b) second step, (c) third step

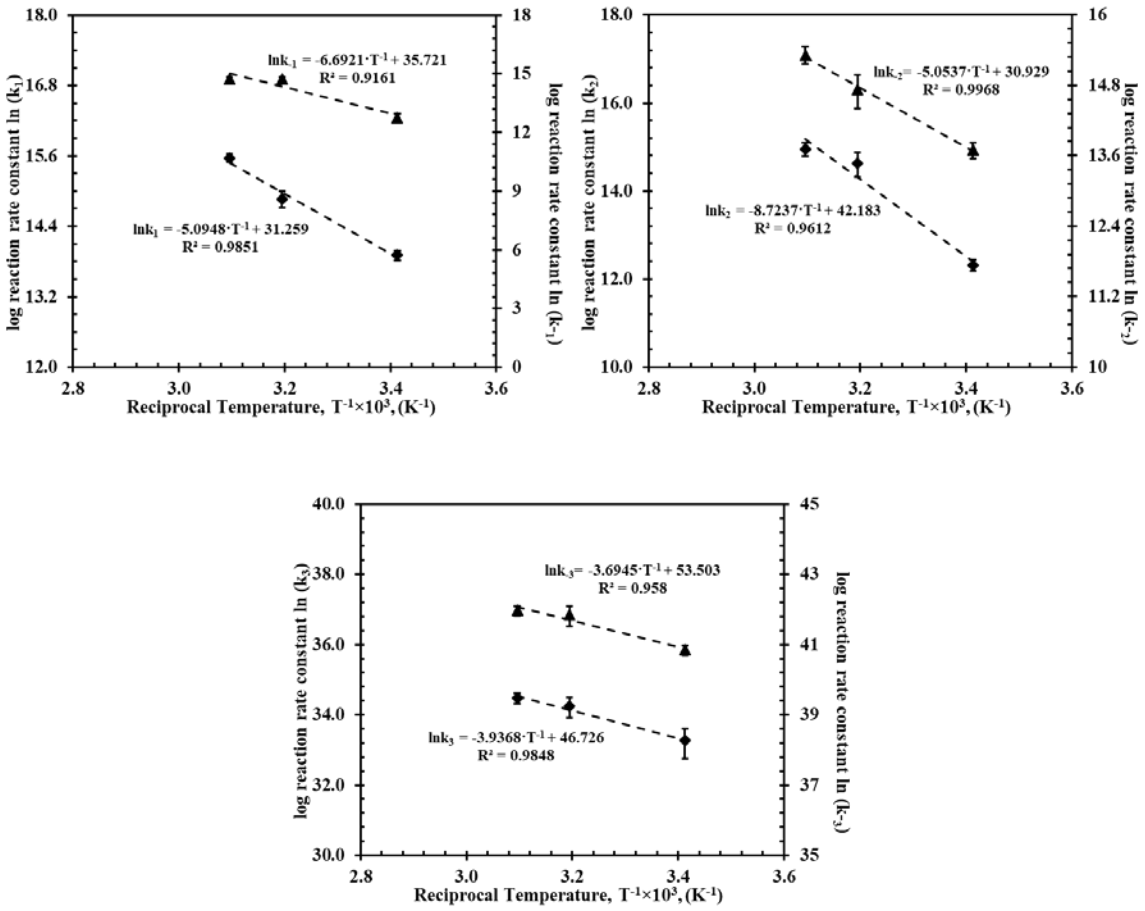

Figure A-13 Arrhenius plot. Parameters estimation from model (i) for heterogeneous reaction for (a) first step, (b) second step, (c) third step

Parameters for calculation of reaction equilibrium constants

Table A-7 Enthalpy and entropy data used for the calculation of reaction equilibrium constants

	MeOH	EC	PC	BC	DMC	EG	PG	BG
Enthalpy of formation kJ/mol	-239.45	-584.2	-614.1	-640.1	-608.76	-455.3	-489	-509.7
entropy J/mol/K	126.98	132.54	210.16	220.46[126]	213.58[127]	155	211	242.27

Parameter estimation for transesterification using Fe-Mn double metal cyanide as catalyst

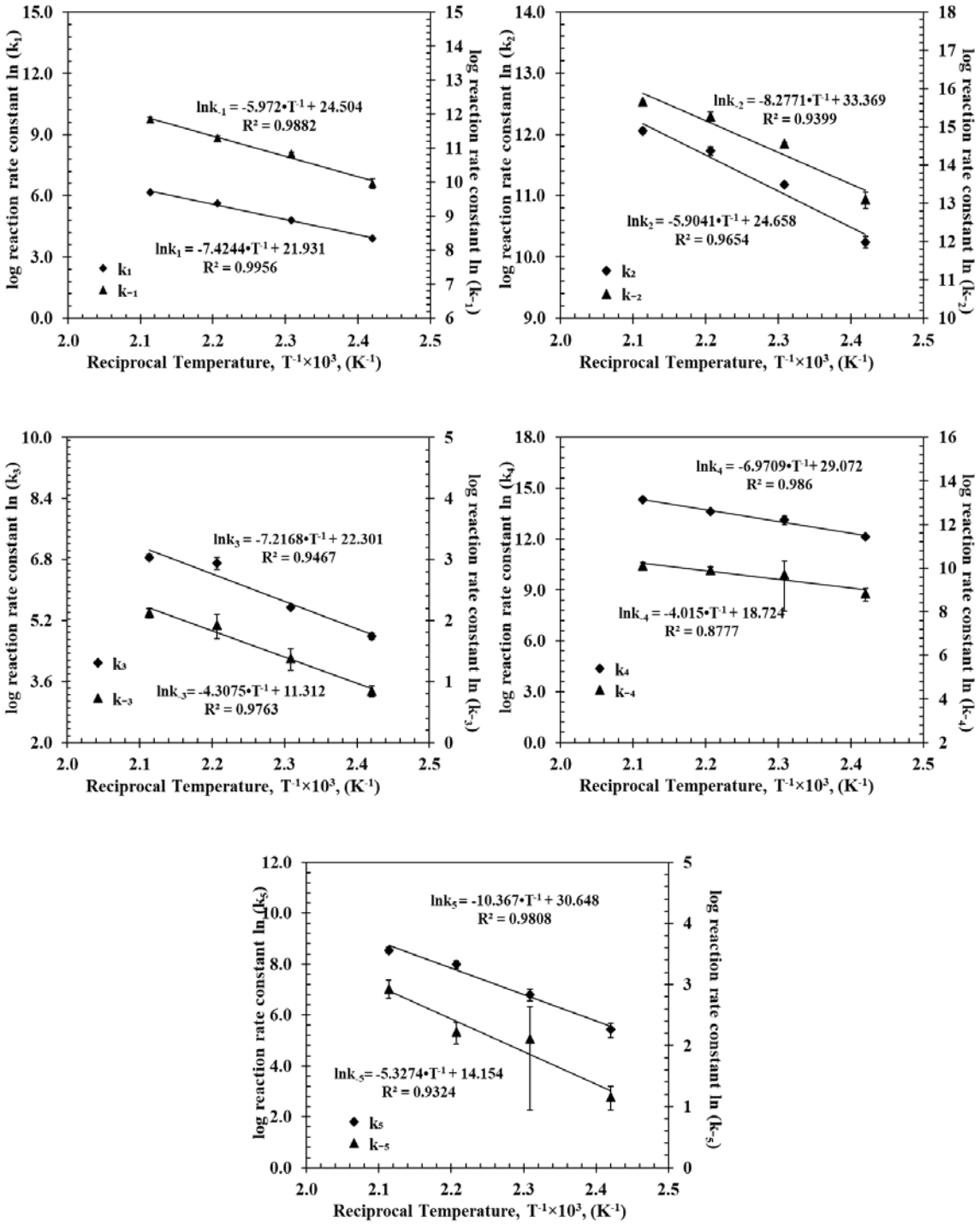

Figure A-14 Arrhenius plot. Parameters estimation from microkinetic modelling for (a) first step, (b) second step, (c) third step, (4) fourth step, (5) fifth step

Parameter estimation for Model (ii)–Model (iv):

Table A-8 Parameter estimation for Model *ii*

Rate Constants	140 °C	160 °C	180 °C	200 °C
k_1, ($m^3 \cdot min^{-1} \cdot kmol^{-1}$)	3.05±1.51	4.46±0.43	11.49±2.14	22.70±1.88
$k_{-1} \times 10^{-4}$, (min^{-1})	1.13±0.15	2.27±0.59	6.61±0.84	8.87±6.64
$k_2 \times 10^{-3}$, ($m^3 \cdot min^{-1} \cdot kmol^{-1}$)	0.37±0.35	1.18±1.02	2.95±3.81	4.54±0.15
$k_{-2} \times 10^{-3}$, (min^{-1})	1.31±0.09	7.88±7.56	9.36±12.91	27.06±33.92
$k_3 \times 10^{-3}$, (min^{-1})	1.34±0.09	2.02±0.06	3.23±0.20	4.54±0.16
$k_{-3} \times 10^{-1}$, ($m^3 \cdot min^{-1} \cdot kmol^{-1}$)	2.07±1.22	0.86±0.17	3.24±0.19	1.36±0.24
$k_4 \times 10^{-3}$, ($m^3 \cdot min^{-1} \cdot kmol^{-1}$)	0.48±0.31	3.38±0.94	3.04±0.88	7.05±1.82
$k_{-4} \times 10^{-2}$, (min^{-1})	3.93±1.03	1.52±0.58	1.71±0.36	1.80±0.44
$k_5 \times 10^{-5}$, (min^{-1})	0.26±0.05	1.00±0.17	5.93±0.65	10.31±0.08
$k_{-5} \times 10^{-3}$, ($m^6 \cdot min^{-1} \cdot kmol^{-2}$)	1.30±0.34	9.53±3.62	9.08±1.87	31.67±7.80

Table A-9 Parameter estimation for Model *iii*

Rate Constants	140 °C	160 °C	180 °C	200 °C
k_1, ($m^3 \cdot min^{-1} \cdot kmol^{-1}$)	4.18±0.30	11.57±4.92	256.64±78.21	11.48±3.01
$k_{-1} \times 10^{-2}$, (min^{-1})	2.36±2.02	Negative	1.28±0.34	1.64±0.53
$k_2 \times 10^{-3}$, ($m^3 \cdot min^{-1} \cdot kmol^{-1}$)	2.26±0.68	2.39±5.36	0.17±0.91	0.31±0.09
$k_{-2} \times 10^{-4}$, (min^{-1})	1.60±0.22	7.44±0.25	1.06±0.89	0.50±0.47
$k_3 \times 10^{-6}$, ($m^3 \cdot min^{-1} \cdot kmol^{-1}$)	2.61±2.76	1.33±3.11	5.23±0.16	19.30±19.58
$k_{-3} \times 10^{-7}$, ($m^3 \cdot min^{-1} \cdot kmol^{-1}$)	2.09±0.14	2.84±0.48	2.12±0.56	4.78±0.15
$k_4 \times 10^{-2}$, (min^{-1})	1.05±0.14	4.98±1.09	11.20±2.82	0.77±0.15
k_{-4}, ($m^3 \cdot min^{-1} \cdot kmol^{-1}$)	4.88±1.07	1362.9±705.9	584.76±315.2	10.42±2.32
$k_5 \times 10^{-4}$, ($m^3 \cdot min^{-1} \cdot kmol^{-1}$)	1.95±0.94	2.48±1.16	4.60±0.91	2.46±0.23
$k_{-5} \times 10^{-4}$, ($m^3 \cdot min^{-1} \cdot kmol^{-1}$)	0.08±0.01	1.76±5.94	0.46±0.36	1.04±0.28
$k_6 \times 10^{-4}$, (min^{-1})	7.86±0.88	1.74±0.46	2.27±0.78	8.64±0.76
$k_{-6} \times 10^{-4}$, ($m^6 \cdot min^{-1} \cdot kmol^{-2}$)	1.24±0.53	3.43±7.79	6.04±4.56	0.43±0.18

Table A-10 Parameter estimation for Model *iv*

Rate Constants	140 °C	160 °C	180 °C	200 °C
k_1, ($m^3 \cdot min^{-1} \cdot kmol^{-1}$)	0.25±0.024	0.37±0.28	3.42±0.38	6.93±0.73
$k_{-1} \times 10^2$, (min^{-1})	1.24±0.36	9.24±1.87	6.08±0.82	9.04±0.95
$k_2 \times 10^{-1}$, ($m^3 \cdot min^{-1} \cdot kmol^{-1}$)	1.24±0.99	2.47±1.98	3.86±0.39	10.42±6.89
$k_{-2} \times 10^{-2}$, (min^{-1})	3.12±3.52	1.32±3.92	2.91±1.64	5.95±0.48
$k_3 \times 10^{-5}$, ($m^3 \cdot min^{-1} \cdot kmol^{-1}$)	0.72±0.05	4.58±0.23	6.39±1.28	43.60±3.49
$k_{-3} \times 10^{-8}$, ($m^3 \cdot min^{-1} \cdot kmol^{-1}$)	0.30±0.022	1.35±0.044	2.86±0.57	5.67±0.45
$k_4 \times 10^{-3}$, (min^{-1})	1.24±0.009	14.94±43.80	19.05±0.69	19.30±0.64
$k_{-4} \times 10^{-3}$, ($m^3 \cdot min^{-1} \cdot kmol^{-1}$)	0.12±0.005	6.01±0.19	12.13±6.85	108.64±3.62
$k_5 \times 10^{-3}$, ($m^3 \cdot min^{-1} \cdot kmol^{-1}$)	1.10±0.002	0.23±0.45	7.29±1.14	38.42±5.34
$k_{-5} \times 10^{-6}$, (min^{-1})	0.89±0.04	0.85±0.13	7.24±1.13	70.23±6.22
$k_6 \times 10^{-7}$, (min^{-1})	0.21±0.009	0.89±1.72	1.50±0.23	5.43±0.48
$k_{-6} \times 10^{-6}$, ($m^6 \cdot min^{-1} \cdot kmol^{-2}$)	0.52±0.02	2.46±2.09	4.67±1.18	7.01±0.62

Appendix IV Additional Experimental Results

Chapter 2

Catalyst Evaluation (Supported CaO)

Six supported CaO was tested using 300 ml Parr reactor at 20 °C. 0.15 mol PC, 3 mol methanol, 1 g supported CaO and about 3 g mesitylene were added into the reactor together. For the convenience of taking samples, 100 psi N_2 was charged. Then the reaction mixture turned into vigorous stirring. From time to time, liquid samples would be taken to analyze using GC. The temporary concentration-time profiles for the six catalysts are shown in Figure A-15. Like the condition of CaO, 10 min to 20 min induction period was observed for all these six catalysts. After the induction period, the reaction rate just picked up quickly. Then, the reaction reached equilibrium quickly.

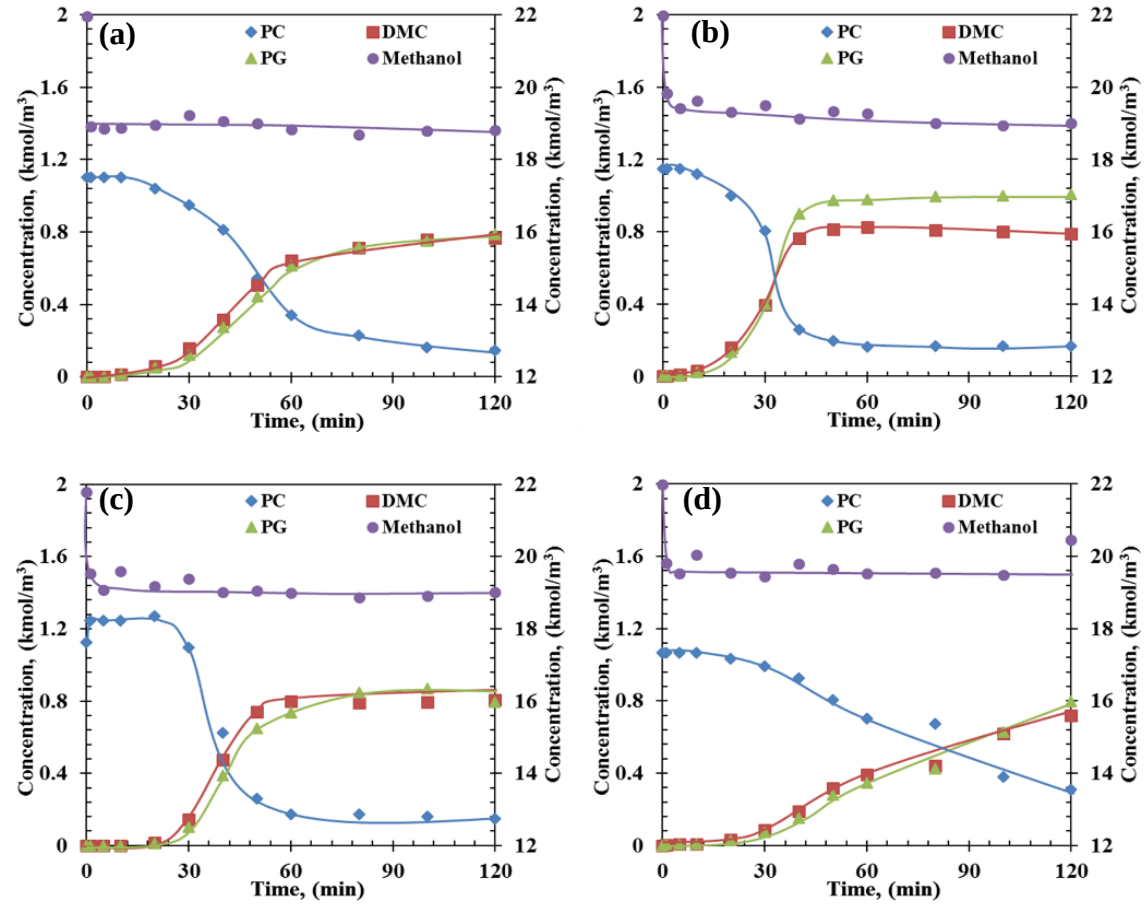

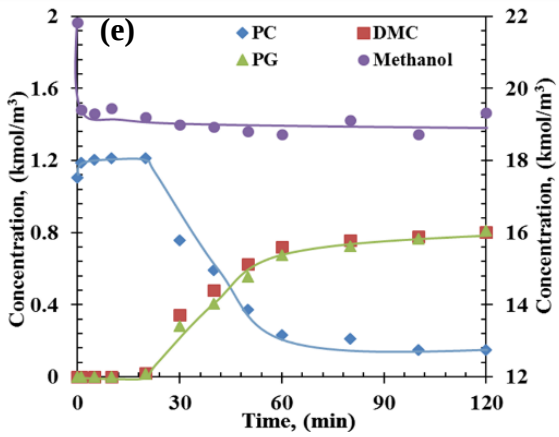

Figure A-15 Concentration-time profile on Supported CaO. (a). CaO/Al_2O_3, (b). CaO/NaY, (C). CaO/13X, (d). CaO/C, (e). CaO/TiO_2 Reaction conditions: PC: 1.07 kmol/m^3, Methanol: 21.4 kmol/m^3, Catalyst: 6.73 kg/m^3, Temperature: 20 °C

Preparation of Supported Ca-Co Mixed Oxides

5 g support was stirred in 100ml distill water vigorously for 1 hr. Then, Na_2CO_3 and NaOH mixture solution was added to the solution to prepare a basic aqueous solution at around pH 11 (As the pH is measured using pH paper, it may not that accurate). Certain amount of $Ca(NO_3)_2{\cdot}4H_2O$ and $Co(NO_3)_2{\cdot}6H_2O$ were mixed and stirred vigorously for 1 h to achieve homogeneous mixing, then drop wised into the prepared basic aqueous solution. Precipitation was controlled at pH 9–10 by adding mix solution of Na_2CO_3 and NaOH when necessary. The resulting precipitations were stirred vigorously for overnight then aged for 2 hr. After aging, the precipitates were filtered and washed thoroughly with distill water until the filtrate remains pH 7. Then the solid was dried in oven under 120 °C for overnight. Finally, the dried solid was calcined at 800 °C for 4 h with the ramp at 1 °C/min. The detail description of the preparation procedure is shown in Figure A-16.

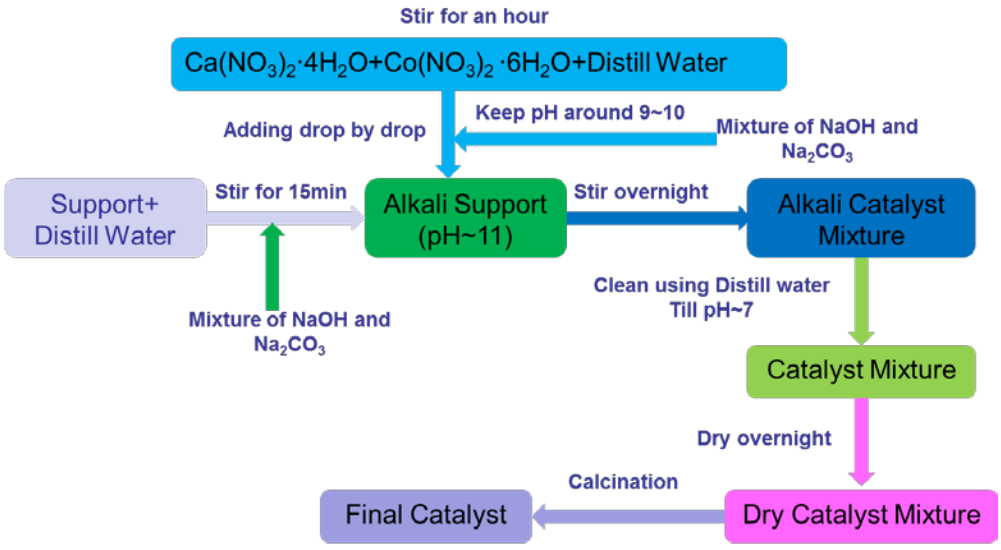

Figure A-16 Catalyst Preparation Procedure

Catalyst Evaluation (Supported Ca-Co Mixed Oxides)

7 different supported Ca-Co mixed oxides have been tested for this reaction, the results listed in Figure A-17. According to the results, Co-Ca/Al_2O_3 is the most active one under the same condition. Thus, Co-Ca/Al_2O_3 was chosen for the following research.

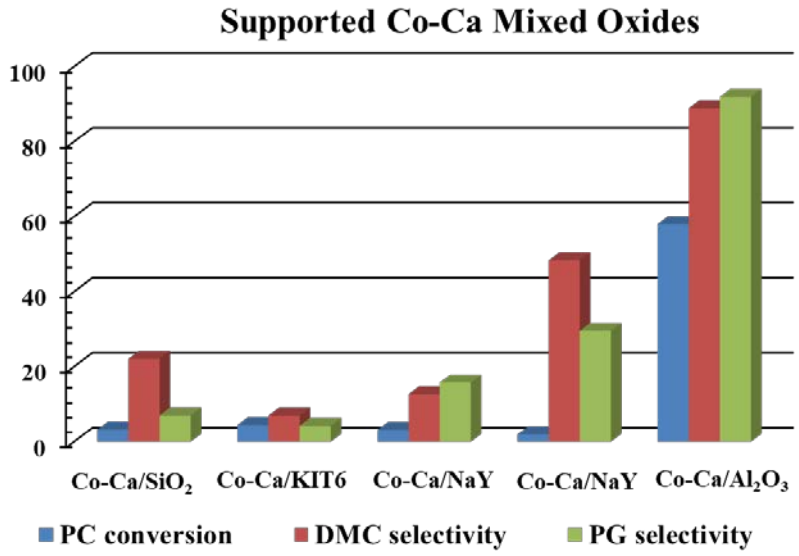

Figure A-17 Catalyst Evaluation. Reaction conditions: Reaction Temperature: 50 °C, Catalyst loading: 0.9 wt%, PC/MeOH=1:20.

Catalyst Preparation Parameters Screening

Calcined in N_2 Flow or in Stable Air

Co-Ca/Al_2O_3 calcined in different environments were tested, the concentration-time profiles of which were shown in Figure A-18. From the comparison, it is clear that when calcined in stable air, Co-Ca/Al_2O_3 showed no activity for the transesterification. However, when calcined in N_2 flow, the PC conversion increased to 58% and the selectivity of DMC increased to 89%. Thus, for the following study, the catalyst used was calcined in N_2 flow.

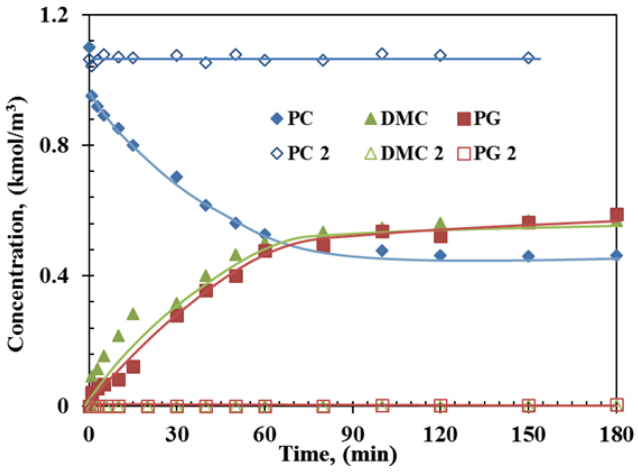

Figure A-18 Comparison of Different Calcination Environment. Solid markers are for catalyst calcined with N_2 flow, hollow markers are for catalyst calcined in stable air. Reaction conditions: Reaction Temperature: 50 °C, Catalyst loading: 0.9 wt%, PC/MeOH=1:20.

Composition Effect

(a) Ca Composition Effect

By keeping the Co composition the same, the Ca composition effect was done. Three different Ca compositions (6.4 wt%, 12.3 wt% and 18.0 wt%) were tested, it is found that with increasing Ca composition, the PC conversion increased, while DMC selectivity kept nearly the same. The temporary concentration-time profiles of different Ca composition effect are shown in Figure A-19. the results showed that when Ca composition increased from 6.4% to 12.3%, slight

increase in activity was observed. However, when the Ca composition increased to 18.0%, significant increase in activity was found. The significant increase of activity may due to the sever leaching of Ca when the Ca composition reaches 18.0%.

Table A-11 Ca Composition Effect

Catalyst	Ca%	Co%	Al_2O_3%	PC X%	DMC S%	PG S%
Co-Ca/Al_2O_3	6.4	32.0	61.6	47.4	88.9	105.5
Co-Ca/Al_2O_3	12.3	32.8	54.9	58.0	89.0	91.9
Co-Ca/Al_2O_3	18.0	33.0	49.0	74.2	91.2	110.6

Reaction conditions: Reaction Temperature: 50 °C, Catalyst (Co-Ca/Al_2O_3) loading: 0.9 wt%, PC/MeOH=1:20.

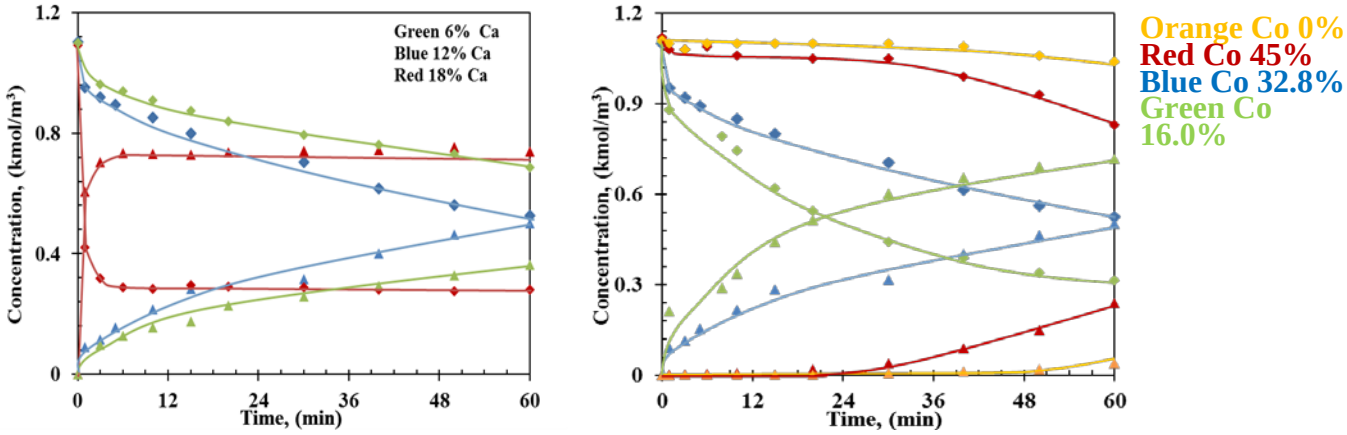

Figure A-19 Ca composition effect and Co composition effect. Reaction conditions: Reaction Temperature: 50 °C, Catalyst loading: 0.9 wt%, PC/MeOH=1:20.

(b) Co Composition Effect

Similar to the Ca composition effect, the Co composition effect was done, the results of which are summarized in Figure A-19. It is clear that, when there is no Co in the catalyst, there is nearly no activity during the first 60 min. After adding Co (about 16%) to the catalyst, the activity increased a lot. There may be two reasons for this phenomenon: first, when Co was added, Co takes all the pores from Al_2O_3, thus $CaCO_3$ is formed free instead of formed on Al_2O_3, the second reason is Co may change the deposition or other properties of Ca/Al_2O_3, the change gives it

activity. However, if increase Co loading even higher, for example, 33 wt%, the activity decreases. This possibly because the surface of CaO is covered by Co.

Table A-12 Co Composition Effect

Catalyst	Ca%	Co%	$Al_2O_{3\%}$	PC X%	DMC S%	PG S%
Co-Ca/Al_2O_3	12.3	32.8	54.9	58.0	89.0	91.9
Co-Ca/Al_2O_3	12.0	45.4	42.3	86.7	90.1	118.4

Reaction conditions: Reaction Temperature: 50 °C, Catalyst (Co-Ca/Al_2O_3) loading: 0.9 wt.%, PC/MeOH=1:20.

Chapter 4

Additional Information About Catalysts

From results in Chapter 4, it is found that the calcination within or without N_2 can have a great difference on the activity of Fe-Mn catalyst. From Figure A-20, it is obvious, the colors of the two catalyst are different. The one calcined with N_2 is grey white, the one in stable air is dark red.

Figure A-20 (a) Catalyst calcined in stable air. (b) Catalyst calcined in N_2 flow

Chapter 5

Additional Concentration-Time Profiles

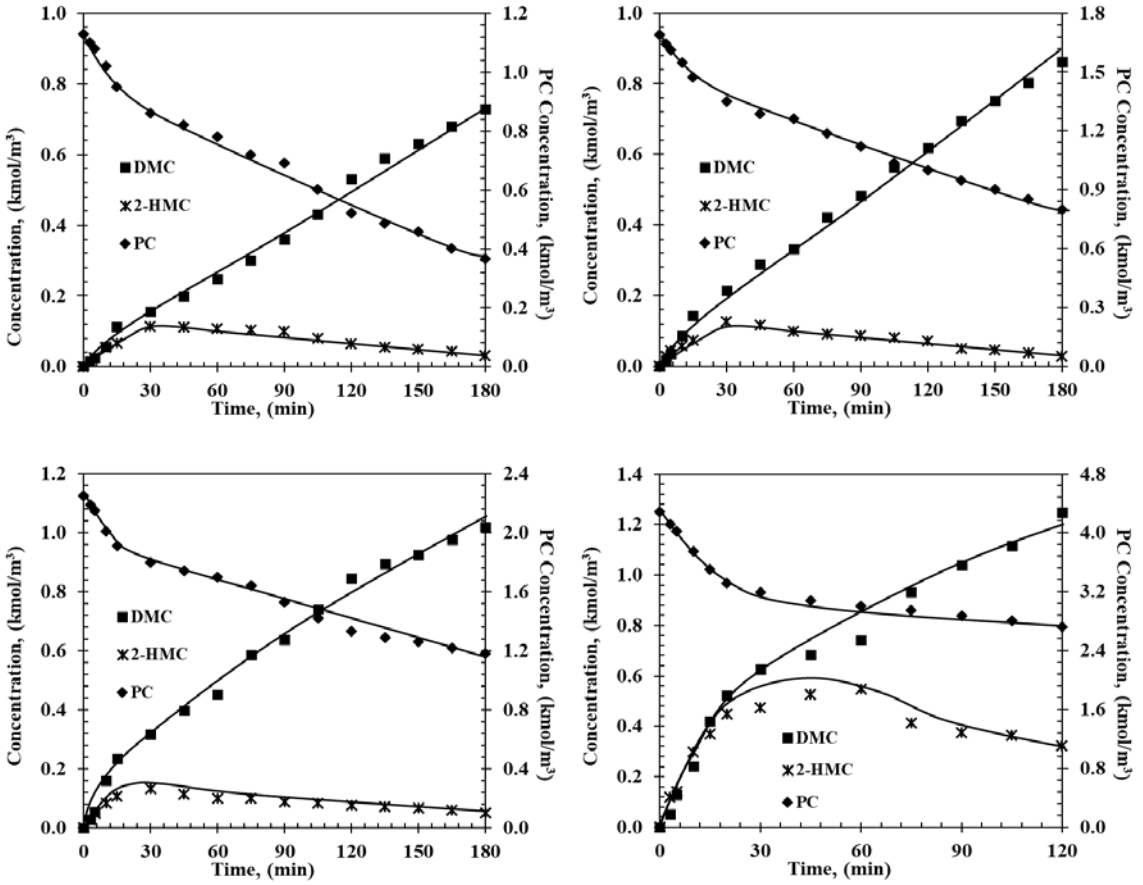

Figure A-21 Concentration-time profiles on Fe-Mn catalyst at 160 °C with different initial PC and methanol concentration

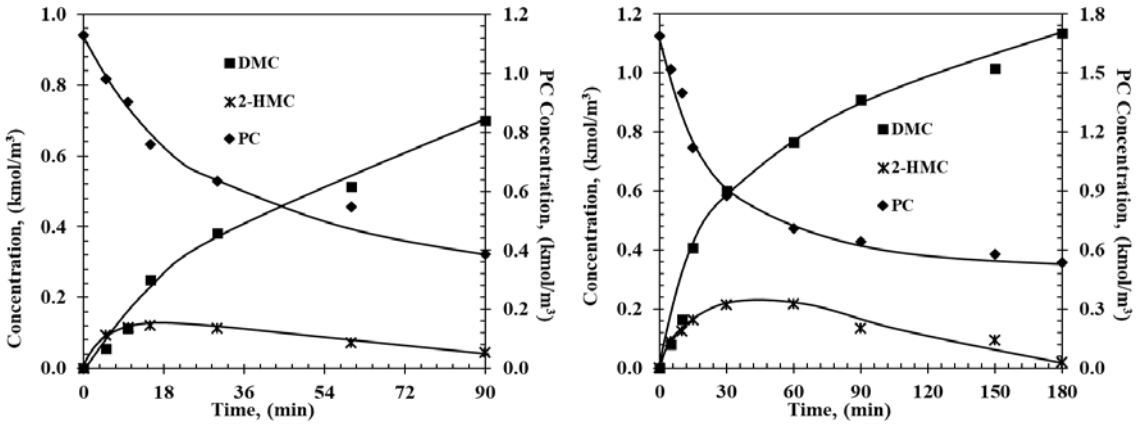

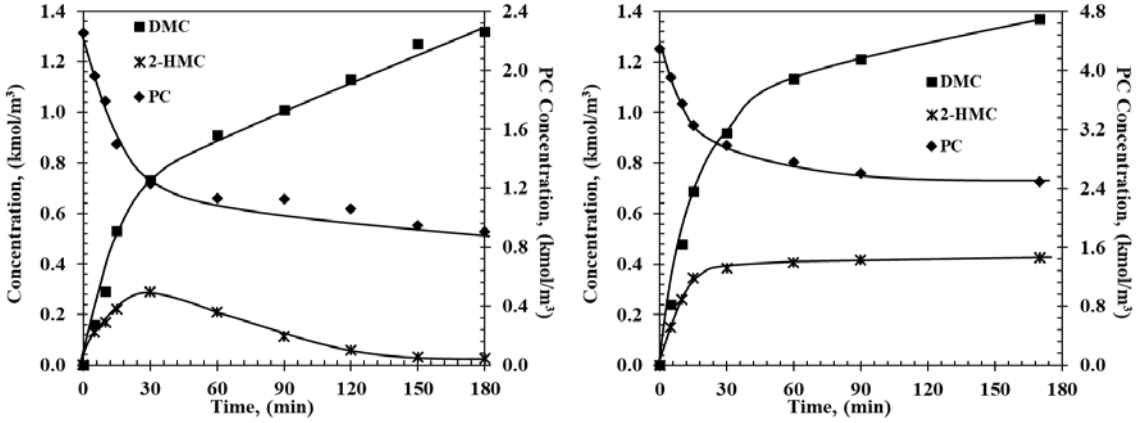

Figure A-22 Concentration-time profiles on Fe-Mn catalyst at 180 °C with different initial PC and methanol concentration

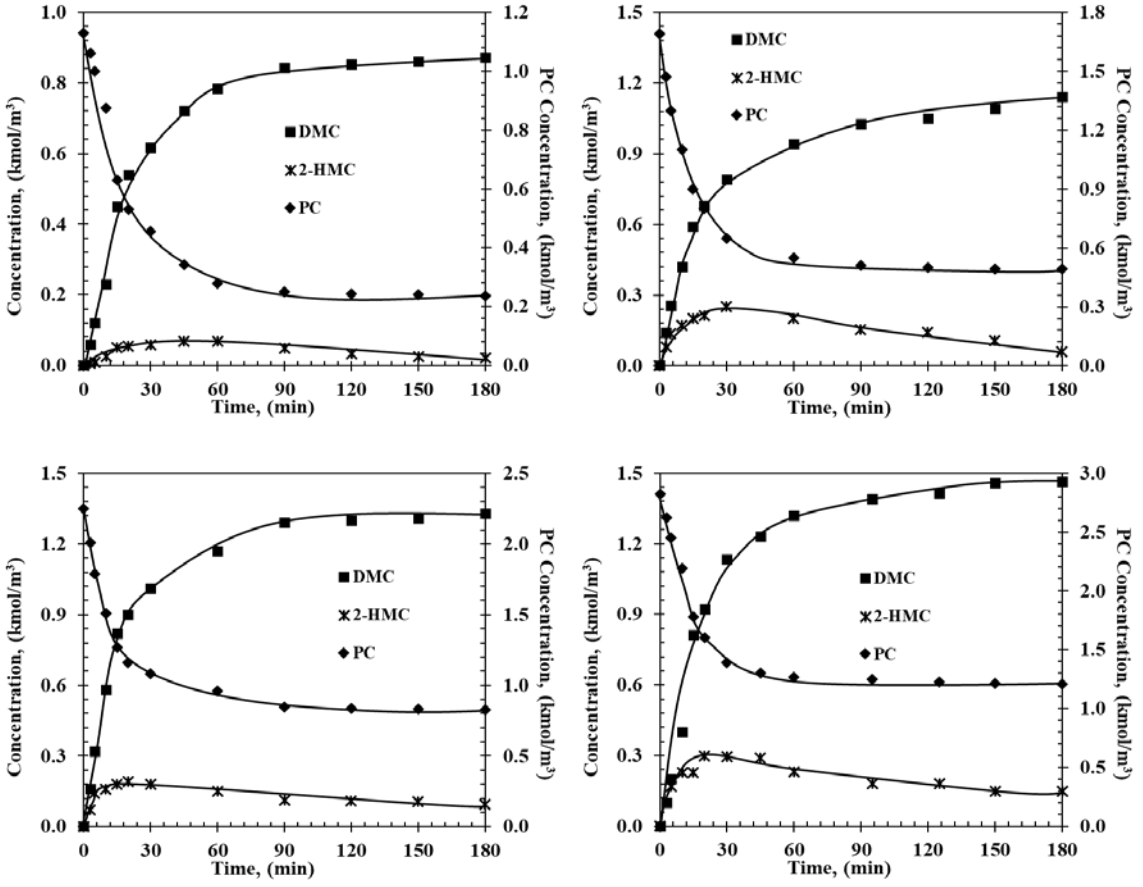

Figure A-23 Concentration-time profiles on Fe-Mn catalyst at 200 °C with different initial PC and methanol concentration

Appendix V Programming Codes for Athena

Example (1) Kinetic Modeling in Chapter 3

Parameter estimation of power law for homogeneous reaction

```
! Declarations and Model Constants
!--------------------------------
 Global k1,k2,a,b,c,D As Real
 Global RxnTime,w As Real
 w=0.0014       ! catalyst loading in kmol/m3

@Initial Conditions
 U(1)=Xu(3)
 U(2)=Xu(4)
 U(3)=Xu(5)
 U(4)=Xu(6)

@Model Equations
Dim CO1,CO2,CO3,CO4 As Real
! CO1 concentration of PC, CO2 concentration of Methanol, CO3 and CO4 concentration for
DMC and PG
Dim R As Real
CO1=U(1)
CO2=U(2)
CO3=U(3)
CO4=U(4)
R=k1*w*(CO1^a)*(CO2^b)-k2*w*(CO3^c)*(CO4^D)   ! reaction rate
F(1)=-R                              ! reaction rate of PC
F(2)=-2*R                             ! reaction rate of methanol
F(3)=R                               ! reaction rate of DMC
F(4)=R                               ! reaction rate of PG

@Response Model
 Y(1)=U(1);
 Y(2)=U(2);
 Y(3)=U(3);
 Y(4)=U(4);

@Connect Parameters
 k1=Par(1);
 k2=Par(2);
 a=Par(3);
 b=Par(4);
 c=Par(5);
 D=Par(6);
```

```
 RxnTime=Xu(2);

@Solver Options
 Headers=RunID;RxnTime;Cao;Cb0;Cc0;Cd0;Ca;Cb;Cc;Cd;w(1);w(2);w(3);w(4);Replicate
```

Parameter estimation of kinetic model based on reaction mechanism for homogeneous reaction

```
! Declarations and Model Constants
!--------------------------------
 Global k1,k2,k3,k4,k5,k6 As Real

@Connect Parameters
 k1=Par(1)
 k2=Par(2)
 k3=Par(3)
 k4=Par(4)
 k5=Par(5)
 k6=Par(6)

@Initial Conditions
 U(1)=Xu(2)
 U(2)=Xu(3)
 U(3)=Xu(4)
 U(4)=Xu(5)
 U(5)=Xu(6)
 U(6)=Xu(7)
 U(7)=Xu(8)

@Model Equations
 Dim R1,R2,R3 As Real
 R1=k1*U(1)*U(5)-k2*U(6)          ! reaction rate for step 1
 R2=k3*U(6)*U(2)-k4*U(7)          ! reaction rate for step 2
 R3=k5*U(7)*U(2)-k6*U(3)*U(5)*U(4)    ! reaction rate for step 3

 F(1)=-R1                  ! reaction rate of PC
 F(2)= -R2-R3              ! reaction rate of Methanol
 F(3)= R3                  ! reaction rate of DMC
 F(4)= R3                  ! reaction rate of PG
 F(5)= -R1+R3              ! reaction rate of S
 F(6)= R1-R2               ! reaction rate of Intermediate I
 F(7)= R2-R3               ! reaction rate of Intermediate II
```

```
@Response Model
 Y(1)=U(1)
 Y(2)=U(2)
 Y(3)=U(3)
 Y(4)=U(4)

@Solver Options
```

Parameter estimation of power law for heterogeneous reaction

```
! Declarations and Model Constants
!---------------------------------
 Global k1,k2,a,b,c,D As Real
 Global RxnTime,w,w1 As Real
 w=0.00662          ! total catalyst, in kmol/m^3
 w1=0.003839         ! solubility of catalyst, in kmol/m^3

@Initial Conditions
 U(1)=Xu(3)
 U(2)=Xu(4)
 U(3)=Xu(5)
 U(4)=Xu(6)

@Model Equations
Dim CO1,CO2,CO3,CO4 As Real
Dim R As Real

CO1=U(1)
CO2=U(2)
CO3=U(3)
CO4=U(4)
R=0.448*0.003839*(CO1^1)*(CO2^2)-213*0.003839*(CO3^1)*(CO4^1)+k1*(w-
w1)*(CO1^a)*(CO2^b)-k2*(w-w1)*(CO3^c)*(CO4^D)
F(1)=-R            ! reaction rate of PC
F(2)=-2*R           ! reaction rate of methanol
F(3)=R             ! reaction rate of DMC
F(4)=R             ! reaction rate of PG

@Response Model
 Y(1)=U(1);
 Y(2)=U(2);
 Y(3)=U(3);
 Y(4)=U(4);

@Connect Parameters
 k1=Par(1);
```

```
 k2=Par(2);
 a=Par(3);
 b=Par(4);
 c=Par(5);
 D=Par(6);
 RxnTime=Xu(2);

@Solver Options
 Headers=RunID;RxnTime;Cao;Cb0;Cc0;Cd0;Ca;Cb;Cc;Cd;w(1);w(2);w(3);w(4);Replicate
```

Parameter estimation of kinetic model based on reaction mechanism for heterogeneous reaction

```
! Declarations and Model Constants
!---------------------------------
 Global w,w1,k1,k2,k3,k4,k5,k6,k7,k8,k9,k10,k11,k12 As Real
 w=0.00662
 w1=0.003839

@Connect Parameters
 k1=Par(1)
 k2=Par(2)
 k3=Par(3)
 k4=Par(4)
 k5=Par(5)
 k6=Par(6)
 k7=Par(7)
 k8=Par(8)
 k9=Par(9)
 k10=Par(10)
 k11=Par(11)
 k12=Par(12)

@Initial Conditions
 U(1)=Xu(2)
 U(2)=Xu(3)
 U(3)=Xu(4)
 U(4)=Xu(5)
 U(5)=Xu(6)
 U(6)=Xu(7)
 U(7)=Xu(8)
 U(8)=Xu(9)
 U(9)=Xu(10)
 U(10)=Xu(11)
```

```
@Model Equations
 Dim R1,R2,R3,R4,R5,R6 As Real
 R1=k1*U(1)*U(5)-k2*U(6)            ! reaction rate of step 1 for homogeneous reaction
 R2=k3*U(6)*U(2)-k4*U(7)            ! reaction rate of step 2 for homogeneous reaction
 R3=k5*U(7)*U(2)-k6*U(3)*U(4)*U(5)     ! reaction rate of step 3 for homogeneous reaction
 R4=k7*U(2)*U(8)-k8*U(9)            ! reaction rate of step 1 for heterogeneous reaction
 R5=k9*U(8)*U(1)-k10*U(10)           ! reaction rate of step 2 for heterogeneous reaction
 R6=k11*U(9)*U(9)*U(10)-k12*U(3)*U(4)*U(8)*U(8)*U(8)       ! reaction rate of step 3 for
heterogeneous reaction

 F(1)=-R1-R5               ! reaction rate of PC
 F(2)= -R2-R3-R4              ! reaction rate of Methanol
 F(3)= R3+R6               ! reaction rate of DMC
 F(4)= R3+R6               ! reaction rate of PG
 F(5)= -R1+R3              ! reaction rate of active species for homogeneous reaction
 F(6)= R1-R2               ! reaction rate of intermediate I for homogeneous reaction
 F(7)= R2-R3               ! reaction rate of intermediate II for homogeneous reaction
 F(8)= -R4-R5+3*R6            ! reaction rate of active species for heterogeneous reaction
 F(9)= R4-2*R6              ! reaction rate of intermediate I for heterogeneous reaction
 F(10)= R5-R6              ! reaction rate of intermediate II for heterogeneous reaction

@Response Model
 Y(1)=U(1)
 Y(2)=U(2)
 Y(3)=U(3)
 Y(4)=U(4)

@Solver Options
```

Example (2) Kinetic Modeling in Chapter 5

Parameter estimation of power law

```
! Declarations and Model Constants
!--------------------------------
 Global k1,k2,k3,k4 As Real
 Global RxnTime,w As Real
 w=0.004164              ! catalyst loading in kmol/m3

@Initial Conditions
 U(1:5)=Xu(3:7)


@Model Equations
```

```
Dim C1,C2,C3,C4,C5 As Real
Dim R1,R2 As Real

C1=U(1)
C2=U(2)
C3=U(3)
C4=U(4)
C5=U(5)

R1=k1*w*(C1^1)*(C2)-k2*w*(C5)        ! reaction rate of step 1
R2=k3*w*(C5)*(C2)-k4*w*(C3)*(C4)     ! reaction rate of step 2


F(1)=-R1                      ! reaction rate of PC
F(2)=-R1-R2                     ! reaction rate of methanol
F(3)=R2                      ! reaction rate of DMC
F(4)=R2                      ! reaction rate of PG
F(5)=R1-R2                     ! reaction rate of 2-HMC


@Response Model
 Y(1:5)=U(1:5);

@Connect Parameters
 k1=Par(1);
 k2=Par(2);
 k3=Par(3);
 k4=Par(4);

 RxnTime=Xu(2);

@Solver Options
Headers=RunID;RxnTime;Cao;Cb0;Cc0;Cd0;Ci0;Ca;Cb;Cc;Cd;Ci;w(1);w(2);w(3);w(4);w(5);R
eplicate
```

Parameter estimation of kinetic model based on reaction mechanism

```
! Micro Kinetic Modeling of Transesterification 1
!-----------------------------------------
 Global k1,k2,k3,k4,k5,k6,k7,k8,k9,k10 As Real

@Connect Parameters
 k1=Par(1)
 k2=Par(2)
 k3=Par(3)
 k4=Par(4)
```

```
 k5=Par(5)
 k6=Par(6)
 k7=Par(7)
 k8=Par(8)
 k9=Par(9)
 k10=Par(10)

@Initial Conditions
 U(1)=Xu(2)
 U(2)=Xu(3)
 U(3)=Xu(4)
 U(4)=Xu(5)
 U(5)=Xu(6)
 U(6)=Xu(7)
 U(7)=Xu(8)
 U(8)=Xu(9)
 U(9)=Xu(10)

@Model Equations
 Dim R1,R2,R3,R4,R5 As Real
 R1=k1*U(2)*U(6)-k2*U(7)      ! reaction rate of step 1 for kinetic model
 R2=k3*U(1)*U(7)-k4*U(8)      ! reaction rate of step 2 for kinetic model
 R3=k5*U(8)-k6*U(5)*U(6)      ! reaction rate of step 3 for kinetic model
 R4=k7*U(8)*U(7)-k8*U(9)*U(6)   ! reaction rate of step 4 for kinetic model
 R5=k9*U(9)-k10*U(3)*U(4)*U(6)  ! reaction rate of step 5 for kinetic model

 F(1)=-R2                  ! reaction rate of PC
 F(2)= -R1                 ! reaction rate of methanol
 F(3)= R5                  ! reaction rate of DMC
 F(4)= R5                  ! reaction rate of PG
 F(5)= R3                  ! reaction rate of 2-HMC
 F(6)= -R1+R3+R4+R5          ! reaction rate of Intermediate I
 F(7)= R1-R2-R4              ! reaction rate of Intermediate II
 F(8)= R2-R3-R4              ! reaction rate of Intermediate III
 F(9)= R4-R5                ! reaction rate of Intermediate IV


@Response Model
 Y(1)=U(1)
 Y(2)=U(2)
 Y(3)=U(3)
 Y(4)=U(4)
 Y(5)=U(5)

@Solver Options
```

Appendix VI List of Publications, Presentations and Awards

Publications/Manuscripts

1. **Ziwei Song**, Bala Subramaniam, and Raghunath V. Chaudhari. Kinetic Modeling and Mechanistic Investigations of Transesterification of Propylene Carbonate with Methanol over Fe-Mn Double Metal Cyanide Catalyst. (Chemical Engineering Science, under review)
2. **Ziwei Song**, Bala Subramaniam, and Raghunath V. Chaudhari. Transesterification of Propylene Carbonate with Methanol using Fe-Mn Double Metal Cyanide Catalyst. (ACS Catalysis, under review)
3. **Ziwei Song**, Bala Subramaniam, and Raghunath V. Chaudhari. Kinetic Study of Homogenous and Heterogeneous CaO-Catalyzed Transesterification of Cyclic Carbonates with Methanol. (In preparation)
4. **Ziwei Song**, Xin Jin, Yongfeng Hu, Bala Subramaniam, and Raghunath V. Chaudhari. Intriguing Catalyst (CaO) Pretreatment Effects and Mechanistic Insights during Propylene Carbonate Transesterification with Methanol. ACS Sustainable Chemistry & Engineering, 2017, 5,
5. Xin Jin, Pallavi Bobba, Nicolas Reding, **Ziwei Song**, Prem S.Thapa, Guru Prasad, Bala Subramaniam, and Raghunath V.Chaudhari. Kinetic Modeling of Carboxylation of Propylene Oxide to Propylene Carbonate Using Ion-Exchange Resin Catalyst in A Semi-Batch Slurry Reactor. Chemical Engineering Science, 2017, 168, 189-203.
6. Xin Jin, Meng Zhao, Chun Zeng, **Ziwei Song**, Prem S.Thapa, Bala Subramaniam, and Raghunath V.Chaudhari. Oxidation of Glycerol to Dicarboxylic Acids Using Cobalt Catalysts. ACS Catalysis, 2016, 6, 4576-4583.

Presentations

1. **Ziwei Song**, Xin Jin, Guru Prasad, and Raghunath V. Chaudhari. "Transesterification of Propylene Carbonate (PC) with Methanol over CaO Catalysts: Pre-Treatment Effects" ACS Midwest Regional Meeting, Oct. 2015 in St. Joseph, MO. (Oral)
2. **Ziwei Song**, Xin Jin, Bala Subramaniam, and Raghunath V. Chaudhari. "Transesterification of Propylene Carbonate with Methanol: Catalyst Pre-treatment Effects" AIChE Annual Meeting, Nov. 2015 in Salt Lake City, UT. (Poster)
3. **Ziwei Song**, Xin Jin, Bala Subramaniam, and Raghunath V. Chaudhari. "Transesterification of Propylene Carbonate to Dimethyl Carbonate (DMC) with CaO Catalyst" 24th ISCRE Meeting, Jun. 2016 in Minneapolis, MN. (Oral)
4. **Ziwei Song**, Anand Ramanathan, Bala Subramaniam, and Raghunath V. Chaudhari. Transesterification of Propylene Carbonate with Methanol to Dimethyl Carbonate using Supported Alkali Metal Oxides Catalysts. Feb. 2017 in Baltimore, MD. (Oral)

Awards

Lyder Fellowship Award

University of Kansas, 2014

Young Researcher Travel Award

International Symposia on Chemical Reaction Engineering, 2016